UNIVERSITY OF ALBERTA

VELOCITY ANISOTROPY DETERMINATION IN THE τ-p DOMAIN

by

AHMED KEBAILI ©

A thesis submitted to the Faculty of Graduate Studies and Research in partial fulfillment
of the requirements for the degree of Doctor of Philosophy
in
Geophysics

Department of Physics

Edmonton, Alberta
Spring, 1996

National Library
of Canada

Acquisitions and
Bibliographic Services Branch

395 Wellington Street
Ottawa, Ontario
K1A 0N4

Bibliothèque nationale
du Canada

Direction des acquisitions et
des services bibliographiques

395, rue Wellington
Ottawa (Ontario)
K1A 0N4

Your file   Votre référence

Our file   Notre référence

The author has granted an irrevocable non-exclusive licence allowing the National Library of Canada to reproduce, loan, distribute or sell copies of his/her thesis by any means and in any form or format, making this thesis available to interested persons.

L'auteur a accordé une licence irrévocable et non exclusive permettant à la Bibliothèque nationale du Canada de reproduire, prêter, distribuer ou vendre des copies de sa thèse de quelque manière et sous quelque forme que ce soit pour mettre des exemplaires de cette thèse à la disposition des personnes intéressées.

The author retains ownership of the copyright in his/her thesis. Neither the thesis nor substantial extracts from it may be printed or otherwise reproduced without his/her permission.

L'auteur conserve la propriété du droit d'auteur qui protège sa thèse. Ni la thèse ni des extraits substantiels de celle-ci ne doivent être imprimés ou autrement reproduits sans son autorisation.

ISBN 0-612-10600-4

Canada

UNIVERSITY OF ALBERTA

LIBRARY RELEASE FORM

NAME OF AUTHOR: Ahmed Kebaili

TITLE OF THESIS: Velocity Anisotropy Determination in the τ-p Domain.

DEGREE: Doctor of Philosophy

YEAR THIS DEGREE GRANTED: 1996

Permission is hereby granted to the University of Alberta Library to reproduce single copies of this thesis and too lend or sell such copies for private, scholarly or scientific research purposes only.

The author reserves all other publication and other rights in association with the copyright in the thesis, and except as herein before provided neither the thesis nor any substantial portion thereof may be printed or otherwise reproduced in any material form whatever without the author's prior written permission.

(signed) ....

4103-7 Avenue
Calgary, Alberta
T3C 0E3

Date: January 30, 1996

UNIVERSITY OF ALBERTA

FACULTY OF GRADUATE STUDIES AND RESEARCH

The undersigned certify that they have read, and recommend to the Faculty of Graduate Studies and Research for acceptance, a thesis entitled Velocity Anisotropy Determination in the τ-p domain submitted by Ahmed Kebaili in partial fulfillment of the requirements for the degree of Doctor of Philosophy in Geophysics.

Dr. D. R. Schmitt

Dr. E. R. Kanasewich

Dr. F. Hron

John Beamish
Dr. J. Beamish

Dr. Robert Luth

f RJB
Dr. R. J. Brown

Date: January 24, 1996

Dedication

To my wife Cherifa, my son Mohamed-Amine, my daughters Hassina, Hadjer, Safa and Maroua, and my parents.

Abstract

Slant stack (τ-p) mappings of expanding spread seismic profiles have long been used in the recovery of subsurface velocities and layer thicknesses under the assumption that the earth is a stack of isotropic layers. Because the ray parameter p is directly a function of the angle of incidence θ, variations of velocity with θ within an anisotropic medium should be naturally identified in the τ-p domain. Existing τ-p formulations are readily modified to a geometry consisting of surface sources and wellbore receivers in a stack of anisotropic layers. A layer stripping operation in the τ-p mapping for an offset vertical seismic profile (VSP) is conducted for small p (near offset) and large p (far offset) ranges. In models consisting of anisotropic layers, the velocities recovered in this research using this strategy differ from those input by less than 1 percent. The method was applied to data acquired in a shallow borehole, which revealed a velocity difference between the near-vertical and oblique directions of 15 percent in lithology of alternating thin (~ 1 m) sands and shales. A further modification of this technique is developed in this thesis to determine the slowness surfaces from τ-p curves. The method directly provides phase velocities as a function of phase angle. In all the investigated models, the discrepancies between the observed and modeled slowness curves are relatively small with a mean error being less than 0.5 percent in each case. This method was also applied to a set of data acquired in a shallow borehole in Northern Alberta. The layered sand-shale sequence studied exhibits a phase velocity that increases by 12.5 percent from vertical to about 50°. The method was also applied to determine ultrasonic velocities for both isotropic (plexiglass) and anisotropic (phenolic) samples. The recovered velocity from the τ-p curves for the isotropic sample differs from the directly measured velocity by less than 1 percent. The results show that the phenolic sample exhibits anisotropies that varies from 4 percent on the x-y plane to 22 percent for the y-z plane.

Acknowledgements

First and foremost, I thank Allah who gave me the strength to make this final product and the wisdom to find a balance between my studies and my family obligations during all these years full of struggle and challenges.

I would like to thank my supervisor, Doctor Douglas R. Schmitt for his relentless moral and material support. His financial support allowed me to present my work at scientific meetings in North America (SEG, CSEG, CGU) and in Europe (Norway) at the Sixth International Workshop on Seismic Anisotropy.

I also would like to thank all my committee members, professors E. R. Kanasewich, F. Hron, J. Beamish, R. Luth, and J. Brown, with a special mention to Franta Hron for his fruitful discussions about phase and group velocities, and Jim Brown (University of Calgary) for supplying me with the phenolic sample I used in my experiments, and his tremendous contributions to the CSEG and the International Workshops on Seismic Anisotropy.

I would also like to thank Lawrence Le for providing me with synthetic seismograms to investigate P and S-wave anisotropies due to thin layering.

I thank Len Tober and Jay Haverstock, very talented technicians, who were of great help to me. Len always listens to the problems and suggests solutions using the experience he acquired through the years he spent in the physics department working with geophysicists. Jay supplied me with all the equipment needed for the laboratory measurements. Jay knows where to find answers when unexpected things occur, and is ready to help. Len and Jay helped in acquiring the VSP data in Fort MacMurray and helped overcome all the technical difficulties.

In addition to sharing an office with my fellow graduate students Jo Molyneux, Yan Wang, Yongyi Li, and Gilbert Dubuc we also shared computers and knowledge. I can't forget the quality time I spent with them discussing scientific matters. I thank them for their help and collaboration and good understanding. I must also mention Marko Mah who digitized the well logs I used.

I would like to acknowledge Norman Udey and Jim MacKinnon who were very helpful to me and kept the computer system working properly. I am very grateful to them.

This work was supported in part by Petroleum Research Fund administered by the American Chemical Society, by the Alberta Oil Sands Technology and Research Authority, and the National Sciences and Engineering Research Council of Canada. The program SAC, version 10.5d developed by William C. Tapley and Joseph E. Tull at the Lawrence Livermore National Laboratory, California was used for plotting of the hodograms.

Last but not least I would like to thank Lynn Chandler, the administration Clerk at the general office, for the help in administration matters she is offering to the graduate students of the Physics Department.

Table of contents

1. Introduction 1
    - 1.1 Background 1
    - 1.2 Causes of Anisotropy 2
    - 1.3 Theoretical Overview 5
    - 1.4 Observations of Anisotropy in Geophysics 10
    - 1.5 The τ-p Transformation 12
    - 1.6 Outline of Thesis 17

2. Velocity Anisotropy Estimation From Slant Stacks of Wellbore Seismics 31
    - 2.1 Introduction 31
    - 2.2 Velocity Recovery in The τ-p Domain 35
    - 2.3 The τ-p Mapping For Directly Transmitted Arrivals in a Borehole 37
    - 2.4 Phase And Ray Velocities in Anisotropic Media 38
    - 2.5 Anisotropy in The Borehole Case 41
    - 2.6 Test of The Method on Calculated Seismic Models 43
        - 2.6.1 Model1: Anisotropic Half-Space 43
        - 2.6.2 Isotropic Layer Over Anisotropic Half-Space 45
    - 2.7 Conclusion 46

3. Velocity Anisotropy Observed in Wellbore Seismic Arrivals: Combined Effects of Intrinsic Properties And Layering 60
    - 3.1 Introduction 60
    - 3.2 Theoretical Backgound 61
    - 3.3 Application 65
        - 3.3.1 Geologic Setting 65

3.3.2 Field Acquisition 66
3.3.3 Three Component Data Processing 67
3.3.4 τ-p Mapping And Velocity Determination 68
3.4 Discussion 73
3.5 Conclusion 75

4. Slowness Surface Determination From Slant Stack Curves 89
4.1 Introduction 89
4.2 Theoretical Background 91
4.2.1 Phase Slowness Determination 91
4.2.2 Phase And Ray Velocities 94
4.3 Tests on Synthetic Data 96
4.3.1 Multilayered Isotropic Medium 96
4.3.2 Elliptically Anisotropic Medium 97
4.3.3 Transversely Isotropic Medium 99
4.4 Application to Real Data 101
4.5 Conclusion 103

5. Ultrasonic phase velocities determined using a radon transformation 122
5.1 Introduction 122
5.2 Theory 124
5.3 Experimental Configuration 129
5.4 Results And Discussion 130
5.4.1 Acrylic Sample 130
5.4.2 Phenolic Sample 132
5.5 Conclusion 135

6 Conclusions 153

6.1 Near-Vertical to Oblique Anisotropy
Delineation From Offset VSP Data 153

6.2 Slowness Surface Determination
From VSP Experiments 154

6.3 Ultrasonic Velocity Anisotropy Determination 156

6.4 Future Directions 157

6.4.1 Application in Reflection Seismology 157

6.4.2 Application to Shear Waves 158

6.4.3 Application to Development Geophysics 158

Appendix A 161

Wave-Forms (1 cm) And Their τ-p Mapping For Plexiglass 161

Wave-Forms (2cm) And Their τ-p Mapping For Plexiglass 162

Wave-Forms (2 cm) And Their τ-p Mapping For Phenolic in x-z Plan 163

Wave-Forms (3 cm) And Their τ-p Mapping For Phenolic in x-z Plan 164

Wave-Forms (4 cm) And Their τ-p Mapping For Phenolic in x-z Plan 165

Wave-Forms (3 cm) And Their τ-p mapping For Phenolic in y-z Plan 166

Wave-Forms (2 cm) And Their τ-p mapping For Phenolic in x-y Plan 167

Wave-Forms (3 cm) And Their τ-p mapping For Phenolic in x-y Plan 168

Wave-Forms (4 cm) And Their τ-p mapping For Phenolic in x-y Plan 169

Wave-Forms (2 cm) And Their τ-p mapping For Phenolic (diagonal line) ... 170

Wave-Forms (3 cm) And Their τ-p mapping For Phenolic (diagonal line) ... 171

Wave-Forms (4 cm) And Their τ-p mapping For Phenolic (diagonal line) ... 172

Appendix B 174

SYNT_VSP.F: to generate synthetic VSP data 174

STATIC.F: for static corrections 181

EQUAL.F: for trace equalization 183

TPMAP.F: for slant-stack (τ-p mapping) 185

WINDOW.F: for windowing of the wavelets 188

LSTRIP.F: for layer stripping 191

TPICK.F: for automatic pick of the intercept times 194

VELAN.F: for velocity analysis 197

VELCAL.F: to compute velocities using Backus's equations 201

List of Figures

Figure **Page**

1.1 Slant stack procedure 27

1.2 Ray tracing through a layered medium: Snell's law 28

1.3 Forward and inverse τ-p transforms of hypothetical seismic events 29

1.4 Multi-offset and depth VSP ray geometry 30

2.1 x-t and corresponding τ-p curves for a muti-offset VSP experiment 52

2.2 Hypothetical phase slowness and wave surface of an anisotropic medium 53

2.3 Half-space model and its ray velocity function 54

2.4 x-t seismogram and corresponding τ-p mapping 55

2.5 Velocities input (model) and recovered for the anisotropic half-space 56

2.6 Isotropic layer over anisotropic half-space: model and velocity relation 57

2.7 τ-p mapping of the x-t seismogram for the one layer model 58

2.8 Velocities input and recovered for the one layer model 59

3.1 VSP downgoing ray through an anisotropic an inhomogeneous medium 80

3.2 Lithology compared to focus electric and sonic logs 81

3.3 Recorded VSP three component traces and horizontal-plane hodogram 82

3.4 Vertical, computed radial and P-wave traces, and vertical-plane hodogram .. 83

3.5 P-traces for the 25-m depth receiver, and their τ-p mapping 84

3.6 Composite τ-p for a multi-receiver depth VSP experiment 85

3.7 Semblance and energy maps for oblique portion of τ-p mapping 86

3.8 Recovered near vertical and oblique velocities compared to sonic logs 87

3.9 Layer between 74 m and 120 m divided into thin layers 88

4.1 Seismic rays through an inhomogeneous and anisotropic half-space 107

4.2 Phase and ray velocities, and plane wave decomposition of wave surface 108

4.3 VSP experiment for an isotropic layered medium 109

4.4 x-t and τ-p seismograms for the isotropic layered medium 110

4.5 Recovered and actual slowness surfaces for isotropic layered medium 111

4.6 Velocity model for an elliptically anisotropic medium 112

4.7 x-t seismogram and τ-p mapping for the elliptically anisotropic medium 113

4.8 Recovered phase and ray velocities for elliptically anisotropic medium 114

4.9 Vertical and horizontal x-t seismograms for a TI medium 115

4.10 Calculated P and S wave seismograms for TI medium 116

4.11 τ-p mappings of the calculated P and SV seismograms for the TI medium .. 117

4.12 Recovered and modeled qP and qSV slowness surfaces 118

4.13 Sonic log showing shale-sand sequence 119

4.14 x-t and τ-p seismograms for a receiver at 75 m depth in a borehole 120

4.15 Recovered phase velocity curve for a shale-sand sequence 121

5.1 Slant stack procedure 139

5.2 Ray path and through-transmission traveltime curve 140

5.3 Transmitter-receiver configuration for the laboratory measurements 141

5.4 Hypothetical phase slowness and wave surface of an anisotropic medium ... 142

5.5 Observed wave-forms and their τ-p mapping for plexiglass sample 143

5.6 Recovered velocity and slowness curve for the plexiglass sample 144

5.7 Schematic of the phenolic sample showing the investigated planes 145

5.8 Wave-forms (2 cm) and their τ-p mapping for phenolic in the y-z plan 146

5.9 Wave-forms (4 cm) and their τ-p mapping for phenolic in the y-z plane 147

5.10 Recovered phase velocities in the y-z plane for phenolic sample 148

5.11 Recovered phase and ray velocities in the y-z plane for phenolic sample 149

5.12 Recovered phase and ray velocities in the x-z plane for phenolic sample 150

5.13 Recovered phase and ray velocities in the x-y plane for phenolic sample 151

5.14 Recovered phase velocities in the y-z plane for the phenolic sample 152

A.1 Wave-Forms (1 cm) And Their τ-p Mapping For Plexiglass 161

A.2 Wave-Forms (2 cm) And Their τ-p Mapping For Plexiglass 162

A.3 Wave-Forms (2 cm) And Their τ-p Mapping For Phenolic in x-z Plan 163

A.4 Wave-Forms (3 cm) And Their τ-p Mapping For Phenolic in x-z Plan 164

A.5 Wave-Forms (4 cm) And Their τ-p Mapping For Phenolic in x-z Plan 165

A.6 Wave-Forms (3 cm) And Their τ-p mapping For Phenolic in y-z Plan 166

A.7 Wave-Forms (2 cm) And Their τ-p mapping For Phenolic in x-y Plan 167

A.8 Wave-Forms (3 cm) And Their τ-p mapping For Phenolic in x-y Plan 168

A.9 Wave-Forms (4 cm) And Their τ-p mapping For Phenolic in x-y Plan 169

A.10 Wave-Forms (2 cm) And Their τ-p mapping For Phenolic (diagonal line) .. 170

A.11 Wave-Forms (3 cm) And Their τ-p mapping For Phenolic (diagonal line) ... 171

A.12 Wave-Forms (4 cm) And Their τ-p mapping For Phenolic (diagonal line) ... 172

Chapter 1

1. Introduction

1.1 Background

For the sake of computational convenience, the earth or its components are usually assumed to be isotropic in seismic analysis. However, seismic anisotropy exists more generally in the real earth. Earth materials are intrinsically anisotropic as a result of preferred grain orientations and cracks. Geologic effects, such as thin layering, also produce variations of velocity with angle of propagation. Ignoring this anisotropy can result in erroneous geologic interpretations. Quantitative measurement of this anisotropy can yield important information about in-situ geologic conditions and structures. A better understanding of the earth and its internal processes requires a better understanding of its seismic anisotropy; and methods of extracting this information are required.

Velocity anisotropy is observed in the earth's mantle and crust. The discrepancy between Rayleigh and Love waves (both surface waves) observed by Anderson (1961, 1967), and Harkrider and Anderson (1962) is clear evidence that the upper mantle of the earth is seismically anisotropic and is explained by P-wave and *S*-wave velocity anisotropies of 7 and 8 percent, respectively. The anisotropy of the mantle is mainly intrinsic; it contains information about alignment of minerals with respect to the direction of convective flow. For example, a relatively large azimuthal P-wave anisotropy of 5 percent is observed in the oceanic upper mantle; this result indicates that the crystallographic axis of olivine with the maximum velocity is preferentially aligned in the direction of convective flow from a spreading oceanic ridge (Peselnick, 1974; Christensen and Salisbury, 1979).

Three-component microearthquake data recorded globally (e. g., Crampin, 1987), surface reflection seismology (e. g., Alford, 1986), and three-component borehole seismic experiments (e. g., Johnston, 1986) also reveal that the earth's crystalline and sedimentary basins are also seismically anisotropic.

Velocity anisotropy in sedimentary basins has been extensively studied as improvements in the interpretation of reflection seismics have substantial economic benefits. During the last few decades, a large number of surface and borehole seismic experiments have been conducted. Larner et al. (1993), computed the migration errors involved in assuming anisotropic media to be isotropic, and showed that the quality of the migrated seismic sections is greatly dependent upon the velocity anisotropy. Daley and Hron (1977) showed that variation of the reflection coefficient at an interface between two anisotropic media is substantially affected by the velocity anisotropy. Further, laboratory measurements carried out on various types of samples (e. g., Vernik and Nur, 1992) show that many sedimentary rocks are anisotropic.

Seismic velocity anisotropy is an important but poorly understood characteristic of the earth. It is important that further methods be developed to extract this anisotropy in seismic data sets. In this thesis, I propose a new method for velocity anisotropy determination in the τ-p domain from ray multioffset and multidepth VSP data sets. First, I describe a layer stripping technique in the τ-p domain and then test it on both synthetic and real data, the latter being acquired in a shallow borehole in Northern Alberta. I further developed the method to recover the slowness curves for both qP-waves and qSV-waves for a simulated VSP for a transversely isotropic (TI) medium, and later applied to a field data set for which the P-wave velocity function from normal incidence to an incidence angle of 55° is determined. I finally adapted the τ-p method to laboratory measurements, where qP-wave phase velocity was measured as a function of incidence angle determined for four different planes within a material of orthorhombic symmetry.

1.2 Causes of Anisotropy

The elastic behavior of an isotropic material is specified by 2 elastic constants. In contrast, the elastic behavior of a material which completely lacks symmetry is characterized by 21 independent elastic constants. Any symmetry within the structure of a material reduces the number of independent elastic constants required to describe it. As a result, both compressional and shear velocities depend on the orientation in a three-dimensional system of coordinates. Some examples of velocities for a few minerals are shown in table 1.1.

The mineral anisotropies will influence rock anisotropy if, on average, the grains within a given rock have a preferred crystallographic, or lattice-preferred, orientation. The aggregates of crystals that form rocks are also anisotropic On this basis, Nicholas and Christensen (1987) describe the main source of the high anisotropy observed in the mantle of the earth. They showed that static deformation resulting from simple shear on minerals with a dominant slip system will preferably align the crystals; therefore, mantle flow indirectly produces seismic anisotropy. The acoustic-wave anisotropy observed (Christensen et al., 1982) on peridotite from the upper mantle is consistent with the anisotropy of their dominant minerals (olivines and orthopyroxene) and their orientation. In crustal metamorphic rocks, anisotropy is caused similarly by preferred orientation of the constituent crystals. Preferred orientations can be produced by crystal rotation during straining, recrystallization in a nonhydrostatic stress field, or by preferential crystal settling in magma chambers.

Deviatoric stress fields are also known to influence the elastic properties of rocks. This fact is important to both in-situ stress measurements and to the interpretation of crustal seismic data because stress will influence seismic velocity. For example, Tocher (1957) and Matsushima (1960) showed that uniaxial stresses applied to rocks with microcracks produce changes in their elastic properties. The anisotropy is produced by oriented microcracks within the rock mass. To help understand the effects of microcracks on wave velocities Walsh, (1965) modeled the microcracks producing a certain porosity. A nonhydrostatic stress applied to a cracked specimen will close cracks in some directions and leave cracks in other directions open. Cracked rocks that are intrinsically isotropic and subject to nonhydrostatic stresses exhibit an anisotropy that depends on the elastic properties of the matrix, the porosity, the aspect ratios of the cracks, and the bulk modulus of the pore fluid (Nur, 1971; Anderson et al., 1974).

Oriented cracks are also important in crustal seismic studies, and it has been suggested these are an indicator of the prevailing stress orientations. The least compressive principal stress is generally horizontal in normal strike-slip faulting environments (Jamison and Cook, 1980; Hickman et al., 1988; Evans et al., 1989); consequently those cracks most open are aligned in a vertical plane striking parallel to the maximum horizontal stress orientation (Crampin, 1978). Crampin (1978) showed that if the seismic wavelength is large relative to the typical crack spacing, the cracked medium is transversely isotropic with a horizontal axis of symmetry perpendicular to the plane of the cracks. As a result, it has been suggested that variability of the stress field near active faults can be monitored by changes in anisotropy. For example, a gradual increase in the delays between the fast shear waves (polarized along the fractures) and slow shear waves (polarized perpendicular to the fractures) over a period of 3 years at a station of the Anza seismic network monitoring the Anza seismic gap on the San Jacinto fault in southern California was observed by Peacock et al. (1988). This anisotropy was reported to end near the time of the North Palm Springs earthquake only 33 km north of the station; this interpretation remains controversial. The polarization of shear waves along and perpendicular to the fractures, and their decoupling as they travel with different speeds is referred to in the literature as "shear wave splitting" or "birefringence".

Aligned cracks are not the only source of crustal anisotropy. The layering of the sediments over geologic time scales can also be a source of seismic velocity anisotropy. In fact, if the typical layer thickness is small compared to the seismic wavelength, the layered medium is equivalent to a homogeneous transversely isotropic medium with a vertical axis of symmetry (e.g. Postma, 1955; Backus, 1962). There is a direct relationship between anisotropy and heterogeneity. Such a transversely isotropic medium is characterized by 5 independent elastic constants. The seismic velocities in a transversely isotropic medium (whose axis of symmetry is vertical) are azimuthally independent and vary only with the angle of incidence (Backus, 1962). Unlike crystals exhibiting hexagonal symmetry, the 5 independent elastic constants of an equivalent transversely isotropic medium cannot take arbitrary values as will be seen later. The inequalities given by Postma (1955), Backus (1962), and Berryman (1979) show that for most cases of physical interest the velocity of a wave propagating along the layers will be larger than that propagating in a direction perpendicular to the layers.

Sedimentary basins can combine both transverse isotropy due to thin horizontal layering and anisotropy due to vertically aligned cracks. This type of medium has an orthorhombic symmetry described by an elastic tensor with 9 independent elastic constants (Bush and Crampin 1987). In addition to these geometric effects of thin layering and aligned cracks in the earth's crust, most of the rocks are intrinsically anisotropic (Freund, 1992). The matrix minerals may themselves be anisotropic, and create preferential orientations for wave propagation (Gieske and Allred, 1974, Brocher and Christensen., 1990, Rokhlin and Wang, 1992, Johnston and Christensen, 1995).

1.3 Theoretical Overview

A brief summary of the mathematical background of elastic wave anisotropy is necessary to set the stage for the work in this thesis. The reader is directed to texts such as Fedorov (1968) and Musgrave (1970) for more complete descriptions of the fundamental relationships between elasticity and anisotropy, and Aki and Richards (1980) for introductory explanations of the implications to seismology. Most recently, Miller and Chapman (1991), and Chapman and Pratt (1992) showed that the inclusion of seismic anisotropy yields a better resolution in tomographic imaging. Larner and Cohen (1993) showed that some migration errors are a result of the fact that velocity anisotropy was not introduced into the processing of reflection data. Because shales are very abundant and important hydrocarbon sources, a large number of studies have been undertaken dealing with their seismic properties. Most of the studies have revealed that the shales in various parts of the world exhibit a strong velocity anisotropy (Banik et al., 1984, Vernik and Nur, 1992, Sayers, 1994). Further, crosswell tomographic imaging has been widely used during the last decade to recover the velocity structure between wellbores. However, the resolution of the images is closely tied to the inclusion of anisotropy of the layers traversed by the rays (Saito, 1991; Chapman and Pratt, 1992).

For an anisotropic medium, the stress-train relationship is given by the generalized Hooke's law

$$\sigma_{ij} = C_{ijkl}\varepsilon_{kl} \tag{1.1}$$

where C_{ijkl} is a component of the fourth-order stiffness tensor, **C**, and σ_{ij} and ε_{ij} are the components of the stress and strain tensors, respectively. The symmetries of the stress and strain tensors reduce the number of independent elastic constants of the **C** tensor to 36. The number can be reduced even further to 21 without losing generality by using the fact that straining a medium must produce a positive change in its internal energy (Musgrave, 1970).

The equations of motion in terms of the components of displacement d_i using Einstein's indexing notation may be written as:

$$C_{ijkl}d_{k,lj} - \rho\ddot{d}_i = 0 \tag{1.2}$$

where ρ is the density, d_i is the ith component of the displacement, and ".." denotes the second time derivative.

To determine the phase velocities for a generally anisotropic medium with 21 independent elastic constants, consider a plane-wave propagating through the medium. One component of the displacement vector **d** that satisfies the equations of motion [equation (1.2)] would have a solution of the form (Musgrave, 1970):

$$d_k = A\mathbf{e_k}\exp i\omega(u_r x_r - t) = A\mathbf{e_k}\exp i(k_r x_r - \omega t) \qquad (1.3)$$

where: A is a scalar amplitude, $\mathbf{e_k}$ a unit displacement vector, ω the angular frequency of the wave, and x_r, u_r, and k_r are the components of the space vector, slowness vector, and the wave number, respectively. Note that a summation is performed over the repeated dummy index r.

Note that the displacement vector in equation (1.1.3) is complex. However, physical displacements are obtained from the average of the complex displacement d_k and its complex conjugate $\overline{d_k}$;

$$D_k = (d_k + \overline{d_k})/2. \qquad (1.4)$$

Alternatively, the physical displacement is simply the real part of d_k.

The wave number k_r may be written as:

$$k_r = \frac{2\pi}{\lambda}(n_r + in'_r) \qquad (1.5)$$

where n_r and n'_r are the real and imaginary parts of the complex wave front normal (i. e. the normal to the wavefront), and λ is the wavelength. By substituting k_r by its expression in equation (1.5), equation (1.3) becomes

$$d_k = A\mathbf{e_k}\exp\left[\frac{-2\pi\, n'_r x_r}{\lambda(n_r)}\right] \exp i\,\frac{2\pi}{\lambda(n_r)}\left[n'_r x_r - v(n_r)t\right] \qquad (1.6)$$

where v is the phase velocity of an elastic wave propagating in the direction of the real n_r. Substituting equation (1.6) into the equations of motion [equation (1.2)], one obtains

$$(C_{ijkl}n_jn_l - \rho v^2\delta_{ik})e_k = 0 \tag{1.7}$$

which may be solved for the real displacements $\boldsymbol{e_k}$ and real phase velocities v. The phase velocities can be obtained by solving the characteristic equation of equation (1.7) which is

$$\det |C_{ijkl}n_jn_l - \rho v^2\delta_{ik}| = 0 \tag{1.8}$$

and which is commonly given in the form

$$\det |\Gamma_{ik} - \rho v^2\delta_{ik}| = 0 \tag{1.9}$$

as Christoffel's characteristic equation. The Γ_{ik} are also known as Kelvin-Christoffel stiffnesses.

The elastic tensors for media of hexagonal symmetry have 5 nonzero independent elastic constants. If the axis of symmetry is parallel to the vertical (x_3) axis the elastic tensor C_{mn}, where both m and n run from 1 to 6, and such that

ij , kl =	11,	22,	33,	23 or 32,	31 or 13,	12 or 21
m , n =	1	2	3	4	5	6

then **C** takes the form

$$\mathbf{C} = \begin{pmatrix} C_{11} & C_{12} & C_{13} & & & \\ C_{12} & C_{11} & C_{13} & & 0 & \\ C_{13} & C_{13} & C_{33} & & & \\ & & & C_{44} & & \\ & 0 & & & C_{44} & \\ & & & & & C_{66} \end{pmatrix} \tag{1.10}$$

where $C_{12} = C_{11} - 2C_{66}$, and the Kelvin-Christoffel stiffnesses are given by:

$$\begin{aligned}
\Gamma_{11} &= n_1^2 C_{11} + n_2^2 C_{66} + n_3^2 C_{44} \\
\Gamma_{22} &= n_1^2 C_{66} + n_2^2 C_{11} + n_3^2 C_{44} \\
\Gamma_{33} &= n_1^2 C_{44} + n_2^2 C_{44} + n_3^2 C_{33} \\
\Gamma_{23} &= n_2 n_3 (C_{13} + C_{44}) \\
\Gamma_{13} &= n_1 n_3 (C_{13} + C_{44}) \\
\Gamma_{12} &= n_1 n_2 (C_{12} + C_{66}) \ .
\end{aligned} \tag{1.11}$$

Note that in a transversely isotropic medium, energy considerations require that the elastic constants meet certain conditions:

$$C_{11} \geq C_{66} \geq 0, \quad C_{33} \geq 0, \quad C_{44} \geq 0, \quad C_{13}^2 \leq C_{33}(C_{11} - C_{66}) \tag{1.12}$$

(Postma, 1955; Backus, 1962). When the transversely isotropic medium is constructed of thin isotropic layers, Backus (1962) showed that the following additional constraints must be imposed:

$$C_{11} > C_{13}, \quad C_{33} > \frac{4}{3} C_{44}, \quad C_{66} \geq C_{44} \tag{1.13}$$

The constraints (1.12) and (1.13) on the elastic constants give a transversely isotropic medium a particular case of hexagonal symmetry for which the horizontal velocity is larger than the vertical velocity for most of materials of this type.

Media of orthorhombic symmetry are described by 9 independent elastic constants that can be grouped in a 6x6 matrix as

$$\mathbf{C} = \begin{pmatrix} C_{11} & C_{12} & C_{13} & & & \\ C_{12} & C_{22} & C_{23} & & 0 & \\ C_{13} & C_{23} & C_{33} & & & \\ & & & C_{44} & & \\ & 0 & & & C_{55} & \\ & & & & & C_{66} \end{pmatrix}. \tag{1.14}$$

1.4 Observations of Anisotropy in Geophysics

In the upper-mantle olivine is the most abundant mineral and has a preferred orientation more pronounced than the other minerals. The olivine mineral that has an orthorhombic symmetry is easily oriented by the ambient stress or flow field. The direction of maximum P-wave velocity in olivine (9.89 km/s) coincides with that of the flow in the horizontal plane and the minimum velocity (7.72 km/s) points generally vertical, perpendicular to the horizontal flow plane. The velocity along the third axis orthogonal to the first two, away from the ridge has a magnitude of 8.43 km/s. However, the olivine and orthopyroxene-rich aggregates exhibit an azimuthal P-wave anisotropy of 4 to 6 percent, which is less than that exhibited by the pure olivine, due partly to the misalignment of the crystals. This olivine and orthopyroxene-rich aggregates exhibit an S-wave azimuthal anisotropy of only 1 to 2 percent that is small compared to the transverse anisotropy.

Shear waves propagating through an anisotropic medium produce shear-wave polarization anomalies that can be used to estimate the anisotropy of materials (Crampin, 1981). Unfortunately, the shear waves are usually contaminated by the preceding P-wave and by the S to P conversions. The P-wave polarization vector may deviate significantly from the wave front normal (phase-velocity direction) and can be as large as 30° in strongly anisotropic materials like the x-cut alpha-quartz (trigonal symmetry) described by Crampin and McGonigle (1981). For P-wave propagation in the symmetry planes of cubic, hexagonal, tetragonal, and orthorhombic systems, the deviation of the polarizations may deviate significantly from the wave front normal. However, the apparent deviation of the polarization from the ray path is small (Crampin, 1981).

Ando et al. (1983) studied the shear-waves splitting at near-vertical incidence angles from earthquakes of intermediate to deep focus. They observed, over a region of 100 km, a time delay as large as 1 s between the fast and slow shear-waves, possibly due to oriented cracks produced by the earthquakes, which corresponds to a velocity difference of 4 percent.

For rigid, fractured bodies, stress is a direct cause of anisotropy. Nur and Simmons (1969) measured velocities of a granite sample subjected to various uniaxial pressures. He showed that at a 300-bar pressure the sample exhibits a P-wave velocity in the stress direction increased by about 20 percent, while the increase in the direction perpendicular to the stress was about 5 percent only.

An experiment conducted in the fractured Austin chalk (O'Connell and Budiansky, 1974) showed a velocity for shear-waves polarized along the orientation of the fractures of 2.44 km/s versus 1.83 km/s for shear-waves polarized perpendicular to the fractures, leading to a shear-wave anisotropy of about 30 percent. Most of the observed leading shear waves are consistent with the orientation of the cracks. For instance, for 60 microseismic events with magnitude between 1.8 and 3.0, observed and monitored by Peacock et al. (1988) in the Anza stretch of the San Jacinto fault in southern California, the time lags between the fast and slow shear waves had an average value of 55 ms, with a standard deviation of 25 ms. Velocity measurements performed by Rabbel (1994) on rock samples taken from the KTB (Continental Deep Drilling Site) in Germany showed that the rocks traversed by the 3500-m deep borehole are anisotropic and that the metamorphic rocks exhibit an anisotropy larger than 10 percent.

Miller et al. (1994) carried out an experiment on a shale sequence in the southern part of China and showed a qP-wave anisotropy of 12 percent. White et al. (1983) used three-component receivers and two sufficiently closely spaced boreholes to calculate the horizontal and vertical phase slowness components $\partial t/\partial x$ and $\partial t/\partial z$, respectively; from which the qP, qSV, and qSH phase velocities for various incidence angles have been calculated. The results of White et al. (1983) show that the horizontal qP-wave velocities were 10 to 20 percent larger than the vertical velocities.

1.5 The τ-p transformation

The modification of the τ-p transformation to the determination of velocity anisotropy in the geometry of a VSP experiment is one of the most important contributions in this thesis. An overview of the τ-p transformation and a brief review of some of its many applications in geophysics is necessary. Further, the rationale for employing the τ-p method over more conventional analyses is described.

A seismogram is a plot of the particle motions, or more usually, the particle's velocity or acceleration versus time in response to the passing of a seismic wave. A single seismogram, obtained at a given fixed position at the surface or within the earth yields a very limited amount of information. As a result, a seismogram record consists of numerous seismograms from a series of spatial positions x versus a common time base t. The changes in the times of arrival across the array of observation points yields information about the earth structure in terms of its material velocities. Consequently, both surface and borehole seismic data are generally analyzed in what is referred to as the offset-time (x-t) domain. Often, however, in this domain it is difficult, if not impossible, to segregate different seismic arrivals such as reflections and critical refractions from geologic interfaces in surface seismics, and downgoing and upcoming waves in a borehole experiment. In the intercept time-ray parameter domain (τ-p) these seismic events are mapped to different positions within the τ-p space where they are more easily separated and distinguishable.

The mathematical developments related to the τ-p mapping were introduced by Radon (1917); and the τ-p is a type of Radon transformation. The application of the τ-p to a series of seismic traces was introduced by Rieber (1936) who developed the concept of delay-and-add of seismic (analog) recordings. He used 10 equally spaced ground locations. Another term synonymous with τ-p, especially in the seismic exploration community, is the slant stack introduced by Claerbout (1975). The slant stack refers to the method used to compute the τ-p data, and consists of summing the amplitudes in the offset-time domain (Figure 1.1) along a straight line of slope p and intercept time τ. However, more than one method can be used to compute the τ-p map of a set of wave-forms, and I will outline three of them briefly) the x-t method that is used here, 2) the (x, f) method, and 3) the (k, f) method.

In the x-t slant stack method, each amplitude in the τ-p map is obtained by summing the amplitudes of the wave-forms in x-t space along a straight line of intercept time τ and slope p. The τ-p amplitudes are computed for all the ray parameters present in the acquired data. Details of this method will appear in later chapters.

The (x-f) method is based on the Fourier transforms of the wave-forms. The wave-forms are transformed to the Fourier domain and the coefficients for each frequency are grouped into a row vector. The summation over x in the x-t method becomes a multiplication of the coefficient row vector by a rectangular matrix that has a number of rows and columns equal to the number of wave-forms and number of p's, respectively. For each frequency a matrix multiplication is performed and the τ-p mapping is obtained by performing an inverse Fourier transform on the computed data.

The (f, k) method uses the projection-slice theorem (Wade and Gardner, 1988) which states that the amplitudes relative to each p in the τ-p domain are identical to those picked along a radial line of slope p in the 2-D Fourier transform of the x-t data.

The method used here, is the (*x-t*) slant-stack, which is the simplest, takes the fewest steps, and is the most commonly used method. I implemented the ratio filter (Moon et al., 1986) in the τ-p mapping to assure that the lines of slope p are tangent to the time curves, and the hyperbolic filter (Tatham, 1984) to attenuate the edge effects resulting from the band-limited data. The programs to carry out these calculations are included in the appendices.

The p-axis in the τ-p domain represents the ray parameter (horizontal component of the slowness) of a plane-wave passing through a medium, while the τ-axis represents the intercept time defined as the vertical-slowness-thickness aggregate of the layers through which the ray is traveling (Diebold and Stoffa, 1981). For a given ray path taken by a seismic wave through the earth (Figure 1.2), for each phase angle θ corresponding to a ray angle ϕ, and a phase velocity v corresponding to a ray velocity V, p remains constant and satisfies Snell's law;

$$p = \frac{\sin\theta_1}{v_1} = \frac{\sin\theta_2}{v_2} = \ldots = \frac{\sin\theta_i}{v_i} = \ldots = \frac{\sin\theta_n}{v_n},$$

As a result, the τ-p mapping of seismic data has the great advantage that a given seismic event is plotted according to its apparent horizontal slowness, p, and not according to its traveltime. This makes the τ-p domain useful for velocity determination.

Consider the traveltime curve for a wave generated by a source placed at the surface, propagated through an isotropic medium, reflected from a horizontal interface separating two media of different acoustic impedance, and finally recorded by a receiver placed at the surface. This traveltime curve is a hyperbola crossing the time axis at the two-way vertical traveltime (Figure 1.3b). This hyperbola maps in τ-p space to an ellipse that crosses the p-axis at 1/v, where v is the velocity of the medium, and the τ-axis at the two-way vertical traveltime. Additionally a line in offset-time space (Figure 1.3a) that could represent a head wave in this experiment maps to a point in the τ-p space.

Although the τ-p transform had been used to filter wellbore seismic arrivals (Moon et al., 1986), to our knowledge the work in this thesis is the first use of the transform for velocity determination in a VSP experiment. The combination of the τ-p analysis with the known depths of the detectors in the wellbore allows for a particularly simple, and powerful, analysis.

In the case of an offset VSP experiment where a receiver is placed in a borehole at a known depth and sources are placed on the surface along a line radiating from the wellbore, the common-receiver ray geometry is similar to that of a hypothetical reflector at the depth of the receiver. The only difference, however, is that for the VSP experiment the traveltime is half of what would be observed for a reflection (Figure 1.3). A downgoing-transmitted-wave traveltime curve for an offset VSP experiment for receivers placed within an isotropic medium is a hyperbola (Figure 1.3c). As explained in Chapter 2 this hyperbolic curve will map to an ellipse that crosses the p-axis at the reciprocal of the velocity of the medium (1/v), and the τ-axis at the one-way vertical traveltime.

Analysis of τ-p data is more complicated when the geology consists of a stack of layers with different velocities. The problem is that the reflection time curves are no longer hyperbolic. Conventionally, the interval velocities are inverted from the root-mean-square velocities using Dix's (1955) equation restricted to flat layers and small source-offset reflector-depth ratios. This method is extremely error-prone. As an alternative, Schultz (1982) suggested a layer-stripping technique in the τ-p domain to determine the interval velocities from a long-offset surface-to-surface seismic experiment. Schultz's method does not employ Dix's equation, and hence entails no restriction on the source-offset/reflector-depth ratio.

The τ-p method has been used beyond the velocity determination described here, for example, to migrate reflection seismic data (Shultz and Claerbout, 1978), and to attenuate multiple reflections (Hampson, 1986). In fact, the diffracted waves generated at a diffracting point in the subsurface propagate up to the receivers placed on the surface at various angles. If a medium is anisotropic the diffraction curve is not hyperbolic and an offset-dependent velocity function is required for proper migration of seismic events, especially those with large offsets.

With the development of three-component seismic data processing, shear waves are increasingly being used in reservoir characterization and lithology discrimination. Tatham and Stoffa (1982) and Robertson and Pritchett (1985) showed, using surface seismic data, that the ratio of the P-wave velocity to the S-wave velocity (VP/VS) is more sensitive to reservoir gas saturation than to the P-wave velocity. Unfortunately the segregation of the S-waves from the rest of the waves is a seismic seismogram in not trivial in the *x-t* domain. However, the shear waves which are characterized by relatively low velocities, map in the *τ-p* domain at large ray parameters, while the P-waves map in the low p-range. By selecting each of these 2 wave types in *τ-p* space and mapping them back to the offset-time domain, the S-waves and P-waves can be separated. Tatham (1984) suggested a hyperbolic filter that can be used in the forward *τ-p* mapping to transform only those seismic events that have velocities within a prescribed velocity range. Tatham applied his technique to separate the P-waves from the converted S-waves for a point-source experiment.

The *τ-p* mapping, often called plane-wave decomposition (Stoffa et al., 1981; Treitel et al., 1982) decomposes a non-plane-wave surface (Musgrave, 1970; Fedorov, 1968) into its component plane, or elementary, waves. Conversely, the wavefront is obtained by drawing the tangent curve to all the component plane-waves. Each ray parameter $p = \sin\theta/v$ corresponds to a plane-wave propagating at a phase angle θ with phase velocity v and passing through the source point at its activation time $t = 0$.

All of the above *τ-p* analyses assume that the earth is composed of thick isotropic layers. However, if the medium is elastically anisotropic the *x-t* curves of seismic events are more complicated, as are their counterparts in *τ-p* space. In particular, the elliptical curves produced for an isotropic earth will no longer be perfect ellipses if anisotropy is present.

Although developed independently, the present work was not the first to suggest that anisotropy could be measured in the τ-p domain. Hake (1986) made an attempt to model the slowness curves of an anisotropic layered medium from the τ-p curves of synthetic surface seismic data. Unfortunately, he was unable to solve for the vertical component of the slowness that requires knowledge of the layer thicknesses, which are not generally known a priori.

White et al. (1983), Gaiser (1990), Miller et al. (1994), and others also compute the vertical and horizontal slownesses ($\partial t/\partial x$, and $\partial t/\partial z$) by measuring the ratios $\Delta t/\Delta x$ and $\Delta t/\Delta z$.

Here, I propose a technique of slowness curve determination from the τ-p curves of downgoing transmitted waves in a multioffset, multidepth VSP experiment. In this case the depths, which are those of the detectors, are known very well and this knowledge greatly constrains the velocities determined.

As will be shown later, a final advantage of this method is that the phase, or plane-wave, velocities are directly determined. This differs from x-t analyses where the ray velocity is found. The phase velocities are useful in recovering the elastic constants of the stiffness matrix and may be converted to ray velocities without too much difficulty in the present method. These ray velocities are indicative of the actual energy flow or path taken by the seismic arrivals and are hence of more utility in tomographic analyses.

1.6 Outline of Thesis

This paper-format thesis consists of four papers produced directly by this research. These papers are chronologically ordered; the reader may note the progression of the analysis and evolution of our understanding of the problem with time. A brief overview of the contents of the thesis is given here.

Chapter 2, published in the Canadian Journal of Exploration Geophysicists (Schmitt and Kebaili, 1993), is the first description of the advantages of the τ-p method in delineating the velocity anisotropy from borehole vertical seismic profile experiments. The text of this chapter has been slightly modified from that published in order to reflect a better understanding of the method. The common receiver ray geometry in a surface-to-borehole seismic experiment is similar to that for reflected waves in a surface-to-surface experiment. Consequently, τ-p techniques used for reflection seismology, such as the τ-p layer-stripping technique suggested by Schultz (1982) to determine the interval velocities, are readily modified to borehole data sets. Shultz's equations are further modified to include anisotropy under the assumption that the velocity is nearly constant over relatively small ranges of incidence angles. The method successfully recovered velocities from calculated seismograms from an elliptically anisotropic half-space. Further, the modified layer stripping technique was able to determine the correct velocities in a more complex geology consisting of an isotropic layer overlaying an anisotropic half-space.

Chapter 3, published in Geophysicist (Kebaili and Schmitt, 1996), describes a case study of an application of the method described in chapter 2 to vertical seismic profile data acquired in a shallow borehole at the AOSTRA Underground Test Facility near Fort McMurray, Alberta. The geology at this site consists of horizontal layers of sands, shales, bituminous sands, and limestones and was an ideal location to test the method. The data acquisition and three-component processing strategies are described. In particular, the particle motions are used to enhance the downgoing directly transmitted arrivals necessary to the anisotropy analysis. Velocities are determined by two different, but complementary, measures of coherency in order to reduce uncertainty. Because certain intervals of the geology consist of rapidly alternating sand and shale layers of dimensions much less than the seismic wavelengths used, it was expected that velocity anisotropy would exceed that expected theoretically. These observations suggest that the layers themselves must be intrinsically anisotropic.

In chapters 2 and 3 the τ-p curves are locally fit by ellipses to determine the near-vertical and oblique velocities, and only a near-vertical and an oblique velocity are determined. Chapter 4, accepted for publication in Geophysics (Kebaili et al., 1996), describes a more mature method of slowness-curve determination from the τ-p curves. Specifically, it is shown that the velocity of a given interval, at any angle of incidence, may be found from simple subtraction of the τ-p curves obtained at the top and bottom of this layer. The theoretical aspects of the τ-p analysis are more fully developed. An important result is that the velocities determined by the method are phase, or plane-wave, velocities and not ray velocities. The relationship between the phase and ray velocities for a transversely isotropic medium is given. The method is tested on three synthetic examples a multilayered isotropic medium, an elliptically anisotropic half-space, for which both phase and ray velocity curves are recovered, and finally a transversely isotropic medium for which the qSV-wave and qP-wave phase slowness curves are determined. The improved method is applied to the same data set used in chapter 3 with the new result that the velocity variations with angle of incidence is determined over a more continuous range. This continuity of the phase velocities allows for an accurate calculation of the ray velocities.

Chapter 5, submitted to the Journal of the Acoustical Society of America (Kebaili and Schmitt, 1996), describes the application of the τ-p method to delineate ultrasonic velocities as a function of incidence angles for anisotropic specimens. Small damped transducers (0.2 x 0.2 cm) were used to generate and receive wave-forms. The transmitter-receiver geometry mimics a reverse vertical seismic profile. The method was tested on an isotropic sample (plexiglass), for which the slowness curve in the plane that contains sources and receivers was determined from the τ-p curves of common-transmitter wave-forms. The method was then applied to an orthorhombic specimen (phenolic). Three planes of symmetry and a diagonal plane of the phenolic sample were investigated. The phase-velocity functions for all four planes were computed, and the ray-velocity functions for the three planes of symmetry were derived from the phase velocities.

Table 1.1

Mineral	Symmetry	$[(V_{max} - V_{min})/V_{mean}]$x100%	
		P	S
Olivine	Orthorhombic	25	22
Garnet	Cubic	0.6	1.0
Orthopyroxene	Orthorhombic	16	16
Clinopyroxene	Monoclinic	21	20
Muscovite	Monoclinic	58	85
Orthoclase	Monoclinic	46	63
Anorthite	Triclinic	36	52
Rutite	Tetragonal	28	68
Nepheline	Hexagonal	24	32
Spinel	Cubic	12	68

References

Aki, K., and Richards, P. G., 1980: Quantitative seismology: theory and methods, Freeman W. H. and company.

Alford, R. M., 1986, Shear data in the presence of azimuthal anisotropy: Dilley, Texas, Paper presented at 56th Annual International meeting: Soc. of Explor. Geophys., Houston, Texas, 476-479.

Anderson, D. L., 1961, Elastic wave propagation in layered anisotropic media: J. Geophys. Res., **66**, 2953-2963.

Anderson, D. L., 1962, Love wave dispersion in heterogeneous anisotropic media: Geophysics, **27**, 445-454.

Anderson, D. L., 1966, Recent evidence concerning the structure and composition of the earth's mantle: Physics and Chemistry of the Earth, **6**, 1-131.

Anderson, D. L., Minster, B. J. and Cole, D., 1974, The effect of oriented cracks on seismic velocities, J. Geophys. Res., **79**, 4011-4015.

Ando, M., Ishikawa, Y. and Yamazaki, F., 1983, Shear wave polarization anisotropy in the upper mantle beneath Honshu, Japan: J. Geophys. Res., **10**, 5850-5864.

Backus, G. E., 1962, Long-wave elastic anisotropy produced by horizontal layering: J. Geophys. Res. **67**, 4427-4440.

Banik, N. C., 1984, Velocity anisotropy of shales and depth estimation in the North sea Basin, Geophysics, **49**, 1411-1419.

Berryman, J. G., 1979, Long-wave elastic anisotropy in transversely isotropic media: Geophysics, **44**, 896-917.

Brocher, T., M., and Christensen, N., I., 1990, Seismic anisotropy due to prefered mineral orientation observed in shallow crustal rocks in southern Alaska: Geology, **18**, 737-740.

Bush, I, and Crampin, S., 1987, Observations of EDA and PTL anisotropy in shear-wave VSPs, paper presented at 57th Annual International Meeting, Soc. of Explor. Geophys., New Orleans, L. A.

Chapman, C.H., and Pratt, R. G., 1992, Traveltime tomography in anisotropic media, -I. Theory: Geophys. J. Int., **109**, 1-19.

Christensen, N. I. and Salisbury, M. H., 1979, Seismic anisotropy in the upper mantle: Evidence from the Bay of Islands ophiolite complex: J. Geophys. Res., **84**, B9, 4601-4610.

Christensen, N. I. and S. Landquist, 1982, Pyroxene orientation within the upper mantle: Bull. Geol. Soc. Am., **93**, 279-288.

Claerbout, J. F., 1975, Slant stack and radial traces: SEP-5, 1-12.

Crampin, S., 1978, Seismic wave propagation through a cracked solid: polarization as a possible dilatancy diagnostic: Geophys. J. R. Astron. Soc., **53**, 467-496.

Crampin, S., and McGonigle, R., 1981, The variation of delays in stress-induced anisotropic polarization-anomalies: Geophys. J. R. Astr. Soc., **64**, 115-131.

Crampin, S., 1981, A review of wave motion in anisotropic and cracked elastic-media: Wave Motion, **3**, 343-391.

Crampin, S., 1987, Geologic and industrial implications of extensive-dilatancy anisotropy: Nature, **328**, 491-496.

Daley, P.F., and Hron, F., 1977, Reflection and transmission coefficients for transversely isotropic media: Bull. Seis. Soc. Am. **67**, 661-675.

Diebold, J. B., and Stoffa, P. L., 1981, The traveltime equation, tau-p mapping, and inversion of common midpoint data: Geophysics, **46**, 238-254.

Dix, C. H., 1955, Seismic velocities from surface measurements: Geophysics, **20**, 68-86.

Evans, K. F., Engelder, T., and Plumb, R. A., 1989, Appalachian stress study, 1, A detailed description of in-situ stress variations in Devonian shales of the Appalachian plateau: J. Geophys. Res., **94**, 7129-7154.

Fedorov, F. I., 1968, Theory of elastic waves in crystals, Plenum Press.

Freund, D., 1992, Ultrasonic compressional and shear velocities in dry clastic rocks as a function of porosity, clay content, and confining pressure: Geophys. J. Int., **108**, 125-135.

Gaiser, J.E., 1990, Transversely isotropic phase velocity analysis from slowness estimates: J. Geophys. Res. **95**, 11241-11254.

Gieske, J. M., and Allred, R. E., 1974, Elastic constants of B-Al composites by ultrasonic velocity measurements: Exp. Mech., **14**, 158-165.

Hake, H., 1986, Slant stacking and its significance for anisotropy: Geophysical Prospecting **34**, 595-608.

Hampson, D., 1986, Inverse velocity stacking for multiple elimination: Houston, 56th International SEG Meeting, (S6.7)

Harkrider, D. G. and Anderson, D. L., 1962, Computation of surface wave dispersion for multi-layered anisotropic media: Bull. Seis. Soc. Am., **52**, 321-332.

Hickman, S. H., Zoback, M. D., and Healy J. H., 1988, Continuation of a deep borehole stress measurement profile at Hi Vista, Mojave Desert, California: J. Geophys. Res., **93**, 15183-15195.

Jamison, D. H., and Cook, N. G., 1980, Note on measured values for the state of stress in the earth's crust: J. Geophys. Res., **85**, 1833-1838.

Johnston, D. H., 1986, VSP detection of fracture-induced velocity anisotropy, Paper presented at 56th Annual International meeting, Soc. of Explor. Geophys., Houston, Texas.

Johnston, J., E., and Christensen, N., I., 1995, Seismic ansotropy of shales: J. Geophys. Res., **100**, 5991-6003.

Kebaili, A., and Schmitt, D. R., 1996, Velocity anisotropy observed in wellbore seismic arrivals: Combined effects of intrinsic properties and layering: Geophysics, **61**, 12-20.

Larner, K., and Cohen, J., 1993, Migration error in transversely isotropic media with linear velocity variation in depth: Geophysics, **58**, 1454-1467.

Matsushima, S., 1960, On the deformation and fracture of granite under high confining pressure: Disaster Prevent. Res. Inst., Kyoto Univ. Bull., **36**, 11.

Miller, D. E., and Chapman, C. H., 1991, Incontrovertible evidence of anisotropy in crosswell data: 61st Ann. Internat. Mtg. Soc. Expl. Geophys., Expanded Abstracts, 825-828.

Miller, D. E., Leaney, S., and Borland, W. H., 1994, An in situ estimation of anisotropic elastic moduli for a submarine shale: Jour. Geophy. Res., (in press).

Moon, W., Carswell, A., Tang, R., Dillston, C., 1986, Radon transform wave field separation for vertical seismic profiling data: Geophysics, **51**, 940-947.

Musgrave, M., J., P., 1970: Crystal acoustics, Holden Day.

Nicholas, A., and Christensen, N. I., 1987, Formation of anisotropy in upper mantle peridotites - A review, in " Composition, Structure and Dynamics of the Geodyn. Sewr. AGU, **16**, 111-123.

Nur, A. and Simmons, G, 1969, Stress-induced velocity anisotropy in rock: an experimental study: J. Geophys. Res., **74**, 6667-6674.

Nur, A., 1971, Effects of stress on velocity anisotropy in rocks with cracks: J. Geophys. Res., **76**, 2022-2034.

O'Connell, R. J., and Budiansky B., 1974, Seismic velocities in dry and saturated cracked solids: J. Geophys. Res., **79**, 5412-5426.

Peacock, S. P., Crampin, S., Booth, D. C., and Fletcher, J. B., 1988, Shear wave splitting in the Anza seismic gap, southern California: J. Geophys. Res., **93**, 3339-3356.

Peselnick, L. A., Nicholas, A. and Stevenson, P. R., 1974, Velocity anisotropy in a mantle peridotite from Ivrea zone: application to upper mantle anisotropy, J. Geophys. Res., **79**, 1175-1182.

Postma, G. W., wave propagation in a stratified medium: Geophysics, **20**, 780-806, 1955.

Rabbel, W., 1994, Seismic anisotropy at the Continental Deep Drilling Site (Germany): Tectonophysics, **232**, 329-341.

Radon, J., 1917, "Uber die Bestimmung von Funktionen durch ihre Intergralwerte langs gewisser Mannigfaltigkeiten" Berichte Sachsische Acadamie der Wissenschaften, Leipzig, Math.-Phys. Kl., **69**, 262-267.

Rieber, F., 1936, A new reflection system with controlled directional sensitivity: Geophysics, **1**, 97-106.

Robertson, J. D., and Pritchett, W. C., 1985, Direct hydrocarbon detection using comparative P-wave and S-wave seismic sections: Geophysics, **50**, 383-393.

Rokhlin, S. I., and Wang, W., 1992, Double through-transmission bulk wave method for ultrasonic phase velocity measurement and determination of elastic constants of composite materials: J. Acoust. Soc. Am., **91**, 3303-3312.

Saito, H., 1991, Anisotropic traveltime tomography at the Buckhorn test facility in Illinois, Proc. 61st Ann. Internat. Mtg., Soc. Expl. Geophys., Exp. Abstr., **1**, 123-126.

Sayers, C. M., 1994, The elastic anisotropy of shales, J. Geophys. Res., **99**, 767-774.

Schmitt, D. R., and Kebaili, A., 1993, Velocity anisotropy estimation from slant stacks of wellbore seismics: Can. J. of Expl. Geophys., **29**, 236-245.

Schultz, P. S., 1982, A method for direct estimation of interval velocities: Geophysics **47**, 1657-1671.

Schultz, P. S., and Claerbout, J. F., 1978, Velocity estimation and downward continuation by wavefront synthesis: Geophysics, **43**, 691-714

Stoffa, P. L., Buhl, P., Diebold, J. B. and Wenzel, F., 1981, Direct mapping of seismic data to the domain of intercept time and ray parameter - A plane-wave decomposition: Geophysics **46**, 255-267.

Tatham, R. H., and Stoffa, P. L., 1982, VP/VS - a potential hydrocarbon indicator: Geophysics, **41**, 837-848.

Tatham, R. H., 1984, Multidimensional filtering of seismic data: Inst. Electr. and Electron. Eng., **72**, 10.

Tocher, D., 1957, Anisotropy in rocks under simple compressions: Trans. Am. Geophys. Union, **38**, 89.

Vernik, L., and Nur, A., 1992, Ultrasonic velocity and anisotropy of hydrocarbon source rocks: Geophysics, **57**, 727-735.

Wade, C. J., and Gardner, G. H. F., 1988, Slant-stack inversion by hyperbolae extraction in the Fourier domain: Expanded abstract, 58 th Annual SEG Meeting, (S1.6), 676 - 679.

Walsh, J. B., 1965, The effect of cracks on the compressibility of rocks, J. Geophy. Res., **70**, 381.

White, J. E., Martineau-Nicoletis, L. and Monash, C., 1983, Measured anisotropy in Pierre shale: Geophysical Prospecting **31**, 709-725.

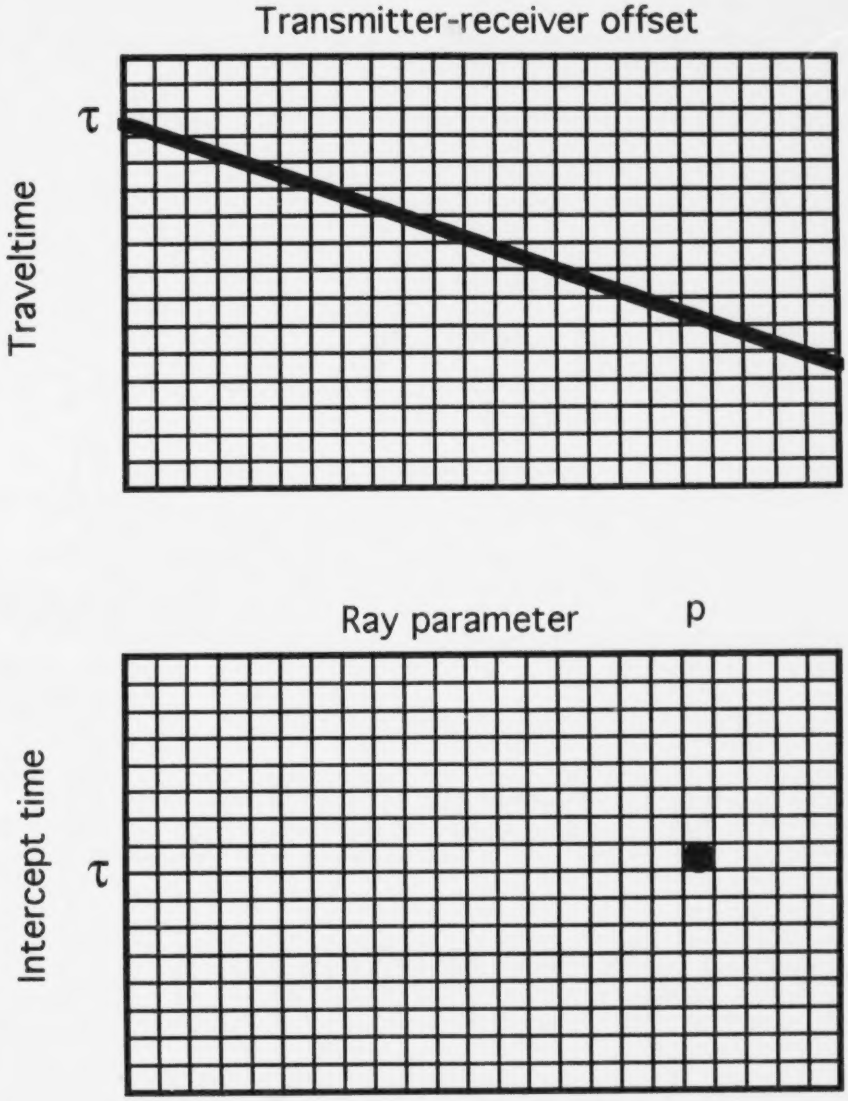
Transmitter-receiver offset
τ
Traveltime
Ray parameter
p
Intercept time
τ

Figure 1.1. Slant stack procedure. The amplitudes in offset-time space on a line of slope p and y-intercept τ are stacked to give the amplitude in τ-p space of x and y coordinates p and τ, respectively.

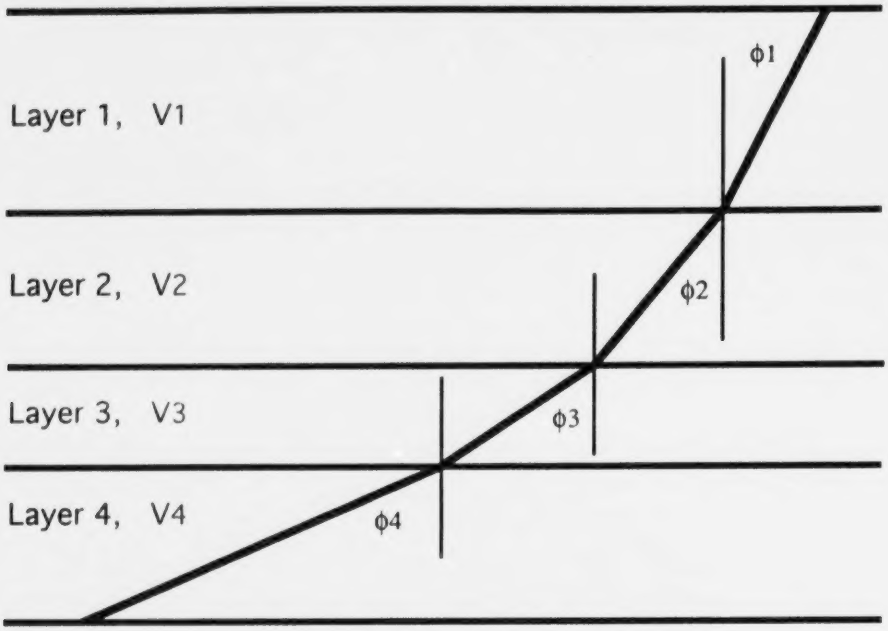
ϕ1
Layer 1, V1
Layer 2, V2
ϕ2
Layer 3, V3
ϕ3
Layer 4, V4
ϕ4

Figure 1.2. Ray tracing through a layered medium. Snell's law states that $\sin\theta_1/v_1 = \sin\theta_2/v_2 = \sin\theta_3/v_3 = \sin\theta_4/v_4 =$ constant $= p$, where p is the horizontal component of the phase slowness, v is the phase velocity that corresponds to the ray velocity V, and θ is the phase angle that corresponds to the ray angle ϕ.

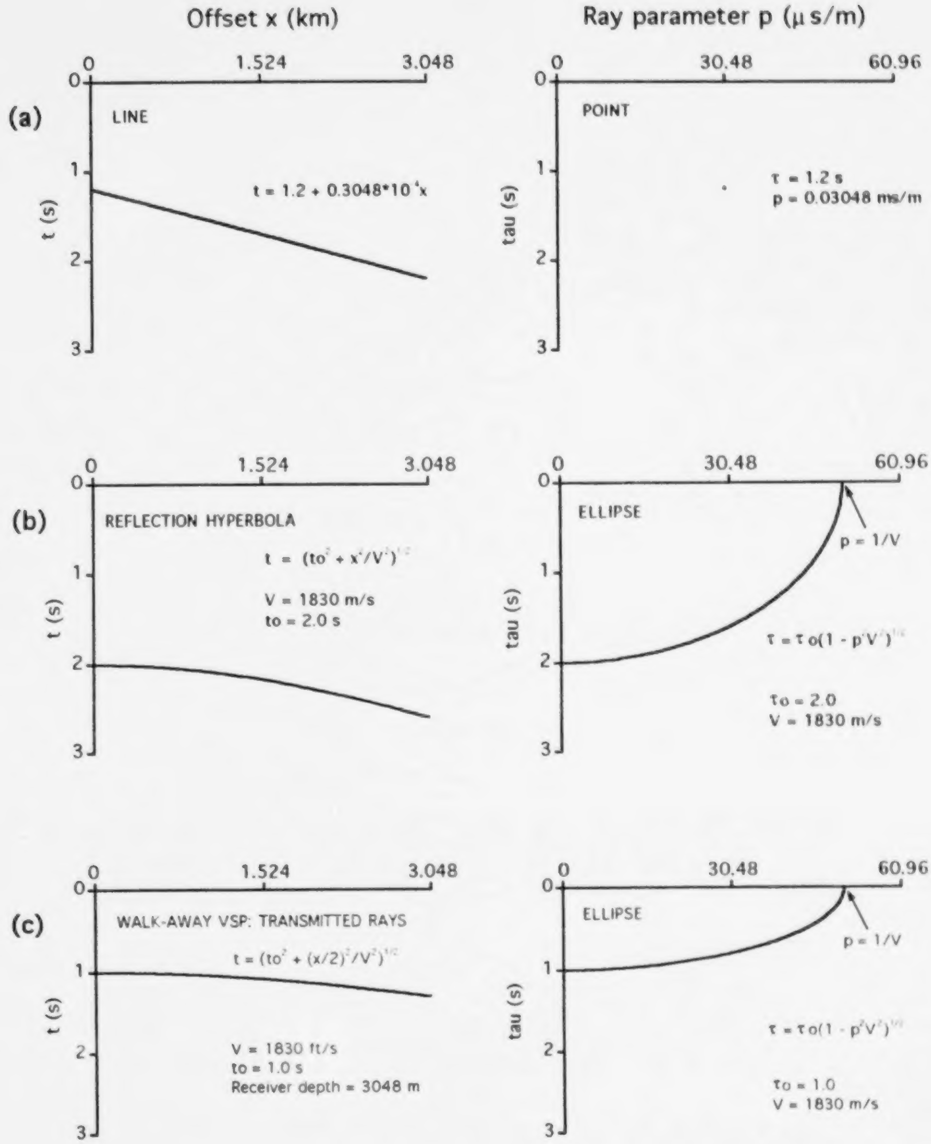

Figure 1.3. Forward and inverse τ-p transforms of hypothetical seismic events. (a) A line in the X-T space maps to a point in the τ-p space, and vice versa. Note that a point in the X-T space maps to a line in the τ-p space. (b) a reflection hyperbola maps to an ellipse (after Thatham, 1984). (c) A walk-away VSP transmitted ray hyperbola in X-T space maps to an ellipse. Note that the τ-p ellipses in (b) and (c) have the same horizontal semi-axes ($1/v$), but different vertical semi-axes (*two*-way, and *one*-way vertical traveltime, respectively).

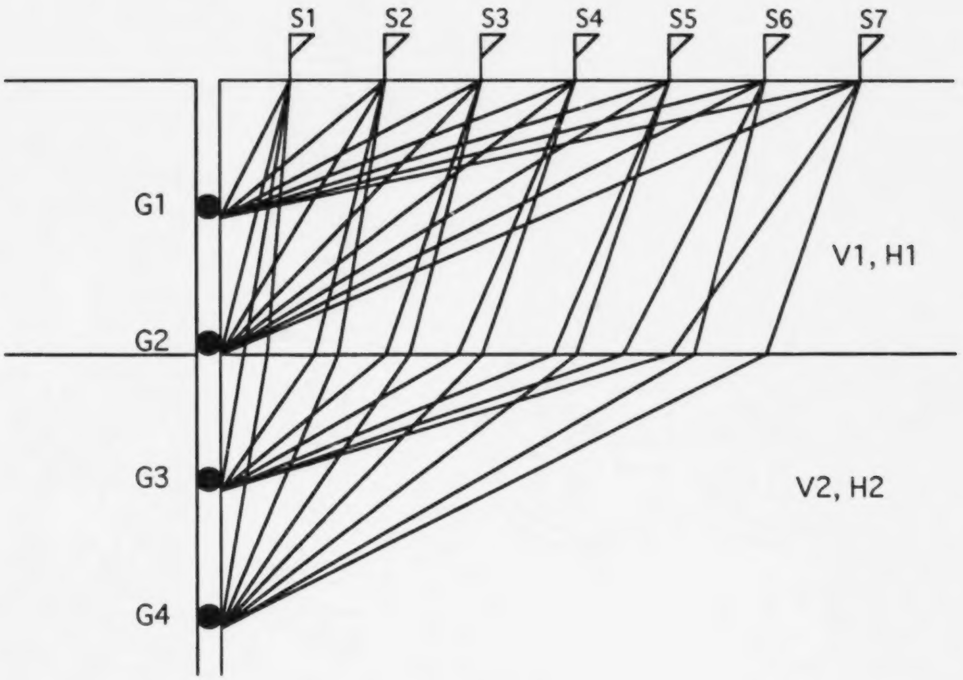
S1
S2
S3
S4
S5
S6
S7
G1
G2
G3
G4
V1, H1
V2, H2

Figure 1.4. Geometry of surface-to-borehole seismic experiment in isotropic layers showing ray paths from surface sources S1, S2, S3,..., and S7 to receivers G1 through G4.

Chapter 2

2. Velocity Anisotropy Estimation From Slant Stacks of Wellbore Seismics

2.1 Introduction

In seismic analyses, the subsurface is often assumed to consist of a series of distinct and elastically isotropic layers. Within such layers the magnitudes of the velocities of elastic waves are independent of the direction of propagation. This assumption has served well in mappings of the gross structure of the earth and in reflection profiling of the crust. However, it has long been recognized that elastic anisotropy is intrinsic to the structure of most rock and, further, seismic theory indicates that a series of thin layers are effectively anisotropic to seismic energy with a large wavelength relative to thicknesses of the layers. In these latter cases, the magnitude of the velocity varies with the direction of propagation. Ignoring these anisotropic effects can adversely influence those analyses that rely on the spatial tracking of the ray paths.

In particular, much of the current interest in seismic anisotropy is motivated by the requirements of various seismic imaging techniques. For example, since the elastic anisotropy of rock controls the ray paths of seismic waves through the earth anisotropy directly affects the accuracy in tomographic imaging (Chapman and Pratt, 1992; Saito, 1991). Additionally, much work has focused on using the variations in wavelet amplitudes with angles of reflection from an interface as a material property diagnostic; these analyses are usually based on the isotropic formulations (e.g. Young and Braile, 1976) but if elastic anisotropy is included, the effects are substantially changed (e.g., Daley and Hron, 1977; Pellisier et al., 1991; Samec and Blangy, 1992). Perhaps of the most practical importance, however, is the realization that erroneous reflector depths will be calculated if anisotropy is not accounted for when determining normal moveout velocities (Banik, 1984; Winterstein, 1986).

Much recent field work has focused on shear waves and their birefringence as observed from recordings in wellbores (e.g., Galperina and Galperin, 1987; Winterstein and Meadows, 1991a, 1991b) but our present study will examine only the first arrivals associated with directly transmitted quasi-compressional waves (qP). The layer stripping techniques described do not preclude analysis of the quasi-shear wave arrivals. Indeed, the direction-dependent slownesses of these modes are substantially more complex and provide useful diagnostic information on the in-situ material properties. However, the unambiguous determination of these arrivals is often difficult as they are often obscured by the coda of the preceding qP arrival.

A number of field measurements of the subsurface seismic anisotropy have been reported in the last four decades. Jolly (1956) measured the traveltimes from surface sources offset as much as 180 m from a wellbore with geophones at depths to 113 m. He suggested on the basis of his traveltime observations that the vertical and horizontal velocities differed by as much as 12%. Levin (1979) used Backus's (1962) formulations and a layered geology of interleaving gypsum and weathered material to simulate Jolly's tests. Levin indicated that a much higher anisotropy would not be untenable or in disagreement with the observations.

Vander Stoep (1966) derived anisotropy factors, *A*, equal to the ratio of the horizontal to vertical velocities, for qP waves by comparing sonic well-log velocities to those obtained from oblique seismic waves propagating down to borehole receivers. In New Mexico, he found $A^2 = 1.077$ and 1.00 in a shale and a salt, respectively. Note that this analysis does not take into account the frequency dispersion. In Texas, Vander Stoep found a small $A^2 = 1.03$ on average which he considered to have negligible effect on the analysis of near-offset reflection seismics. The author also demonstrated, however, that this simple anisotropy factor analysis, that assumed that the incidence-angle-velocity relation was elliptical, was not sufficiently complex to describe the traveltime behavior at far offsets, where the proper theory for a transversely isotropic medium should be used.

White et al. (1983) derive the elastic coefficients for a transversely isotropic medium by finding phase velocities from time differences observed for qP, qSV, and qSH phases from three-component recordings in a pair of closely spaced boreholes. They found in a shale that qP velocities of vertically propagating waves were in general 10% to 20% less than the horizontal velocities. White et al. (1983) also determined the particle motions from the polarizations of the vertical and in-line receiver components of the first arrivals. The phase velocity directions were found from the horizontal and vertical traveltimes between adjacent receivers in the two wells. Because their technique measured the phase velocities, comparison of the observed polarizations with the wave propagation direction is meaningful in theory (Crampin, 1981). In practice, the large relative experimental uncertainties in the polarizations did not allow further delineation of the anisotropy. De Parscau (1991) indicates use of this knowledge may be necessary to accurately define anisotropy parameters.

Gaiser (1990) developed a technique to extract transversely isotropic phase velocities from a vertical seismic profile consisting of six in-line offsets and over 50 receiver depths. His method is, to a degree, similar to that of White et al. (1983) in that vertical and horizontal slownesses are found and used to calculate phase-velocity magnitudes and directions. Since horizontal slowness, p, in particular, will be influenced by variations in the surface properties between adjacent surface source points, the method must assume that the medium is laterally homogeneous. Gaiser observed strong variations in the TI velocities, which apparently correlated with lithology; specifically qP velocity anisotropies increased from 6% to 20% with increased concentration of calcareous and clay materials.

Winterstein and Paulsson (1990) conducted VSP and cross-well experiments in an unconsolidated shale. They calculated the five elastic coefficients required for a transversely isotropic medium from arrival times for all three modes in their crosswell data set. Perhaps somewhat unexpectedly, these coefficients suggested that the shale could be considered isotropic and that the crosswell traveltimes were explained well by a linear increase of velocity with depth.

The above methods were capable of demonstrating that the subsurface was anisotropic. However, the method of Vander Stoep (1966) has the disadvantage that it relies on sonic log velocities which, because of frequency dispersion effects, typically differ from seismic velocities by approximately 5%. This error could adversely affect the determination of the true anisotropy which in many cases is of the same scale. Other methods such as those of White et al. (1983) and Gaiser (1990) determine phase velocities under the assumption that planar wavefronts pass the receivers. The technique of White et al. (1983) is also limited by the fact that two closely spaced boreholes are required for the experiment.

In the present chapter, a method is developed that provides the ray velocity dependence on propagation angle within a given layer between two receiver depths in a single vertical borehole. The advantage of such a technique is that the results could be incorporated into far-offset reflection profiling or traveltime tomography. The analysis exploits the τ-p domain representation of traces collected at a common depth to determine the variations of the velocity over a given depth range. The technique requires no major *a priori* assumptions about the anisotropy. In the following development, a well known layer-stripping technique (Schultz, 1982) is first adapted to the geometry of a vertical seismic profile. These resultant formulas for the τ-p locus of a given set of arrivals at a common depth are modified to include anisotropy. Finally the layer stripping strategy is tested on two seismic traveltime models consisting of anisotropic layered structures. The present results will be useful for the analysis of large data sets consisting of multiple depths and offsets from a borehole. These types of observations are becoming more practical given the recent developments in downhole source technologies applied to a reverse vertical seismic profile geometry.

2.2 Velocity Recovery in The τ-p Domain

The τ-p representation of seismic data has long been employed to determine the radial structure of the earth by approaches based on the Wiechert-Herglotz method (Bullen, 1963; Gerver and Markushevich, 1966). As regards a surface reflection profile, Diebold and Stoffa (1981) derived the following formula for the traveltimes, t, of reflected or refracted rays produced and observed at the surface and propagating through a laterally homogeneous and flat-lying layered structure of elastically isotropic materials:

$$t = px + \sum_{j=1}^{n} q_j z_j \tag{2.1}$$

where z_j is the layer thickness and x is the surface offset between the source and receiver. The horizontal and vertical slownesses for a given ray are

$$p = \frac{\sin i_o}{V_1} \quad \text{and} \quad q_j = \frac{\cos i_j}{V_j} \tag{2.2}$$

respectively, where V_1 is the velocity of the topmost layer, i_o is the take-off angle with respect to vertical of the particular ray leaving the source, i_j is the subsequent angle of the ray transmitted into layer j, and V_j is the isotropic velocity of layer j. By a corollary of Snell's law, the horizontal slowness, or ray parameter, p remains constant over the entire length of the ray path. As noted by Diebold and Stoffa (1981), equation (2.1) describes a line of slope p with intercept

$$\tau = 2\sum_{j=1}^{n} q_j z_j \tag{2.3}$$

dependent only on the changing vertical slownesses and layer thicknesses. Equation (2.3) allows the contribution of a single layer to be written as

$$\Delta\tau_j = 2q_j z_j = 2z_j(u_j^2 - p^2)^{1/2} \tag{2.4}$$

where $u_j^2 = p^2 + q_j^2$ defines the magnitude of the slowness within layer j. The locus of equation (2.4) is an ellipse in the τ-p domain with semi-axes of lengths $2z_j u_j$, corresponding to the two-way vertical traveltime in the layer, and u_j corresponding to the horizontal slowness of the layer for i_j=90°.

For a series of flat-lying and elastically isotropic layers, the traveltimes of the precritical and postcritical reflections, and the critical refraction from the bottom of each layer all fall on the ellipse in the τ-p domain defined by equation (2.4). Note, however, that rays turned by deeper layers map as ellipses distorted by the $\tau(p)$ contributions of shallower layers. A characteristic of this mapping is that the endpoint of the τ-p distorted ellipse for a next lower layer intersect that of the previous layer at the p corresponding to a critically reflected ray in the former layer. Further, critically reflected rays map into a point on the ellipse because their traveltimes have a linear moveout in the x-t domain. The next lower distorted ellipse intersects at this point due to the asymptotic convergence of the traveltimes of the far offset reflections from the next lower interface to those of the critical reflection.

Numerous techniques exist to derive velocity structure from the τ-p domain representation of seismic data sets (see papers in Gardner and Lu, 1991). Schultz (1982), among others, exploits the assumed isotropy and consequent ellipticity of equation (2.8) to derive both isotropic velocities and layer thicknesses from common midpoint reflection data. His interactive method essentially consists of first finding the uppermost τ-p ellipse representing arrivals from the surface layer. An appropriate ellipse is fit, usually by some measure of coherency, to the τ-p curve to provide both the velocity and thickness of this top layer via equation (2.4). With this knowledge, the τ contribution of the surface layer may then be accounted by increasing all τ values at a given p by $\Delta\tau_1(p)$. This flattens the first ellipse and corrects the next lower distorted τ-p locus to an elliptical shape. This procedure is interactively repeated to provide the velocity and thickness of the subsequent layers. Because the τ contributions, and hence the effects of each layer, are successively removed, the technique is referred to as layer stripping; it will be adapted to the case of anisotropy below.

2.3 The τ-p Mapping For Directly Transmitted Arrivals in a Borehole

Moon et al (1986) have discussed separation of upgoing and downgoing wavefields in a vertical seismic profile using the τ-p domain. In the present study, the geometry consists of a series of sources on the surface that radiate outwards along a line from the axis of the vertical borehole with receivers spaced at known depths (Figure 2.1a). Otherwise, the medium remains the same stack of isotropic layers. In this geometry the traveltime T for a wave propagating from a source that is offset a distance X from the borehole to a receiver at a given depth is

$$T = pX + \sum_{j=1}^{n} q_j z_j \tag{2.5}$$

where it is understood that z_n is the depth difference between the last receiver and the immediately shallower interface. Equation (2.5) scales to equation (2.1) by a factor of 0.5 since this geometry is only half that required when both the source and receiver are on the surface. However, the observations under equation (2.1) are constrained to only those rays returning from the interfaces between the layers, whereas equation (2.5) applies to any arbitrary depth within the borehole. In a manner similar to Diebold and Stoffa's (1981) common midpoint analysis we can write

$$\tau = \sum_{j=1}^{n} q_j z_j \tag{2.6}$$

whereupon the layer contribution becomes

$$\Delta\tau_j = q_j z_j = z_j(u_j^2 - p^2)^{1/2} \tag{2.7}$$

which is rewritten as

$$\frac{\Delta\tau_j^2}{u_j^2 z_j^2} + \frac{p^2}{u_j^2} = 1 \tag{2.8}$$

As equation (2.4), equation (2.8) describes an ellipse in the τ-p domain but with a semi-major axis equal to the one-way vertical traveltime through the layer. Otherwise, the other semi-major axis remains equal to the layer slowness (Figure 2.1a).

2.4 Phase And Ray Velocities in Anisotropic Media

Before generalizing the above to consider anisotropic layers, it is first important to carefully define what would be measured in a borehole experiment; a brief review of the propagation of elastic waves in anisotropic layers is necessary.

In the bulk of the literature, velocities in anisotropic media are first introduced from the perspective that the material's complete set of elastic coefficients is known. With this knowledge, one may calculate the phase velocity or, alternatively, the phase slowness vector **s** of a plane-wave propagating through the medium in a specified direction with respect to the elastic coefficient tensor. Calculation of the magnitudes of **s** and the corresponding particle motions for the three different propagation modes possible need not be presented here but is found in many texts (e.g. Musgrave, 1970; Fedorov, 1968; Beltzer, 1988) and reviews (e.g, Crampin, 1981). These calculated slownesses may be mapped with respect to the direction of propagation within the material to provide the phase velocity slowness surface, S, which is also called the refraction surface by Fedorov (1968). The distance from the origin in slowness space to any point on S is equal to the magnitude of **s** in that direction in the material. In an isotropic medium, three concentric and spherical slowness surfaces exist and correspond to one compressional and two shear modes that are possible; because the velocities of both shear waves are the same for this case, two of the spheres coincide (Aki and Richards, 1980). In a perfectly elastic isotropic medium the phase velocity and the ray velocity, defining the speed of energy propagation within the medium, have the same direction and magnitude.

In an anisotropic medium, however, the three phase-slowness surfaces are nonspherical and generally not coincident. Figure 2.2a shows the two-dimensional trace of an imaginary slowness surface within a quadrant of a slowness plane for an anisotropic material. In this projection $\mathbf{s} = \mathbf{s}(\theta)$ where θ is the angle that **s** makes with the vertical; a plane-wave propagating through the medium in the direction specified by θ has a speed $1/|\mathbf{s}|$.

Alternatively, this variation of velocities with incidence angle is described by the shape of the wavefront at any given instant, and Fedorov (1968) refers to the wavefront positions at unit time as the wave surface W. The wave surface is more physically meaningful in that it is a scaled version of instantaneous positions of arrival of the actual disturbance, that is the set of points in space which begin to oscillate at the same time. It is the arrival of this energy of oscillation which is detected in a seismic experiment.

Fedorov (1968) describes how W may be constructed if S is known and vice versa. Figure 2.2b shows the wavefront produced by a point source in the anisotropic medium of Figure 2.2a. Construction of the wavefront requires that the normal $\mathbf{n}(\theta)$ to S at the endpoint of $\mathbf{s}(\theta)$ is in the same direction ϕ as $\mathbf{x}$ (Aki and Richards, 1980) the endpoint of which must fall on the plane-wavefront B-B' that has propagated distance **X** at unit time T. W may most easily be determined graphically, provided the derivative of the slowness surface *S* is easily determinable (Crampin, 1981); this is not necessarily the case for certain quasi-shear mode slownesses that can contain sharp cusps. Direct analytic relations between *W* and the elastic coefficients exist but are difficult to solve (Fedorov, 1968).

The direction of the phase velocity $\mathbf{v} = \mathbf{X}(\theta)/T$ will lie parallel to the normal to the wavefront. As a consequence, point A' in X-Z space corresponds to point A in slowness space. This is an important point because θ and ϕ can differ by 20° or more (e.g. Crampin, 1981). The wavefront defines the arrival of energy from a point source. Consequently, in a homogeneous anisotropic medium, the ray velocity will be given by $\mathbf{u}(\phi) = \mathbf{x}(\phi)/T$ and is a function of the ray direction within the medium (Robertson and Corrigan, 1983; Hake, 1986). An observer within an anisotropic half-space must see an arrival from a point on the surface as traveling along the line from the source to the observer in accordance with Fermat's principle of minimum traveltime. Hence this observer, knowing both his position relative to the seismic source and the traveltime would necessarily determine the magnitude and direction of the ray velocity **u**, not that of the phase velocity. It is this ray velocity, dependent on the actual path taken by the energy flow through the medium, which is crucial to many imaging procedures. However, the present analysis determines the phase velocity.

The present analysis consequently differs from those of White et al. (1983) and Gaiser (1990) who found phase velocities by determining slownesses on the basis of traveltime differences between adjacent detectors. Implicit to their analysis is the assumption that the adjacent receivers are closely enough spaced such that there is negligible curvature of the wavefront between the receivers; that is, from the receiver positions the wavefront appears planar. At point A' in figure 2.2. (b), the equivalent plane-wave is tangent to W and, as noted above, the phase slowness direction **s** is normal to this plane. The advantage of these methods is that one presumably measures directly the phase velocities which in turn may be used to constrain the subsurface elastic coefficients. Such information can be an important diagnostic of the material properties useful for interpretive purposes. Otherwise, in the present study $\mathbf{s}(\theta)$ must be determined indirectly from $\mathbf{u}(\phi)$.

One caveat on the above discussion is that it is assumed that the vertical source-receiver plane also contains the slowness vectors. However, in a layered anisotropic structure this restriction is not necessary; that is, the planes containing the slowness vectors and the source-receiver pair need not coincide. This is not important for the simple case of an anisotropic half-space where the rays travel along straight lines and the shortest directly transmitted traveltime must follow the direct line between the source and the receiver (e.g., Robertson and Corrigan, 1983). For observations below the first layer in a stack of anisotropic layers, however, the first arriving ray does not necessarily remain within the source receiver plane. In this case, the ray velocities found will only be apparent ray velocities under the assumption that they are contained within the sagittal plane.

In the present study, which relies on the analysis of the direct arrivals from the surface source to the borehole receiver, the τ-p analysis assumes that all the rays are contained within the vertical source-receiver plane. The above discussion demonstrates that this may not, in general, be the true case as often the ray paths taken by the energy flow are allowed to leave this plane and hence the velocities determined would necessarily be apparent velocities. Such effects could become problematic in tomographic imaging. If, however, the source-receiver plane coincides with a plane of symmetry of the material then the rays remain within the plane and the analysis is valid. At present, we do not know the magnitude of the errors that would be introduced by the out-of-plane ray paths in the more general case but assume, for the present, that these effects will be small for a weakly anisotropic medium.

2.5 Anisotropy in The Borehole Case

In the case of anisotropic layers and assuming that the vertical source-receiver and the sagittal planes are the same, then the $\Delta\tau$ contribution of each layer becomes, in analogy to equation (2.7),

$$\Delta\tau_j = q_j(p)z_j = z_j(u_j^2(p) - p^2)^{1/2} \tag{2.9}$$

or

$$\frac{\Delta\tau_j^2}{u(p)_j^2 z_j^2} + \frac{p^2}{u(p)_j^2} = 1 \tag{2.10}$$

after Hake (1986). The only difference between equations (2.7) and (2.9) is that u_i becomes essentially a function of the angle θ through the medium. Note that Snell's law

$$\frac{\sin\theta_i}{v_i(\theta_i)} = \frac{\sin\theta_{i+1}}{v_{i+1}(\theta_{i+1})} = p \tag{2.11}$$

remains valid for this case of anisotropy. Equivalently, the ray parameter p remains constant for anisotropic layers over the length of the ray path taken. Because $u_i(\theta)$ will not necessarily take on a simple form, the locus of equation (2.10) in the τ-p domain will not be an ellipse but some other more complex curve, which may be difficult to describe analytically.

The loss of the elliptical τ-p locus for the anisotropic case in equation (2.9), however, eliminates a crucial constraint for recovery of these parameters, and as noted by Hake (1986) they cannot be determined for layers of arbitrary anisotropy unless the depths to the reflectors or the layer thicknesses are known *a priori*. This problem can be overcome in the analysis of common-midpoint reflection profiles if one assumes a simple form for $\mathbf{u}(\theta)$ such as elliptical (e.g. Levin, 1978). However, great care must be exercised in using this assumption, as slowness surfaces have elliptical forms only for a few specialized cases not normally found in nature (e.g. Krey and Helbig, 1956; Helbig, 1983).

If the depths are known, however, then equation (2.9) suggests that $q_j(\theta)$ may be directly calculated from the observed $\Delta\tau(p)$; this fact is a great advantage for traveltime observations in a borehole where the receiver depths are unambiguous.

In theory, one could derive $\mathbf{u}(\theta)$ by simple application of equation (2.9) through a layer stripping approach. One problem with this method, however, is that calculation from the observed τ-p curves on a point-by-point basis could be subject to random fluctuations resulting from noise within the original data, and the advantages of averaging over a τ-p arrival locus are lost. In order to maintain this benefit, the assumption is made that $\mathbf{u}(\theta)$ changes little over sufficiently small ranges of θ. Under these circumstances, the τ-p locus over limited ranges of p will be nearly elliptical allowing use of a coherency measure, piecewise in p and subject to the constraint that the depth is known, to determine $\mathbf{u}(p)$ by layer stripping in an approach similar to that of Schultz (1982). This approach is tested on two calculated models below.

2.6 Test of The Method on Calculated Seismic Models

The above technique is illustrated by the analysis of two seismic forward models both incorporating anisotropic layers.

2.6.1 Model 1: Anisotropic half-space

The first model consists of an anisotropic half-space [Figure 2.3. (a)] with a borehole receiver at an arbitrary depth z and characterized by a hypothetical elliptical P-wave velocity function which increases from a horizontal value of 2000 m/s to 2500 m/s in the vertical direction, as shown in Figure 2.3b. This corresponds to a difference of 25% which is typical of the compressional-wave anisotropy seen in many shales in both the laboratory (Vernik and Nur, 1992) and the field (White et al., 1983). As noted above, compressional-wave slownesses will only rarely have the elliptical form of Figure 2.3b but the velocity function used is only for purposes of illustration, as equation (2.9) will apply to any arbitrary velocity relation. The purpose of this simple model is first to determine whether the piecewise p analysis is sensitive to the directional variations of the velocity.

Figure 2.4a is a set of seismic traces observed at a depth of 50 m in this half-space in Figure 2.3. These traces are the convolution of a Ricker wavelet with the traveltimes from surface sources, at offsets up to 300 m to the receiver at depth. This model does not consider loss of amplitude via geometrical spreading of the wavefront as could be determined from the formulations of Cerveny´ (1972).

These seismic traces, displayed in a common-depth gather, are transformed to the τ-p domain shown in Figure 2.4b by summation along lines of constant moveout in the X-T domain (e.g., Chapman, 1978; Clayton and McMechan, 980). Note that amplitudes (τ-p) within this slant stack have been equalized with respect to p in order to enhance the direct arrival curve. Otherwise the energy in the raw τ-p curve is shifted to higher p values as a consequence of the constant source interval used which has the consequence that the ray path density per unit ray parameter is higher for far offsets; it is this enhanced τ-p relation that was actually used in the velocity analysis.

Two complementary coherency measures are applied to extract the p-dependent velocity from the τ-p curve of Figure 2.4b by piecewise fitting of ellipses described above. The first measure is a windowed semblance M (Taner and Koehler (1969))

$$M(u,\tau) = \frac{1}{n} \frac{\sum_{\tau} \left(\sum_{k=1}^{n} a_{k,\,\tau(k)} \right)^2}{\sum_{\tau} \sum_{k=1}^{n} a^2_{k,\tau(k)}} \qquad (2.12)$$

where k is the index representing the n discrete values of p_k used in the piecewise analysis. $\tau(k)$ represents the point in τ-p space at p_k along a trial ellipse calculated with velocity $\mathbf{u}$ and intercept τ from equation (2.8). The summation further proceeds over a specified τ

window that follows the locus of the trial ellipse. The values of $\mathbf{u}$ and τ that best describe the data are found where M has maximum magnitude. An advantage of the semblance is that its magnitude is independent of the arrival amplitudes (Stoffa et al., 1981) but has the disadvantage that low-noise, narrow time windows are often required for good resolution. To alleviate this problem, the energy E given by:

$$E(u,\tau) = \frac{1}{n}\sum_{\tau}\sum_{k=1}^{n} a^{2}_{k,\tau(k)} \tag{2.13}$$

is used to complement the analysis, because E more easily separates those events also of high coherency but low energy, such as secondary lobes, from those of both high energy and high coherency which contain the necessary information. The values of $\mathbf{u}$ and τ which best describe the data are found where $S(\mathbf{u},\tau)$ and $E(\mathbf{u},\tau)$ have maximum magnitude.

Since I have assumed that the material is approximately isotropic over small ranges of p, then the τ that is determined must be the product of $\mathbf{u}$ and of the layer thickness which is known in the borehole experiment via equation (2.7) . This added constraint is useful as a check on the determined values and also aids in the refinement of the p and τ windows used to find S and E.

Figure 2.5 compares the p-dependent velocities recovered with the original input velocities of the model versus p, or equivalently θ. The τ window used in equations (2.11) and (2.12) is 20 ms (or 21 samples) and the p window varies from 0.25 ms/m for small ray parameters to 0.07 ms/m for large ray parameters. In general, the velocity recovery for this simple half-space model is quite good as the recovered differ from the input velocities by less than 1%.

2.6.2 Model 2: Isotropic layer over anisotropic half-space

Figure 2.6a shows the second simple model consisting of an isotropic layer of 50 m thickness underlain by an anisotropic half-space characterized by the velocity relation of Figure 2.6b. Receivers are placed at the bottom of the layer and within the half-space at a depth of 100 ms. This geometry was selected to determine whether the technique could successfully retrieve the velocity in the half-space after the effects of an upper layer were removed by layer stripping.

The *X-T* common depth gather for the receiver in the half-space is not shown; however these traces again were determined by convolving a spike at the ray traveltime, calculated using Snell's law, with a 50-Hz Ricker wavelet. Again, no corrections were made for geometrical spreading or reflection-transmission coefficients (Daley and Hron, 1977). The corresponding slant stack is shown in Figure 2.7. Note that this τ-p curve is distorted by the τ contribution of the top layer (shown only as a dark line for clarity) which must be first removed.

The velocities recovered in the half-space are shown in Figure 2.8. and again, except for the highest p data point, agree with those input to the model to an accuracy better than 1% . This may be related to the fact that the ray density increases with p. Otherwise, the relatively good agreement at lower ray parameters suggests that the analysis, which is piecewise in p, shows potential for extracting the variations in velocities with incidence angle within the subsurface layers.

2.7 Conclusion

Analysis of borehole seismic arrivals in the τ-p domain can provide a measure of the degree of seismic velocity anisotropy within a vertical plane containing multiple borehole receivers and multiple-offset surface sources. The technique developed exploits the known depth of the receivers to provide an important constraint on the vertical traveltime, τ_o, which must be satisfied by the incidence-angle-dependent velocities determined. Another advantage of the technique is that no assumptions as to the shape of the entire ray slowness-curve within the plane need be made. That is, the technique is able to discriminate velocity variations as a function of incidence angle, or equivalently ray parameter p, within the layer alone. When applied to simple seismic forward models which incorporate velocity anisotropy, recovered velocities differ by those input to the model by less than 1%.

The models used above are, admittedly, deficient in a number of areas. Most crucial, perhaps is that they have not taken into account the amplitude decay resulting from geometrical spreading and energy partitioning at interfaces. Further, the calculated seismic traces were free of random and coherent noise which could have a deleterious effect on the analysis especially for low signal-to-noise ratios.

Other issues relate to the geometry of the structures which are being studied. The present analysis assumes flat layers but dipping beds are more general and even slight dips have been shown to substantially affect traveltimes and subsequent τ-p representations (Hake, 1986; Diebold and Stoffa, 1981). Since the present method relies on the accurate measurement of traveltimes, the influence of surface static corrections is also important since the ray parameter of a given ray is defined by the take-off angle of that ray within the topmost layer (Gaiser, 1990). Recent findings which suggest that the weathered layer is also highly anisotropic constitute an added complication. Finally, as with all analysis that purports to measure the anisotropy of the subsurface, determining whether the observed perturbations from isotropy to the τ-p curves is due to anisotropy or to lateral heterogeneity remains problematic.

A few technical concerns also arise when the measurements are made in a borehole. For example, the present analysis assumes that the arrival directly transmitted from the source to the receiver is easily found. In practice, however, critically reflected rays are often the first arrival, making discrimination of the direct wave within the coda of this first arrival difficult or impossible, especially for source-receiver pairs with large p values. Another unresolved issue is created by the fact that the depth of the receivers within the borehole may not necessarily line up with the changes in the lithology, with the consequence that, if a receiver interval includes one or more geologic boundaries, the effects of the differing velocities of the different beds could appear as an apparent anisotropy of the interval. Another problem arising from the assumption that the receiver intervals are homogeneous is the general increase in velocities within a formation due to compaction which results in refraction of a ray independent of any anisotropic effects (Robertson and Corrigan, 1983). Finally, for a better construction of the τ-p curves, the experiment proposed consists of many depths and surface source offsets, and is in practice difficult and expensive to perform. However, many groups are presently pursuing various forms of borehole sources in reverse vertical seismic profile experiments which have the potential to make the proposed measurements practical.

The method proposed above should, in theory, be applicable to estimation of anisotropy from long-offset reflection seismic profiles provided the depths of the various reflectors are well known from well-log or core information. I have recently performed the required multidepth, multioffset seismic experiment using three-component recording in a borehole drilled into a layered sequence of shales, sands, and limestones; the results of the application of the above analysis to this data set will be forthcoming in a later contribution.

References

Aki, K. and P.G. Richards, 1980, Quantitative seismology, theory and methods, W.H. Freeman and Company.

Backus, G.,E., 1962, Long-wave elastic anisotropy produced by horizontal layering: J. Geophys. Res. **67**, 4427-4440.

Banik, N.C., , 1984, Velocity anisotropy of shales and depth estimation in the North Sea basin: Geophysics **49**, 1411-1419.

Beltzer, A.I., 1988, Acoustics of solids, Springer-Verlag.

Bullen, K.E., 1963, An introduction to the theory of seismology, 3rd ed.,Cambridge University Press.

Cerveny´, V., 1972, Seismic rays and ray intensities in inhomogeneous anisotropic media: Geophys. J. Royal Astr. Soc. **29**, 1-13.

Chapman, C.H., 1978, A new method for computing synthetic seismograms, Geophys. J. R. astr. Soc. **54**, 481-518.

Chapman, C.H., and Pratt, R.G., 1992, Traveltime tomography in anisotropic media - I. theory: Geophys. J. Int., **109**, 1-19.

Clayton, R.W. and G.A. McMechan, 1980, Inversion of refraction data by wave field continuation: Geophysics **46**, 860-868.

Crampin, S., 1981, A review of wave motion in anisotropic and cracked elastic-media: Wave Motion **3**, 343-391.

Daley, P.F., and Hron, F., 1977, Reflection and transmission coefficients for transversely isotropic media: Bull. Seis. Soc. Am. **67**, 661-675.

de Parscau, 1991, Relationship between phase velocities and polarization in tranversely isotropic media: Geophysics **56**, 1578-1583.

Diebold, J.B. and P.L Stoffa, 1981, The traveltime equation, tau-p mapping and inversion of common midpoint data: Geophysics **46**, 238-254.

Fedorov, F.I., 1968, Theory of elastic waves in crystals, Plenum Press.

Gaiser, J.E., 1990, Transversely isotropic phase velocity analysis from slowness estimates: J. Geophys. Res. **95**, 11241-11254.

Galperina, R.M. and Galperin, E.I., 1987, Experimental study of shear waves from shots in anisotropic media: Geophys. J. R. astr. Soc. **91**, 517-533.

Gardner, G.H.F. and Lu, L., 1991, Slant-stack processing, Geophysics reprint series Number 14, Society of Exploration Geophysicists.

Gerver, M. and Markuskevich, V., 1966, Determination of seismic wave velocity from the traveltime curve: Geophys. J. R. astr. Soc. **11**, 165-173.

Hake, H., 1986, Slant stacking and its significance for anisotropy: Geophysical Prospecting **34**, 595-608.

Helbig, K., 1983, Elliptical anisotropy - Its significance and meaning: Geophysics **48**, 825-832.

Jolly, R.N., 1956, Investigation of shear waves: Geophysics **21**, 905-938.

Krey, Th. and Helbig, K., 1956, A theorem concerning anisotropy in stratified media and its significance to reflection seismology: Geophys. Prosp. **4**, 294-302.

Levin, F.K., 1979, Seismic velocities in transversely isotropic media: Geophysics **44**, 918-936.

Levin, F.K., 1978, The reflection, refraction, and diffraction of waves in media with elliptical velocity dependence: Geophysics **43**, 528-537.

Moon, W., A. Carswell, R. Tang and C. Dillon, 1986, Radon transform wave field separation for vertical seismic profiling data: Geophysics **51**, 940-947.

Musgrave, M.J.P., 1970, Crystal acoustics, Holden Day.

Pellisier, M.A., Thomas-Betts, A. and Vestergaard, P.D., 1991, Azimuthal variations in scattering amplitudes induced by transverse anisotropy: Geophysics **56**, 1584-1595.

Robertson, J.D. and Corrigan, D., 1983, Radiation patterns of shear-wave vibrator in near-surface shale: Geophysics **48**, 19-26.

Saito, H., 1991, Anisotropic traveltime tomography at the Buckhorn test facility in Illinois, expanded abstract in Proc. 61st Ann. Int. Meeting Soc. Expl. Geophys., **1**, 123-126.

Samec, P., and Blangy, J.P., 1992, Viscoelastic attenuation, anisotropy, and AVO: Geophysics **57**, 441-450.

Schultz, P.S., 1982, A method for direct estimation of interval velocities: Geophysics **47**, 1657-1671.

Stoffa, P.L., Buhl, P., Diebold, J.B. and Wenzel, F., 1981, Direct mapping of seismic data to the domain of intercept time and ray parameter - A plane-wave decomposition: Geophysics **46**, 255-267.

Taner, M. T., and Koehler, F., 1969, Velocity spectra - digital computer derivation and applications of velocity functions: Geophysics, **34**, 859-881.

Vander Stoep, D.M., 1966, Velocity anisotropy measurements in wells: Geophysics **31**, 900-916.

Vernik, L., 1992, Ultrasonic velocity and anisotropy of hydrocarbon source rocks: Geophysics, **57**, 727-735.

White, J.E., Martineau-Nicoletis, L. and Monash, C., 1983, Measured anisotropy in Pierre shale, Geophysical Prospecting **31**, 709-725.

Winterstein, D.F., 1986, Anisotropy effects in P-wave and SH-wave stacking velocities contain information on lithology: Geophysics **51**, 661-672.

Winterstein, D.F., and Meadows, M.A., 1991a, Changes in shear-wave polarization azimuth with depth in Cymric and Railroad Gap oil fields: Geophysics **56**, 1349-1364.

Winterstein, D.F., and M.A. Meadows, Shear wave polarizations and subsurface stress directions at Lost Hills field, Geophysics, **56**, 1331-1348, 1991b.

Winterstein, D.F, and B. N. P Paulsson, 1990, Velocity anisotropy in shale determined from crosshole seismic and vertical seismic profiles data, Geophysics **55**, 470-479

Young, G.B., and Braile, L.W., 1976, A computer program for the application of Zoeppritz's amplitude equations and Knott's energy equations: Bull. Seis. Soc. Am. **66**, 1881-1885.

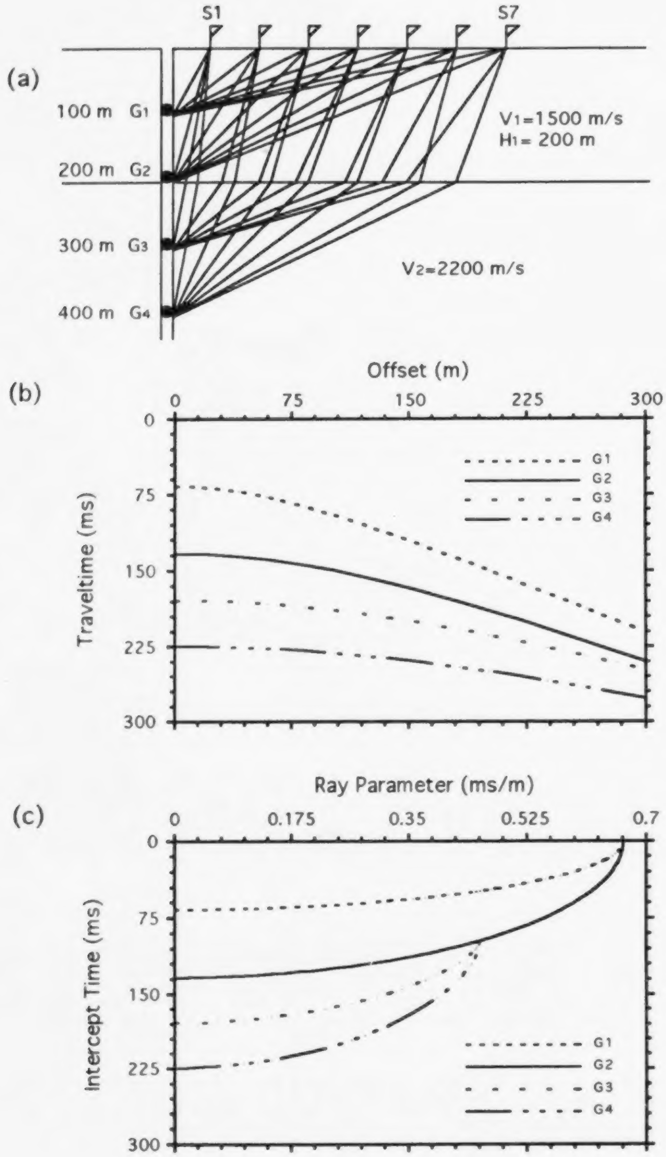

Figure 2.1. (a) Geometry of surface-to-borehole seismic experiment in isotropic layers showing ray paths from surface sources S1, S3 and S7 to receivers G1 through G4 at 50 m intervals from 50 m depth. (b) Traveltimes of rays to receivers G1 through G4 versus the distance of the source offset from the vertical borehole. (c) Traveltime curves of (b) transformed into the τ-p domain. τ-p curves for G1 and G2 are perfect ellipses. Those for G3 and G4 are distorted by $\tau(p)$ contribution of layer 1.

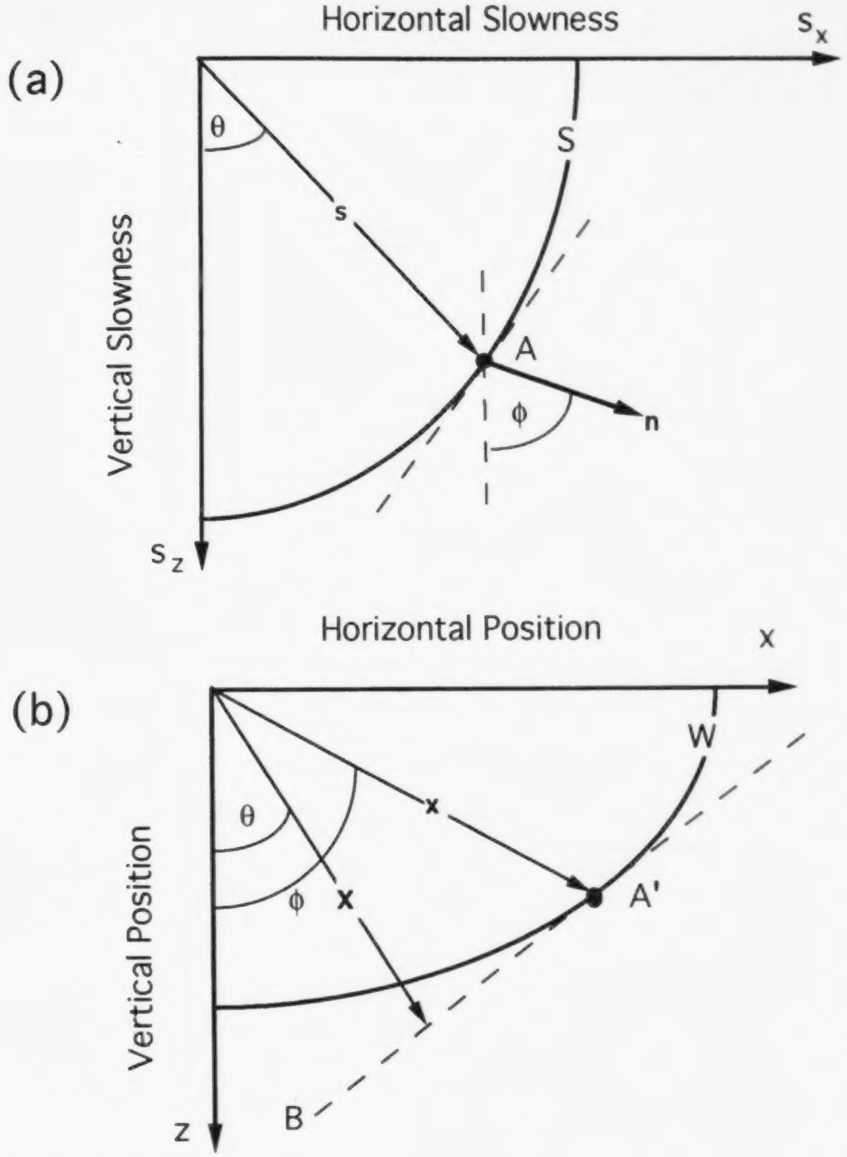
Horizontal Slowness
s_x
(a)
θ
S
s
Vertical Slowness
A
ϕ
n
s_z
Horizontal Position
x
(b)
W
x
θ
ϕ
x
A'
Vertical Position
z
B

Figure 2.2. (a) Hypothetical phase slowness surface S in one plane of an anisotropic material with respect to the vertical and horizontal. The length of **s** is inversely proportional to the velocity of a plane wave propagating through the material in the direction defined by θ. **n** is a unit vector normal to S at the endpoint of s, ϕ defines both the direction of **n** and of the energy flow through the medium. (b) Hypothetical wave surface, W, in x-z space is directly related to phase slowness surface S; A' at the endpoint of spatial vector x at angle ϕ corresponds to A in (a).

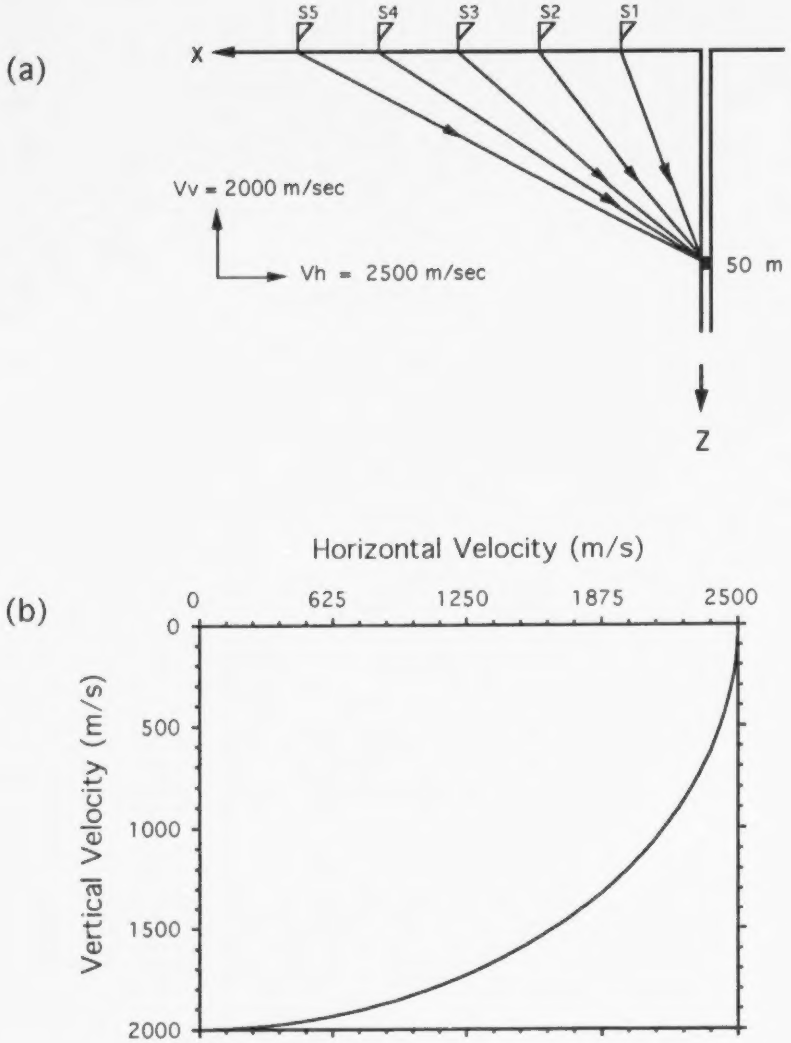
(a)
S5
S4
S3
S2
S1
X
Vv = 2000 m/sec
Vh = 2500 m/sec
50 m
Z
(b)
Horizontal Velocity (m/s)
0
625
1250
1875
2500
Vertical Velocity (m/s)
0
500
1000
1500
2000

Figure 2.3. (a) First model consisting of anisotropic half-space with receiver at 50 m. (b) Ray velocity model of half-space.

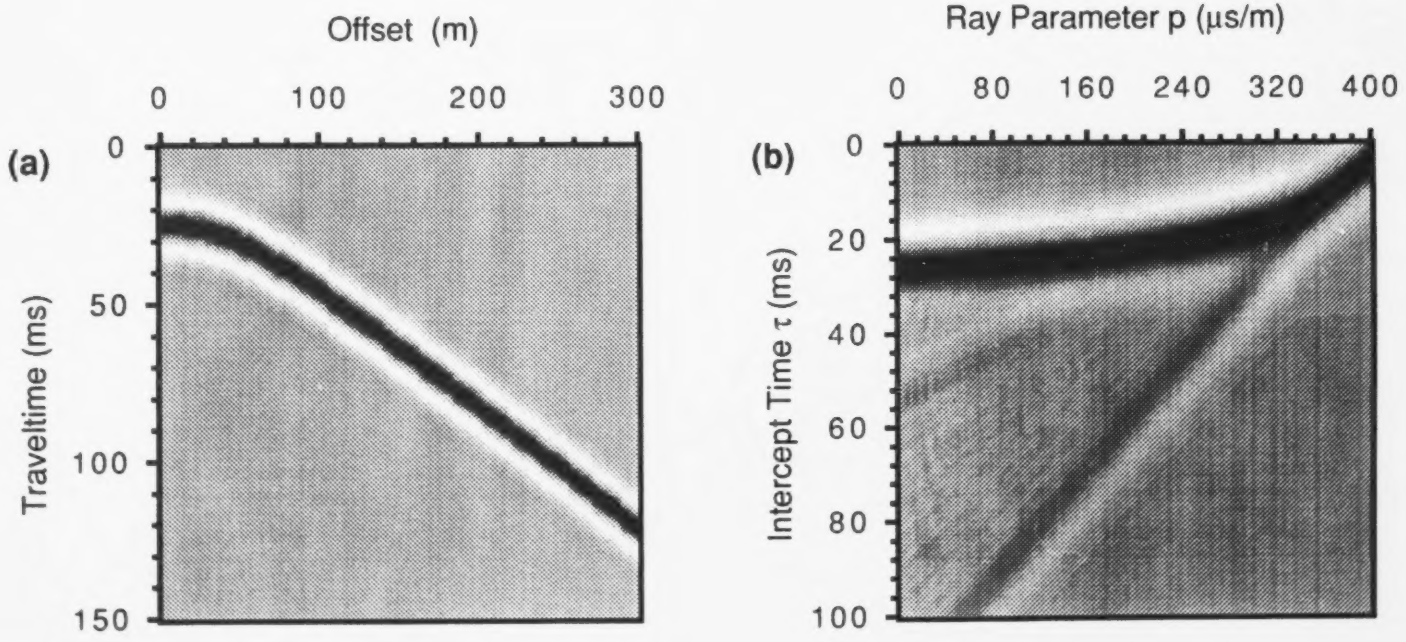

Figure 2.4. (a) Traveltime observed at 50-m receiver of Figure 3 and convolved with a Ricker wavelet versus source offset from borehole. (b) Equalized τ-p amplitude representation of (a).

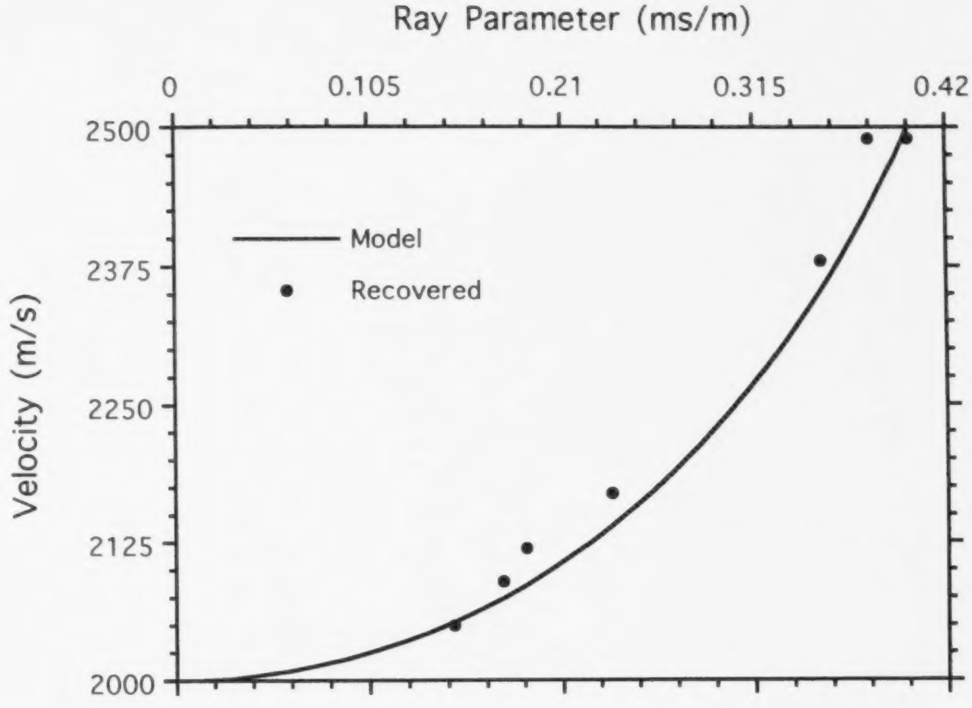

Figure 2.5. Velocities input to Figure 2.4.(a) (model) and recovered from Figure 2.4.(b) (recovered) using method described in text.

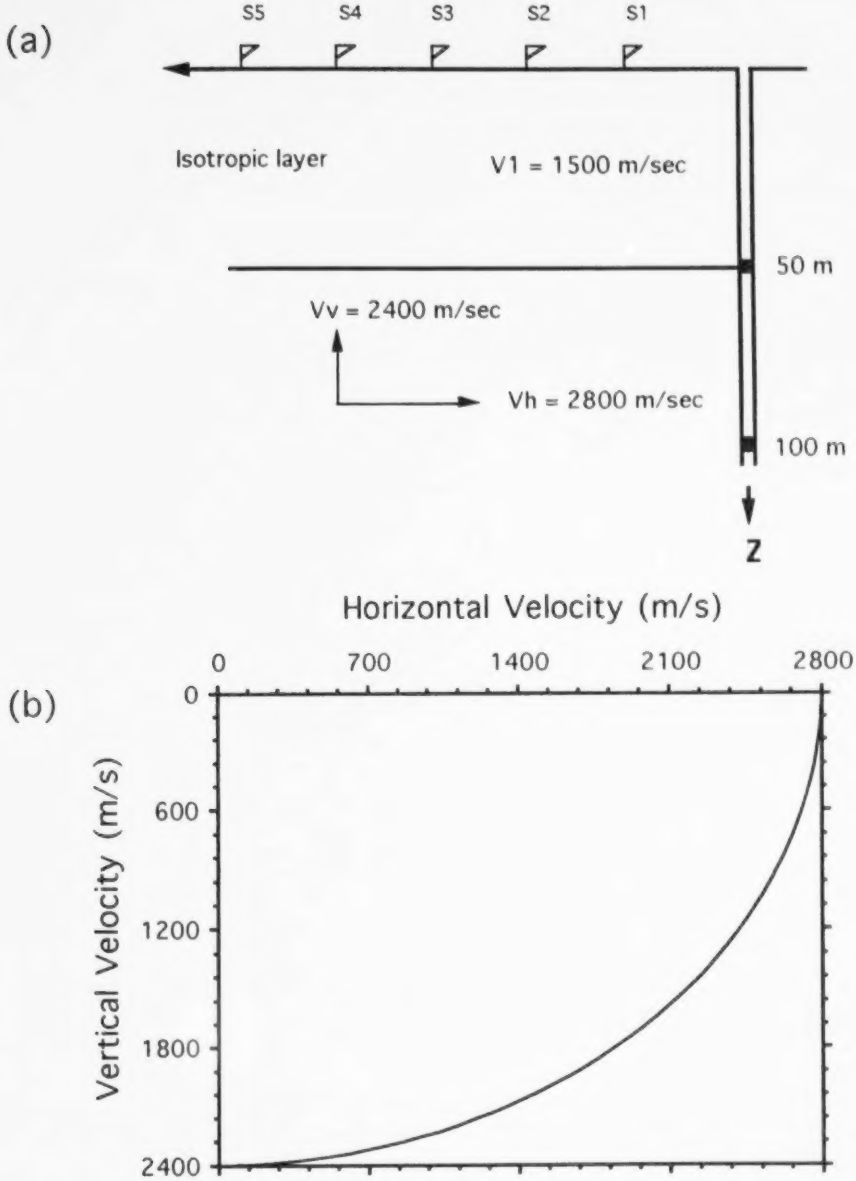
(a)
S5
S4
S3
S2
S1
Isotropic layer
V1 = 1500 m/sec
50 m
Vv = 2400 m/sec
Vh = 2800 m/sec
100 m
Z
(b)
Horizontal Velocity (m/s)
0
700
1400
2100
2800
Vertical Velocity (m/s)
0
600
1200
1800
2400

Figure 2.6 (a) Second model consisting of isotropic 50-m thick surface layer over an anisotropic half-space. (b) Velocity relation of halfspace.

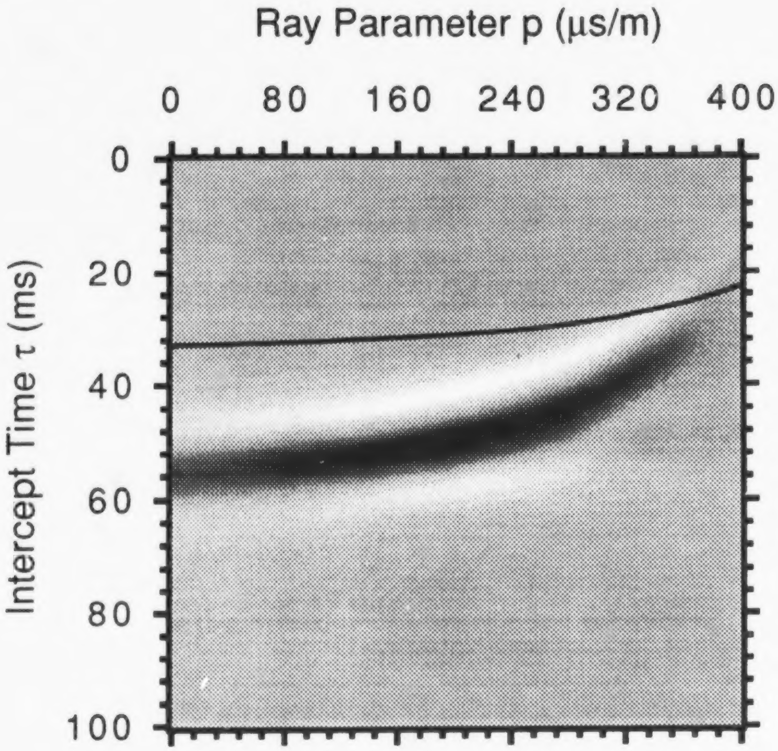

Figure 2.7. Nonequalized τ-p amplitude representation of traveltimes observed at a 100-m depth receiver within anisotropic half-space of Figure 2.6. Continuous line represents τ-p traces derived from a receiver at the bottom of the isotropic layer, the contribution of which must first be removed.

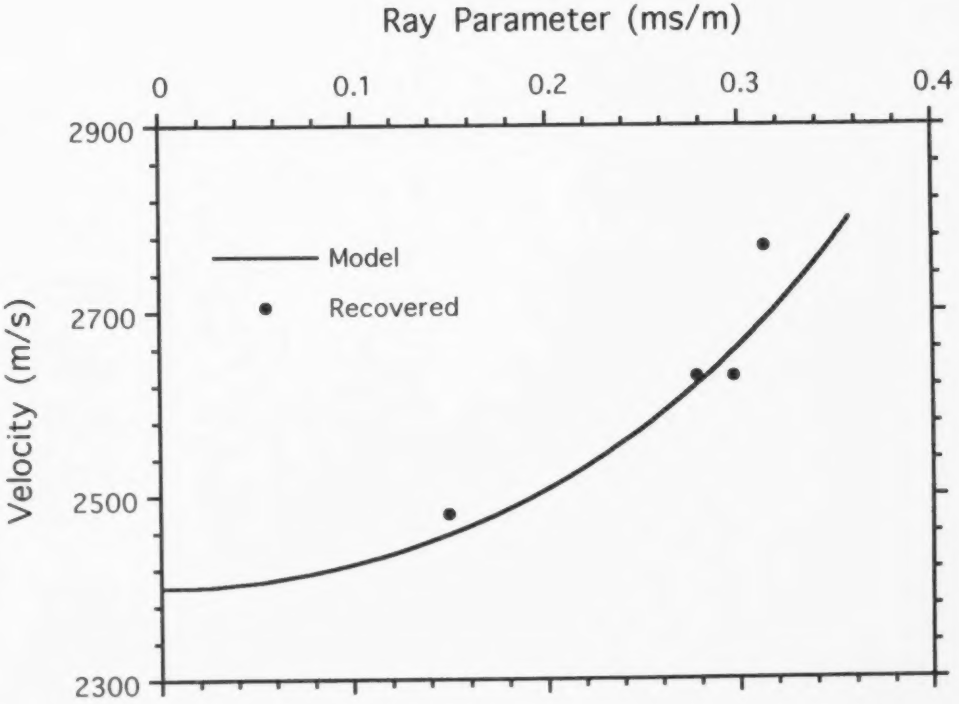

Figure 2.8. Velocities input to the model of Figure 2.6 (model) and recovered from Figure 2.7 (recovered) using the layer stripping method described in text.

Chapter 3

3. Velocity Anisotropy Observed in Wellbore Seismic Arrivals: Combined Effects of Intrinsic Properties And Layering

3.1 Introduction

The earth's crust is seismically anisotropic, but only recently have the implications of this anisotropy in seismic imaging been recognized. For example, inclusion of velocity anisotropy has been shown to produce better resolution in crosswell tomographic imaging (Miller et al., 1991; Chapman and Pratt, 1992; Pratt and Chapman, 1992). Velocity anisotropy also directly impacts migration of seismic reflection profiles (Larner, 1993; Larner and Cohen, 1993). Knowledge of the velocity anisotropy can improve the accuracy of estimates of depths to seismic reflectors (Banik, 1984). Finally, velocity anisotropy of a given layer can in itself be an important lithologic diagnostic in reservoir descriptions (Jones and Wang, 1981; Byun et al., 1989; Vernik and Nur, 1992). Accurately determining or even estimating this anisotropy so that it might be considered in sophisticated analyses is problematic, and, partly for this reason, was ignored in seismic exploration. In production geophysics, however, features within or near a reservoir must be located more precisely and this elevated level of resolution requires a more complete understanding of the seismic character of the subsurface. As a result, methods for extracting this anisotropy are needed.

Anisotropy, and in particular the variation of velocity with angle of incidence within the vertical plane, has previously been estimated using various methods from seismic data collected in one or more wellbores (e.g., Jolly, 1956; White et al., 1983; Gaiser, 1990; Winterstein and Paulsson, 1990). These studies have been reviewed by Schmitt and Kebaili (1993) who also proposed that this variation of velocity might be extracted from the τ-p mapping of the direct arrivals recorded on a detector at a known depth in a wellbore.

In the present study, this τ-p analysis is applied to a multioffset, multidepth wellbore seismic data set. Both near-vertical and oblique velocities are derived under the simplifying assumption that the velocity within a given range of incidence angles is nearly constant. This chapter includes a brief description of the basis of the method but focuses more on its implementation and the results of a field experiment.

3.2 Theoretical Background

The slant stack or τ-p mapping has been widely used during the last decade for velocity inversion and wave separation in surface reflection and refraction profiles (Stoffa et al., 1981; Schultz, 1982). Here, p is called the ray parameter, which is the same as the horizontal component of the phase slowness, and τ is the delay intercept time equivalent to the zero-offset arrival time. Under the assumption that the crust consists of stratified isotropic layers, Schultz (1982) derived a layer stripping technique in τ-p space to estimate the interval velocities from expanding-spread surface profiles. In this method, the interval velocities between successive strong reflecting and critically refracting geologic interfaces were obtained independent of Dix's (1955) estimates and without any restrictive assumptions regarding depths to the different layers. The Schultz analysis was modified by Hake (1986) to include velocity anisotropy and applied to a theoretical data set. Unfortunately, without the additional knowledge of the depth to a given lithologic interface, Hake's (1986) analysis is unable to determine the slowness curves from surface seismic data without the additional knowledge of the layer thicknesses.

However, if the receivers are instead placed at known depths in a wellbore and are activated by energy arriving from a series of source points placed on the surface, the ray geometry for each receiver is equivalent to that of the downgoing ray in a common depth point reflection profile. This similarity in ray geometry is readily exploited by modifying Schultz's (1982) technique to determine interval velocities for the case of isotropic layers and the equations may be further adapted to include vertical-to-horizontal velocity anisotropy (Schmitt and Kebaili, 1993).

To see this, consider a vertical borehole drilled into a vertically inhomogeneous (i.e. layered) and anisotropic medium in which a series of receivers R_i are located at increasing depths z_i (Figure 3.1). Also, consider a seismic ray generated at the surface, at an offset distance X from the borehole, propagating through this medium down to receiver R_n. Since the medium is inhomogeneous and anisotropic, the ray velocity V at any point depends on both the ray parameter p and the depth z. The ray traveltime from the source S to receiver R_n at depth z_n in the borehole (Hake, 1986) can be generalized to an anisotropic and inhomogeneous medium as

$$t_n = pX + \tau_n \tag{3.1}$$

where τ_n is the intercept time or zero-offset time to receiver n (Schultz and Claerbout, 1978) given by:

$$\tau_n = \sum_{i=1}^{n} \Delta z_i q_i \ , \tag{3.2}$$

where the layer thickness $\Delta z_i = z_{i+1} - z_i$.

The parameters p and q are the horizontal and vertical phase slownesses, respectively, and are given by:

$$p = \frac{dt}{dx} = \frac{\sin\theta}{v} = u\sin\theta \qquad\qquad q = \frac{dt}{dz} = \frac{\cos\theta}{v} = u\cos\theta \tag{3.3}$$

where θ is the angle of incidence, v is the magnitude of the phase velocity, and u is the magnitude of the phase slowness. Hereafter I refer to p as the ray parameter, p, and q are related by

$$p^2 + q^2 = u^2 . \tag{3.4}$$

Using these relations, equation (3.2) may be written in terms of the ray parameter, p and the magnitude of the slowness in layer i, u_i;

$$\tau_n(p) = \sum_{i=1}^{n} \Delta z_i (u_i^2 - p^2)^{1/2} , \tag{3.5}$$

and for a particular ray parameter p, the contribution from layer i to the total intercept time τ_n is:

$$\Delta\tau_i(p) = \Delta z_i (u_i^2 - p^2)^{1/2} , \tag{3.6}$$

which can be written in the form (Schultz, 1982):

$$\frac{\Delta\tau_i^2(p)}{\Delta z_i^2 u_i^2(p)} + \frac{p^2}{u_i^2(p)} = 1 . \tag{3.7}$$

If all the layers are isotropic (i.e., u_i is independent of θ i.e independent of p), then equation (3.7) defines an ellipse. Equation (3.7) does not define an ellipse in the $\Delta\tau$-p system of coordinates when the slowness u_i is a function of the ray parameter p (Helbig, 1984), and in this case determining the velocity as a function of the incidence angle is problematic. However, if I assume that over a given limited range of ray parameters denoted p_o the material is nearly isotropic such that the velocity does not change considerably and may be taken as a constant $\langle u_i \rangle$, then an ellipse of the form

$$\frac{\Delta\tau_i^2(p)}{\Delta z_i^2 \langle u_i(p_o) \rangle^2} + \frac{p^2}{\langle u_i(p_o) \rangle^2} = 1 \tag{3.8}$$

will describe the loci of the direct arrivals in the τ-p domain over that limited range of p. Consequently, the local shape of the τ-p curve provides information on the incidence-angle-dependent velocity which may be extracted using the layer-stripping technique (Schultz, 1982) for anisotropic layered earth. Modified to include anisotropy (Schmitt and Kebaili, 1993), the slownesses of the layers can be recursively determined. Note that the two recoverable quantities $\langle u_i(p_o) \rangle$ and $\Delta z_i \langle u_i(p_o) \rangle$ are not independent; and the knowledge of the receiver spacings in the wellbore can be used as an important constraint in the slowness determination.

In this chapter I investigate the near-vertical and oblique velocities for each layer bounded by two successive receivers. Each τ-p curve is divided into two portions: one representing the near-vertical rays with angles of incidence $0<\theta<30°$, and the other one for oblique rays ($\theta>30°$). The delimiting ray parameter, $p = \sin(30°)/v$, is obtained using Snell's law, where the velocity v is calculated from the traveltimes observed at a source offset of 5 m (i.e essentially zero offset). This angle of 30° was arbitrarily selected but represents the approximate median ray angle for most of the common wellbore depth gathers.

The observed τ-p curves were separated into near-vertical (i.e., small p) and oblique (i.e. large p) segments on this basis. Each segment was examined independently to provide the two measures of velocity for a given depth interval. The near-vertical interval velocity of the first layer was obtained by fitting this first portion of the corresponding τ-p

curve with ellipses, assuming that the material to be nearly isotropic, according to equation (3.8). Once this velocity is known, the contribution of the first depth interval to the second τ-p curve can be eliminated by calculating the layer stripping correction

$$\delta\tau_1(p) = \tau_1(0) - \tau_1(p) = \tau_1(0) - \Delta z_1[\langle u_1(p_o)\rangle^2 - p^2]^{1/2} , \qquad (3.9)$$

and shifting the portion of the second τ-p curve downward by the amount calculated using equation (3.9). This correction eliminates the contribution of the first layer and is equivalent to changing the datum plane from depth zero to depth z_1, allowing us to determine the velocity of the second layer for the first p-range. I carried out this procedure all the way down to the deepest detector in a manner similar to that described by Schultz (1982) in order to obtain the set of near vertical velocities. The procedure was then repeated on the larger p portions of the τ-p curves to provide the oblique velocities.

3.3 Application

3.3.1 Geologic setting

I conducted a field experiment in a 230-m deep, steel-cased wellbore drilled through an oil sand formation near Fort McMurray, Alberta. The geology in this region essentially consists of a 150-m thick, flat-lying Cretaceous sequence of marine sands and shales, which unconformably overlie dense Devonian limestones. At the surface, a 10-m thick overburden consists of Quaternary glacial and postglacial sands and silt. Mossop et al. (1979) delineate a number of zones within the Cretaceous (Figure 3.2). The uppermost section is a 16-m thick layer of dark grey marine shales of the Grand Rapids Formation. These overlie the Clearwater Formation, which is approximately 96 m thick from depths of 26 m to 122 m and is composed of grey marine shales separated by thin beds of water-saturated sands. These sand beds are characterized by velocities and resistivities that are large relative to the surrounding shales; these units are distinctive in both the sonic and focused electric logs (Figure 3.2). The sonic velocity generally increases with depth throughout this zone and this may be a consequence of the corresponding increase in sand content with depth. The sonic log indicates a jump in the shale velocities at a depth near 70 m but there are no obvious lithologic changes at this depth. The Clearwater terminates at a 2.5-m thick gas sand. The lowermost Cretaceous section is called the McMurray Formation and is approximately 37 m thick. The uppermost 17 m of this zone consists of a mixture of shales with thin beds of oil-saturated sand, while the lowest 20 m is a thick oil sand with shale layers sufficiently thin and resolvable by their low resistivity in the electric log. The transition from the oil sands to the underlying Devonian limestones is sharp with a transitional zone of no more than 1 m thickness in the core.

3.3.2 Field acquisition

I acquired a multioffset VSP data set at 13 depth levels from 25 m to 225 m in the wellbore. The three-component data was recorded at a 0.1-ms sampling rate on three channels of a Bison series 5000 data acquisition unit. The energy was generated on the surface by the "Betsy gun" model 979 and detected by an SIE T42 type detector in three orthogonal directions: one vertical component, V, and two horizontal components, H_1 and H_2. The geophone tool was clamped to the borehole casing. Each geophone was calibrated on a shake table over the frequency range 5 to 500 Hz. Over the range of frequencies from 0 to 150 Hz, typical of the field experiments, the amplitudes of these three geophones differed at most by 7%. The seismic source provided energy by firing into water-filled holes at increasing offsets from 5 to 300 m from the wellbore. An antialiasing band-pass filter of 20 – 2000 Hz was used in the field. This primarily attenuated problems associated with low-frequency vibration of the wireline cable. For each source-receiver pair, enough shots were taken to provide an acceptable signal-to-noise ratio determined from real-time monitoring of the accumulating stack. This process is, admittedly, somewhat subjective but the number of stacked shots for a given pair generally increased from three for near-offset shallow receivers to seven for far-offset deep records.

An uneven source-offset spacing was adopted to produce better spatial resolution of the τ-p curves, especially at shallow receiver depths. The source spacing was dense near the wellbore where p changes rapidly with offset. This pattern of increasing source spacing with radial distance from the wellbore produces a relatively uniform ray density.

3.3.3 Three-component data processing

The onsets of the times of the directly transmitted compressional arrivals were found using hodograms. As an example, Figure 3.3 shows the vertical and two horizontal components recorded by the downhole geophones at 25-m depth for a source fired at a 30-m offset from the wellbore. These traces were digitally filtered with a 50 – 150 Hz band-pass and individually normalized for display purposes only. The peak energy reaches the three orthogonal geophones in the time interval of 30-60 ms. The maximum amplitude on the H2 component is nearly 1.5 times that of the vertical, as would be expected for this source-receiver geometry. The amplitude responses for the two horizontal components in the time window of 0-70 ms are plotted as an hodogram in Figure 3.3b; the difference between the polarization of the hodogram trace and the H2 direction is +18°. Under the assumption that the plane containing the arriving rays also contains the polarization vector (Ahmed et al., 1986), the two horizontal components were rotated through the appropriate angle to yield components that are transverse (Ht) and radial (Hr) to the projection of the incoming ray on the horizontal plane (Figure 3.4a). Again, under the assumption that the direct compressional wave stays in the plane of incidence, a second hodogram was plotted using the observed vertical (V) and the calculated radial components (Hr), which for the example shown has a polarization that suggests an angle of incidence of 56° (Figure 3.4b). Finally, the vertical and radial components were rotated to this angle to produce a trace whose components are parallel to the direction of the first arrival. Note that this rotated P arrival in the 30-60 ms interval (Figure 3.4a) has a maximum amplitude which is 76 percent greater than the vertical component alone.

The above analysis was performed for each source-receiver pair. The maximally rotated direct P-wave seismograms for the 2- m depth receiver are displayed as a common receiver gather in Figure 3.5a. In some cases, these particle motions were used to discriminate the directly transmitted downgoing P-arrival from earlier arriving refractions. The primary difficulty encountered in processing these data was the estimation of the amplitude and time of the compressional transmitted wave using the three-component data. For some receiver-shot point pairs, the first-break wavelet is not the downgoing P-wave but, rather, the upcoming head wave. This is most apparent for the shallow receiver depths at large offset, where a refraction is observed from the base of the weathered layer at 20 m depth. The search for the downgoing direct arrival must be conducted carefully by examining particle motion hodograms in the vertical plane and over a variety of time windows.

3.3.4 τ-p mapping and velocity determination

These final, maximally rotated traces were mapped into the τ-p domain using the slant-stack procedure of Diebold and Stoffa (1981) using Chapman's (1978) discrete equation

$$F(\tau_i, p_j) = \sum_{k=1}^{N} f(t=\tau_i + p_j X_k, X_k), \tag{3.10}$$

where $F(\tau_i, p_j)$ is the data sample in the τ-p domain for trace p_j at intercept time τ_i, and $f(t, X_k)$ is the data sample in the x-t domain at time t for trace offset X_k.

The spatial sampling of the data introduces an aliasing if the sampling interval Δx does not satisfy the condition $\Delta x \leq V_{\min}/f_{\max}$, leading to a Nyquist ray parameter equal to $p_N = 1/\Delta x f_{\max}$. In the present study with a $V_{\min}$, minimum horizontal velocity of 1340 m/s and an $f_{\max}$, maximum frequency of ~200 Hz, this limit indicates a maximum source spacing of 6.5 m. To attenuate the spatial aliasing, a ratio filter (Moon et al., 1986) was incorporated in the forward τ-p transformation. This selective filter allows into the summation of equation (3.10) only those $F(t, x_k)$ whose ratio to neighboring sample values lies within the range 0.7 to 1/0.7. This procedure assures that the line of slope p over which the summation is performed in the x-t domain is tangent to the offset-time curve of the downgoing rays.

The maximum ray parameter allowed for a given common-receiver gather varies with the receiver depth due to the geometrical constraints. For example, for the 25 m depth gather Figure 3.5b, the maximum ray parameter is 700 ms/m; this is equivalent to a horizontal velocity of about 1430 m/s. The direct arrivals which appear near 40 ms for normal incidence at $p=0$ are organized along a hyperbola-like curve in offset-traveltime space, and Figure 3.5b map into an ellipse-like curve in the τ-p domain as seen for $30<\tau_0<50$ ms in Figure 3.5b. In this range of intercept times, more than one ellipse-like curve is seen and these are an artifact of the successive lobes of the wavelet in the offset-time domain. Only one of these is used in the velocity determinations. These τ-p arrivals were further enhanced for cosmetic purposes by multiplication with a symmetric Gaussian window. In this process, a time window containing the maximum energy lobes on an ellipse-like curve is selected; the maximum amplitudes within this time window are then automatically determined, and the data at constant p are multiplied by Gaussian curves centered at these maxima. As a result of this operation, the data points on both sides of the ellipse-like curve are multiplied by a coefficient less than unity whose magnitude decreases from the center of the window. Note that any of the ellipse-like curves for $30<\tau_0<50$ ms could be used to determine the velocity. However, the windowed ellipse-like curve must be tied to the one-way vertical traveltime, because the intercept time τ_0 for $p=0$ should be equal to the one-way vertical traveltime to the geophone at the depth considered. I corrected the τ-p data by a simple τ shift to agree with this value. This time was determined from the shortest offset x-t seismogram.

The data processing steps given above were performed on the common geophone traces at 9 depths, and a composite of the resulting common geophone τ-p curves for six of these is displayed in Figure 3.6. This figure is similar to that which would be observed for an hypothetical seven layer model with reflecting lithologic interfaces at the receiver depths in a reflection profile.

The vertical lines dividing each τ-p curve into two segments mark the 30° angle of incidence for each geophone depth. The near-vertical velocity was derived from the small p segment of each curve to the left of the 30° incidence angle mark. Similarly, the oblique velocities were determined from the large p segments to the right of this mark.

Velocities are determined using combined semblance and maximal-energy coherency measures. The semblance (Taner and Koehler, 1969) for a given point in the slowness-τ_0 space is defined as:

$$S(u,\tau_0) = \frac{1}{n}\frac{\sum_{j=1}^{m}(\sum_{i=1}^{n} A_{j,i})^2}{\sum_{j=1}^{m}(\sum_{i=1}^{n} A_{j,i}^2)} \tag{3.11}$$

where n is the number of traces in the τ-p domain, m is the number of data samples in the semblance calculation window, and $A_{j,i}$ is the ith data sample in the semblance calculation window of trace j. Equation (3.11) measures the degree of coherency between the actual

τ-p curves and an ellipse of horizontal and vertical semi-axes u and τ_0, respectively. For each trial of the pair u-τ_0, a correction $\delta\tau(p)$ is calculated according to

$$\delta\tau(p) = \tau(p) - \tau(0) = [\ \tau(0)\ ][\ 1 - (1 - p^2 v^2)^{1/2}\ ], \tag{3.12}$$

after which the p-traces are shifted downward by the amount $\delta\tau(p)$. A semblance value is then calculated using equation (3.11). When the trial u-τ_0 coincides with that of the analyzed τ-p curve, the $\delta\tau(p)$ correction flattens the actual curve, and the semblance reaches its maximum.

The power of the semblance function resides in the fact that it is normalized, and hence independent of the energy of the seismic events. However, this turns out to be a disadvantage in the case of narrow calculation windows. The semblance becomes sensitive to the side lobes of the wavelets, which leads to more than one maximum in the semblance map for the same depth. To discriminate the main lobe from the side ones, the energy $E(u, \tau_0)$ is also calculated for each trial ellipse u-τ_0 using

$$E(u, \tau_0) = \frac{1}{n} \sum_{i=1}^{m} \sum_{j=1}^{n} A_{j,i}^2. \tag{3.13}$$

An example of semblance mapping for the oblique rays at 25-m depth is shown in Figure 3.7a; this mapping was calculated using a 5-ms t-window with 0.6-ms increments. The mapping displays a maximum at 28.4 ms with two local maxima at 23.6 ms and 33.8 ms. The projection of the absolute maximum to the horizontal axis yields the oblique velocity which is 1340 m/s. The corresponding energy mapping is shown in Figure 3.7b; and the peak of the energy appears at 29.0 ms and 1330 m/s in good agreement with the semblance. The relatively high coherencies in the semblance mapping at 23.6 ms and 33.8 ms do not appear in the energy mapping, indicating that these are side lobes of lower energy which may be ignored.

The semblance and energy mappings for the near-vertical section of the 25-m depth τ-p curve are constructed in a similar manner. The semblance mapping showed a maximum peak at 27.8 ms with a velocity of 1210 m/s. This velocity is lower than the value of 1340 m/s observed for the oblique rays. The energy mapping presented only one maximum at 28.4 ms and 1200 m/s which nearly coincides with the maximum of the semblance mapping and further suggests that the near-vertical velocity is less than the oblique velocity. To check the stability of the technique and the reliability of the recovered velocities, the semblance and energy mappings were calculated with a variation of window widths (3 ms to 9 ms) and velocity increments (5 m/s to 20 m/s). The results show that the recovered velocities are in error by little more than 2 percent.

These determined characteristics for the near-vertical and oblique portions of the 25-m depth τ-p curve are used in the layer-stripping procedure to correct the next receiver depth at 50 m from which, again, the two different ray parameter ranges are analyzed to produce near-vertical and oblique velocity estimates for the interval lying between 25 m and 50 m depth.

This procedure was carried out for all the receiver depths with both near-vertical and oblique rays. Velocities found from the two complementary coherency measures are summarized in Figure 3.8 which suggests that the oblique velocity is larger than the near-vertical velocity for all the layers. Within a given interval between receivers, these velocities can vary from each other by 2 percent to 15 percent (Figure 3.8). This difference is possibly attributed to velocity anisotropy. Other workers, too, have observed that horizontal velocities are generally higher than vertical velocities, although this in no way validates the present observations.

3.4 Discussion

The anisotropy observed may be a manifestation of the fine layering of the formation (Backus, 1962; Berryman, 1979; Levin, 1979), or may be due to an intrinsic anisotropy of the rock (Winterstein et al., 1990). To test the first possibility, I calculated the degree of anisotropy. The elastic constants *A* and *C* for a transversely isotropic medium that is equivalent to a stack of thin isotropic layers, in the notation of White (1965) are given by:

$$\begin{aligned} A &= \left\langle 4\rho\beta^2\left[1-\left(\beta^2/\alpha^2\right)\right]\right\rangle + \left\langle 1-\left(2\beta^2/\alpha^2\right)\right\rangle^2 \Big/ \left\langle\left(\rho\alpha^2\right)^{-1}\right\rangle \\ C &= \left\langle\left(\rho\beta^2\right)^{-1}\right\rangle^{-1}, \end{aligned} \tag{3.14}$$

where α and β are the P-wave and S-wave velocities in the isotropic medium, respectively, and ρ is the density. The brackets in equation (3.14) denote averages. The horizontal v_h and vertical v_v velocities for the equivalent transverse isotropic medium (Backus, 1962) are then given by:

$$v_h = \sqrt{A/\rho} \quad \text{and} \quad v_v = \sqrt{C/\rho}\ , \tag{3.15}$$

and the anisotropy may be defined as the ratio $(v_h - v_v)/v_v$. Calculations were carried out over the intervals between receiver depths of 74 m to 100 m and 100 m to 120 m, both characterized by thin alternating sand-shale layers, which were divided into thin layers of 0.5 to 3 m thicknesses on the basis of the sonic and focused electric logs (Figure 3.9). These two intervals differ in shale content, the first interval from 74 m to 100 m having less sand. The densities for the shale and sand constituents are taken as 2.38 g/cm^3 and 2.3 g/cm^3, respectively, as determined from bulk measurements on core. The P-wave velocities are obtained from the sonic logs, and the *S*-wave velocities are assumed to be $\beta = \alpha/1.82$ for both rock types for a characteristic Poisson's ratio, σ, of 0.28. This procedure predicts degrees of anisotropy of 14.2 percent and 6.0 percent for the intervals from 74 m to 100 m and 100 m to 120 m, respectively.

In contrast, the observed anisotropies for these two intervals were 15 percent and 7 percent, respectively (Figure 3.8.). It must be kept in mind that these observed anisotropies compare the vertical velocity to that observed at an angle of incidence of about 45°. In a transversely isotropic medium which may be representative of the site of the present investigation, the P-wave velocity is known to vary monotonically as a function of incidence angle between two given axes of symmetry, which for a horizontally stratified medium are parallel to the vertical and any horizontal direction. The increase of observed velocity with angle of incidence suggests that the in-situ horizontal velocity and the true anisotropies will be larger than those observed.

The magnitudes of the observed vertical-to-oblique and the calculated vertical-to-horizontal anisotropies are comparable; consequently, the true anisotropy will exceed that calculated under the assumption that the layers are isotropic. Intrinsic anisotropy of the rock material itself, which is not considered in the theoretical predictions, possibly explains this discrepancy. This is not necessarily that surprising as a large portion of the lithology in the two intervals consist of shales, which for a wide variety of differing types have display anisotropies to ultrasonic compressional waves ranging from 5 percent to nearly 30 percent (Podio et al., 1968; Schock et al., 1974; Jones and Wang, 1981; Tossaya, 1982; White et al., 1983; Thomsen, 1986; Vernik and Nur, 1992). As a result, the observed anisotropies, which are high relative to those calculated, may result from the combination of fine layering and intrinsic anisotropy within the lithology.

3.5 Conclusion

Multi-offset VSP data contains information about variations of the seismic velocity with angle of incidence. I have recovered such variations using a layer-stripping technique in the τ-p domain. The structure of the τ-p mapping, in particular the fact that the ray parameter so naturally relates to the angle of incidence at a given point of the ray path, aids the extraction of incidence-angle variations in velocity. The incidence-angle-dependent interval velocities are directly recovered without recourse to Dix's (1955) equation and without restrictive assumptions regarding the offset-depth ratio, although this ratio must be large to recover velocities at large angles of incidence in the x-t domain.

The near-vertical and oblique velocities that I determined from the borehole experiment are not exact. The main source of error in the present implementation lies in the fact that a number of rays must be used to determine the velocity assigned to the midpoint of the p range over which the velocity analysis is conducted. This results in an averaging of any variations in velocity over the range such that the full range of the anisotropy is underestimated. Further, if receivers have not been placed at lithologic boundaries, the recovered velocities will be an average for the given interval. Finally, the near-vertical to near-horizontal velocity differences could be caused by the combination of both anisotropy and lateral inhomogeneity, factors that are not easy to dissociate.

In practical terms, the experiment requires that records be obtained at numerous offsets and depths. This can be problematic if surface source positions are used. However, the present method is equally valid if, instead, the sources are within the wellbore and the detectors on the surface. This reverse vertical seismic profile geometry has the advantage that more source positions can easily be added at the surface, but implementation awaits the development of suitable wellbore seismic sources.

Despite the limitations, reasonable results were obtained in a multidepth multioffset

VSP data set acquired in a nearly flat-lying sedimentary formation. In all cases, the oblique velocity is greater than the near-vertical velocity. The maximum vertical-to-oblique velocity variation (15 percent) was observed over the interval bounded by receivers at 75 m and 100 m depth through the section of the wellbore distinguished by alternating sand and shale beds. The difference between the vertical and horizontal velocities in this interval will probably be larger than the observed 15 percent. Simple estimates of the anisotropy calculated under the assumption that the formation consists of isotropic layers as delineated from the sonic logs were of the same magnitude of the observed vertical to oblique anisotropies and hence are less than might be expected for the true vertical to horizontal anisotropy. This discrepancy may be due to the fact that the layers are intrinsically anisotropic. This hypothesis can only be tested from laboratory measurements on core or from cross-well seismics.

References

Ahmed, H., Dillon, P.B., Johnstad, S.E. and Johnston, C. D., 1986, Northern Viking Graben multilevel three-component walkaway VSPs-a case history: First Break, **4**, 10, 9-27.

Backus, G. E., 1962, Long-wave elastic anisotropy produced by horizontal layering: J. Geophys. Res., **67**, 4427-4440.

Banik, N. C., 1984, Velocity anisotropy of shales and depth estimation in the North Sea basin: Geophysics, **49**, 1411-1419.

Berryman, J. G., 1979, Long wavelength anisotropy in TI media: Geophysics, **44**, 896-917.

Byun, B. S., Corrigan D., and Gaiser J. E., 1989, Anisotropy velocity analysis for lithology discrimination: Geophysics, **54**, 1564-1574.

Chapman, C.H., 1978, A new method for computing synthetic seismograms, Geophys. J.

R. astr. Soc., **54**, 481-518.

Chapman, C.H., and Pratt, R. G., 1992, Traveltime tomography in anisotropic media, -I. Theory: Geophys. J. Int., **109**, 1-19.

Diebold, J.B. and P.L Stoffa, 1981, The traveltime equation, tau-p mapping and inversion of common midpoint data: Geophysics, **46**, 238-254.

Dix, C. H., 1955, Seismic velocities from surface measurements: Geophysics, **20**, 68-86.

Gaiser, J.E., 1990, Transversely isotropic phase velocity analysis from slowness estimates: J. Geophys. Res., **95**, 11241-11254.

Hake, H., 1986, Slant stacking and its significance for anisotropy: Geophys. Prosp., **34**, 595-608.

Helbig, K., 1984, Transverse isotropy in exploration seismics: Geophys. J. Roy. Astr. Soc., **76**, 79-88.

Jolly, R.N., 1956, Investigation of shear waves: Geophysics, **21**, 905-938.

Jones, L.E.A, and Wang, H.F., 1981, Ultrasonic velocities in Cretaceous shales from the Williston basin: Geophysics, **46**, 288-297.

Larner, K., 1993, Dip-moveout error in transversely isotropic media with linear velocity variation in depth: Geophysics, **58**, 1442-1453.

Larner, K., and Cohen, J., 1993, Migration error in transversely isotropic media with linear velocity variation in depth: Geophysics, **58**, 1454-1467.

Levin, F.K., 1979, Seismic velocities in transversely isotropic media: Geophysics, **44**, 918-936.

Miller, D. E., and Chapman, C.H., 1991, Incontrovertible evidence of anisotropy in crosswell data: 61st Ann. Internat. Mtg. Soc. Expl. Geophys., Expanded Abstracts, 825-828.

Moon, W., A. Carswell, R. Tang and C. Dillon, 1986, Radon transform wave field separation for vertical seismic profiling data: Geophysics, **51**, 940-947.

Mossop, G. D., Kramers, J. W., Flach, P. D., and Rottenfusser, B. A., 1979, Geology of Alberta's oil sands and heavy oil deposits, *in*: Meyer, R. F. and Steele, C. T. Eds., The future of heavy crude oil and tar sands, McGraw Hill, 197-207.

Podio, A. L., Gregory, A. R., and Gray, K. E., 1968, Dynamic properties of dry and water saturated Green River shale under stress: J. Soc. Petr. Eng., 389-404.

Pratt, R. G., and Chapman, C. H., 1992, Traveltime tomography in anisotropic media, -II. Application: Geophys. J. Int., **109**, 20-37.

Schmitt, D.R., and Kebaili, A., 1993, Velocity anisotropy estimation from slant stacks of wellbore seismics: Can. J. Expl. Geophys., **29**, 236-245.

Schock, R. N., Bonner, B. P., and Louis, H., 1974, Collection of ultrasonic velocity data as a function of pressure for polycrystalline solids: Lawrence Livermore Nat. Lab. Rep. UCRL-51508.

Schultz, P. S., and Claerbout, J. F., 1978, Velocity estimation and downward continuation by wavefront synthesis: Geophysics, **43**, 691-714.

Schultz, P.S., 1982, A method for direct estimation of interval velocities: Geophysics, **47**, 1657-1671.

Stoffa P. L., Buhl, P., Diebold, J. B., and Wenzel, F., 1981, Direct mapping of seismic data to the domain of intercept time and ray parameter - a plane-wave decomposition: Geophysics, **46**, 255-267.

Taner, M. T., and Koehler, F., 1969, Velocity spectra - digital computer derivation and applications of velocity functions: Geophysics, **34**, 859-881.

Thomsen, Leon, 1986, Weak elastic anisotropy: Geophysics, **51**, 1954-1966.

Tossaya, C. A., 1982, Acoustic properties of clay-bearing rocks: Ph. D. thesis, Stanford Univ.

Vernik, L., and Nur, A., 1992, Ultrasonic velocity and anisotropy of hydrocarbon source rocks: Geophysics, **57**, 727-735.

White, J.E., 1965, Seismic waves: radiation, transmission, and attenuation: McGraw-Hill, Inc.

White, J.E., Martineau-Nicoletis, L. and Monash, C., 1983, Measured anisotropy in Pierre shale: Geophys. Prosp., **31**, 709-725.

Winterstein, D.F, and B. N. P Paulsson, 1990, Velocity anisotropy in shale determined from crosshole seismic and vertical seismic profiles data: Geophysics, **55**, 470-479.

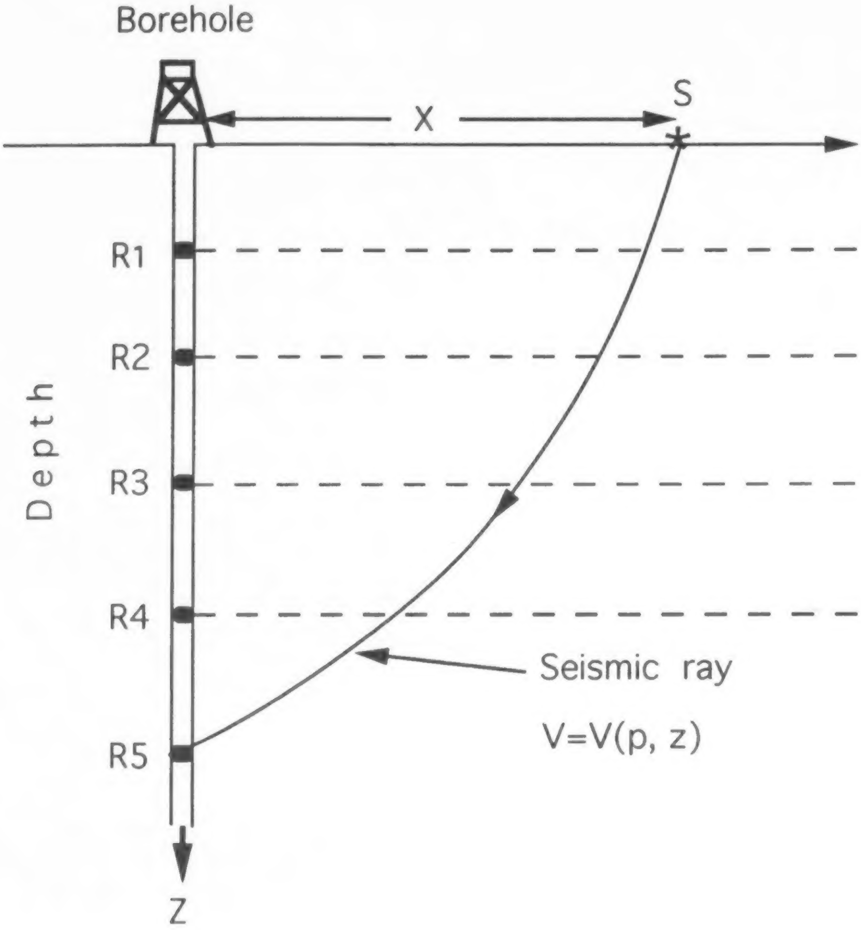
Borehole
X
S
R1
R2
R3
R4
R5
Depth
Seismic ray
V=V(p, z)
Z

Figure 3.1. Seismic ray downgoing to a receiver through an anisotropic and inhomogeneous medium.

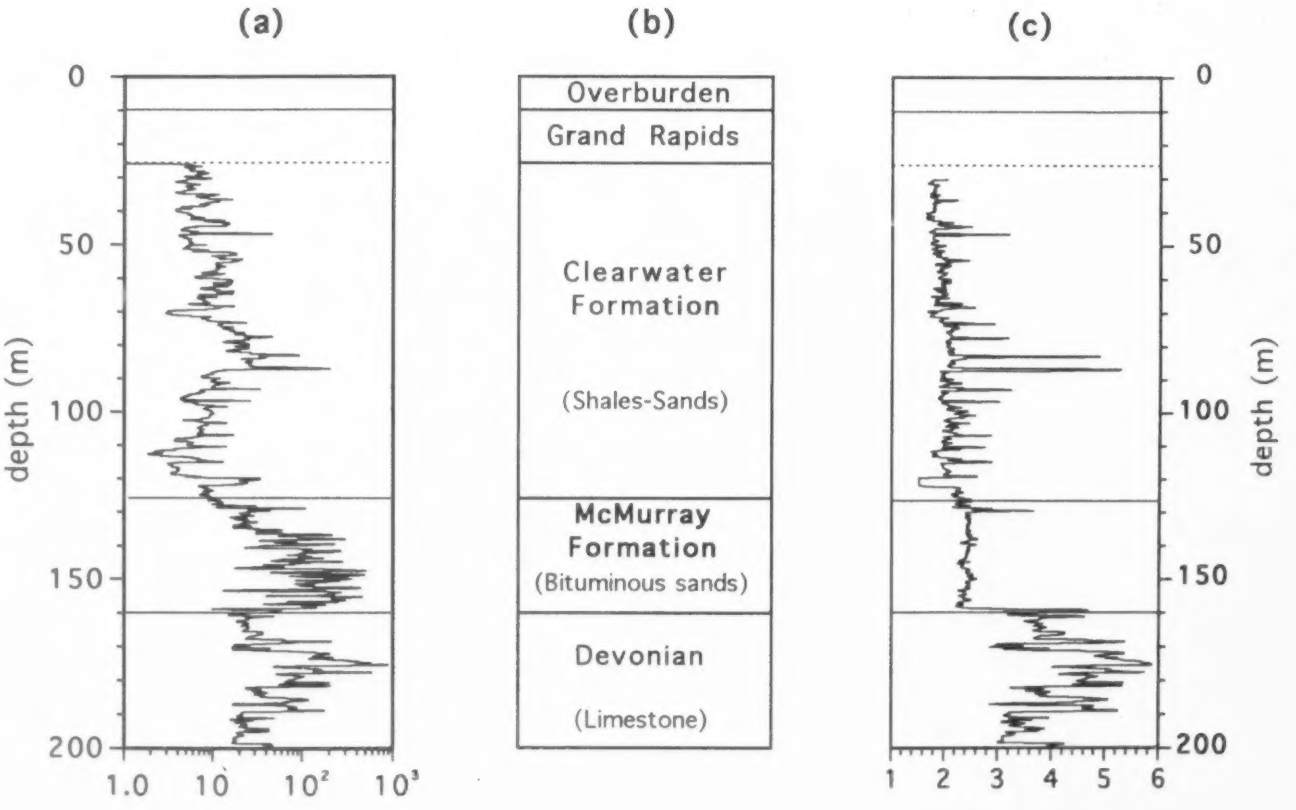

Figure 3.2. Lithology (b) compared to focused electric (a) and sonic log (c) through the wellbore.

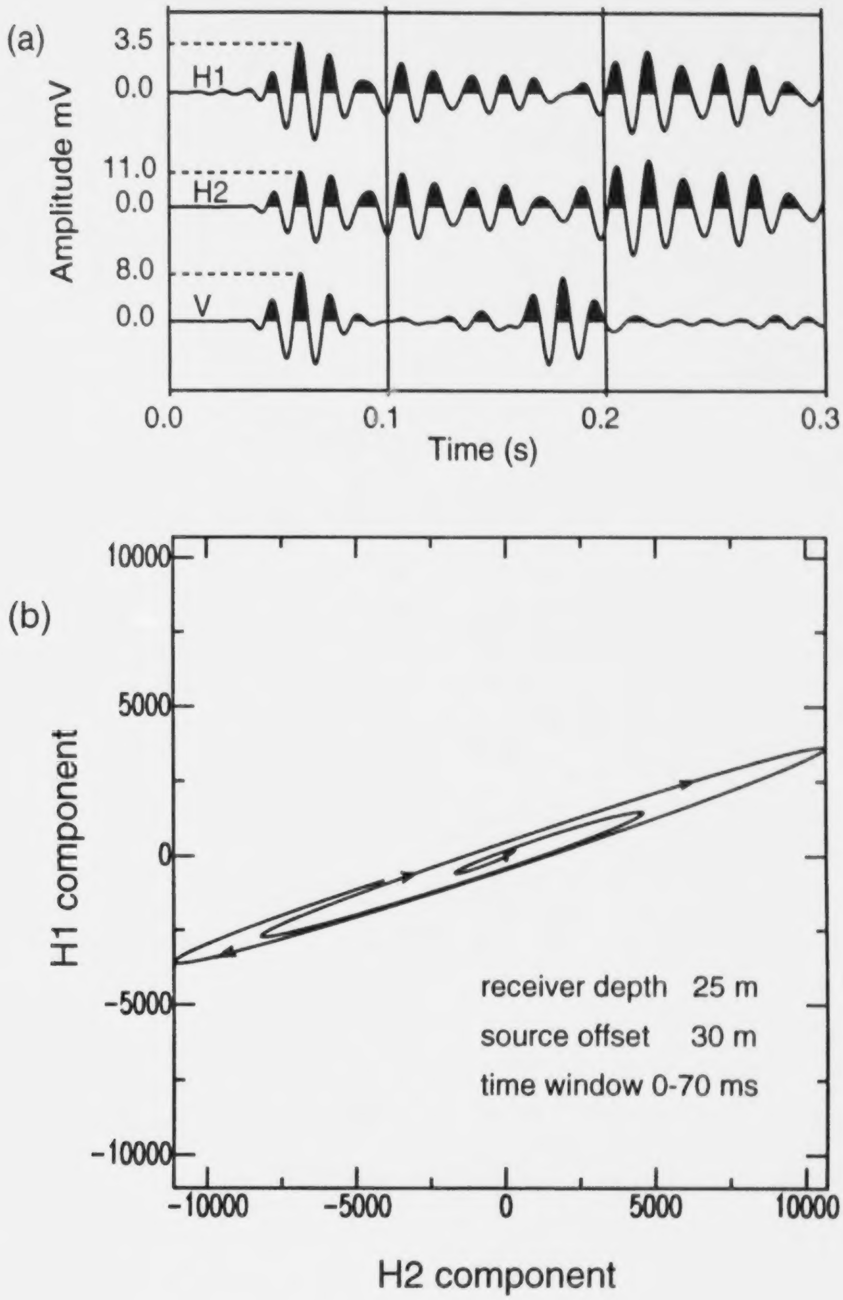

Figure 3.3. (a) The three downhole components H1, H2 and V recorded at 25 m depth for a surface source offset of 30 m, and individually normalized. The peak amplitude between 0 and 0.1 s for H1, H2, and V are 3.5, 11.0, and 8.0, respectively. (b) Hodogram of the horizontal particle motions between 0 and 70 ms. The arrows show the direction of time.

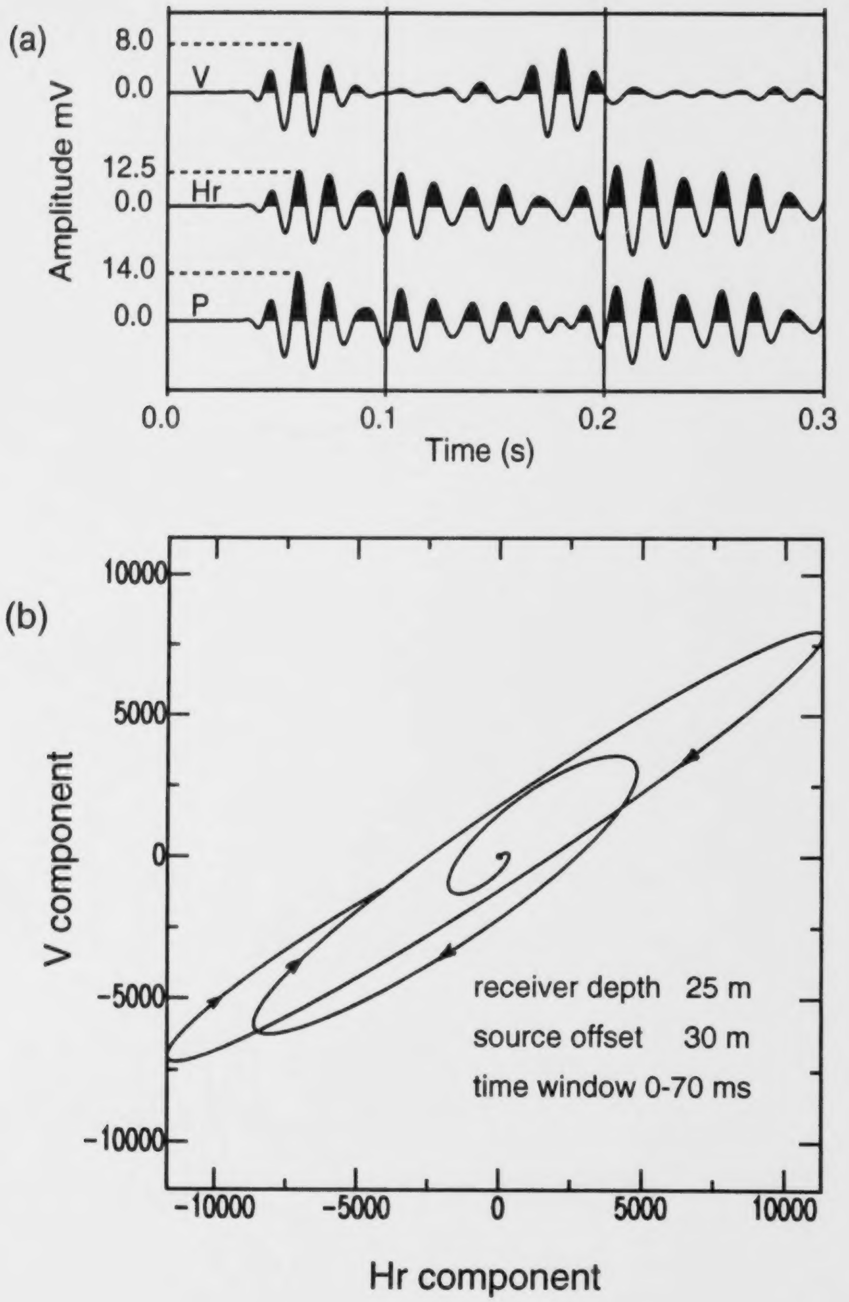

Figure 3.4. (a) Normalized components V, Hr, and P (see text for details). The peak amplitude between 0 and 0.1 s for V, Hr, and P are 8.0, 12.5, and 14.0, respectively. (b) Vertical-radial hodogram used to find polarization direction for calculation of P trace.

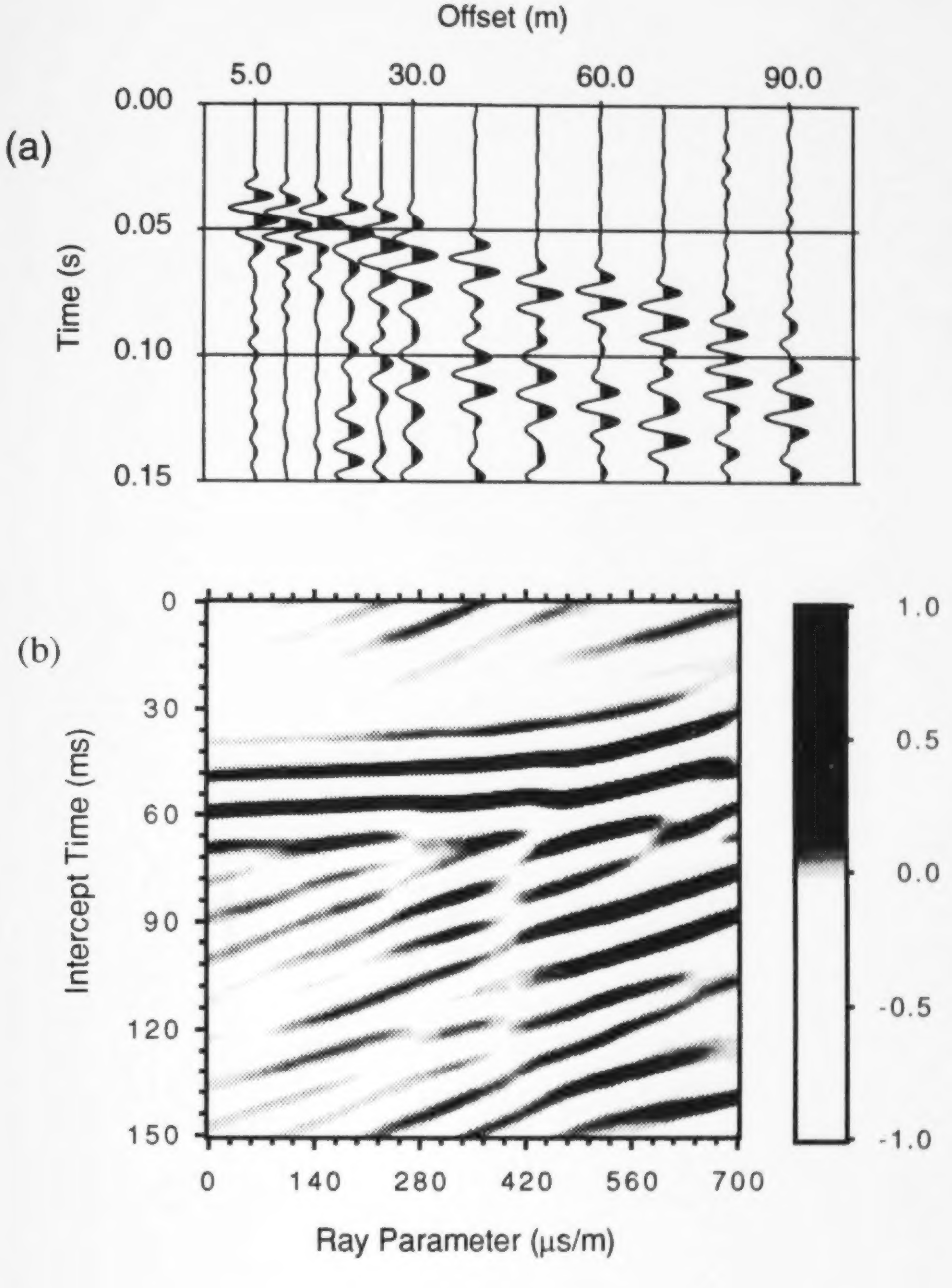

Figure 3.5. (a) P-traces for the 25-m depth receiver.
(b) τ-p mapping of the seismogram in (a).

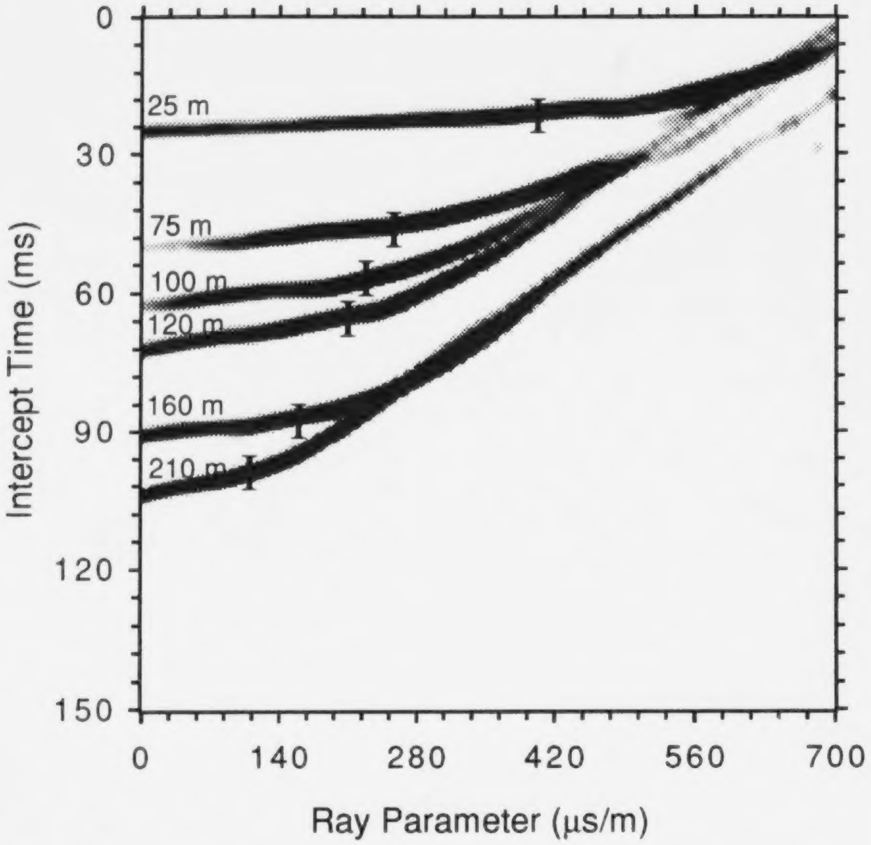

Figure 3.6. Composite *τ-p* of 6 depths from 25 m to 210 m. Each curve is Gaussian windowed and τ_0-corrected. The vertical line segments represent the horizontal ray parameter corresponding to a 30-degree angle of incidence, and which delineates the near-vertical and oblique *τ-p* sections to the left and right, respectively.

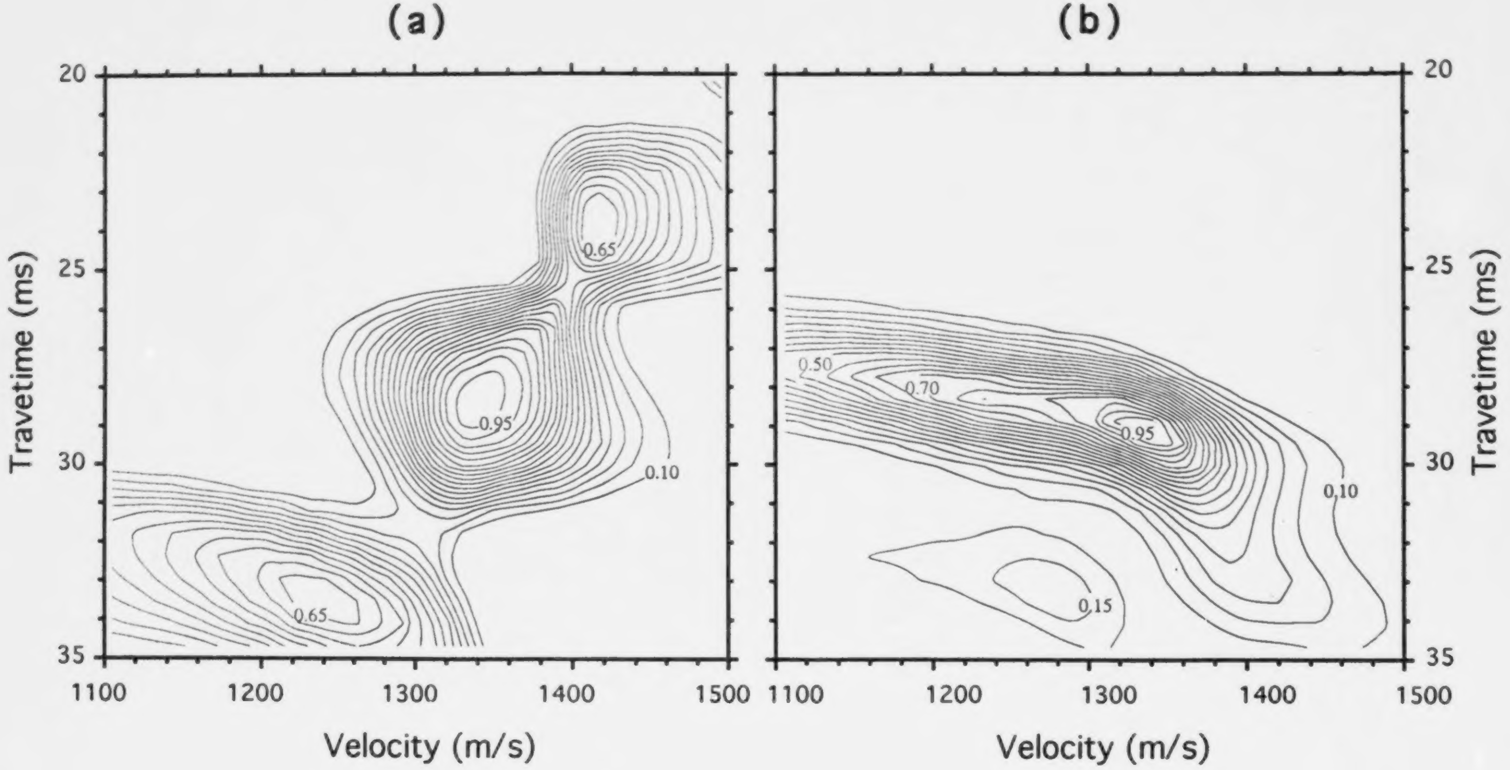

Figure 3.7. (a) Semblance map for the oblique portion of the 25-m depth curve. (b) Corresponding energy map.

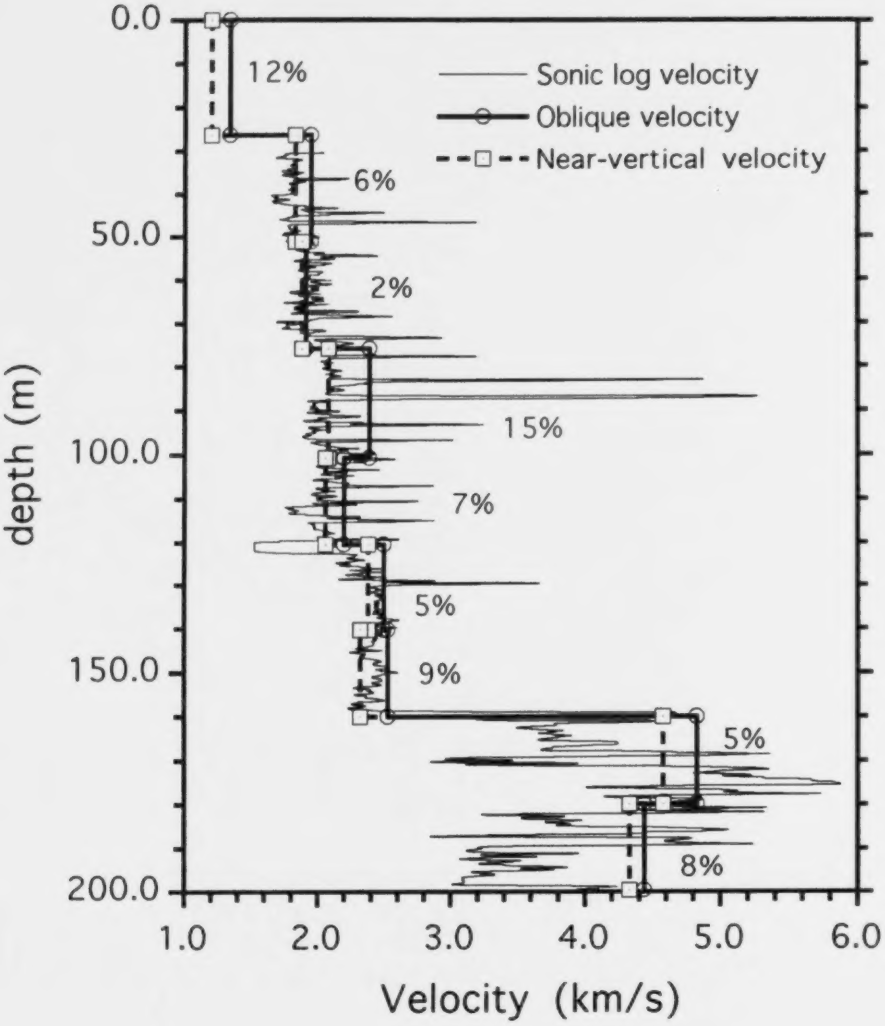

Figure 3.8. Recovered near-vertical and oblique velocities compared to sonic log velocities

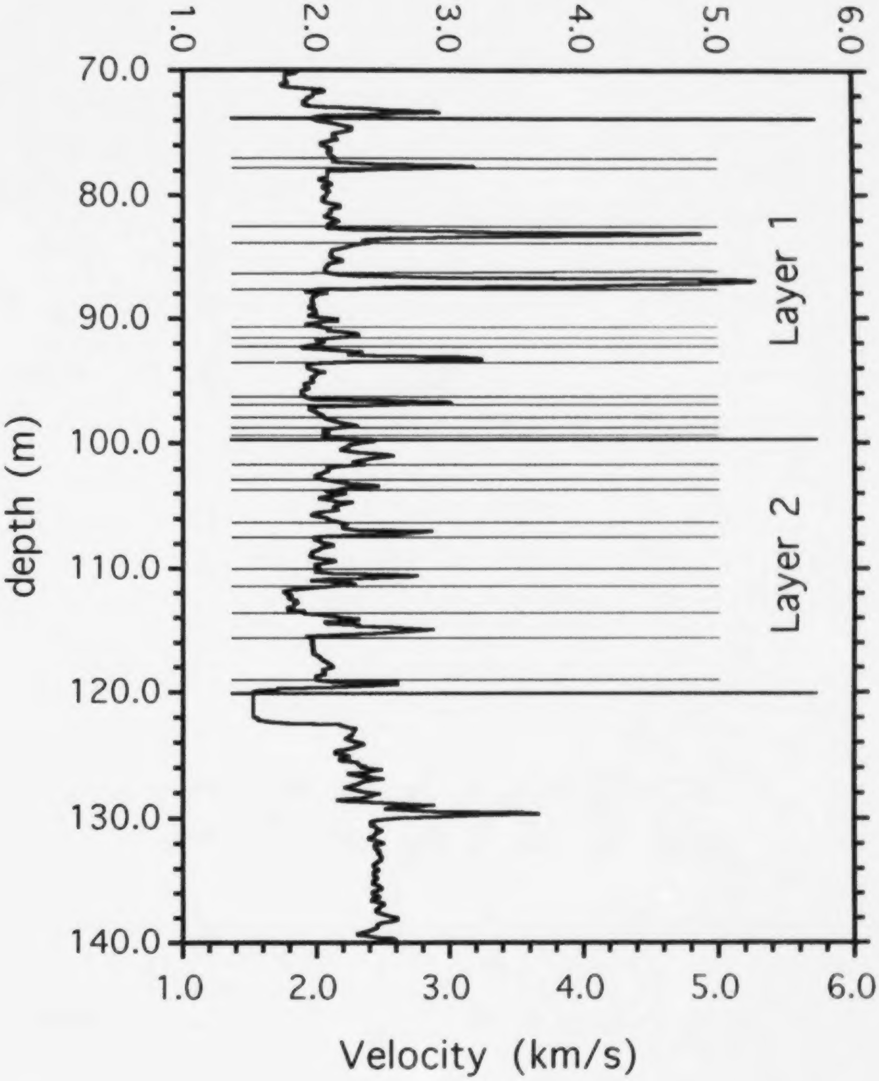

Figure 3.9 Layer between 74 m and 120 m divided into thin layers according to sonic-log velocities.

Chapter 4

4. Slowness Surface Determination From Slant Stack Curves

4.1 Introduction

Both geologic structure and rock material properties conspire to make the subsurface anisotropic to seismic wave energy. Unfortunately, this anisotropy has, until recently, been ignored because of the additional complexity it introduces in the analysis of seismic data. However, studies on seismic anisotropy carried out during the last decade show that tremendous improvements can be made when the velocity anisotropy is considered as part of a seismic analysis algorithm. Larner and Cohen (1993) showed that including the anisotropy of the subsurface layers greatly improves the quality of the final reflection seismic section. The resolution of crosswell tomographic imaging is positively affected by the inclusion of the velocity anisotropy of the subsurface (e.g. Chapman and Pratt, 1992). Further, the anisotropy of the subsurface can in itself be a good indicator of lithology, and has been successfully used as an aid in reservoir engineering (e.g. Byun et al., 1989; Vernik and Nur, 1992).

There is a long, but discontinuous, history of attempts to measure in situ anisotropy. These techniques have usually involved wellbore seismic measurements (Jolly, 1956; White et al., 1983). More recently, a three-component VSP experiment carried out by Winterstein and Paulsson (1990) on a near-surface shale formation in a shallow borehole showed that a clear shear-wave birefringence can be seen when the medium is anisotropic. Gaiser (1990) showed that both components of the slowness vector can be recovered from the spatial and depth traveltime derivatives of a ray multioffset and multidepth VSP experiment for which the sources are placed on the surface and the receivers in the wellbore that traverses a transversely isotropic medium. Miller and Spencer (1994), rearranged the dispersion equation in a linear fashion that permits a direct measurement of the elastic constants for a transversely isotropic medium with vertical axis of symmetry from the components of the slowness. In another paper (in press), Miller et al. (1994) showed that a shale sequence in the South China Sea exhibits a qP-wave vertical-to-horizontal anisotropy of 12%. Most of the above studies have exploited the wellbore geometry to extract incidence angle-dependent velocities from observed arrival times.

Schmitt and Kebaili (1993) described an approximate method of near-vertical to oblique velocity anisotropy determination in the τ-p domain using ray multioffset and multidepth VSP data. The τ-p domain has been widely used in the velocity analysis of surface seismics because of the advantages it presents over the conventional offset-time (x-t) domain. Schultz (1982), who employed a correction method called layer stripping, showed that the interval velocities for a layered isotropic medium can be directly determined from the τ-p transformation of the surface seismic data with no restriction on the source-offset reflector-depth ratio. Unfortunately, the layer-stripping technique used to determine the interval velocity for a particular layer of a sedimentary sequence requires the knowledge of the velocities and one-way vertical traveltime of all the overlaying layers, and this can lead to a large uncertainty in the interval velocities of the deeper layers. Another useful application of the τ-p mapping in seismology is plane-wave decomposition (Stoffa et al., 1981), for which the reflection and refraction events are automatically determined. The wave surface (Musgrave, 1970, 77) which is defined as the locus of the wavefront at unit time, is decomposed by the τ-p transformation procedure into plane-waves passing through the source point at time zero and propagating at phase velocities through the medium by a simple mapping of the seismic data into the τ-p domain.

The τ-p domain is a natural domain for slowness surface determination since one of its axes p; the horizontal component of the slowness, implicitly contains the angle of incidence. Further, as will be shown the τ axis can be easily converted to the vertical component of the slowness by a simple division of it by the receiver spacing of two geophones placed in the wellbore. Hake (1986) showed that the τ-p curves for a surface seismic data experiment carried out for a layered anisotropic medium have shapes that are similar to the slowness surfaces for each layer interval. However, Hake could not solve for the vertical component of the slowness from the intercept time τ because the depth of the reflectors are themselves unknown. Schmitt and Kebaili (1993) showed that layer stripping can be used to approximately determine the vertical to oblique anisotropy from the τ-p curves of a multioffset VSP data set, where the receiver depths are well known, and measured variations in anisotropy at different depth intervals along a wellbore (Kebaili and Schmitt, 1996). The technique of slowness surface determination presented here overcomes both the uncertainty of Hake's method and the cumulative layer stripping errors of Schmitt and Kebaili (1993). Here, this method is applied to determine the interval velocity in hypothetical geologies consisting of a half-space overlain by a stack of isotropic layers, of an elliptically anisotropic medium, and of a transversely isotropic medium. The theoretical basis of the τ-p method is more fully investigated and it is demonstrated that the technique extracts the plane-wave, or phase, velocities (Musgrave, 1970) of the anisotropic medium. Finally an example of an application of the modified τ-p analysis to a VSP data set acquired in a shallow borehole in northern Alberta is given.

4.2 Theoretical Background

4.2.1 Phase slowness determination

Consider a vertically inhomogeneous and anisotropic medium through which is drilled a vertical borehole. To determine the in situ anisotropy of the interval bounded by depths z_1 and z_2, let us place two receivers R_1 and R_2 at depths z_1 and z_2, respectively (Figure 4.1.).

Two seismic rays of identical ray parameter p are generated at the surface at offsets X_1 and X_2, and propagate downwards to receivers R_1 and R_2, respectively. The traveltime for each ray (Hake 1986) through this inhomogeneous and anisotropic medium from the surface to each receiver is given by:

$$t_i = \int_0^{Xi} p\ dx + \int_0^{z_i} q(z)\ dz \qquad (4.1)$$

Where $i=\{1,2\}$. The parameters p and q are the horizontal and vertical components of the slowness u, respectively, that is

$$p = \frac{\sin\theta}{v} = u \sin\theta \qquad\qquad q = \frac{\cos\theta}{v} = u \cos\theta,$$

where θ is the phase velocity angle, and v the magnitude of the phase velocity (Figure 4.2). p and q are related to the slowness u by the relation:

$$p^2 + q^2 = u^2\ . \qquad (4.2)$$

Since for a laterally homogeneous medium, the ray parameter, p, remains constant along the ray (Kennett, 1981), equation (4.1) may be written as

$$t_i = pX_i + \int_0^{z_i} q(z)\ dz\ . \qquad (4.3)$$

On the other hand, the traveltime, t_i, to receiver i can be expressed in terms of the intercept time τ_i (Schultz and Claerbout, 1978),

$$t_i = pX_i + \tau_i\ , \qquad (4.4)$$

By comparing equations (4.3) and (4.4), we get an expression for the intercept time τ_i

$$\tau_i = \int_0^{z_i} q(z)\, dz \,. \tag{4.5}$$

Suppose now that the layer interval between the receivers R_1 and R_2 is homogeneous but anisotropic. The rays could then propagate through this interval along straight lines, and the integral in equation (4.3) for receiver R_2 could be cast into the sum of an integral from the surface (z=0) to depth z_1 and the term $q(z_2 - z_1)$; that is, the product of the layer interval between the two receivers (known) and the vertical component of the slowness (unknown):

$$\tau_2 = \int_0^{z_1} q(z)\, dz + q(z_2 - z_1). \tag{4.6}$$

Combining equations (4.6) and (4.5) for the case i=1, the intercept-time difference $[\tau_2(p) - \tau_1(p)]$ is then equal to:

$$\tau_2(p) - \tau_1(p) = q(z_2 - z_1). \tag{4.7}$$

Equation (4.7) shows that the intercept-time difference for the two receivers divided by the receiver spacing $(z_2 - z_1)$ yields the vertical component of the slowness as a function of the ray parameter p:

$$q(p) = \frac{\tau_2(p) - \tau_1(p)}{z_2 - z_1} \,. \tag{4.8}$$

The phase velocity function $v(p)$ can be obtained by replacing $q(p)$ with this expression in equation (4.2), thus:

$$u(p) = 1/v(p) = \left(\left[\frac{\tau_2(p) - \tau_1(p)}{z_2 - z_1}\right]^2 + p^2\right)^{1/2}. \qquad (4.9)$$

Since the intercept time $\tau_1(p)$ represents the contribution in the τ-p domain of all the layers from the surface down to receiver R_1, and $\tau_2(p)$ from the surface to receiver R_2, the intercept time difference $[\tau_2(p) - \tau_1(p)]$ is equivalent to a stripping of the contributions above receiver R_1 in a single operation. This is equivalent to a change of datum from the surface to a horizontal plane which includes receiver R_1. This change of datum plane does not require knowledge of the velocities and thicknesses of the layers above receiver R_1, which makes equations (4.8) and (4.9) valid even if this medium is vertically inhomogeneous (e.g. layered) and anisotropic. This is advantageous over the layer-stripping method applied by Kebaili and Schmitt (1996) in that errors do not increase as a result of the successive corrections used.

4.2.2 Phase and ray velocities

The analysis of elastic-wave propagation in anisotropic media is complicated. In the case of anisotropic media, the ray velocity, $V(\phi)$, which is the velocity of propagation of energy along a path, differs from the phase velocity, $v(\theta)$, which is the velocity measured for a plane-wave propagating through the medium (Musgrave, 1970, 92-93). θ and ϕ are the angles of incidence of the phase and ray velocities, respectively (Figure 4.2a). Equation (4.9) allows us to determine the phase velocity of a plane-wave propagating in an anisotropic medium along the direction specified by the unit vector $\mathbf{n}(r)$, that is normal to the wavefront (Figure 4.2b) at any time t. When plane-waves cover the whole space, the unit vector $\mathbf{n}(r)$ takes all the possible directions, and hence the wavefront can be constructed by drawing the envelope of the plane-waves passing through the source at time $t = 0$ (Musgrave, 1970, 76). This envelope at unit time, $t = 1$, describes the wave surface. In the case of a transversely isotropic medium, the unit vector $\mathbf{n}(r)$ can be specified by the angle θ along which the plane-wave propagates, the velocity being constant for a fixed angle θ. Using Snell's law, each plane-wave can be characterized by its ray parameter $p=\sin\theta/v$. As a consequence, the mapping of the seismogram into the τ-p domain is identical to a plane-wave decomposition (Stoffa et al., 1981), and the velocity $v(p)$ in equation (4.9) is indeed the phase velocity, not the ray velocity. How comparable the ray and phase velocities are depends on how anisotropic the medium is. Berryman (1979) demonstrated that the magnitude of the ray $V(\phi)$ and phase $v(\theta)$ velocities are related by:

$$V^2(\Phi) = v^2(\theta) + \left(\frac{dv}{d\theta}\right)^2. \tag{4.10}$$

As a result, if $\frac{dv}{d\theta}$ is small, the ray velocity $V(\phi)$ can be expanded using a truncated Taylor series approximation to:

$$V(\Phi) = v(\theta)[1+\frac{1}{2v^2(\theta)}\ (\frac{dv}{d\theta})]. \tag{4.11}$$

Note that the above relations between ray and phase velocities deal with magnitudes only and not to the propagation directions corresponding to ray and phase angles ϕ and θ [Figure 4.2. (a)]. these are related via the expression (Thomsen 1986):

$$\tan(\Phi(\theta)) = (\tan\theta + \frac{1}{v}\frac{dv}{d\theta})/(1 - \frac{\tan\theta}{v}\frac{dv}{d\theta}). \tag{4.12}$$

The technique of determining phase velocity versus phase angle from the τ-p curves of common-receiver VSP traces described here is valid even for large anisotropy, since no restrictions on the τ-p mapping of the x-t seismograms, nor on the shape of the $[\tau_2(p) - \tau_1(p)]$ curve used in equation (4.9) to calculate the phase velocity, were made. The recovered phase velocities can then be converted to ray velocities versus ray angles using equations (4.10) and (4.12) if necessary. Below this technique is tested on a number of different hypothetical geologic models.

4.3 Tests on Synthetic Data

4.3.1 Multilayered isotropic medium

Consider a model consisting of three layers overlaying a half-space as described in Figure 4.3. This model is intended to represent a simple sedimentary sequence that might be encountered in practice. To determine the velocity of the half-space two receivers R_1 and R_2 are placed in the borehole at depths 300 m and 700 m, respectively (Figure 4.3.). The source was allowed to move radially along the surface from 10 m to 1500 m offset in increments of 10 m. The seismogram for this model (Figure 4.4a) is obtained by a simple convolution of the time series calculated for receivers R_1 and R_2 with an 80 Hz Ricker wavelet.

The seismogram in Figure 4.4a is then mapped to the τ-p domain using the slant-stack technique described by Stoffa et al. (1981) with the ratio filter of Moon et al. (1986) applied as described by Kebaili and Schmitt (1994). In the present study all data samples whose amplitude ratio with respect to the neighboring samples is within the range 0.7 to 1/0.7 are allowed into the slant-stack summation.

Due to the contrasting velocities and resultant bending of the rays downgoing to the receivers, the offset-time curves shown in Figure 4.4a are nearly hyperbolic, and the velocity of the half-space cannot be exactly inverted from those traveltimes. However, by combining equations (4.2) and (4.7), the ratio $\Delta\tau(p)/\Delta z$ as a function of p [equation (4.9)] represents a circle whose radius is the slowness u of the half-space; that is

$$\frac{[\Delta\tau(p)/\Delta z]^2}{u^2} + \frac{p^2}{u^2} = 1, \qquad (4.13)$$

which allows the computation of the interval velocity $v(p)$ for each ray parameter p. Note that for the isotropic case the phase and ray velocities are equal [equation (4.10) with $dv/d\theta = 0$]. The seismogram in Figure 4.4a is mapped to the τ-p domain using the technique described above, and displayed in Figure 4.4b. Given that the offset-time curves for both receivers R_1 and R_2 are nearly hyperbolic, their τ-p mappings are nearly elliptical as each is corrupted by the contributions of the layers above the receivers. The intercept time difference [$\tau_2(p)$ - $\tau_1(p)$] is computed for each ray parameter p. Then the slowness u is calculated using equation (4.9) and displayed in Figure 4.5a. The + symbols in Figure 4.5. (a) are the recovered slownesses and the solid line is the actual slowness curve which is a circle with a radius of the reciprocal of the velocity (1/3000 m/s).

To quantify the uncertainty of the recovered velocity, a q^2-versus-p^2 curve, which is a straight line of slope -1 and y-intercept the slowness u is plotted in Figure 4.5b. The solid line in Figure 4.5b represents the least-square fit line. The recovered velocity is 2984 m/s which differs from the actual velocity of 3000 m/s by 16 m/s leading to an uncertainty of 0.5%. Note that this interval-velocity determination technique is valid even if the layers overlaying the half-space are anisotropic, since no assumptions on the vertical component of the slowness [$q(z)$] in the integral term of equation (4.6) are made.

4.3.2 Elliptically Anisotropic Medium

The second synthetic example I are considering consists of an elliptically anisotropic half-space (Figure 4.6), whose vertical and horizontal ray velocities are 2000 m/s and 2500 m/s, respectively. Eventhough most sedimentary rocks will realistically have an anelliptical qP-wave anisotropy [as Thomsen's parameters are usually such that $\varepsilon \neq \delta$, (see table 1 of

Thomsen (1986)], this simple case of anisotropy is a good example for a test of the method. Further, the horizontal shear-wave component displays elliptical anisotropy in nature (Daley and Hron, 1979) and, although such waves remain to be studied fully, the present method will be applicable to this case. In the model, a receiver is placed at depth 200 m in a borehole, and sources are activated at increasing offsets radially from the borehole from 10 m to 1500 m in increments of 10 m. Since the medium is homogeneous, the traveltimes are simply the quotient of the straight-line distance between the source and the receiver and the ray velocity at the corresponding ray angle (Figure 4.2a).

A seismogram that would be recorded by the receiver is formed by convolving the time series with an 80 Hz Ricker wavelet and displayed in Figure 4.7a. Due to the variation of velocity with angle of incidence, the offset-time curve in Figure 4.7a is nearly hyperbolic and again maps into a near-ellipse in the τ-p domain (Figure 4.7b). In the case of a half-space, no second receiver is required, and no layer-stripping is needed to recover the phase velocities. For each ray parameter p of the curve in Figure 4.7. (b) the intercept time $\tau(p)$ is picked automatically and divided by the receiver depth (200 m) to yield the vertical component of the slowness. The magnitude of the phase velocity is computed using equation (4.9). This operation is carried out for all the values of p present in Figure 4.7b.

Since our velocity model is defined in terms of ray velocity versus ray angle, the ray parameters p and the recovered phase velocities v are converted back to the ray angles and ray velocities, respectively, via Snell's law and equations (4.10) and (4.12). The results are displayed in Figure 4.8, which shows that for all angles the recovered phase velocities are smaller than the actual ray velocities (solid line) as expected from examination of Figure 4.2a except at near-normal and near-horizontal incidences where the phase and ray velocities converge as they become parallel to the axes of symmetry of the medium.

The uncertainty of the fit of the observed velocities to the modeled velocities calculated via

$$E(\widehat{v}_i, v_i) = 100\,\frac{\widehat{v}_i - v(\theta_i)}{v(\theta_i)}, \tag{4.14}$$

where $\widehat{v}_i$ is the velocity of the ith measured phase velocity and $v(\theta_i)$ is the model velocity for the angle θ_i, has a mean of 0.2% and a standard deviation of 0.1% indicating that the velocity reconstruction method operates well.

4.3.3 Transversely Isotropic Medium

Sedimentary formations are usually composed of flat-lying horizontal layers of differing lithology and physical properties. Such geologic structures are rotationally symmetric about the vertical axis and are quite often considered as transversely isotropic (Helbig et al., 1987; Gaiser, 1990; Miller et al., 1994; among others). Since most sedimentary formations are expected to be transversely isotropic, it is important to apply the τ-p method to retrieve the slowness curves. I consider a transversely isotropic medium formed as the long-wavelength equivalent to a composite solid composed of 25% limestone and 75% sandstone (table 1) similar to that modeled by Carcione (1992). The elastic moduli in GPa ($=10^9\text{N/m}^2$) for the equivalent homogeneous transversely isotropic solid with a density $\rho = 2400\ Kg/m^3$ are:

$$A_{ij} = \begin{pmatrix} 33.50 & 12.10 & 9.70 & & & \\ & 33.50 & 9.70 & & & \\ & & 24.50 & & & \\ & & & 7.41 & & \\ & & & & 7.41 & \\ & & & & & 10.70 \end{pmatrix}$$

following the Voight notation (Thomsen, 1986). Synthetic vertical seismic profile seismograms are calculated for the equivalent homogeneous transversely isotropic whole space. The computation method used is the frequency-wavenumber integral method (see for example Takeuchi and Saito, 1972) combined with the complex frequency technique of Mallick and Frazer (1987). The geometry of the experiment consists of a receiver with sources deployed at a level of 500 m above the receiver. The depth axis containing the receiver simulates the borehole and the horizontal axis containing the sources simulates the earth surface. 150 synthetic traces with 10 m spacing are calculated with the closest offset trace being 10 m away from the borehole.

The calculated vertical and horizontal displacement components are shown in Figure 4.9. Both components are sensitive to qP and qSV-wave motions. This procedure predicts horizontal and vertical qP-wave ray velocities in the structure of 3736 m/s and 3195 m/s, respectively, and a qSV-wave axial velocity of 1757 m/s with a maximum value of 1978 m/s at 42°. For a transversely isotropic medium the radial component allows us to recover the energy that propagates in the horizontal plane, and allows separation of the qP and qSv waves on the basis of their particle motions. These vertical and radial component data are then rotated into the direction of propagation of the incoming rays (Figure 4.10). Figure 4.10 shows that the amplitudes of both qP and qSV-waves are enhanced by this change of coordinate frame especially those at far source offsets. After rotation, the qSV-wave component of the estimated qP-wave seismogram was greatly attenuated, and similarly for the qP-wave on the qSV-wave seismogram. This residual on both rotated seismograms is due to the fact that the polarization angle differs from the ray propagation angle in anisotropic media (Crampin, 1981).

These qP and qSV-wave seismograms are then mapped into the τ-p domain and plotted in Figure 4.11. Each ray parameter p on the ellipse-like curves in Figure 4.11 corresponds an intercept time $\tau(p)$ which is then divided by the receiver depth (500 m) to yield the vertical component of the slowness $q(p)$ by equation (4.8). The slowness curves $q(p)$ (Figure 4.12) are obtained by carrying out this intercept-time pick and simple computation for all ray parameters p used in the τ-p mappings which produced Figure 4.11.

Figure 4.12 shows the recovered (+) and actual (solid line) qP and qSV-wave phase slowness curves. The qP-wave phase slowness curve (Figure 4.12) has been successfully recovered for phase velocity angles between zero and 55°. The mean error [equation (4.14)] between the reconstructed and the input qP-wave velocities calculated using equation (4.14) is 0.4% with a standard deviation of 0.2%. Note that the maximum observed phase angle of 55° is less than the maximum ray angle (~63°) calculated for the largest source offset of 1500 m, which is in agreement with the expected phase-ray angle relationship [Figure 4.2a and equation (4.12)].

Figure 4.12 also shows that the reconstructed qSV-wave slowness curve is comparable to the modeled curve. The mean error between the reconstructed and input slownesses for phase incidence angles from 17° and 74° was 0.2% with a standard deviation of 0.2%. Note that as predicted by equation (4.12) the maximum phase angle (74°) is larger than the maximum ray angle possible (63°).

4.4 Application to Real Data

The method described above was applied to real data acquired in a shallow borehole near Fort McMurray in northern Alberta. The target layer consists of flat-lying marine shales interbedded with thin layers of high-velocity sand between depths of 75 m and 120 m (Figure 4.13). The purpose of this test is to determine if the sand-shale layer is apparently anisotropic. The layering of this interval as indicated in Figure 4.13 suggests that it will appear anisotropic to long-wavelength seismic energy according to the theoretical predictions of Backus (1962), Berryman (1979), and others.

Details of much of the experimental data acquisition have been described previously, and only a brief discussion is given here. An SIE T42 type three-component receiver was lowered in the borehole within the depth limits of the layer between depths of 75 m and 120 m, and a "Betsy gun" model 979 type was activated on the surface at increasing offsets radially from the borehole from 10 m to 160 m. A relatively uniform ray density was achieved by an uneven source offset increment, where the offset increased by 10 m for the first 80 m and by 20 m for the rest of the source locations. The seismic traces were acquired at a sampling rate of 0.1 ms on a 12 channel BISON series 5000. A piezoelectric trigger attached to the Betsy gun provided the zero time break fiducial.

The data was common depth sorted, and band pass filtered (50 – 120 Hz). The three-components were rotated to the incoming ray via hodogram analysis to estimate the downgoing transmitted qP-waves used in the analysis. The rotated qP-wave traces were normalized and static corrections applied. The final offset-time qP-wave seismogram for a depth of *75* m is displayed in Figure 4.14. (a) and shows the qP-wavelets lying along an hyperbola-like curve.

The data in Figure 4.14a are then mapped into the τ-p domain using the slant-stack technique, and implementing both the ratio and hyperbolic filters described earlier. The amplitude ratio for this filter was chosen to be equal to 0.7 and the minimum and maximum velocities for the hyperbolic filter were 1200 m/s and 3000 m/s. The τ-p mapping of these seismograms in Figure 4.14a is displayed in Figure 4.14b; the most energetic downgoing transmitted qP-wave (Figure 4.14a) has the largest amplitude in Figure 4.14b displaying three main lobes on ellipse-like curves. The intercept times for each lobe (1, 2, and 3) for various ray parameters are picked and compared with their counterpart in the *120* m depth τ-p image to determine the phase velocities using equation (4.9). Note that only one τ-p curve for each depth is required for the velocity determination. More than one τ-p curve is used for each τ-p image in order to attenuate the effects of incoherent noise that occurred during the τ-p transformation and a short discussion on how these velocities are calculated is in order. For example the circles in Figure 4.15a correspond to the velocities determined at a given ray parameter by picking the intercept times $\tau_1(p)$ from the maximum magnitude for lobe (1) and $\tau_2(p)$ for lobe 1 from the τ-p mapping for the receiver at depth *120* m (not shown). The phase velocity $v(p)$ is then computed using equation (4.9) and the two intercept times $\tau_1(p)$ and $\tau_2(p)$. This procedure is carried for each lobe leading to three velocity curves shown in Figure 4.15. (a) where the mean phase velocity (solid line) is also displayed. Figure 4.15. (a) shows that the phase velocity increases in a nonlinear fashion from 1990 m/s at normal incidence to 2235 m/s for a phase velocity angles of about 50°. The normal incidence velocity is calculated from the 10 m source offset traveltimes. The mean phase velocity curve (solid) in Figure 4.15a is the fourth order best fit polynomial to the observed phase velocities. This polynomial fit does not have any physical significance but was chosen only to allow a convenient determination of the derivative $dv/d\theta$ as required in the calculation of the ray velocity via equation (4.10). The ray velocities versus ray angle are displayed in Figure 4.15. (b). Figure 4.15. (b) shows that for impinging rays at incidence angles ranging from 0° up to about 52° the ray velocity increases in the same fashion as the velocity from 1990 m/s to 2245 m/s, which corresponds to a ray velocity variation of 12.8%.

4.5 Conclusion

The τ-p domain, for which one of the axes (p) represents the horizontal component of the slowness, is a natural domain for determination of the variations in phase velocity with incidence angle. For a ray multioffset and multidepth VSP experiment for which the receiver spacing is known, the intercept time τ can be converted to the vertical component of the slowness for each ray parameter p leading to the slowness curve. After the determination of both components of the slowness vector from vertical incidence to as near-horizontal as possible given the experimental geometry, the magnitude of the velocity for various angles of incidence can be computed. The method for slowness surface determination proposed was applied to both various synthetic models and VSP data acquired in a shallow borehole. These showed that the technique is useful even for the case of isotropic layered medium where the interval velocity was directly recovered from the τ-p

curves with no restriction on the depth of the layer interval. The observed interval velocity for the theoretical models tested differs from the actual by only 0.5%. The second example consisted of an elliptically anisotropic half-space and demonstrates that phase velocities are measured and that these may successfully be converted to ray velocities with a small error. A transversely isotropic medium is a good approximation to the elastic response of a sedimentary sequence when the typical layer thickness is small relative to the seismic wavelength. Both the qP-wave and qSV-wave slowness surfaces were recovered from a multioffset multi-component VSP experiment carried out in this medium. The match of these curves with their corresponding actual curves is quite good to a discrepancy of less than 0.4%. In application to real data, the recovered velocities for the layer interval between two receivers placed at 75 m and 120 m show that the ray velocity increases from 1990 m/s at normal incidence to 2245 m/s for a ray angle of incidence of about 52° giving rise to an anisotropy of at least 12.8% over this range of incidence angles.

References

Backus, G.,E., 1962, Long-wave elastic anisotropy produced by horizontal layering: J. Geophys. Res. **67**, 4427-4440.

Byun, B. S., Corrigan D., and Gaiser J. E., 1989, Anisotropy velocity analysis for lithology discrimination: Geophysics **54**, 1564-1574.

Berryman, J. G., 1979, Long wavelength anisotropy in TI media, Geophysics, **44**, 896-917.

Carcione, J. M., 1992, Anisotropic Q and velocity dispersion of finely layered media, Geophys. Prosp. **40**, 761-783.

Chapman, C.H., and Pratt, R. G., 1992, Traveltime tomography in anisotropic media, -I. Theory, Geophys. J. Int., **109**, 1-19.

Crampin, S., 1981, A review of wave motion in anisotropic and cracked elastic-media:

Wave Motion, **3**, 343-391.

Daley, P. F., and Hron, F., 1979, SH waves in layered transversely isotropic media-an asymptotic expansion approach: Bull. Seism. Soc. Am., **69**, 689-711.

Gaiser, J. E., 1990, transversely isotropic phase velocity analysis from slowness estimates: J. Geophys. Res., **95**, 11241-11254.

Hake, H., 1986, Slant stacking and its significance for anisotropy: Geophysical Prospecting **34**, 595-608.

Helbig, K., and Schoenberg, M., 1987, Anomalous polarization of elastic waves in transversely isotropic media: J. Acoust. Soc. Am., **81**, 1235-1245.

Jolly, R.N., 1956, Investigation of shear waves: Geophysics **21**, 905-938.

Kebaili, A., and Schmitt, D. R., 1996, Velocity anisotropy observed in wellbore seismic arrivals: Combined effects of intrinsic properties and layering: Geophysics, **61**, 12-20.

Larner, K., and Cohen, J., 1993, Migration error in transversely isotropic media with linear velocity variation in depth: Geophysics, **58**, 1454-1467.

Mallick, S., and Frazer, L. N., 1987, Practical aspects of reflectivity modeling, Geophysics: **52**, 1355-1364.

Miller, D. E., and Spencer, C., 1994, An exact inversion for anisotropic moduli from phase slowness data, J. Geophys. Res., (in press).

Miller, D. E., Leaney, S., and Borland, W. H., 1994, An in situ estimation of anisotropic elastic moduli for a submarine shale, Jour. Geoph. Res., (in press).

Moon, W., A. Carswell, R. Tang and C. Dillon, 1986, Radon transform wave field separation for vertical seismic profiling data: Geophysics **51**, 940-947.

Musgrave, M., J., P., 1970, Crystal acoustics, Holden Day.

Schmitt, D. R., and Kebaili, A., 1993, Velocity anisotropy estimation from slant stacks of wellbore seismics, Can. J. Expl. Geophys., **29**, 236-245.

Schultz, P.S., 1982, A method for direct estimation of interval velocities: Geophysics, **47**, 1657-1671.

Schultz, P. S., and Claerbout, J. F., 1978, Velocity estimation and downward continuation by wavefront synthesis: Geophysics, **43**, 691-714.

Stoffa, P.L., Buhl, P., Diebold, J.B. and Wenzel, F., 1981, Direct mapping of seismic data to the domain of intercept time and ray parameter - A plane-wave decomposition: Geophysics **46**, 255-267.

Takeuchi, H., and Saito, M., 1972, Seismic surface waves, vol. **11**, Methods in Computational Physics (ed. Bolt, B. A.), Academic Press, New York.

Thomsen, L., 1986, Weak elastic anisotropy: Geophysics **51**, 1954-1966.

Vernik, L., and Nur, A., 1992, Ultrasonic velocity and anisotropy of hydrocarbon source rocks: Geophysics **57**, 727-735.

White, J.E., Martineau-Nicoletis, L. and Monash, C., 1983, Measured anisotropy in Pierre shale, Geophys. Prosp. **31**, 709-725.

Winterstein, D.F, and Paulsson B. N. P, 1990, Velocity anisotropy in shale determined from crosshole seismic and vertical seismic profiles data, Geophysics **55**, 470-479.

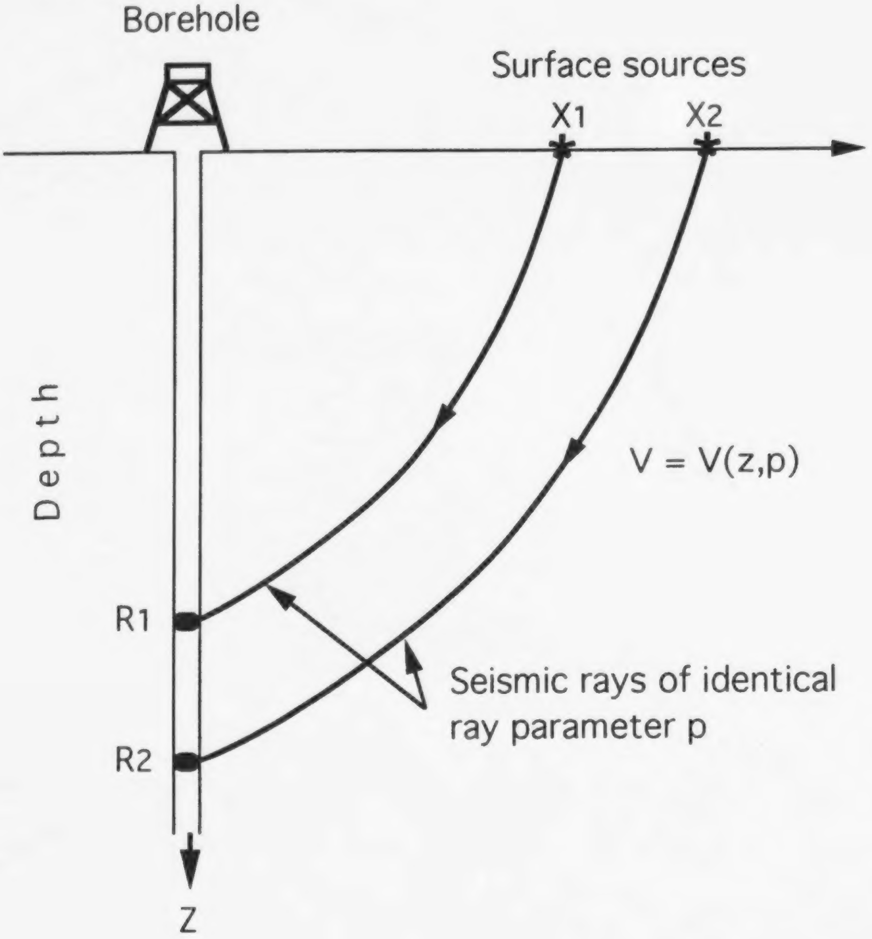
Borehole
Surface sources
X1
X2
Depth
V = V(z,p)
R1
R2
Seismic rays of identical ray parameter p
Z

Figure 4.1. Seismic rays of identical ray parameter p downgoing to receivers R1 and R2 placed in a borehole. Case shown is for isotropic media; in anisotropic media rays and corresponding plane wave normals are not generally coincident.

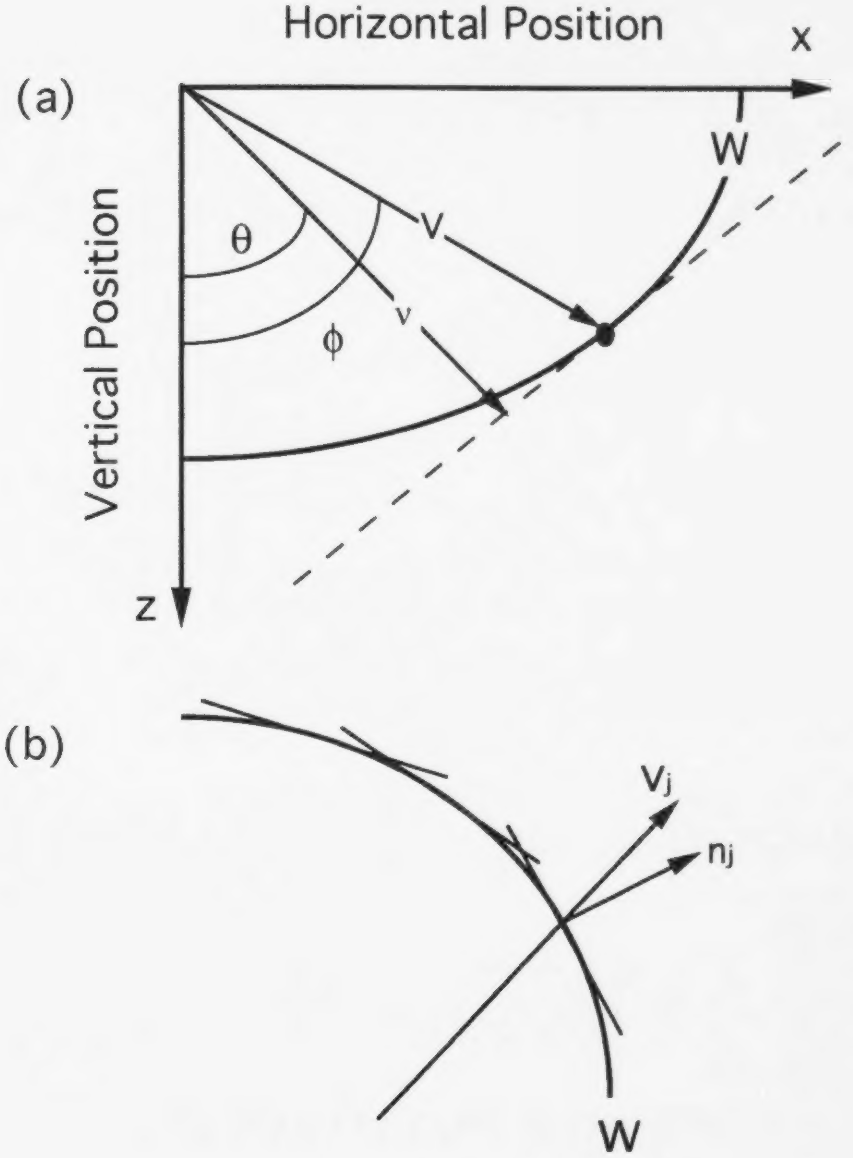
Horizontal Position
x
(a)
W
Vertical Position
V
θ
ν
ϕ
z
(b)
V_j
n_j
W

Figure 4.2. (a) Ray angle, ϕ, and phase angle, θ, in the case of an anisotropic medium. The ray and phase velocities, V, and v, do not point in the same direction. (b) Plane waves of different orientations enveloping a segment of wave surface (after Musgrave, 1970).

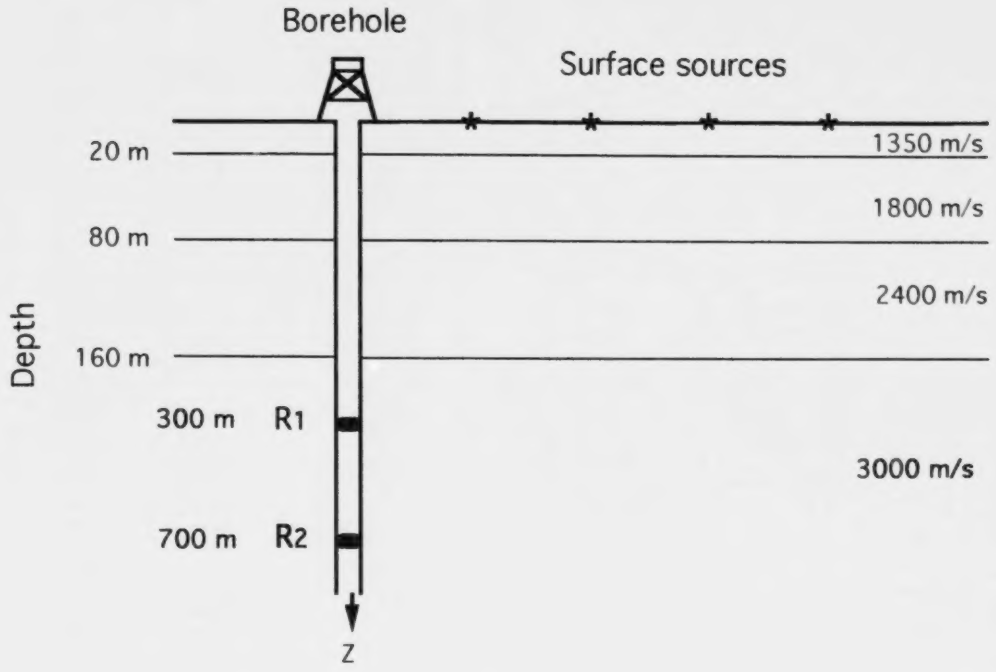
Borehole
Surface sources
Depth
20 m
80 m
160 m
300 m
700 m
R1
R2
1350 m/s
1800 m/s
2400 m/s
3000 m/s
Z

Figure 4.3. Isotropic layered medium overlying a half-space of velocity 3000 m/s. Two receivers R_1 and R_2 placed in the borehole within the half-space, are perturbed by waves generated at the surface at various offsets from the wellbore.

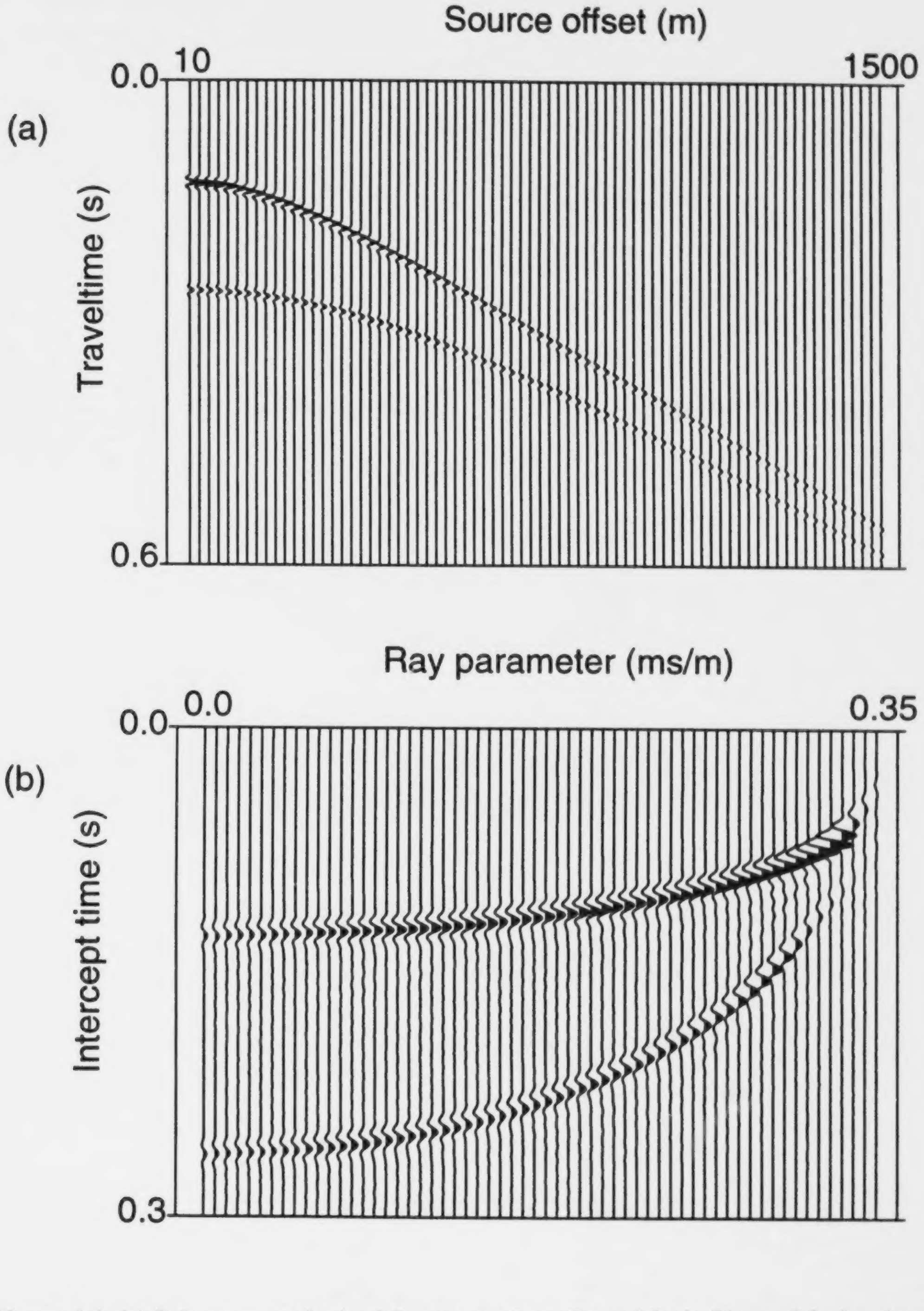

Figure 4.4. (a) Seismogram obtained for the receivers R_1 and R_2 in Figure 4.3. by simple convolution of the time series with an 80 Hz Ricker wavelet. (b) Slant stack of the seismogram in Figure 4.3a for the layered medium case.

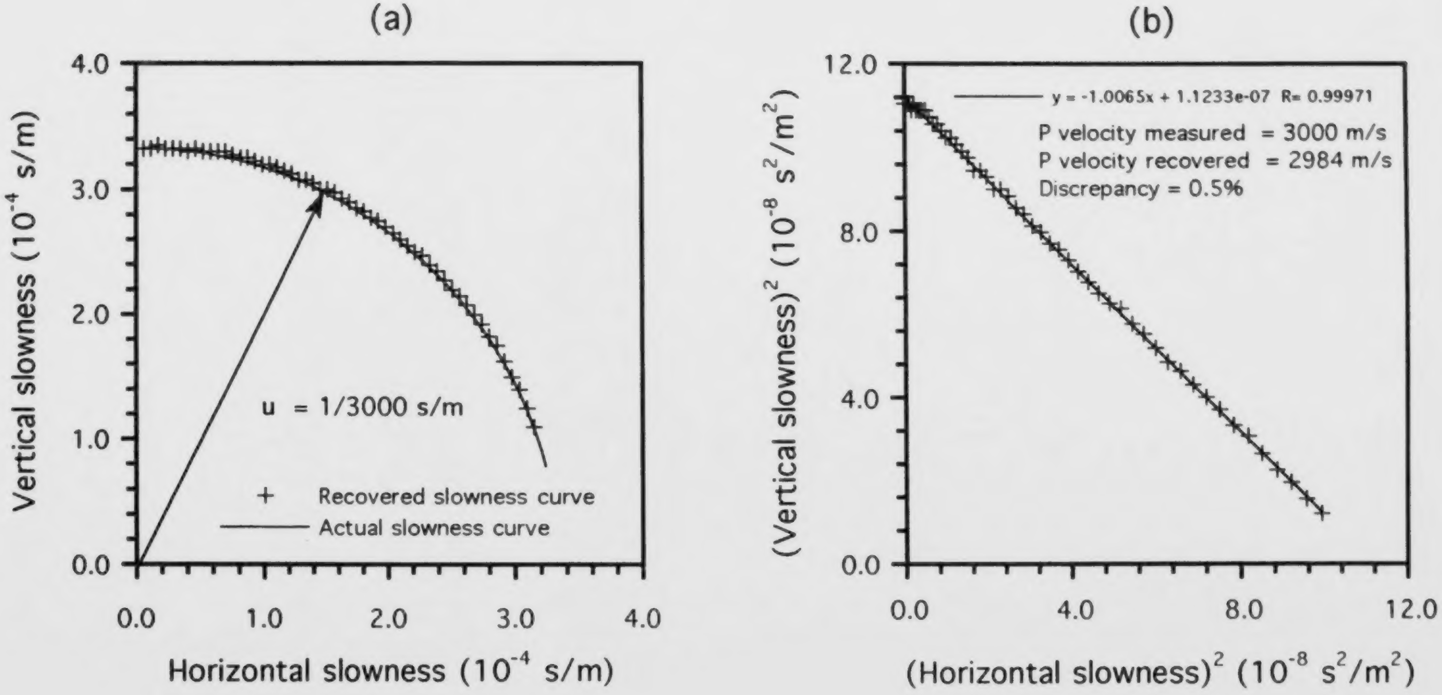

Figure 4.5. (a) Recovered and actual slowness surfaces for the isotropic half-space of Figure 4.3. (b) Recovered horizontal slowness component squared versus horizontal component squared. The graph is a straight line of y-intercept the velocity of the half-space in Figure 4.3.

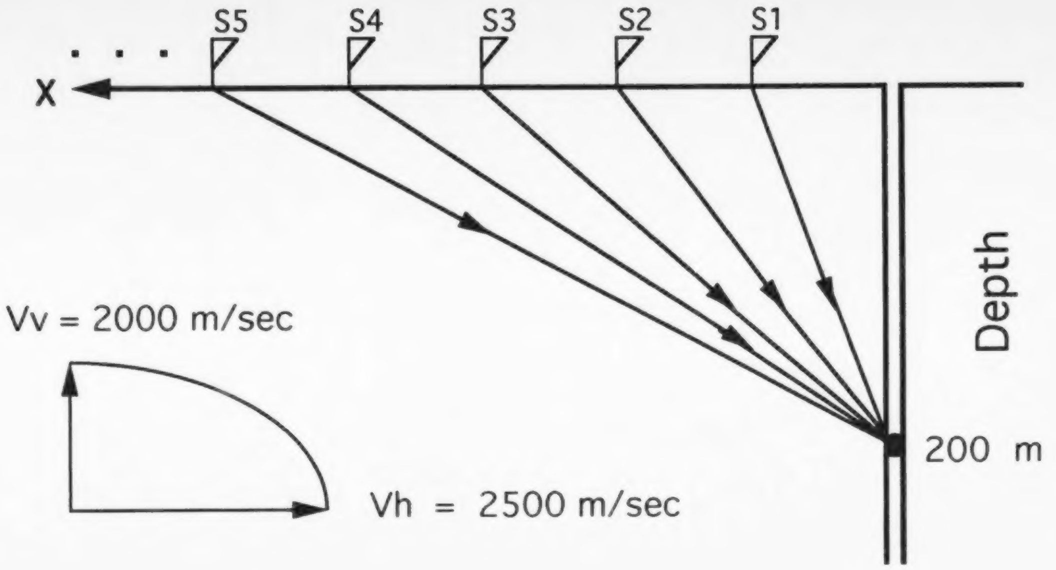

. . .
X
S5
S4
S3
S2
S1
Depth
200 m
Vv = 2000 m/sec
Vh = 2500 m/sec

Figure 4.6. Elliptically anisotropic half-space of vertical and horizontal velocities 2000 m/s and 2500 m/s, respectively, traversed by a borehole. To determine the velocity function of the half-space, a receiver is placed at depth 200 m in the wellbore.

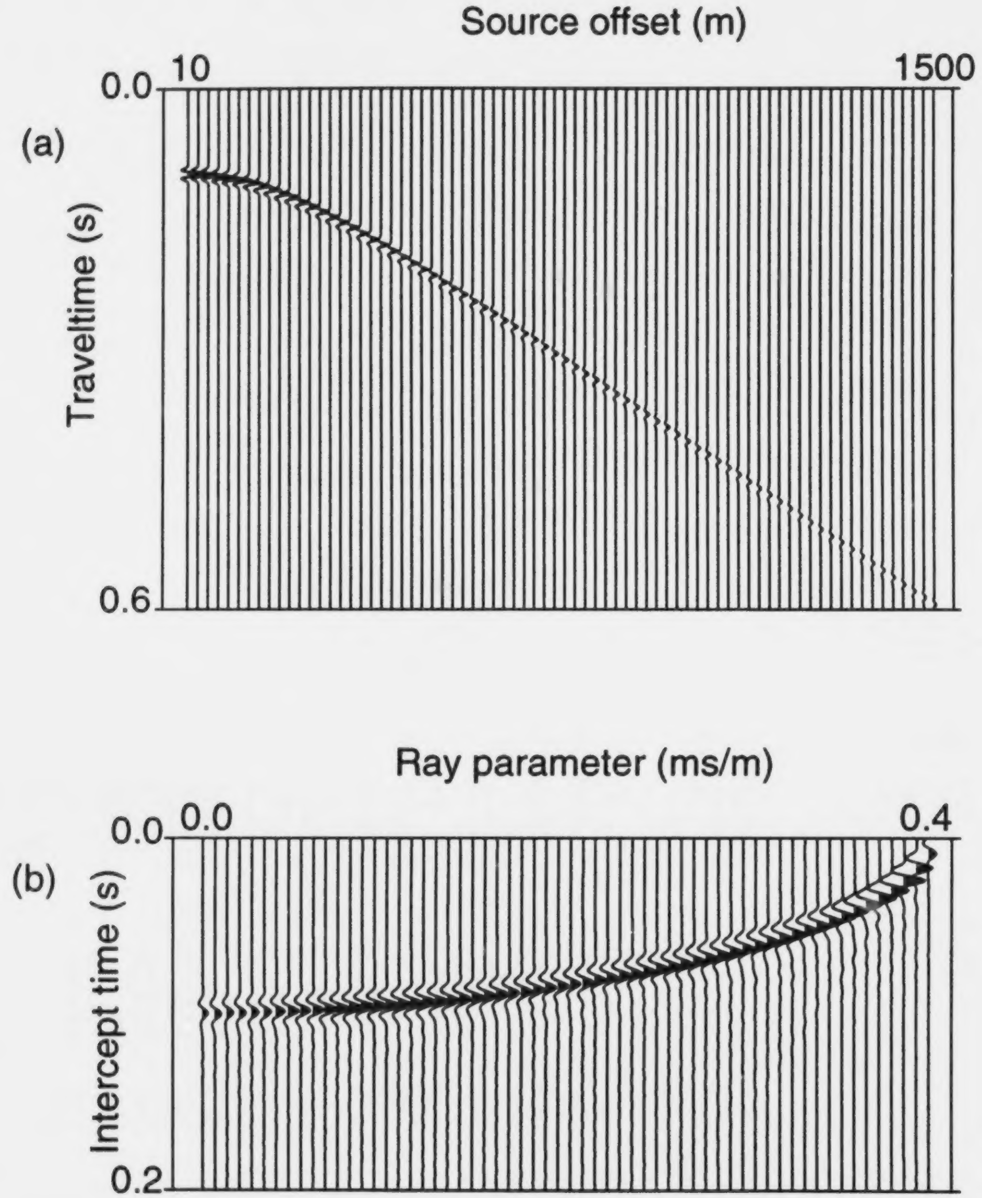

Figure 4.7. (a) Offset-time seismogram that would be recorded by the receiver at 200 m in Figure 4.6. The seismogram is obtained by a simple convolution of the time series with an 80-Hz Ricker wavelet. (b) τ-p mapping of the seismogram in (a).

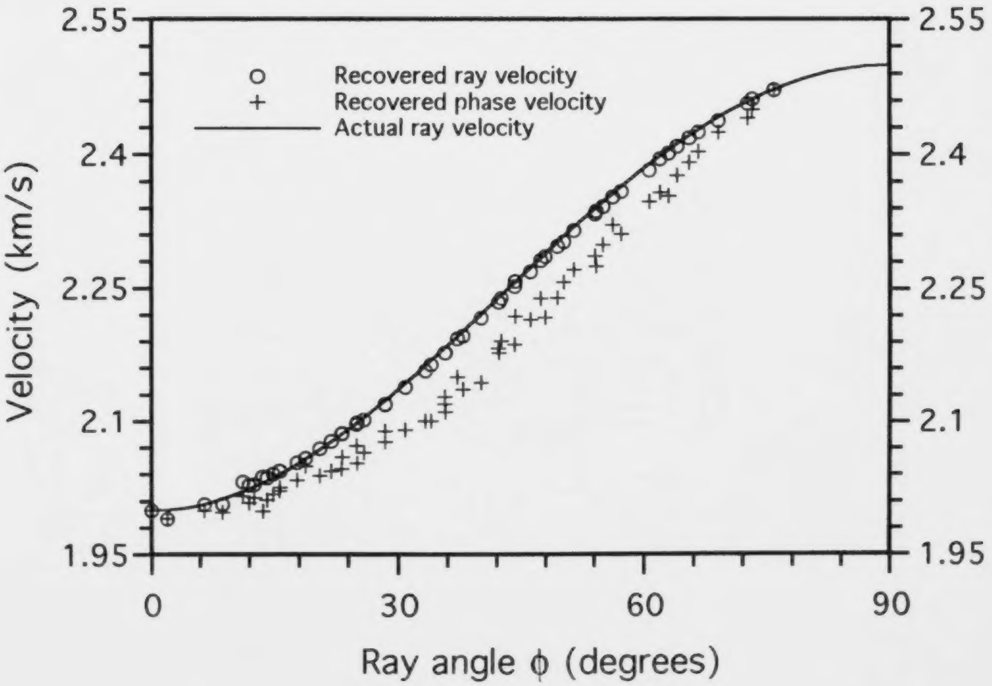

Figure 4.8. Recovered phase (crosses) and ray (open circles) velocities versus ray angle ϕ for the elliptically anisotropic medium of Figure 4.6. The actual ray velocity relationship input to the forward modeling is shown as the curved line.

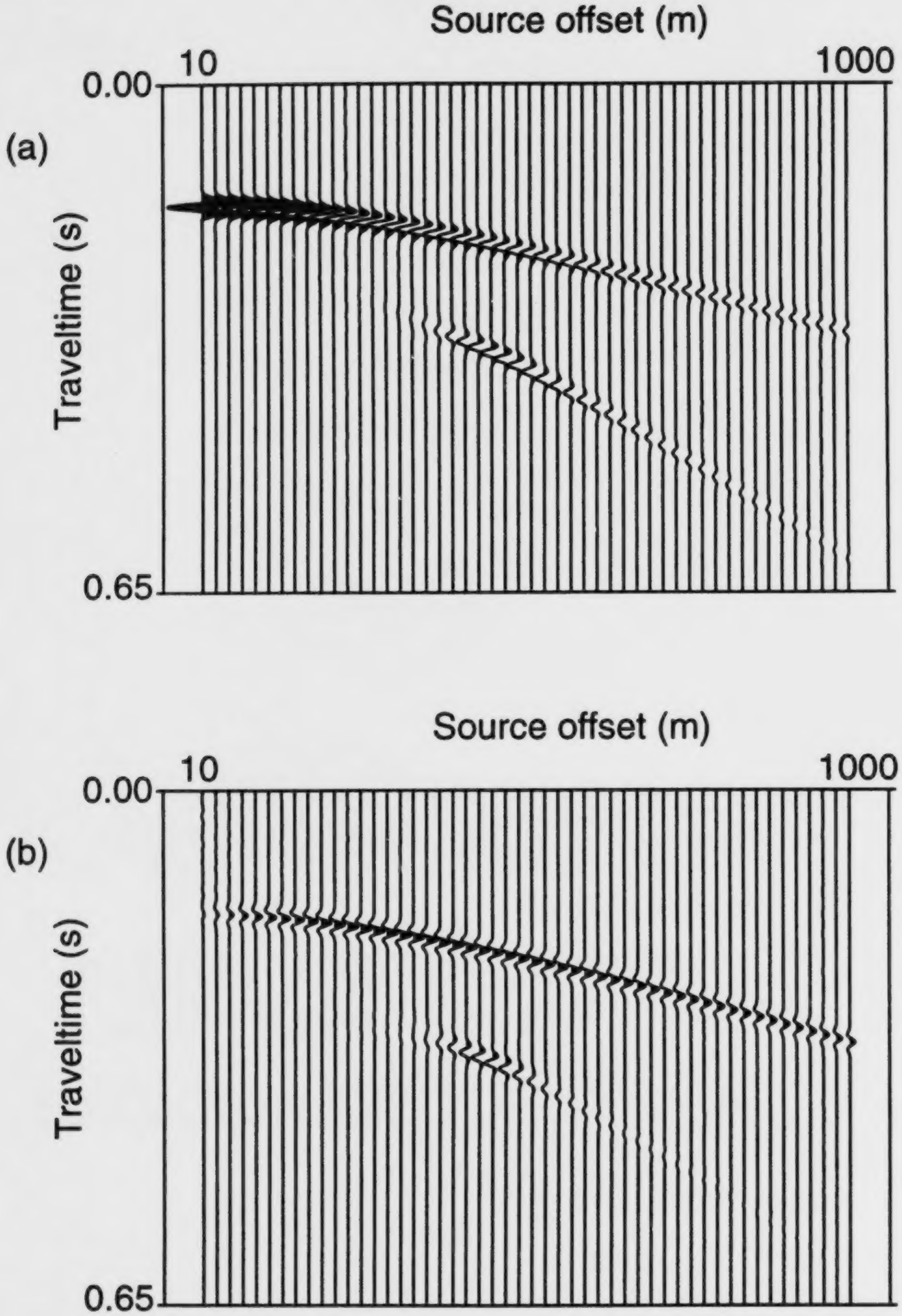

Figure 4.9. Calculated (a) vertical and (b) horizontal component seismograms for a receiver placed at 500 m in a wellbore traversing a transversely isotropic medium.

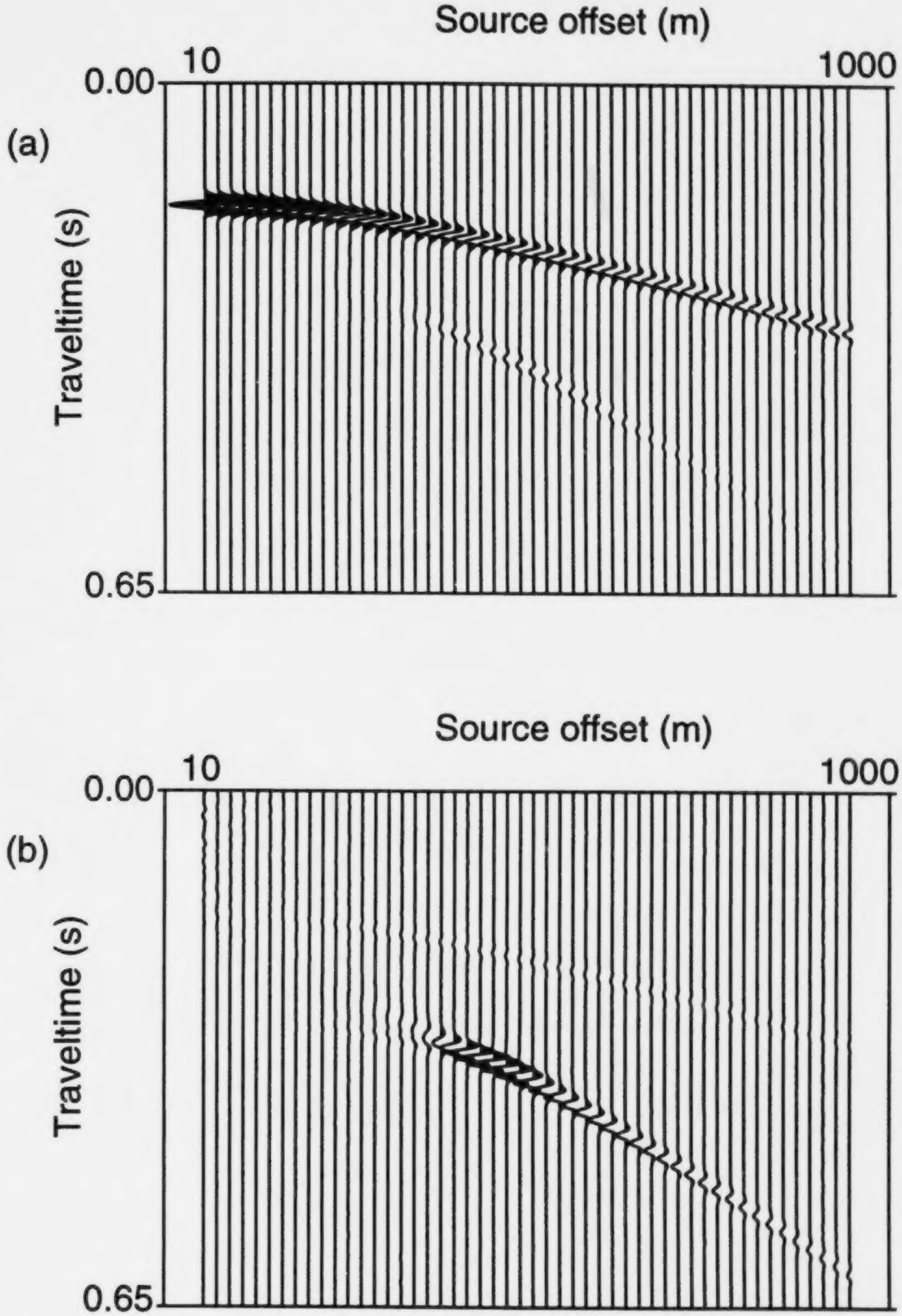

Figure 4.10. Estimated (a) P-wave and (b) SV-wave seismograms after rotation of seismograms in Figure 4.9.

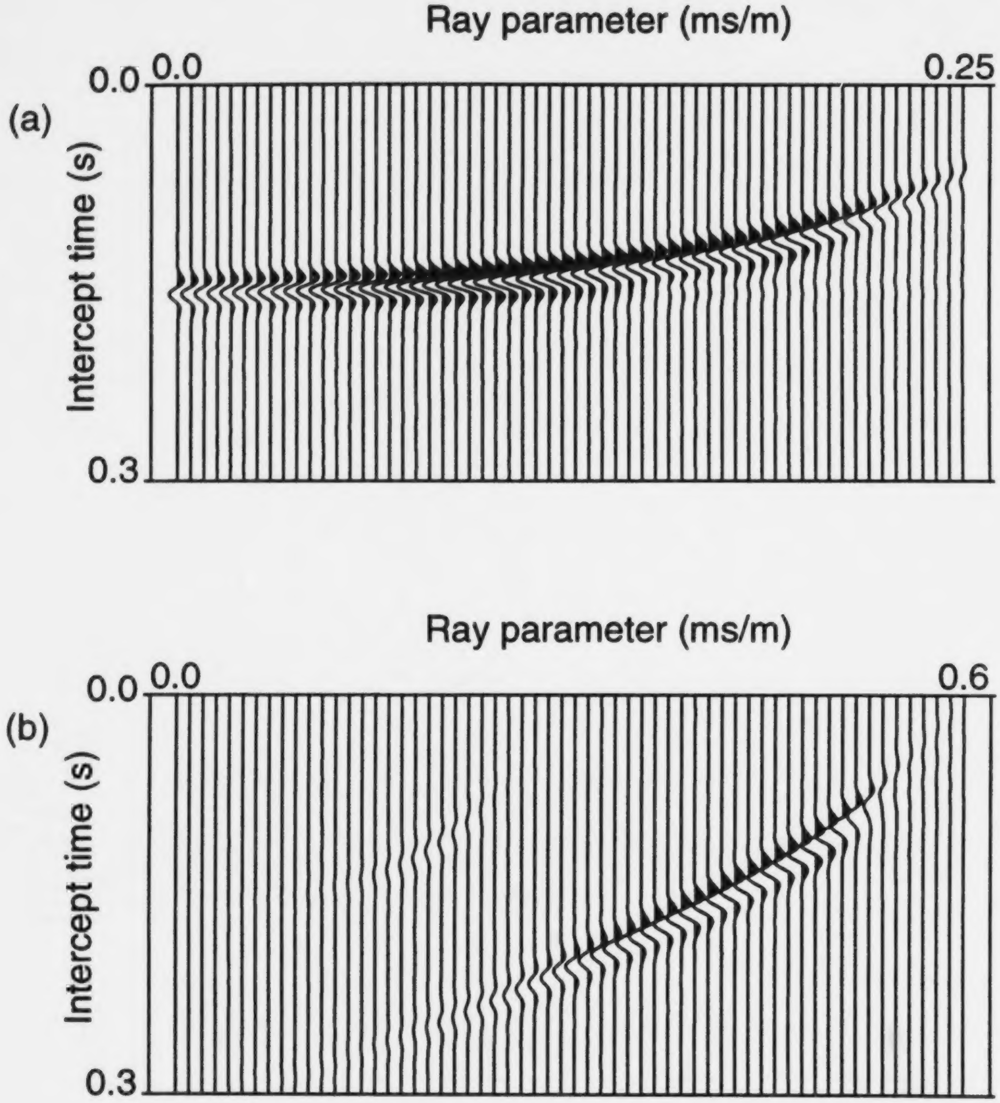

Figure 4.11. τ-p mapping of (a) rotated P-wave and SV-wave seismograms in Figure 4.10.

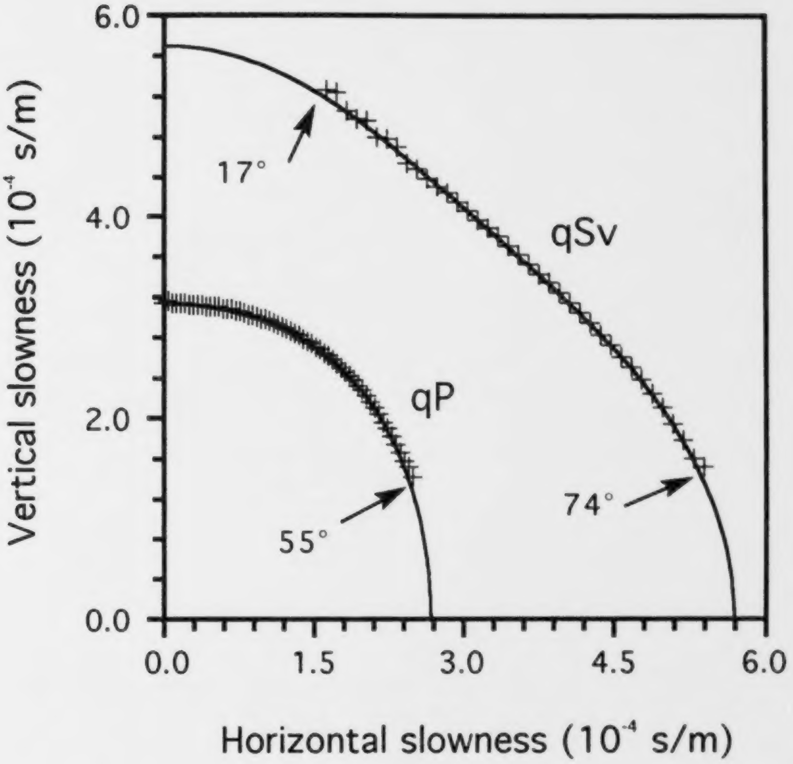

Figure 4.12. Recovered (+) and true (solid line) qP-wave and qSv-wave phase slowness surfaces.

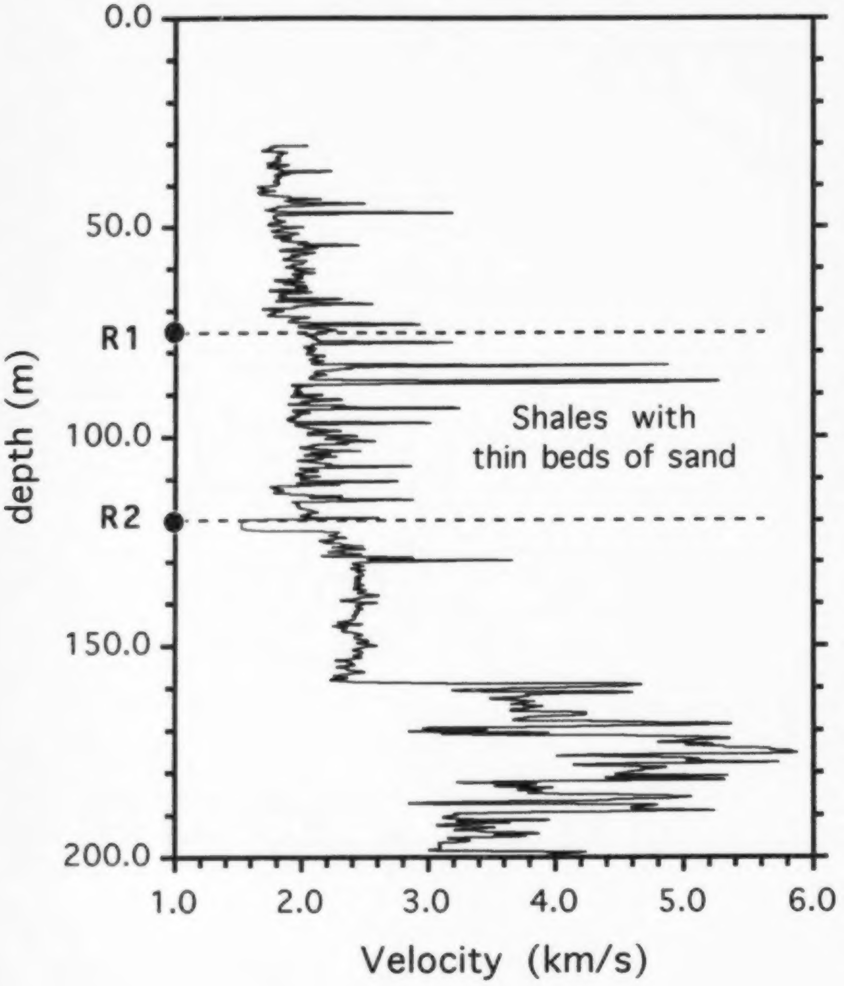

Figure 4.13. Sonic-log velocities from the borehole in which two receivers R1 and R2 are placed at depths 75 m and 120 m within a shale-sand sequence.

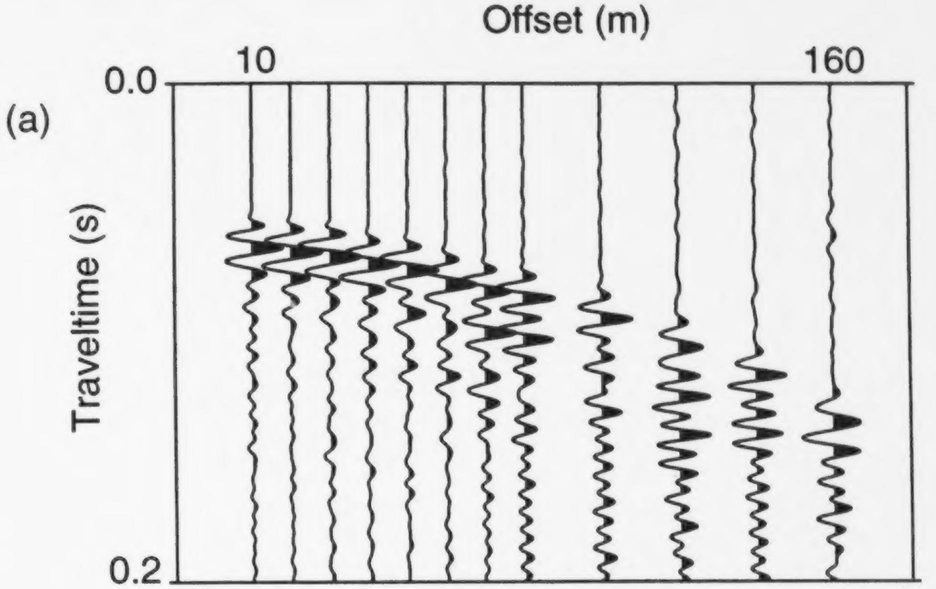

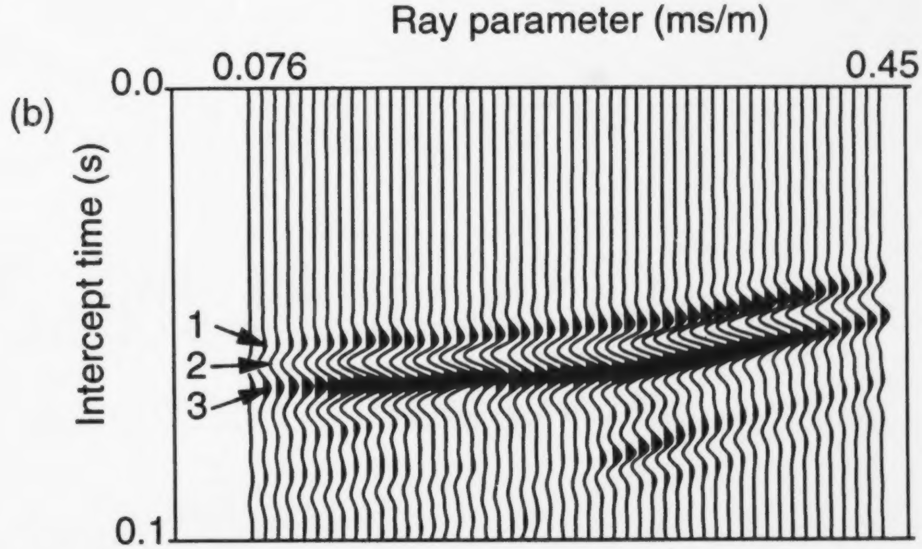

Figure 4.14. (a) P-wave seismogram for the receiver at 75 m depth. (b) τ-p mapping of the seismogram in (a).

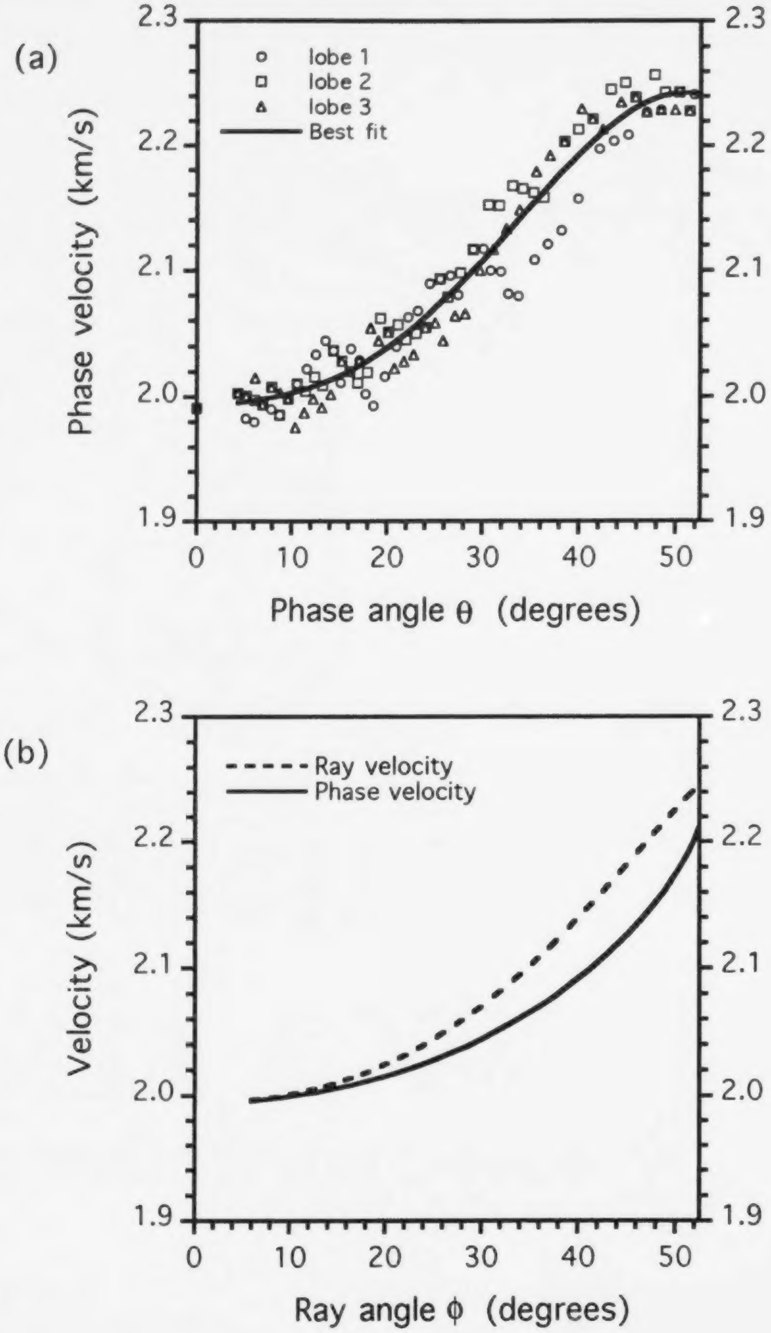

Figure 4.15. Recovered phase velocities for the layer interval bounded by the receivers at 75 m and 120 m in the wellbore.

Chapter 5

5. Ultrasonic Phase Velocities Determined Using a Radon Transformation

5.1 Introduction

Knowledge of a material's elastic properties provides important clues as to the quality of both manmade and natural materials. In principle, up to 21 independent elastic constants may be required to completely characterize a material. These could be obtained by 21 independent observations of longitudinal and shear-wave phase velocities measured in appropriate directions. In practice, however, many more observations are required for inversion of velocities to elastic constants and inversion methods usually lose generality by assuming that the measurements are made with respect to known symmetries within the material. Actual experiments are further complicated by difficult sample machining, by the question of whether phase or ray velocities are observed, and by traveltime picking errors. Resolving these experimental problems will improve our ability to determine a material's elastic properties.

Two types of velocity are defined for an anisotropic material: the ray velocity which is the velocity of energy transport along the ray path, and the phase velocity defined as the velocity of a plane-wave through the medium (Musgrave, 1970). The ray velocity is determined from the traveltime between a point source and a point receiver at a known separation. This velocity is important in applications such as acoustic tomography where the ray paths through the object must be known to invert traveltimes for structure. In contrast, the elastic constants of a material are directly related to the phase velocity via Christoffel's equation (Musgrave, 1970). Any attempt to determine the elastic tensor requires a knowledge of the phase velocities; but which velocity is determined in a given experimental configuration may not always be clear (Vestrum, 1994).

A number of ray-velocity measurement methods have been proposed. Markham, (1970) describes a point-source, point-receiver technique exploiting Snell's law for velocity measurements of an anisotropic material immersed in a fluid (water). Using similar methods, Smith (1972) determined the five elastic constants of carbon fiber composites and Gieske and Allred (1974) found the 9 elastic constants of B-Al composites.

More recently Castagnede et al. (1991) suggested a laser-generated ultrasonic point-source point-receiver technique of elastic constants determination by measuring transmitter-receiver transit times.

In the above, ray velocities are determined. However, phase velocities are required in Christoffel's characteristic equation for the determination of the elastic constants. Direct phase-velocity measurement requires that a plane-wave be propagated through the medium (e.g. Vestrum, 1994). In practice, this means that transducers must be large relative to the sample. This limits the number of measurements that may be obtained as the sample must be specially cut to allow placement of the areally large transducers and thus permits measurements along different directions. There have been a number of attempts to measure phase velocity. Rokhlin and Wang (1989), and Mignogna (1990) showed that the phase velocities may be determined from Markham's (1970) transducer arrangement. The method relies on placing the detecting transducer at the position for which the energy of the arriving pulse is maximum. In practice, the receiving transducer must scan two orthogonal axes to find this position, and positioning must be repeated for each incidence angle. Rokhlin and Wang (1992) eliminated this restriction in a double-through-transmission technique where a large reflector returns the beam through the same path to the transmitter which is used also as the receiver. However, a small nonparallelism in the sample can slightly change the refraction angle resulting in deviation of the acoustic path (Rokhlin and Wang, 1992). Further, in highly attenuative samples the wave-form shape differs from that of the reference making traveltime determination inaccurate and introducing error in the phase velocity.

Here, a Radon transformation of ultrasonic wave-forms recorded over an array of point-receivers placed on one surface of a sample is used to directly determine the phase velocity as a function of the phase angle of incidence. In the present method the experimental geometry is greatly simplified in that the sample need only be machined as a rectangular prism. A differential analysis procedure is employed which further minimizes traveltime picking errors. The laboratory method described here is a modification of a technique developed to extract phase-velocity anisotropy over depth intervals in the earth from wellbore seismic measurements (Schmitt and Kebaili, 1993, and Kebaili and Schmitt, 1996). The method is described and tested on both an isotropic plastic and an orthorhombic phenolic composite.

5.2 Theory

The Radon transform is a mapping of two dimensional function $f(x, t)$ offset-time defined in the (x, t) coordinate system into a second (τ, p) system where τ and p are the τ-intercept and slope, respectively, of a line in the x-t plane. As defined by Robinson (1982) the Radon transform is equivalent to

$$F(\tau, p) = \int_{-\infty}^{\infty} f(x, \tau + px)\, dx \tag{5.1}$$

which integrates the amplitudes $f(x,t)$ which lie along a line $y = \tau + px$; this integration maps to the point (τ, p) in the τ-p domain (Figure 5.1). In the discrete Radon transform (Chapman, 1981), the integral in equation (5.1)is replaced by a summation

$$F(\tau_i, p_j) = \sum_{k=1}^{n} f(X_k, \tau_i + p_j X_k).$$

(5.2)

In the geophysical literature, this discrete transformation is often referred to as the slant stack, in recognition of the summation of amplitudes along lines of constant slope.

Consider a prismatic sample as shown in cross-section in Figure 5.2a. Disturbances generated by a point source on one surface of the specimen will reach in-line receivers placed on another surface along rays with angles of incidence which increase with offset. If the specimen is anisotropic, each disturbance travels at a velocity dependent on the incidence angle. If the block is made of a typical plastic, the arrival times for a transmitter at a distance 2 cm from the top surface to the receiving transducers along the top surface are described by the thick black hyperbolic line in Figure 5.2b. The slant stack essentially decomposes the locus of the directly arriving wave-forms into the equivalent set of plane-waves according to their direction of propagation. This direction of propagation is represented by the horizontal slowness (ray parameter) $p = \sin\theta/v$ where θ is the angle of propagation. Alternatively, the ray parameter p is the instantaneous slope of the traveltime curve and as such the τ-p mapping is a plane-wave decomposition (Stoffa et al., 1981). Such a sorting of the received wave-forms is particularly advantageous in anisotropy analysis as the velocity varies with θ which is implicit within p.

Equation (5.2) is employed to map ultrasonic wave-forms observed by a series of in-line receiving transducers placed on the top of the surface sample and at various distances from a transmitting transducer on the side (Figure 5.3). The coordinates x and t correspond to the distance x, the receiving transducers are offset from the sample edge and the time t after the transmitting transducer has been activated, respectively. The two-dimensional function $f(x,t)$ is the amplitude of a wave-form acquired by a receiving transducer at offset positions x and time t. The coordinates τ and p in equation (5.2) correspond to the intercept time and slope of a slant line in the x-t domain, respectively. The two-dimensional function $F(\tau, p)$ is the mapped amplitude of the transformed wave-form to the τ-p domain at intercept time τ and horizontal slowness p.

It is important to illustrate why the wave-forms mapped to τ-p space can be used to determine phase velocity for various incidence angles. The phase velocity, **v**, lies along the wave normal, **n** (Figure 5.4) at an angle θ (phase angle) to the z-axis. This differs from the ray velocity, **V**, along a direction from the origin of the coordinate system to the wave surface (Schmitt and Kebaili, 1993) and makes an angle ϕ (ray angle) with the z-axis. Consider now a ray propagating through an anisotropic medium. The traveltime t of energy transport from a transmitter placed at the origin of a coordinate system to a receiver defined by a vector **x** of coordinates (x, y, z) can be written in terms of the phase slowness, **s**, (Figure 5.4b) as:

$$t = \mathbf{x} \cdot \mathbf{s} \tag{5.3}$$

where **s** is the phase slowness vector, or explicitly

$$t = x\frac{\partial t}{\partial x} + y\frac{\partial t}{\partial y} + z\frac{\partial t}{\partial z} \tag{5.4}$$

Considering only the x-z plane, equation (5.4) reduces to

$$t = x\,p + z\,q \tag{5.5}$$

where $p = \partial t/\partial x$ and $q = \partial t/\partial z$ are the horizontal and vertical components of the phase slowness vector **s**, respectively. Note that the traveltime in equation (5.3) has been expressed in terms of the phase slownesses in equation (5.5). Note that in an anisotropic medium, however, the vertical slowness q will be dependent on the angle at which the wave propagates through the material and consequently may also be considered a function of p.

With this in mind, the traveltime t for a given ray path may also be written (Figure 5.2) as

$$t = \tau + x\,p \tag{5.6}$$

By comparing equations (5.5) and (5.6) the intercept time, τ, for each ray parameter p is equal to:

$$\tau\,(p) = q(p)z \tag{5.7}$$

The vertical component of the phase slowness q in equation (5.5) may then be obtained by dividing equation (5.7) by the vertical distance between the transmitter and the top surface, at the level of the receiver line.

The magnitude of the phase velocity, **v**, is the reciprocal of the slowness and is computed from the horizontal and vertical components of the slowness, p and q, respectively:

$$v = 1/|\,\mathbf{s}\,| = \left[p^2 + q^2(p)\right]^{-1/2} = \left[p^2 + \left(\frac{\tau(p)}{z}\right)^2\right]^{-1/2} \tag{5.8}$$

Equation (5.8) involves known quantities that allow the computation of the phase slowness.

As with picking of the first arriving energy in ultrasonic wave-forms, the intercept time, τ, is not always evident to pick on a τ-p mapping. To minimize this problem, the difference between the τ-p curves for two transmitting transducers placed at different known distances from the receiving line on the top surface (Figure 5.3) is used. If z_i is the vertical distance from the top surface of the specimen for transmitter i, the intercept time τ_i

for that transmitter is from equation (5.7).

$$\tau_i(p) = q_i z_i \tag{5.9}$$

For two transmitters at distances z_1 and z_2 with $z_1 < z_2$, then, for each ray parameter p, the intercept time τ_1 for the transmitter at distance z_1 can be subtracted from that of the transmitter at distance z_2 to yield an expression for the vertical slowness component q as a function of the transmitter spacing

$$q(p) = \frac{\tau_2(p) - \tau_1(p)}{z_2 - z_1}. \tag{5.10}$$

Equation (5.8) may then be adapted simply as

$$v(p) = \left[p^2 + \left(\frac{\tau_2(p) - \tau_1(p)}{z_2 - z_1} \right)^2 \right]^{-1/2} \tag{5.11}$$

The advantage equation (5.11) presents over equation (5.8) is that a corresponding phase of the wave-form (e.g. peak or trough) is selected for both τ-p mappings and the difference $\tau_2(p) - \tau_1(p)$ is then used in equation (5.11) to compute the phase velocities. Use of equation (5.11) assumes that the wave-forms are not substantially changed by attenuative processes.

It is worthwhile to note that equation (5.11) provides a continuous measure of the velocity versus the horizontal slowness p. This continuity of measurement allows ready conversion between phase and ray velocities which requires knowledge of the derivative of phase velocity with angle of incidence.

In planes of material symmetry only the ray angle, ϕ, and ray velocity, V, are related to the phase angle, θ, and phase velocity, v (Thomsen, 1986) by:

$$V^2(\phi) = v^2(\theta) + \left(\frac{dv}{d\theta}\right)^2 \tag{5.12}$$

$$\phi(\theta) = \theta + \tan^{-1}\left(\frac{1}{v}\frac{dv}{d\theta}\right) \tag{5.13}$$

Note that this technique can be used to determine the phase velocities in any plane containing the transmitters and receivers. The ray velocities in directions not coincident with a plane of symmetry may be separately obtained using conventional transmission methods.

5.3 Experimental Configuration

The analysis described above is tested on two materials. The first is an isotropic acrylic annealed after machining to relax residual stresses. Velocities were also measured by the pulse transmission method on the acrylic sample using 2.54-cm diameter, 0.7-MHz piezoelectric ceramic transducers along the three orthogonal directions *(x, y, and z)*. The observed velocities of 2826 m/s, 2780 m/s, and 2795 m/s, respectively, confirm that the sample is isotropic to within experimental errors adding up to about 1.5 percent. The second is an orthotropic phenolic with three planes of symmetry (Brown et al., 1991; Cheadle et al., 1991; Nayfeh et al., 1995). This industrial laminate is composed of canvas fibers arranged in two orthogonal orientations and bonded by a phenolic resin. The fibers are straight in one direction (the wrap) and woven in the direction perpendicular to it (the weave or woof). The system of coordinates adopted for this experiment is such that the *x*-axis coincides with the weave, the *y*-axis with the warp, and the *z*-axis with the planes perpendicular to the fibers. Both samples were machined into right rectangular prisms. The plexiglass and phenolic samples have dimensions 9.7 x 4.7 x 13.6 cm measured to an accuracy of 0.05 cm. The phenolic specimen is cut along the three planes of symmetry.

Ultrasonic transducers were cut to dimensions of approximately 2 mm x 2 mm from

PZT5 piezoelectric ceramic (American Piezoceramic). The transducers were coupled to the samples with a silver paint and damped by backing with a tungsten-epoxy matrix. The same sensor configuration was used for both the isotropic and anisotropic samples. A line of equally spaced receiving transducers on one surface of the specimen and transmitters on another surface perpendicular to the first, and such that the transmitters and receivers are within the plane of interest (Figure 5.3).

For the isotropic acrylic sample, only one plane was investigated with 20 receivers aligned on the top surface with 0.5 cm spacing, and 3 transmitters placed on a side surface in the same plane as the receivers at distances 1 cm, 2 cm, and 3 cm from the receiving line (Figure 5.3).

In the orthorhombic sample, transducer arrays were placed along the three planes of symmetry (*x*-*z*, *y*-*z*, and *x*-*y*) and one diagonal plane containing the 2 axis and at 43° from the *y*-*z* surface. Four transmitters at depths of 1 cm, 2 cm, 3 cm, and 4 cm below the surface containing a receiving line of transducers were used in each of the arrays.

The transmitters were activated by a 300-V spike provided by a high-voltage pulse generator/receiver (JSR SYNERGETIC, model PR 35). The response of the receiving transducer was preamplified and band-pass filtered with a 0.3-to-10 MHz pass-band prior to digitization at an 8-ns sampling rate on a Tektronix TDS 520 digital oscilloscope. A final acquired wave-form represents an average from at least 100 individual pulses. The final digitized wave-forms were transferred to a Quadra 650 computer over the GPIB bus and to a Sun SPARC 5 workstation for analysis.

5.4 Results And Discussion

5.4.1 Acrylic sample

A series of the recorded wave-forms which share the same transmitting transducer are digitally band-pass filtered (300 – 850 KHz) and plotted. An example of such an *x*-*t* plot obtained on the plexiglass sample is shown in Figure 5.5a. The first arriving pulses follow the expected locus of a hyperbola in Figure 5.5. These are the longitudinal waves transmitted directly through the sample. Other later arrivals include surface waves and the longitudinal waves reflected from the bottom surface. Using equation (5.2) the wave-forms in Figure 5.5a are mapped into the τ-p domain and plotted as shown in Figure 5.5b. Each data point in the τ-p domain is obtained by summing data samples in Figure 5.5a along a straight line (slant-stack) that is tangent to the curve of slope p and y-intercept τ. A tangency condition is satisfied by implementing in the mapping code the ratio filter suggested by Moon et al. (1986). This selective filter checks each sample on the line of summation against its left and right neighboring points. The data sample is accepted into the summation only if the ratio of its amplitude to that of each neighboring sample is larger than a predetermined value. In our case this ratio is fixed at 0.5 for all τ-p mappings. Additionally, a velocity-sensitive hyperbolic filter (Tatham, 1984) is introduced in the τ-p mapping to attenuate the edge effects due to band-limited data, and to map only those acoustic wave-forms falling within a predetermined velocity range of $V_{\min} = 2200$ m/s to $V_{\max} = 3500$ m/s. Since ray parameter p and velocity V are related to each other by Snell's law, this restriction in velocity will allow each sample $f(x,t)$ in equation (5.2) to contribute to a certain number of slopes or p-values in the range $p_{\min}$–$p_{\max}$ (Tatham, 1984). The results in the τ-p domain were finally band-pass filtered with the same filter applied to the recorded wave-forms (300–850 KHz).

To determine the slowness curve of the specimen in the plane containing the transmitters and receivers, a coherent trace-to-trace feature (a trough or a peak) of the wave-forms in the τ-p domain (Figure 5.5 b) is selected, and the intercept times $\tau_1(p)$ of this feature at each p is determined. The intercept times $\tau_2(p)$ for the same feature on a corresponding τ-p mapping for a different transmitter are also found. The difference for each ray parameter p, $[\tau_2(p) - \tau_1(p)]$ is then calculated and divided by the spacing $(z_2 - z_1)$ of the two transmitters to yield the vertical component q of the phase slowness [equation (5.10)].

In practice, the τ times are chosen for a number of different troughs and peaks in the τ-p wave-forms in order to reduce random error. The resulting slowness curves can then be used to compute an average curve such as the one displayed in Figure 5.6a. The symbols along the p and q axes of Figure 5.6a show the directly measured slownesses for vertical and horizontal incidence angles. For this particular case where the sample is isotropic the data in Figure 5.6a fall closely as expected along a circle of radius $|\mathbf{s}|$; the solid-line arc of a circle in Figure 5.6a represents the slowness curve calculated using this velocity. Further, equation (5.8) may be written as

$$q^2 = (1/|\mathbf{s}|)^2 - p^2. \qquad (5.14)$$

The graph q^2 versus p^2 is linear for the isotropic acrylic and has a y-intercept equal to the reciprocal of the velocity of the specimen as shown in Figure 5.6 (b). Linear regression of the data in Figure 5.6b yields a velocity of 2776 ± 20 m/s, which compares favourably with 2830 ± 23 m/s measured independently by pulse transmission along the axes; this discrepancy is less than 1%.

The velocities computed using equation (5.11) are sensitive to the receiver spacing and the errors on the intercept-time picks. The errors in recovered velocities are proportional to the reciprocal of the squre of the receiver spacing, and to the relative error on the intercept-time difference as well. The larger the receiver spacing is, the more accurate the recovered velocities are. However, as the receiver spacing increases, the maximum available angle of incidence decreases. One needs to find a balance between the range over which velocities may be determined and the accuracy of their determination.

5.4.2 Phenolic sample

The phenolic specimen is anisotropic with three planes of symmetry as described in Cheadle et al. (1991) and more recently by Vestrum (1994), who used the pulse-transmission method to measure the traveltimes that were then inverted to obtain slowness surfaces. He first measured longitudinal and transverse phase velocities using large aperture transducers in 9 directions on an 18-face specimen. Ray velocities were recovered from a 23-cm diameter sphere of the same phenolic with the pulse-transmission method using small aperture transducers.

Here, the anisotropy of the sample is investigated in each of the three planes of symmetry and in one nearly diagonal plane aligned perpendicular to the *x-y* plane (plane of fibers) and at an angle of 43° with respect to the *y-z* plane (Figure 5.7). The data were analysed using the same sequence as described above for the isotropic acrylic sample. As a reminder, the velocities are recovered from intercept time differences, $\Delta\tau$, which makes the method less sensitive to systematic traveltime pick errors. The methodology is outlined only for the *(y-z)* plane, which contains the straight fibering, but the final results for all planes will be presented. Two series of wave-forms and their τ-p mappings corresponding to transmitters at 2 cm and 4 cm are shown in Figures 5.8 and 5.9, respectively. The null traces at small ray parameters, p, result from the hyperbolic filter. The intercept times, τ, for three different coherent features of these τ-p wave-forms are selected and labeled (1, 2, and 3) for both depths, and the intercept times, τ, for each of them are determined for both transmitters. Equation (5.11) is finally used to compute the phase velocity for each ray parameter present in the data.

Figure 5.10 summarizes the variations of phase velocity versus p for the *y-z* plane obtained for the plots in Figures 5.8b and 5.9b. The average phase velocity in the *y-z* plane increases with ray parameter from 2826 m/s along the *z*-axis (perpendicular to the fibers) to 3300 m/s for the maximum ray parameter corresponding to a phase incidence angle, θ, of 80°: a velocity anisotropy of 17% over this range of incidence angles. An uncertainty of 20 m/s is estimated from the variation in the velocities determined by picking of the different wave-form features. Having a near-continuous measure of the phase velocity with ray parameter, as in Figure 5.10, is a considerable advantage in that the corresponding ray velocities may be determined using equations (5.12) and (5.13). The ray parameters are easily converted to phase angles, θ, allowing $dv/d\theta$ in equations (5.12) and (5.14) to be determined. The recovered phase velocity as a function of the phase angle θ was fit with a fourth-order polynomial that has no physical significance and was chosen for convenience only. Figure 5.11a shows that, for all ray angles between 15° and 80°, the ray velocity is larger than the phase velocity as it must be.

The phase velocities recovered using the τ-p method are in good agreement with those directly measured by Vestrum (1994) with an average discrepancy of 1%. However, Figure 5.11a shows that between incidence angles of 30° and 80°, Vestrum's ray velocities are systematically larger than those calculated here. This discrepancy may result from errors in distances and traveltimes and are consistent with Vestrum's estimated relative velocity error of 2%. The τ-p method used here to compute the velocities does not use the traveltime through the sample but intercept time *difference*, $\Delta\tau$, which eliminates any systematic traveltime error.

I measured the velocities along the axes using the transit-time method between a transmitter/receiver pair of transducers glued on opposite faces of the specimen. 1-MHz transducers, 2.54 cm in diameter, were placed opposite to each other to measure the phase velocities. Small 1 x 1 mm, 1 MHz ceramics provided the measured ray velocities (Vestrum, 1994). The phase and ray velocities along the axes have been measured and summarized in Table 1.

Along the axes of symmetry the phase and ray velocities should be identical, which is not the case here, especially for the y-axis where the phase and ray velocities differ by as much as 3.5%. This discrepancy may result from traveltime measurement errors and the numerical errors involved in the τ-p method.

Similar curves are obtained for the $(x$-$z)$ and $(x$-$y)$ planes of symmetry. The phase and ray velocities for these two planes are shown in Figures 5.11b and c, respectively. Figure 5.11b is very similar to that for the y-z plane and reveals a velocity anisotropy of

22%. The computed ray velocities are comparable to those measured by Vestrum (1994). However, Vestrum's phase velocity at 45° is 3% larger than our recovered phase velocity for the same angle using the τ-p method. Figure 5.11 (c) shows that the phase velocity in the x-y plane decreases from 3320 m/s at 15° from the y-axis to 3220 m/s for an incidence angle of 68°. A phase velocity decrease of only 3%. In this plane the computed ray and phase velocities differ little because of the weak anisotropy. The discrepancy of about 1.5% observed along the axes could again be due to the traveltime determination errors. The slight increase in velocity from 70° to 90° was also observed by Vestrum (1994). Unlike the other three planes, the diagonal plane is not a plane of symmetry. The phase velocities recovered from the τ-p curves relative to this plane show that the phase velocity increase from 2826 m/s in a direction perpendicular to the plane of the fibers to 3160 m/s for an incidence angle of 66° (Figure 5.12). The ray velocities have not been computed because equations (5.13) and (5.14) are valid for planes of symmetry only.

5.5 Conclusion

I applied the Radon transform to ultrasonic wave-forms plotted in the x-t space to the intercept time-horizontal slowness τ-p domain. Since the horizontal slowness implicitly contains the angle of incidence, the τ-p domain is a natural space for velocity anisotropy determination. The intercept time τ is converted to the vertical slowness component when the transmitter spacing in known. The experimental transmitter-receiver configuration is particularly simple and easily implemented in a laboratory setting. Small transducers were coupled to the sample and backed with a tungsten-epoxy mixture, which highly attenuates the ringing of the observed wave-forms. Unlike the classical methods of acoustic phase velocity determination, which employ large transducers and are sometimes semi-destructive as the sample must be cut in many different orientations, the τ-p method is nondestuctive and provides a nearly continuous measure of the phase velocity with incidence angle.

On an isotropic plexiglass sample the τ-p method gave a velocity of 2776 m/s which differs from the transmission measurement of 2800 m/s by less than 1%. This technique was then applied to a phenolic sample of orthorhombic symmetry. The phase velocities have been determined for four planes containing transmitters and receivers by exploring the τ-p curves relative to each common-transmitter wave-form. The recovered phase velocities differ from those measured by Vestrum and Brown (1994) on a sample of the same material for 0 and 45° of incidence angles by less than 2%. Even the weak anisotropy of 3% as for the plane of the fibers of the phenolic sample was detected. Since the velocity curves are nearly continuous, the ray velocities in the planes of symmetry are easily computed.

Table 5.1

Phase and ray velocities directly measured along the phenolic axes of symmetry.

	x-axis	y-axis	z-axis
Phase velocity (m/s)	3440	3310	2826
Ray velocity (m/s)	3490	3439	2846

References

Brown, R. J., Lawton, D. C., and Cheadle, S. P., 1991, Scaled physical modelling of anisotropic wave propagation: multioffset profiles over an orthorhombic medium: Geophys. J. Int., **107**, 693-702.

Castagnede, B., Kim, K. Y., and Sachse, W., 1991, Determination of the elastic constants of anisotropic materials using laser-generated ultrasonic signals: J. Appl. Phys., **70**, 150-157.

Chapman, C. H., 1981, Generalized Radon transforms and slant stacks: Geophys. J. Roy. Astr. Soc., **66**, 445-453.

Cheadle, S. P., Brown, R. J., and Lawton, D. C., 1991, Orthorhombic anisotropy: A physical seismic modeling study: Geophysics, **56**, 1603-1613.

Gieske, J. M., and Allred, R. E., 1974, Elastic constants of B-Al composites by ultrasonic velocity measurements: Exp. Mech., **14**, 158-165.

Kebaili, A., and Schmitt, D. R., 1996, Velocity anisotropy observed in wellbore seismic arrivals: Combined effects of intrinsic properties and layering: Geophysics, **61**, 12-20.

Markham, M. F., 1970, Measurements of the elastic constants of fibre composites by ultrasonics: Composites, **1**, 145-149.

Mignogna, R. B., 1990, Ultrasonic determination of elastic constants from oblique angles of incidence in non-symmetry planes, Review of Progress in Quantitative Nondestructive Evaluation, edited by D. O. Thompson and D. E. Chimenti (New York, 1990), **9B**, 1565-1572.

Moon, W., A. Carswell, R. Tang and C. Dillon, 1986, Radon transform wave field separation for vertical seismic profiling data: Geophysics, **51**, 940-947.

Musgrave, M. J. P., 1970, Crystal Acoustics (Holden-Day, San Francisco).

Nayfeh, A. H., 1995, Ultrasonic plate waves in three-dimensional braided composites: J.

Acoust. Soc. Am., **97**, 2057-2062.

Robinson, E. A., 1982, Spectral approach to geophysical inversion by Lorentz, Fourier and Radon transforms: Proc. Inst. Electr. and Electron. Eng., **70**, 1039-1053.

Rokhlin, S. I., and Wang, W., 1989, Critical angle measurement of elastic constants in composite material: J. Acoust. Soc.Am., **86**, 1876-1882.

Rokhlin, S. I., and Wang, W., 1992, Double through-transmission bulk wave method for ultrasonic phase velocity measurement and determination of elastic constants of composite materials: J. Acoust. Soc. Am., **91**, 3303-3312

Smith, 1972, Ultrasonic elastic constants of carbon fibers and their composites: J. Appl. Phys., **43**, 2555-2562.

Stoffa P. L., Buhl, P., Diebold, J. B., and Wenzel, F., 1981, Direct mapping of seismic data to the domain of intercept time and ray parameter - a plane-wave decomposition: Geophysics, **46**, 255-267.

Tatham, R. H., 1984, Multidimensional filtering of seismic data: Proc. Inst. Electr. and Electron. Eng., **72**, No 10.

Thomsen, L., 1986, Weak elastic anisotropy: Geophysics, **51**, 1954-1966.

Vestrum, R. W., and Brown, R. J., 1994, Group- and phase-velocity inversions for the general anisotropy stiffness tensor: Master's Thesis, University of Calgary.

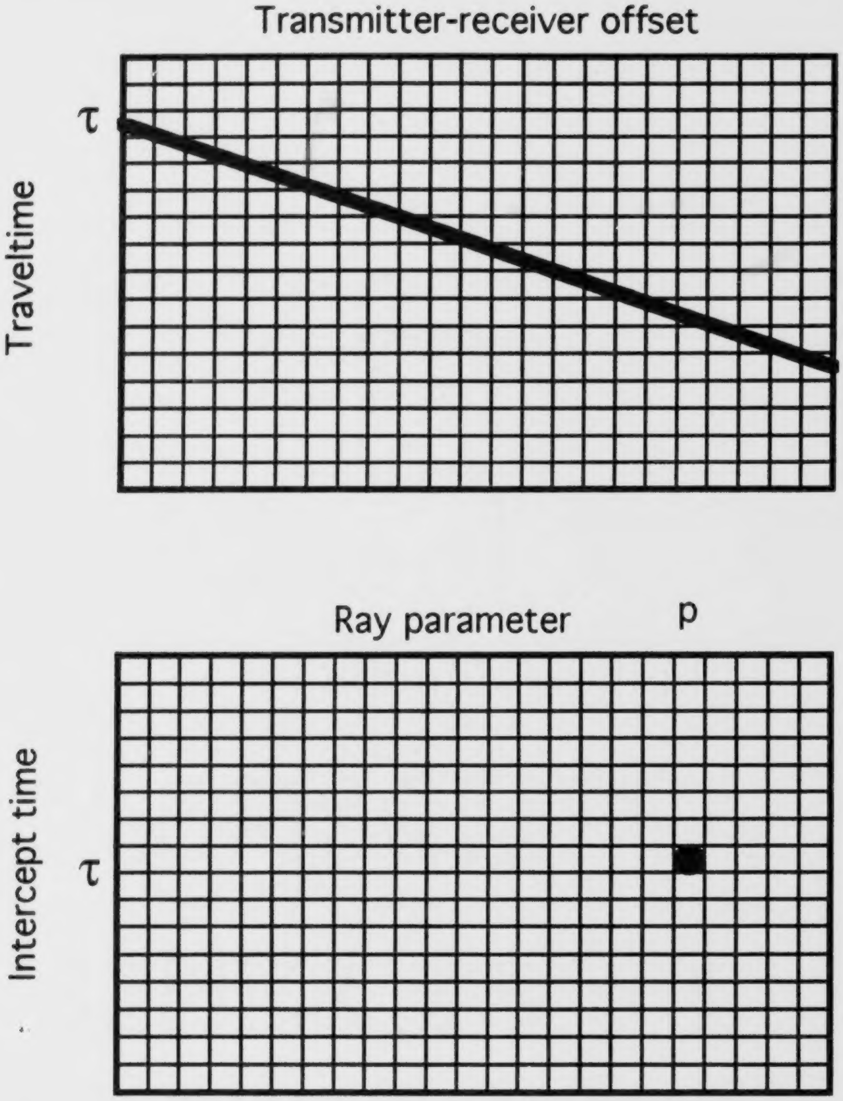
Transmitter-receiver offset
τ
Traveltime
Ray parameter
p
Intercept time
τ

Figure 5.1. Slant-stack procedure. The amplitudes in the offset-time domain on a line of slope p and y-intercept τ are stacked to give the amplitude in the τ-p space of x and y coordinates p and τ, respectively.

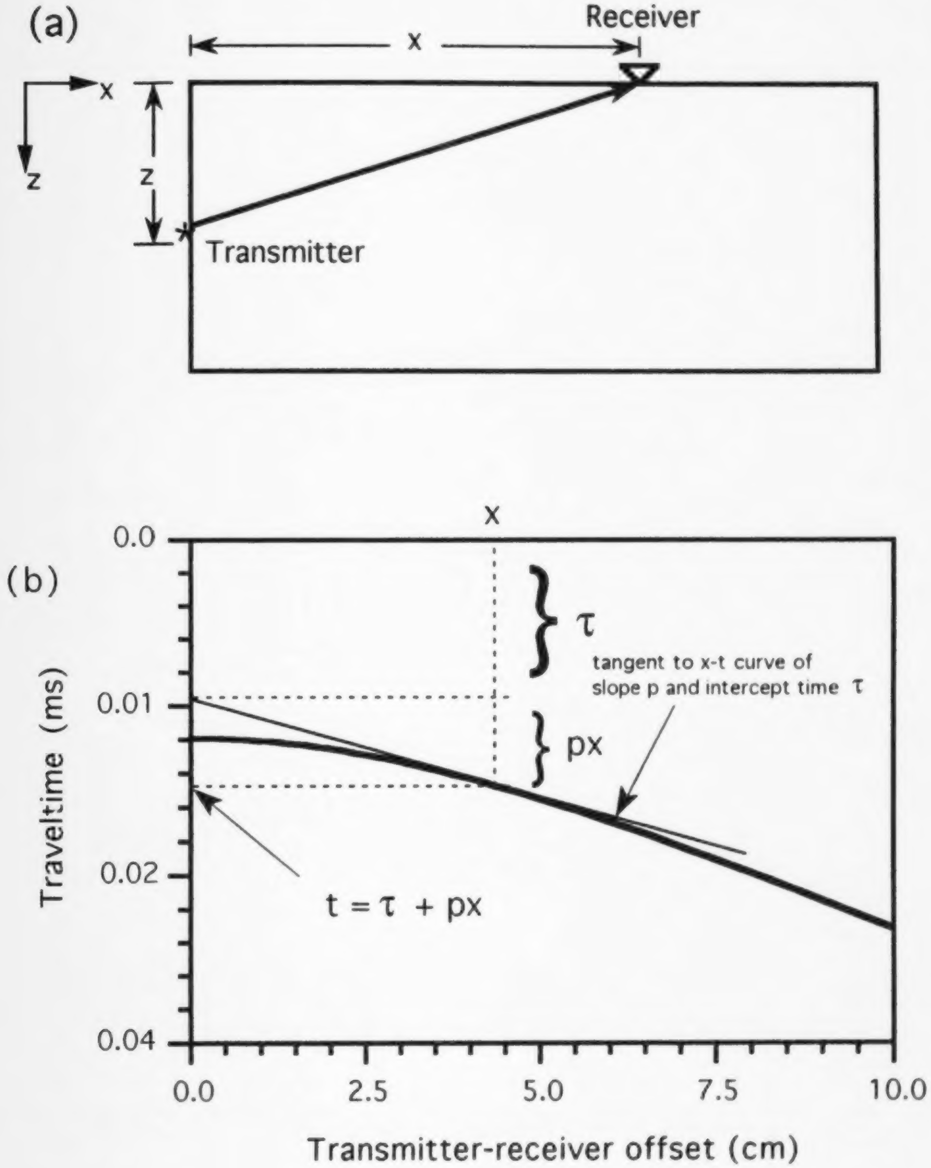
(a)
Receiver
x
x
z
z
Transmitter
(b)
x
τ
tangent to x-t curve of slope p and intercept time τ
px
t = τ + px
Traveltime (ms)
0.0
0.01
0.02
0.04
0.0
2.5
5.0
7.5
10.0
Transmitter-receiver offset (cm)

Figure 5.2. (a) Ray path. (b) Transmission traveltime versus transmitter-receiver offset for receivers aligned on the top surface and a transmitter on a side surface of an anisotropic specimen.

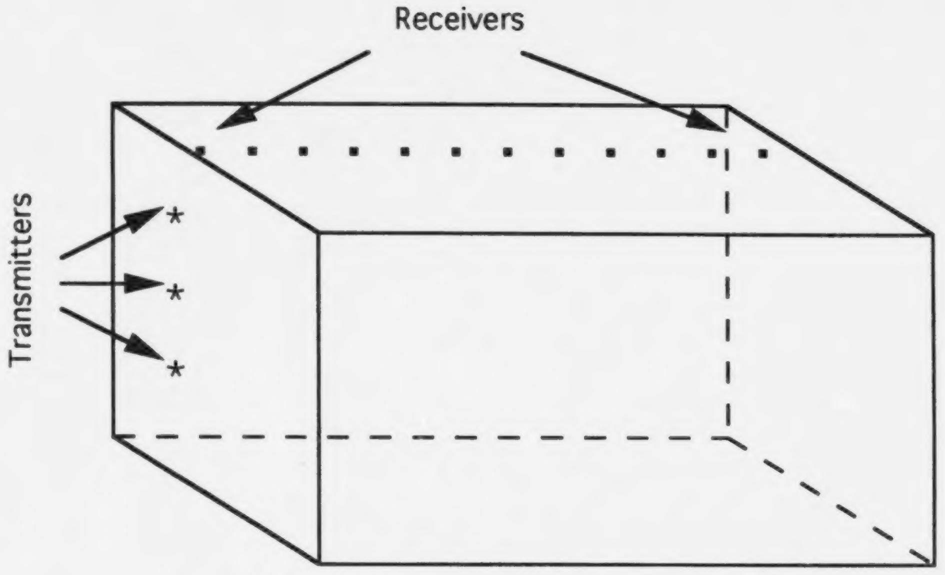
Receivers
Transmitters

Figure 5.3. Transmitter-receiver configuration for the experiments. The receivers are placed on the top surface of the specimen and the transmitters on the side surface in the vertical plane that contains the receivers

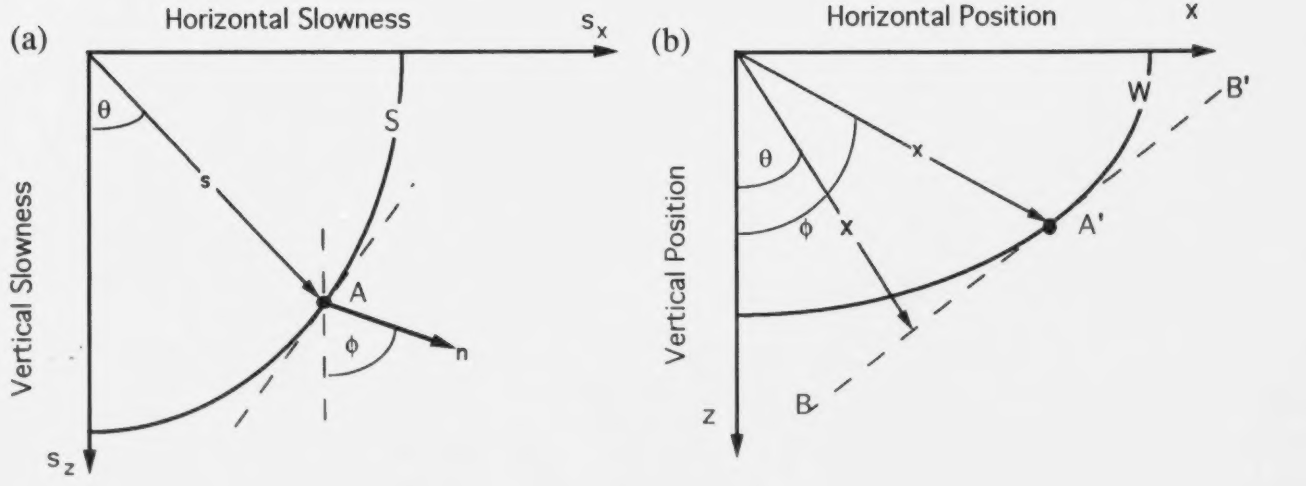
(a)
Horizontal Slowness
s_x
Vertical Slowness
s_z
θ
s
S
A
φ
n
(b)
Horizontal Position
x
Vertical Position
z
θ
φ
x
x
W
A'
B'
B

Figure 5.4. (a) Hypothetical phase slowness surface S in a vertical plane of an anisotropic material. The length of **s** is inversely proportional to the velocity of a plane wave propagating through the material in the direction defined by θ . **n** is a unit vector normal to S at the endpoint of s, ϕ defines both the direction of **n**. and of the energy flow through the medium. (b) Hypothetical wave surface W in *x-z* space is directly related to phase slowness surface S; A' at the endpoint of spatial vector x at angle ϕ corresponds to A in (a).

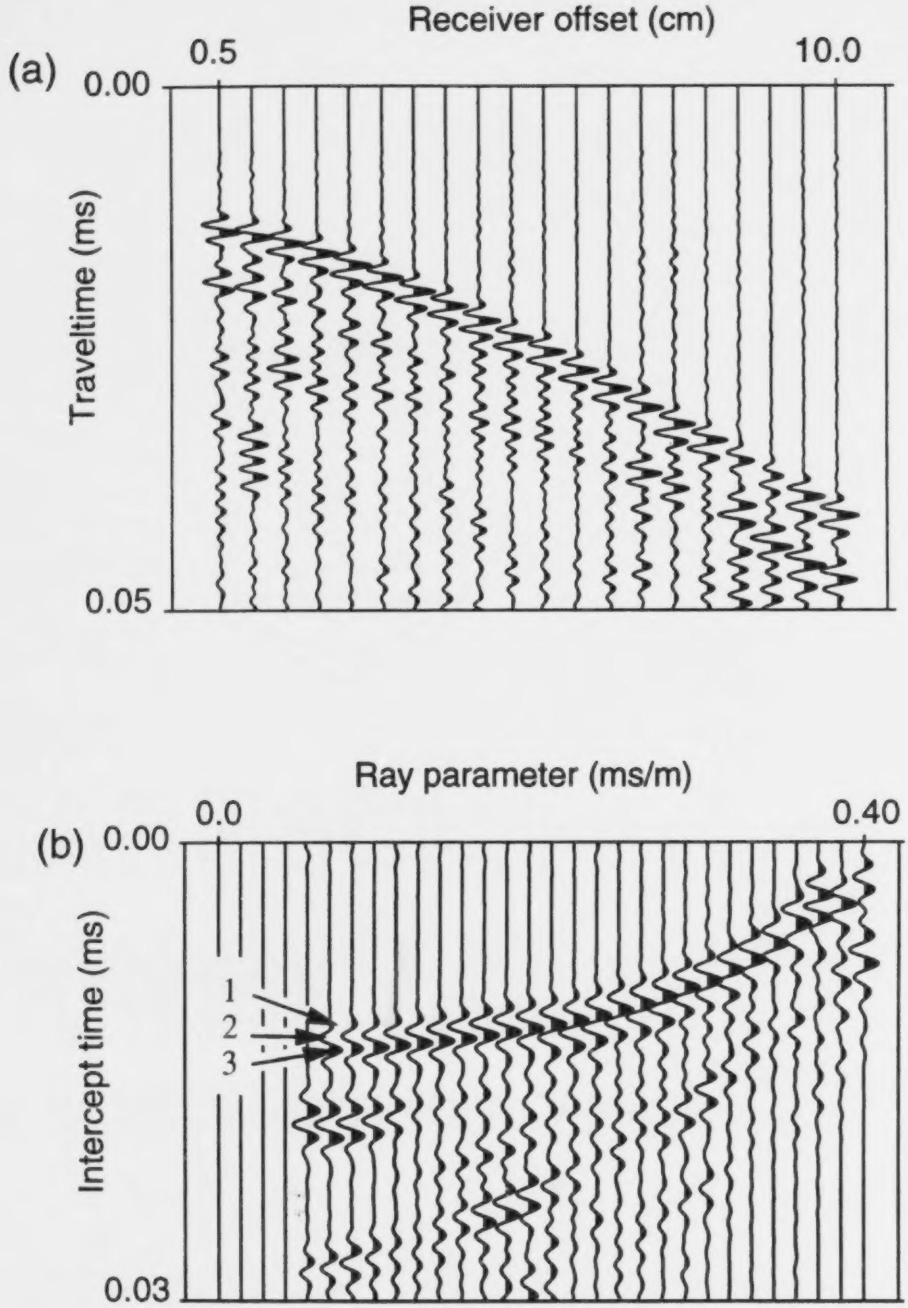

Figure 5.5. (a) Wave-form amplitudes with time observed for a transmitter on the side of the plexiglass specimen at 3 cm from the top surface where 20 receivers are placed along a line in the plane containing the transmitter. (b) τ-p mapping of the wave-forms in (a). Positive values are shaded black to enhance viewing of coherent features.

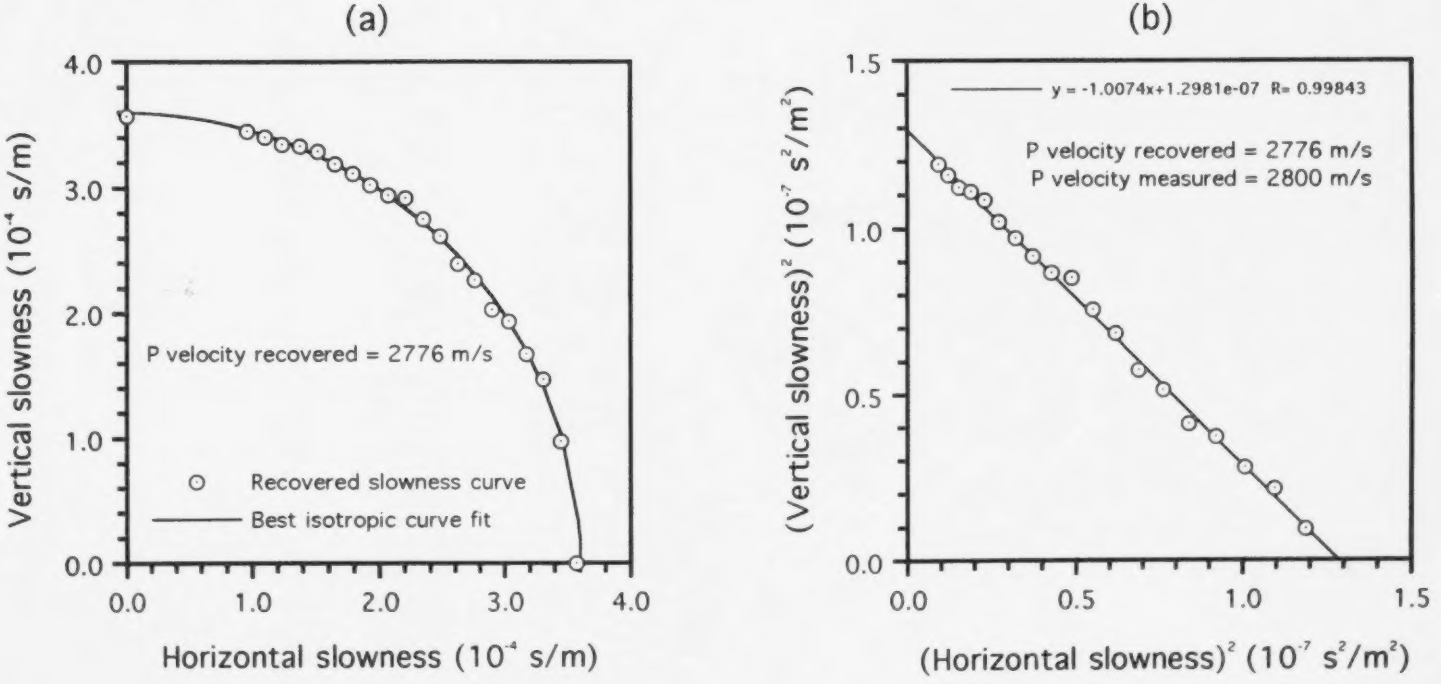

Figure 5.6. Recovered (a) P-slowness surface and (b) P velocity of the isotropic plexiglass sampl

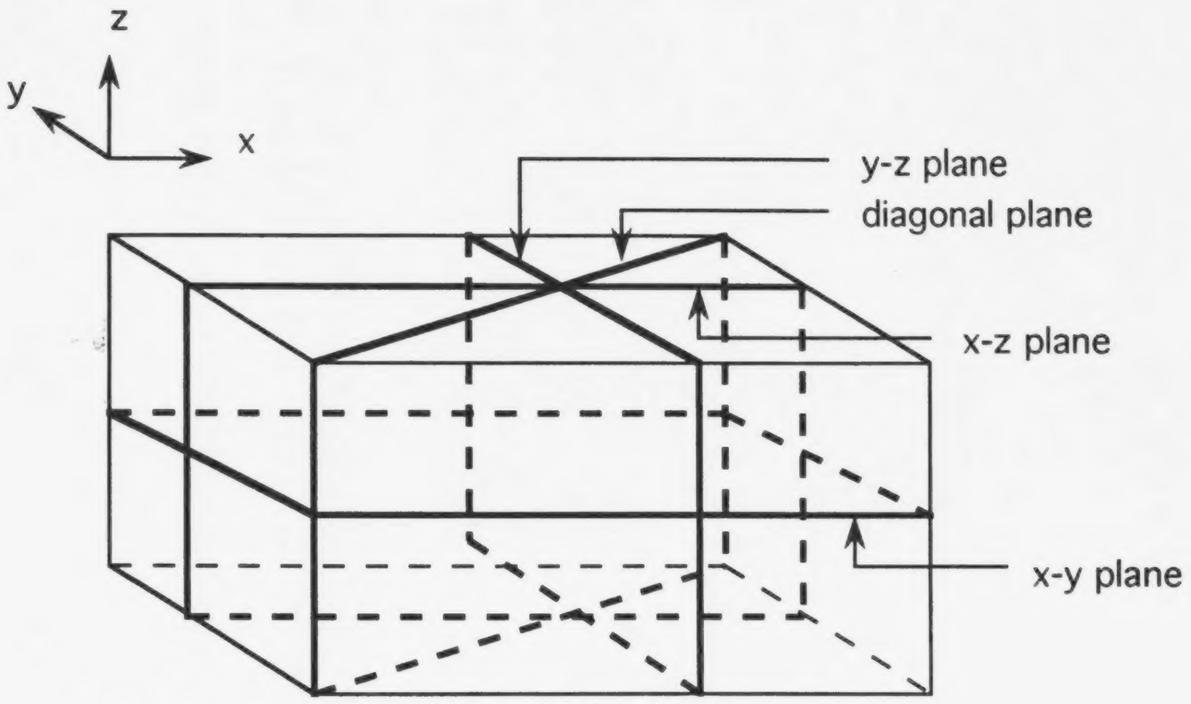
z
y
x
y-z plane
diagonal plane
x-z plane
x-y plane

Figure 5.7. Schematic of the phenolic sample showing the planes along which the P-wave anisotropy has been investigated.

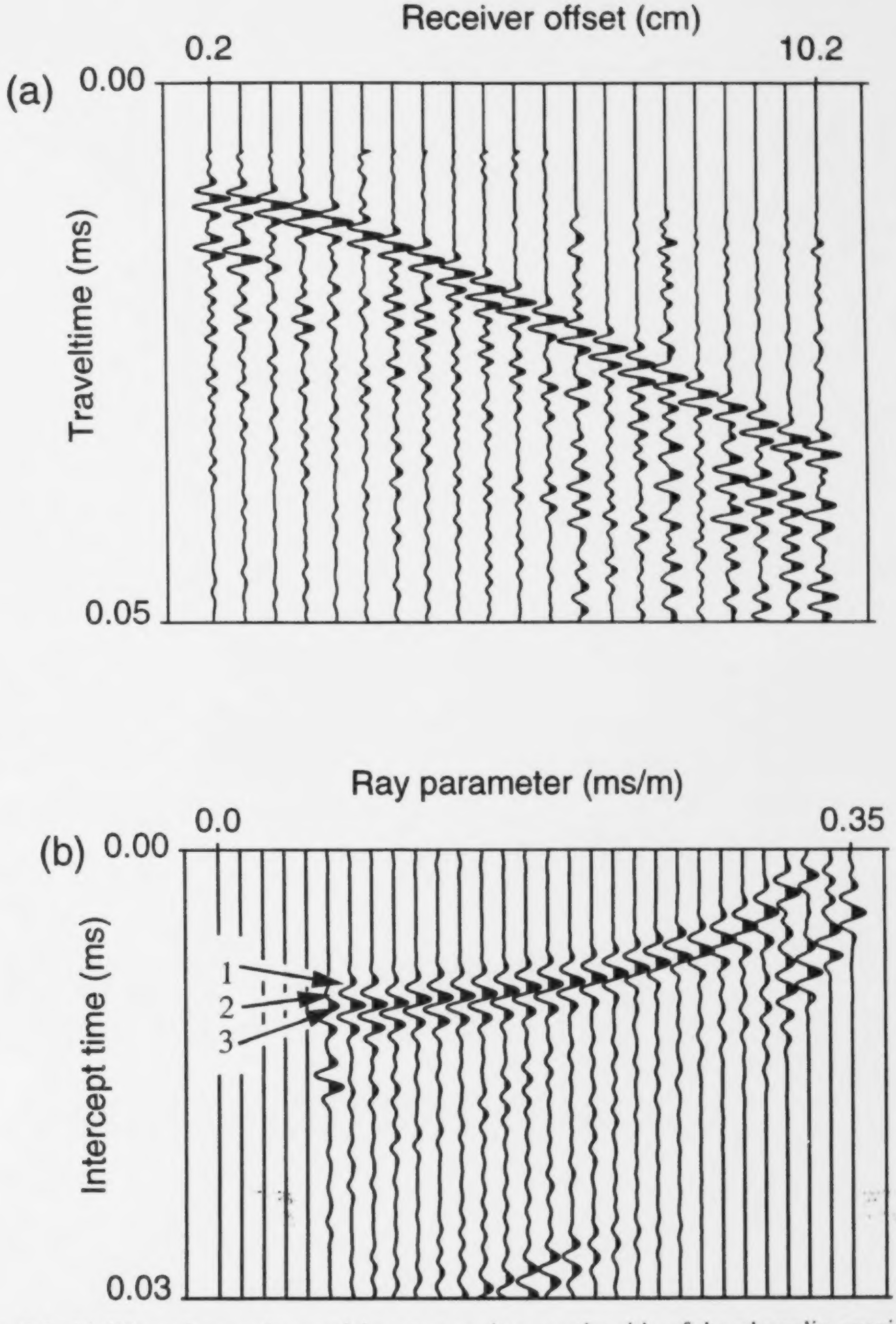

Figure 5.8. (a) Wave-forms observed for a transmitter on the side of the phenolic specimen at 2 cm from the top surface where 21 receivers are placed along a line in the y-z plane that contains the transmitter. (b) τ-p mapping of the wave-forms in (a). Each of the lobes labeled (1, 2, and 3) were used with their counterparts in Figure 5.9 to compute the phase-velocity function.

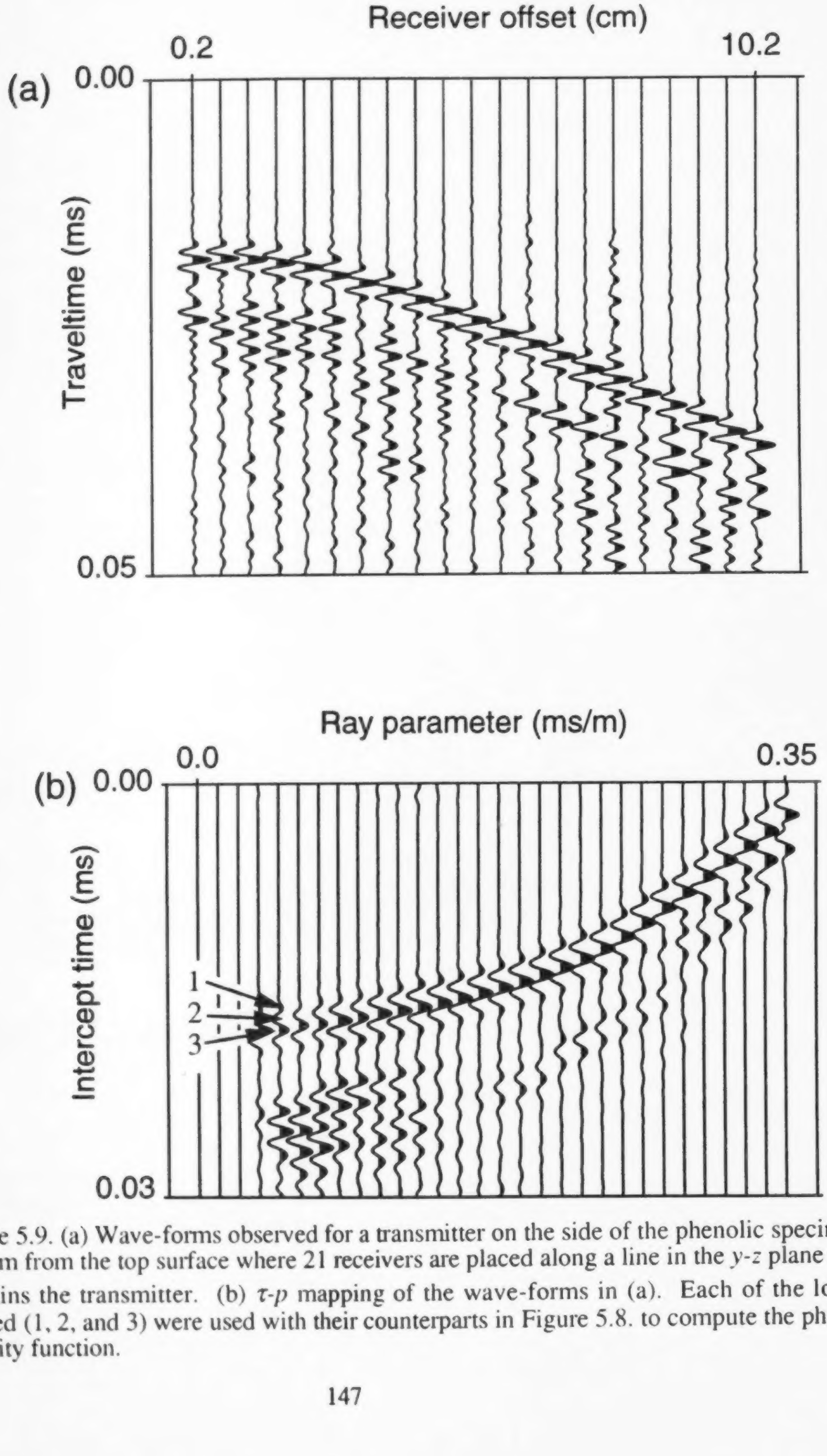

Figure 5.9. (a) Wave-forms observed for a transmitter on the side of the phenolic specimen at 4 cm from the top surface where 21 receivers are placed along a line in the y-z plane that contains the transmitter. (b) τ-p mapping of the wave-forms in (a). Each of the lobes labeled (1, 2, and 3) were used with their counterparts in Figure 5.8. to compute the phase-velocity function.

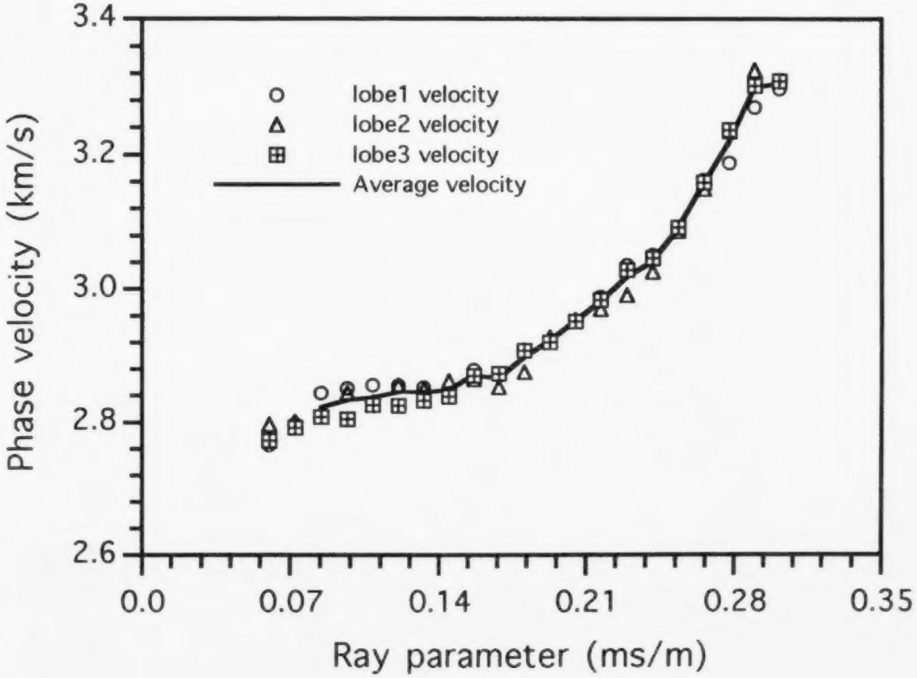

Figure 5.10. Recovered phase velocities for the phenolic sample in the y-z plane from the tau-p curves in Figures 5.8 (b) and 5.9 (b).

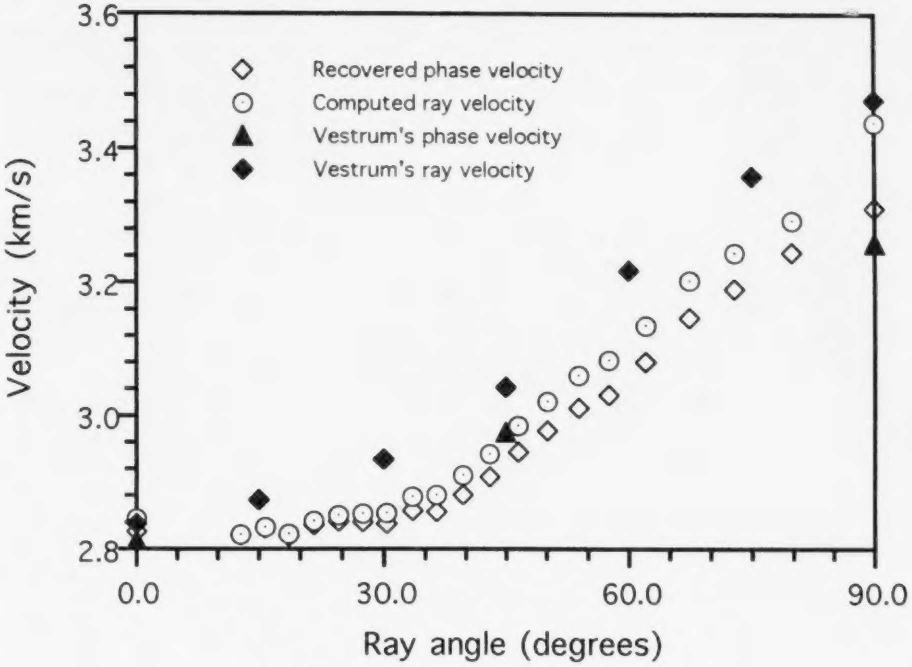

Figure 5.11. Recovered phase and computed ray velocities for the phenolic sample in the y-z plane plotted as a function of the ray angle. The phase and ray velocities as measured by Vestrum et al. are plotted for comparison The angles are measured from the normal to the plane of the fibers.

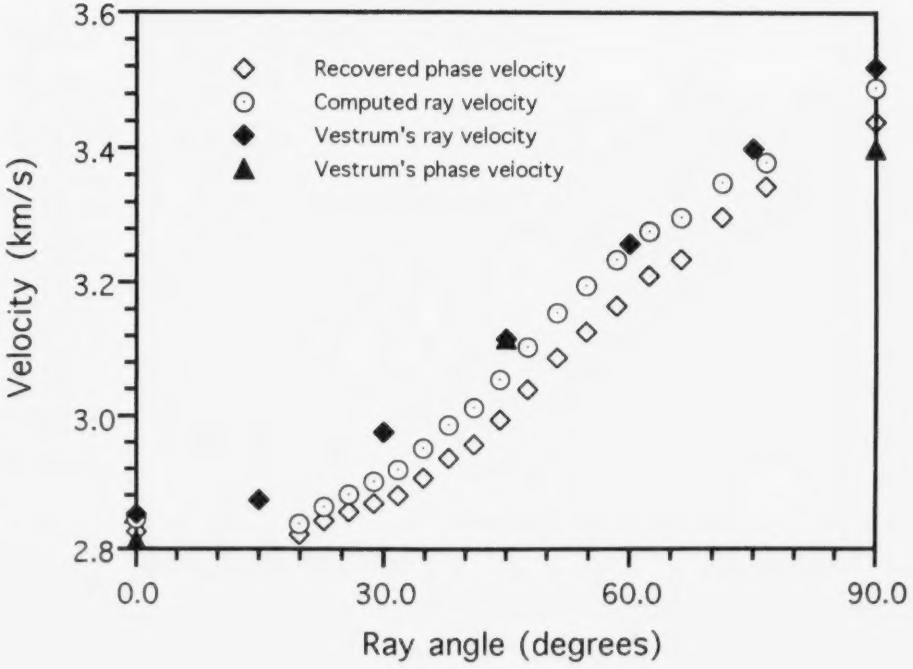

Figure 5.12. Recovered phase and computed ray velocities for the phenolic sample in the x-z plane plotted as a function of the ray angle. The phase and ray velocities as measured by Vestrum et al. are plotted for comparison The angles are measured from the normal to the plane of the fibers.

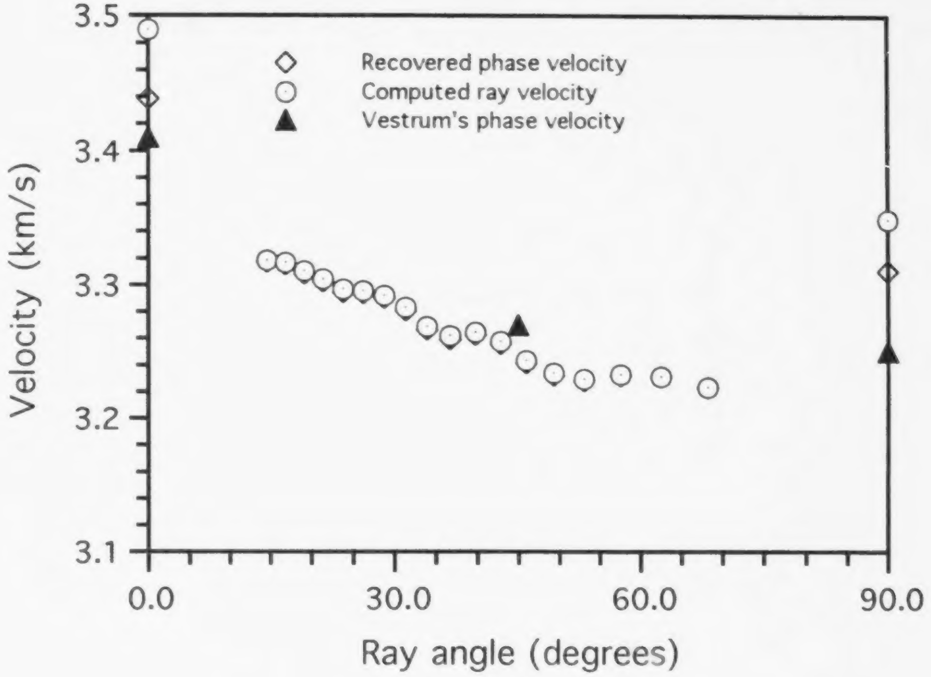

Figure 5.13. Recovered phase and computed ray velocities for the phenolic sample in the x-y plane plotted as a function of the ray angle. The phase velocities as measured by Vestrum et al., 1994, are plotted for comparison

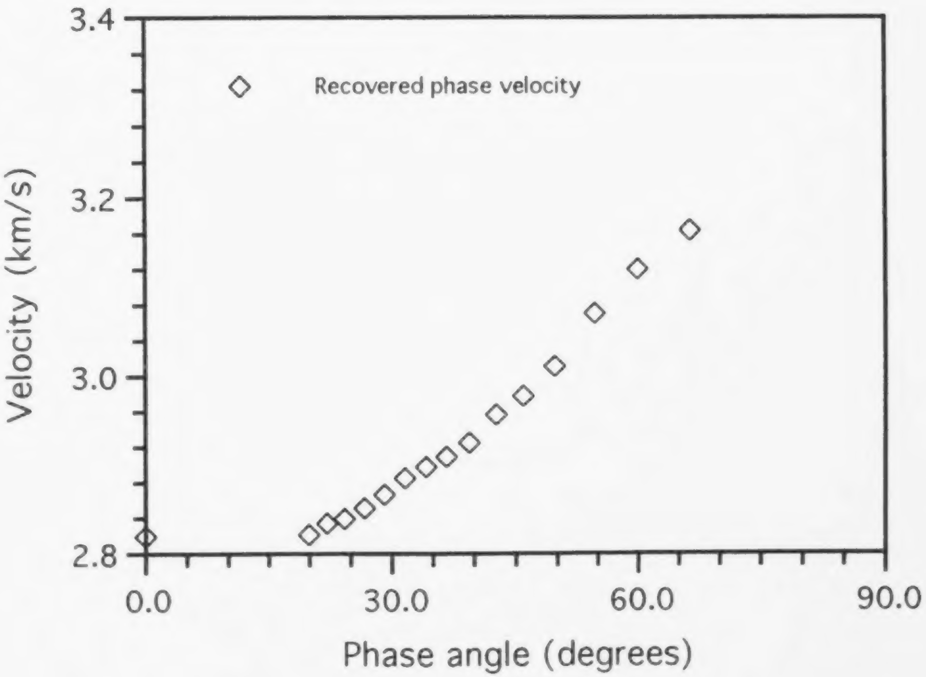

Figure 5.14. Recovered phase velocities for the diagonal plane perpendicular to the x-y plane plotted as a function of the phase angle

Chapter 6

6. Conclusions

6.1 Near-Vertical to Oblique Anisotropy Delineation From Offset VSP data

The dependence of seismic velocities on the angle of incidence is more naturally determined in the τ-p domain. In this domain, τ represents the intercept time and p the ray parameter which readily allows the determination of the phase velocity v and phase angle θ via the relation $p=\sin\theta/v$. The technique is based on the analysis of the τ-p curves of common depth receiver gather for a walkaway vertical seismic profile experiment where the receivers are placed in the borehole and the sources radiate from it at increasing offsets. In this kind of experiment the depth of the receivers is known, this knowledge can be used as a constraint to enhance the accuracy of the recovered velocities from the τ-p curves of successive receivers. The technique is able to determine the velocity changes as a function of the ray parameter without any restriction on the shape of the τ-p curves. In Chapters 2 and 3 the τ-p curves are subdivided into small p ranges within which the velocity is assumed to be constant. To check the accuracy of the recovered velocities for various p-ranges, the method was first applied to two synthetic offset vertical seismic profile experiments. The first example consists of an elliptically anisotropic half-space, for which the recovered velocities differ from the modeled velocities by less than 1 percent. The second example consists of an isotropic layer overlaying an elliptically anisotropic half-space. x-t seismograms were formed for two receivers where the first was placed at the interface separating the two media, and the second receiver within the anisotropic half-space at a known depth. The x-t seismograms were then mapped to the τ-p domain. A layer stripping technique similar to that described by Schultz (1982) was used to subtract the contribution of the isotropic layer to the total intercept time computed for the receiver placed within the anisotropic layer. Again the computed velocities for various p-ranges attributed to the mid-point of the ranges differ from the input modeled velocities by less than 1 percent.

The *p*-range velocity determination from τ-p curves of common-receiver seismograms was then applied to a walkaway vertical seismic profile data set acquired in a shallow borehole (225 m) at the Underground Test Facilities (UTF) near Fort McMurray, Alberta. The three-component receiver was lowered down into the borehole at 13 known depths. Hodogram analyses of the three-component seismic data were used to segregate the downgoing transmitted waves, and enhance their amplitude by the rotations through the appropriate angles. The layer stripping technique was used to calculate the near vertical and oblique velocities for each of the layers bounded by the receivers. The largest difference between oblique and near-vertical velocities (15 percent) was observed for a shale/sand sequence bounded by receivers at 75 m and 100 m. This latter is subdivided into thin shale and sand layers as delineated from sonic and focused electric logs recorded in the same wellbore. Assuming isotropic constituents the horizontal and vertical velocities of the long-wave transversely isotropic medium equivalent to the 75-100 m layer are computed using Backus's (1962) equations. The computed vertical to horizontal anisotropy of the equivalent medium was 14.2 percent which is less than the observed 15 percent near-vertical to oblique velocity anisotropy. This simply suggests that the 75-100 m thin layer components are intrinsically anisotropic.

6.2 Slowness Surface Determination From VSP Experiments

The τ-p method for velocity determination was further developed to recover an almost continuous phase velocity function for the whole range of incidence angles present in the offset vertical seismic profile data set. After mapping the offset-time common receiver data to the τ-p domain, and using the known receiver spacing, the vertical component q of the slowness is computed for each ray parameter (horizontal slowness component) p. The magnitude of the slowness vector can then be computed from its components p and q. The velocity for each ray parameter is then calculated by taking the reciprocal of the already determined slowness ($v=1/u$). The method was applied to various synthetic data sets, then to a real data set acquired in a shallow borehole. The first test to the method consisted of the determination of the slowness surface of an isotropic half-space overlain by a stack of three isotropic layers. Two receivers were placed in a borehole at known depths, and a series of sources are activated on the surface at increasing offsets from the wellbore. Seismograms for the two receivers were formed, than mapped to the τ-p domain. The intercept time differences ($\tau_2 - \tau_1$) for various ray parameters were divided by the well known receiver spacing to yield the vertical component of the slowness [$q = (\tau_2 - \tau_1)/(z_2 - z_1)$]. The slowness curve was circular, which means that the medium in which the receivers are placed is indeed isotropic. Finally the velocity of the medium was graphically determined from the q^2-versus-p^2 plot, where q and p are the vertical and horizontal components of the slowness, respectively. The recovered velocity differs from the input modeled velocity of the half-space by 0.5 percent. This example showed that the τ-p method described in this thesis can be useful even in the case of isotropic media.

The second synthetic example consisted of an elliptically anisotropic half-space of vertical and horizontal velocities of 2000 m/s and 2500 m/s, respectively. Again a seismogram was formed for a receiver placed at 200 m depth, then mapped to the τ-p domain. The phase velocities from normal incidence to a near-horizontal angle fixed by the ray geometry are determined from the τ-p curve. The recovered phase velocities and the derivative of their best polynomial fit were used to compute the ray velocities using the phase-ray velocity relationship in a plane of symmetry. The observed phase velocities were smaller than the input ray velocities for all incidence angles except for normal and horizontal incidences where the velocities are equal as predicted by the theory. The recovered ray velocities deviate from the input modeled ray velocities by 0.2 percent only.

The third example which is probably the most interesting of all consisted of a hypothetical transversely isotropic medium. Radial and vertical component seismograms were calculated for a receiver placed at 500 m depth in a borehole, and sources were activated on the surface at increasing offset from the wellbore (10 - 1000 m). The seismograms were rotated to the incoming rays, and the qP-wave and qSV-wave seismograms were calculated and mapped to the τ-p domain. The qP-wave and qSV-wave slowness curves are in good agreement with the modeled slownesses for the range of incidence angles fixed by the ray geometry.

The method was then applied to a set of data acquired in a shallow borehole. Two receivers were placed within a shale formation with thin beds of sand. The data acquired using a three-component receiver was rotated to the incoming rays via hodogram analysis to obtain the downgoing transmitted qP-wave seismograms. These offset-time seismograms were then mapped into the τ-p domain. Three lobes of the wavelets in the τ-p domain were used to compute three velocities for each ray parameter p, and an averaged velocity is calculated. The observed phase velocities increase with incidence phase angle from 1990 m/s at normal incidence to 2235 m/s for a phase angle of about 50°, which corresponds to an increase in velocity of about 12 percent. The ray velocities are then computed from the phase velocities assuming the plane that contains the source and receivers is a plane of symmetry. The ray velocities show an increase from 1990 m/s at normal incidence to 2245 m/s for a ray angle of about 52°.

6.3 Ultrasonic Velocity Anisotropy Determination

The τ-p method described above was finally used to determine ultrasonic velocities for an isotropic sample of plexiglass and an anisotropic sample (phenolic) that has an orthorhombic symmetry. The transmitter and receivers were arranged in a way similar to that of a reverse vertical seismic profile in seismology. The receivers were aligned on the top surface of the sample and the transmitters were glued on a side surface. The observed wave-forms were filtered than mapped to the τ-p domain. The velocity of the specimen was also directly measured using 1-inch (1 MHZ) transducers glued on opposite faces of the sample. The recovered velocity from the τ-p curves was 2776 m/s which differs from the directly measured (2800 m/s) by less than 1 percent.

The method, being successfully tested on an isotropic sample, was applied to an anisotropic orthorhombic sample (phenolic) along its three planes of symmetry and one diagonal plane. The phase velocities recovered from the τ-p curves show that, as expected, the specimen is anisotropic. The increase in phase velocity from about 15° to about 80° incidence angles for the x-z plane, y-z plane, x-y plane, and the diagonal plane were 17 percent, 22 percent, 4 percent and 12 percent, respectively. The phase velocities for the three planes of symmetry were then converted to ray velocities, and the phase angles to ray angles. The computed ray velocities for the x-z and y-z planes were larger than their phase counterparts for all incidence angles from 15° to about 80° as expected since the phase velocity functions increased monotonically with incidence angle. However, for the x-y plane where the anisotropy was as small as 4 percent, the phase and ray velocities almost coincide, and the discrepancy between them is negligible.

6.4 Future directions

6.4.1 Application in reflection seismology

If the depth of the top and bottom of a layer are approximately known from sonic log information, then the reflection data can be used to determine the change of velocity with incidence angle by substituting the quantity $(z_2 - z_1)$ in equation 4.9 by $2(z_2 - z_1)$. In Alberta where a large number of oil and gas pools are either regional sands trapped by shaly sand channels, or clean sands cutting through silty regional sands, the method described here can be a useful tool for shale sand lithology discrimination. In fact, in most cases the clean and shaly sands cannot be differentiated in sonic logs as their velocities are almost identical. However, since the P-wave and *S*-wave velocities through the shales are highly anisotropic, the spatial variations of anisotropy within a homogeneous, horizontally layered lithology could indicate changes of shale content within the layer.

6.4.2 Application to shear waves

During the recent years, shear waves have received a great deal of attention in industrial geophysics. The τ-p method can also be used to determine shear wave velocity anisotropy by the same technique as applied for P-waves in the earlier chapters. Shear wave anisotropy combined with the P-wave anisotropy would provide useful complementary information.

6.4.3 Application to development geophysics

The focus of petroleum geophysics has shifted from exploration to development and production. In the latter application, structural traps were looked for, and the accuracy in positioning of an exploratory well, while important, was often less crutial than that in production of an existing field. In field development, well spacings might differ only by a few meters and in such cases anisotropy must be considered in order to improve imaging of the subsurface by tomography or migration. For example, locally an active area of research focuses on the temporal monitoring of reservoirs subject to steam assisted enhanced oil recovery processes (e.g. Kalantzis, 1994), Dilay and Eastwood (1995), Schmitt et al. (1995)). In these studies, a variety of seismic traveltime and frequency attributes are employed to map changes in the temperature and fluid content of various sections of the geology. The areal positioning of anomalies is critical in such application; and a small error can mean that substantial reserves may not be recovered. As such increasing importance will be placed on anisotropy determination and the incorporation of this knowledge in data analysis.

Rocks are often intrinsically anisotropic, and fractures and thin layering introduce additional velocity anisotropy. Consequently, rocksmasses cannot be described by only 2 independant elastic parameters, and the isotropy assumption is far from being realistic. Real rockmasses more probably require either five elastic constants if transversely isotropic or nine elastic constants for orthorhombic symmetry. Anisotropy cannot be ignored, and developments of techniques for velocity anisotropy delineation are necessary. The inclusion of anisotropy in seismic data processing schemes improves the quality of the final seismic sections in reflection seismic profiling. Anisotropy may also be used for lithology discrimination. The method proposed in this thesis is only one of the many methods used for velocity anisotropy determination. However, it presents an advantage in that it derives the anisotropy in the τ-p domain which more naturally contains information on the angle of incidence dependent velocities.

Appendix A

Appendix A have plots of the offset-time data acquired in the laboratory and their τ-p mappings for both the plexiglass and phenolic samples.

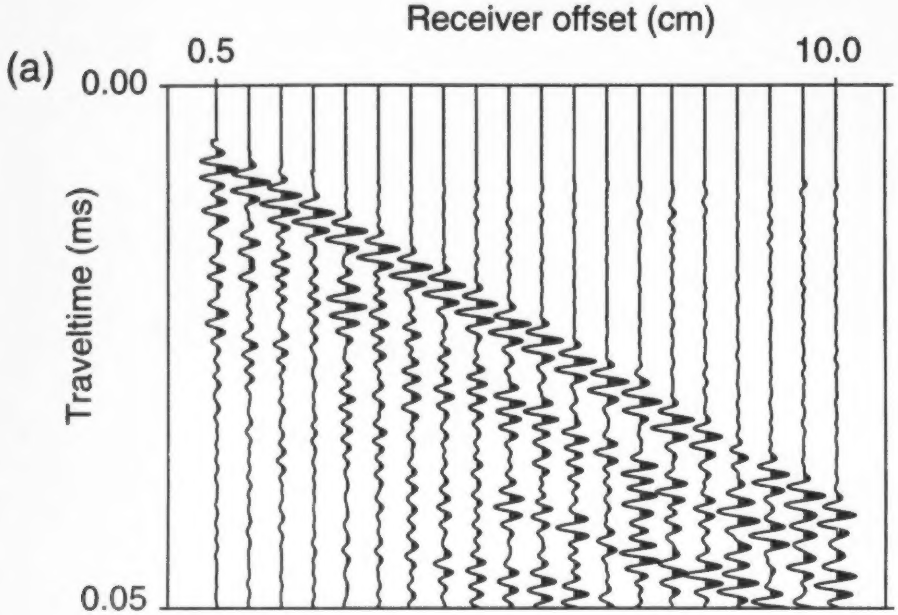

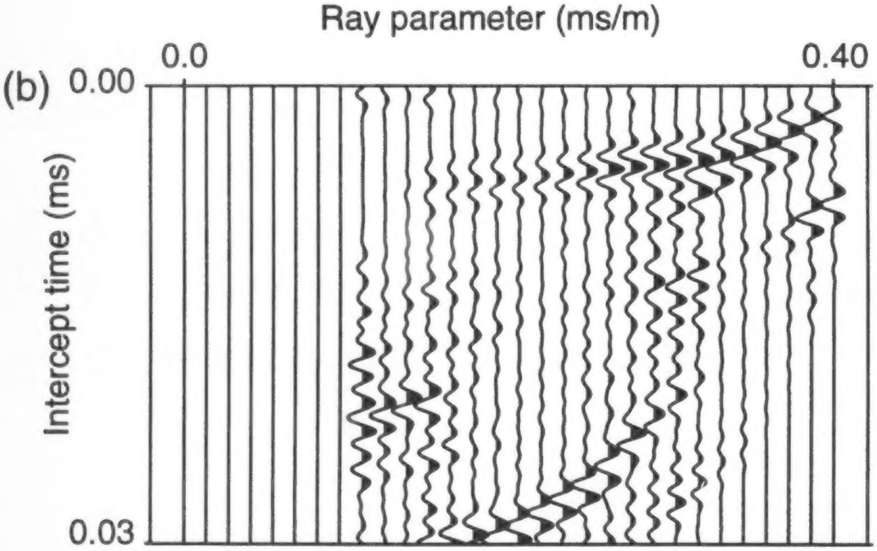

Figure A1. (a) Wave-form amplitudes with time observed for a transmitter on the side of the plexiglass specimen at 1 cm from the top surface where 20 receivers are placed along a line in the plane containing the transmitter. (b) τ-p mapping of the wave-forms in (a). Positive values are shaded black to enhance viewing of coherent features

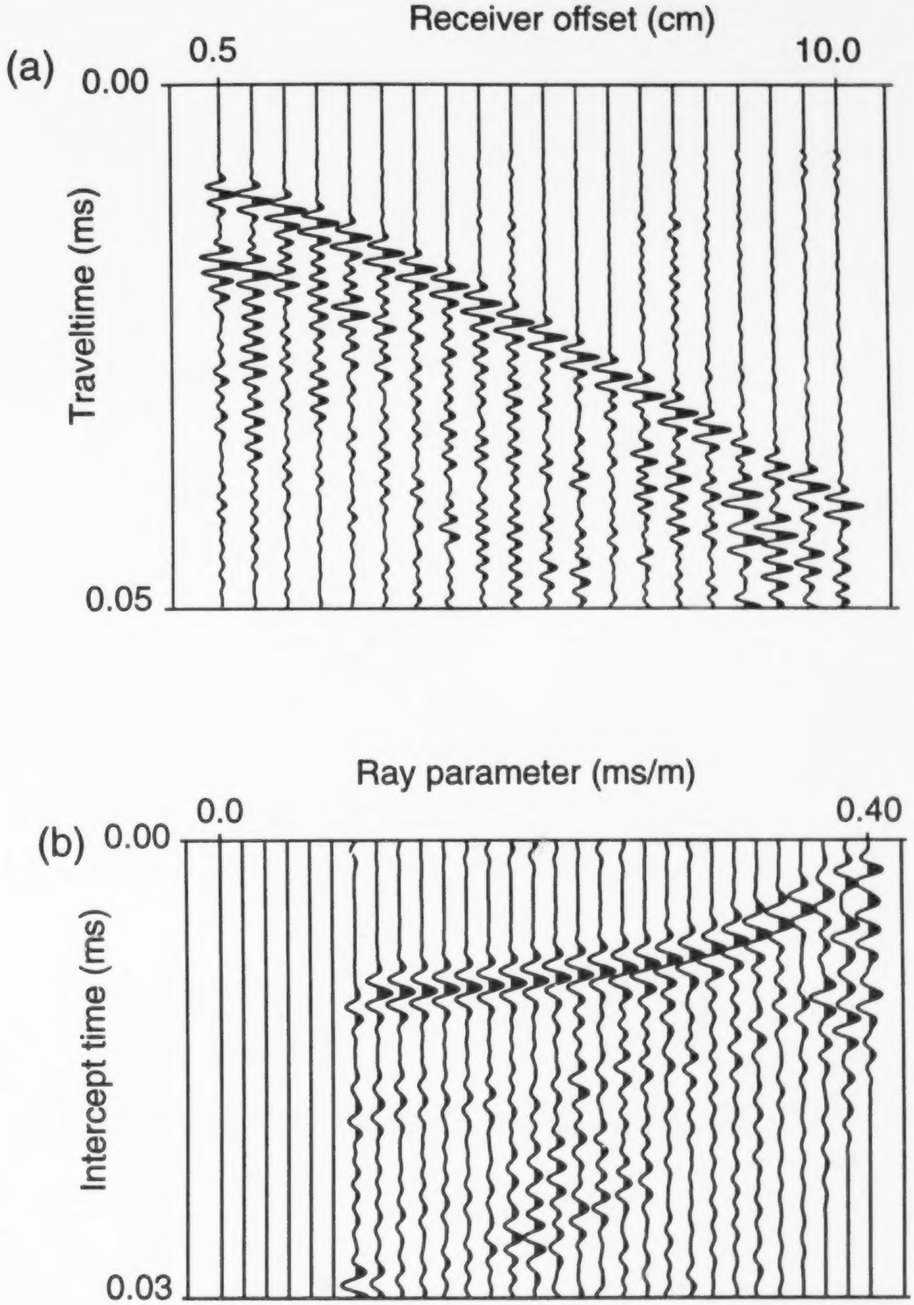

Figure A2. (a) Wave-form amplitudes with time observed for a transmitter on the side of the plexiglass specimen at 2 cm from the top surface where 20 receivers are placed along a line in the plane containing the transmitter. (b) τ-p mapping of the wave-forms in (a). Positive values are shaded black to enhance viewing of coherent features

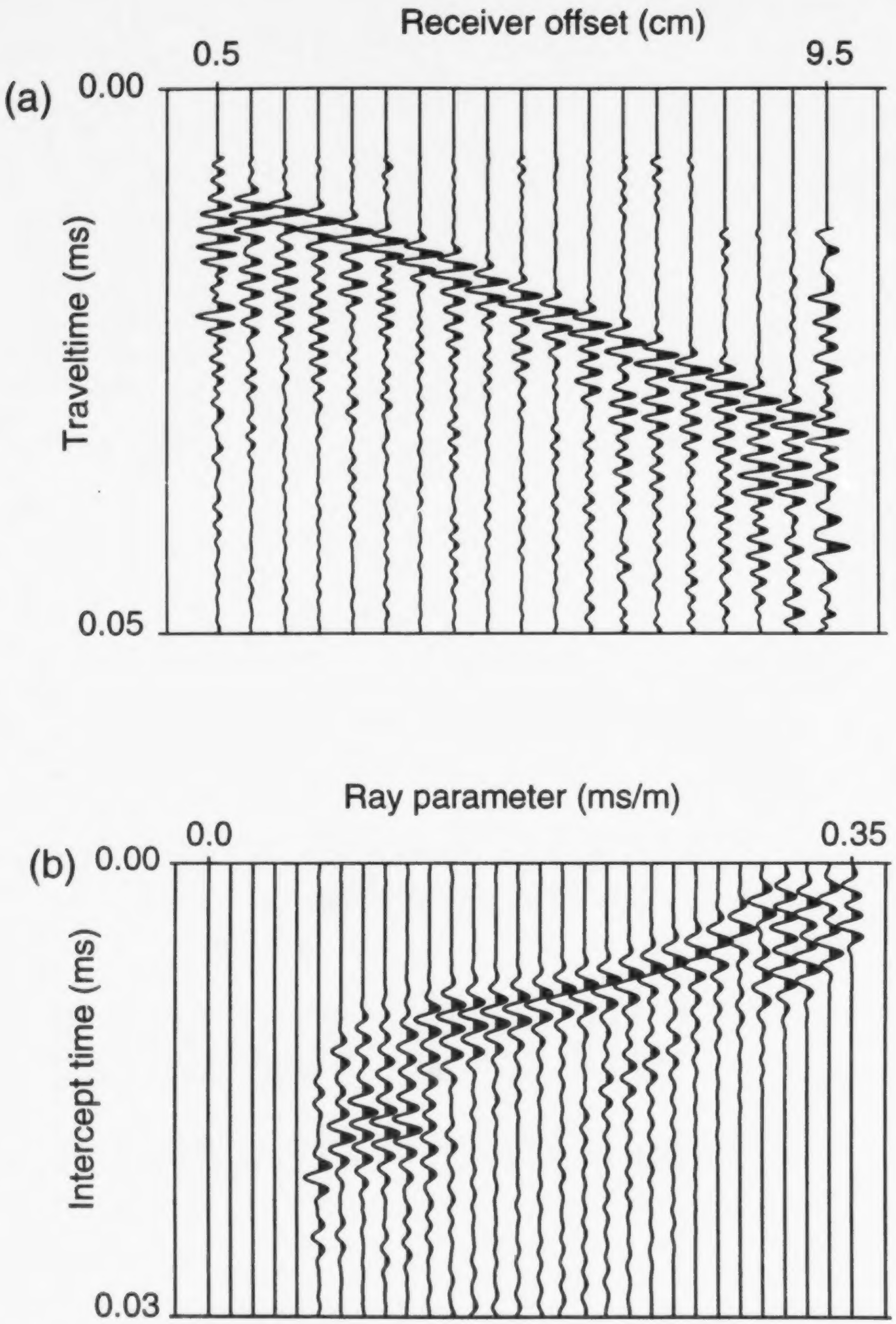

Figure A3. (a) Wave-forms observed for a transmitter on the side of the phenolic specimen at 2 cm from the top surface where 21 receivers are placed along a line in the *x*-*z* plane that contains the transmitter. (b) τ-p mapping of the wave-forms in (a).

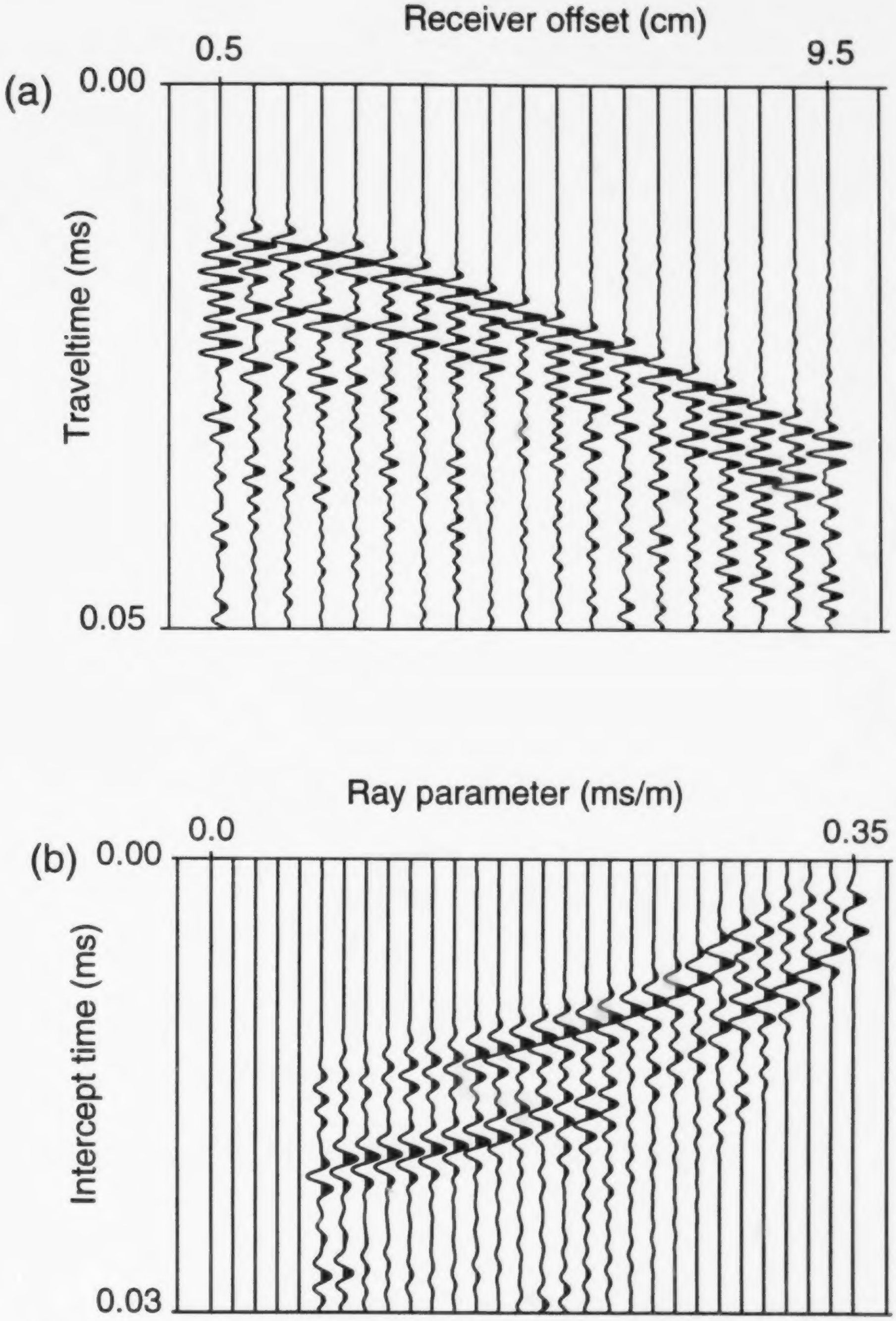

Figure A4. (a) Wave-forms observed for a transmitter on the side of the phenolic specimen at 3 cm from the top surface where 21 receivers are placed along a line in the x-z plane that contains the transmitter. (b) τ-p mapping of the wave-forms in (a).

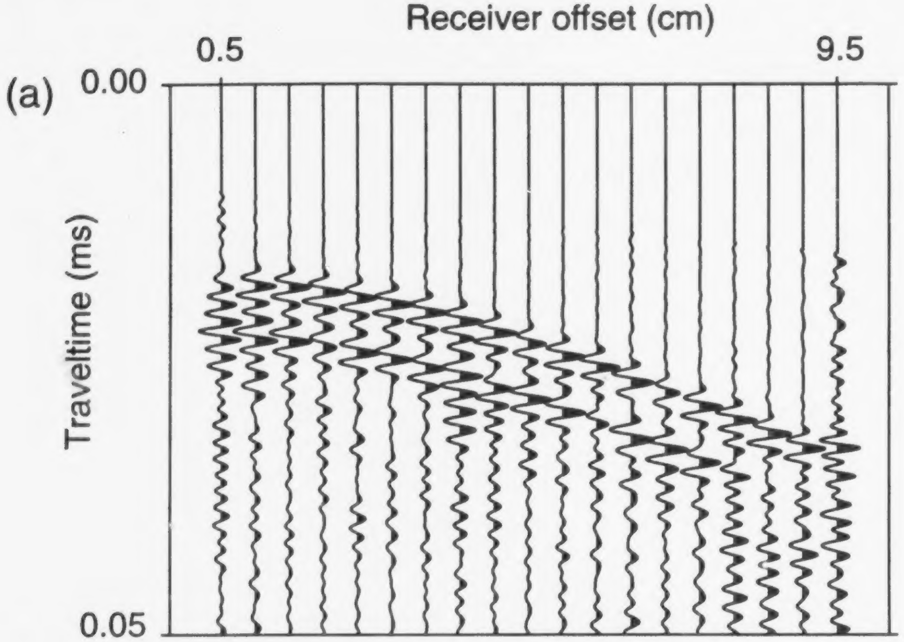

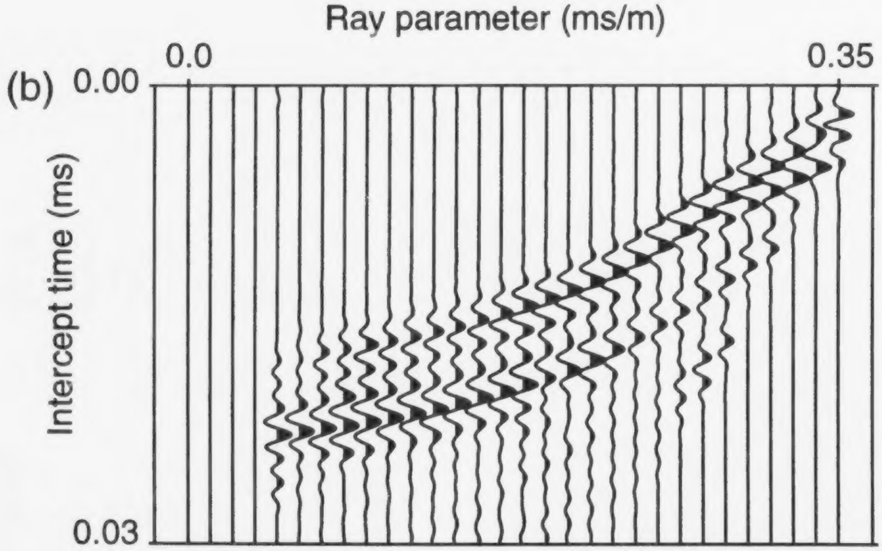

Figure A5. (a) Wave-forms observed for a transmitter on the side of the phenolic specimen at 4 cm from the top surface where 21 receivers are placed along a line in the x-z plane that contains the transmitter. (b) τ-p mapping of the wave-forms in (a).

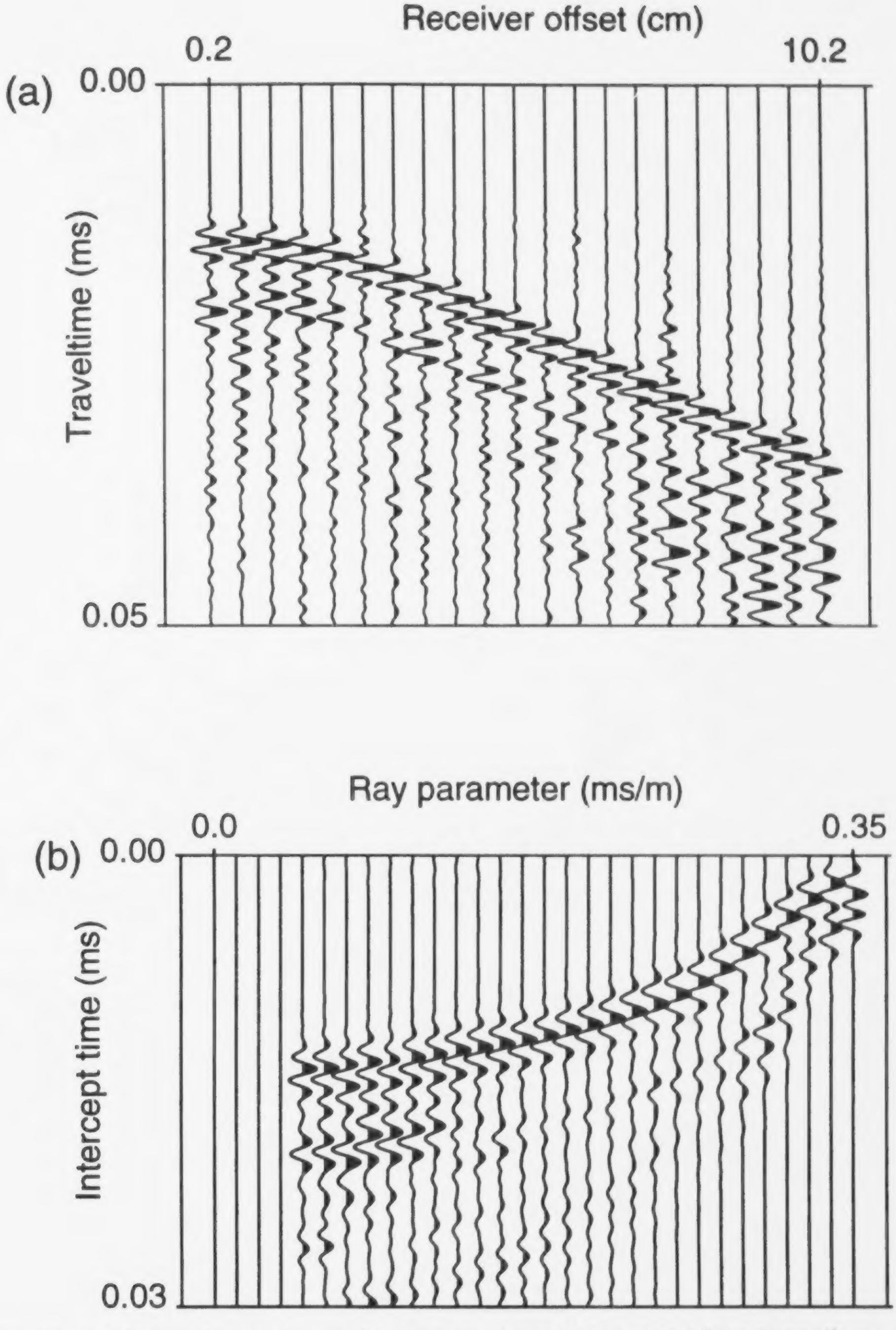

Figure A6. (a) Wave-forms observed for a transmitter on the side of the phenolic specimen at 3 cm from the top surface where 21 receivers are placed along a line in the y-z plane that contains the transmitter. (b) τ-p mapping of the wave-forms in (a).

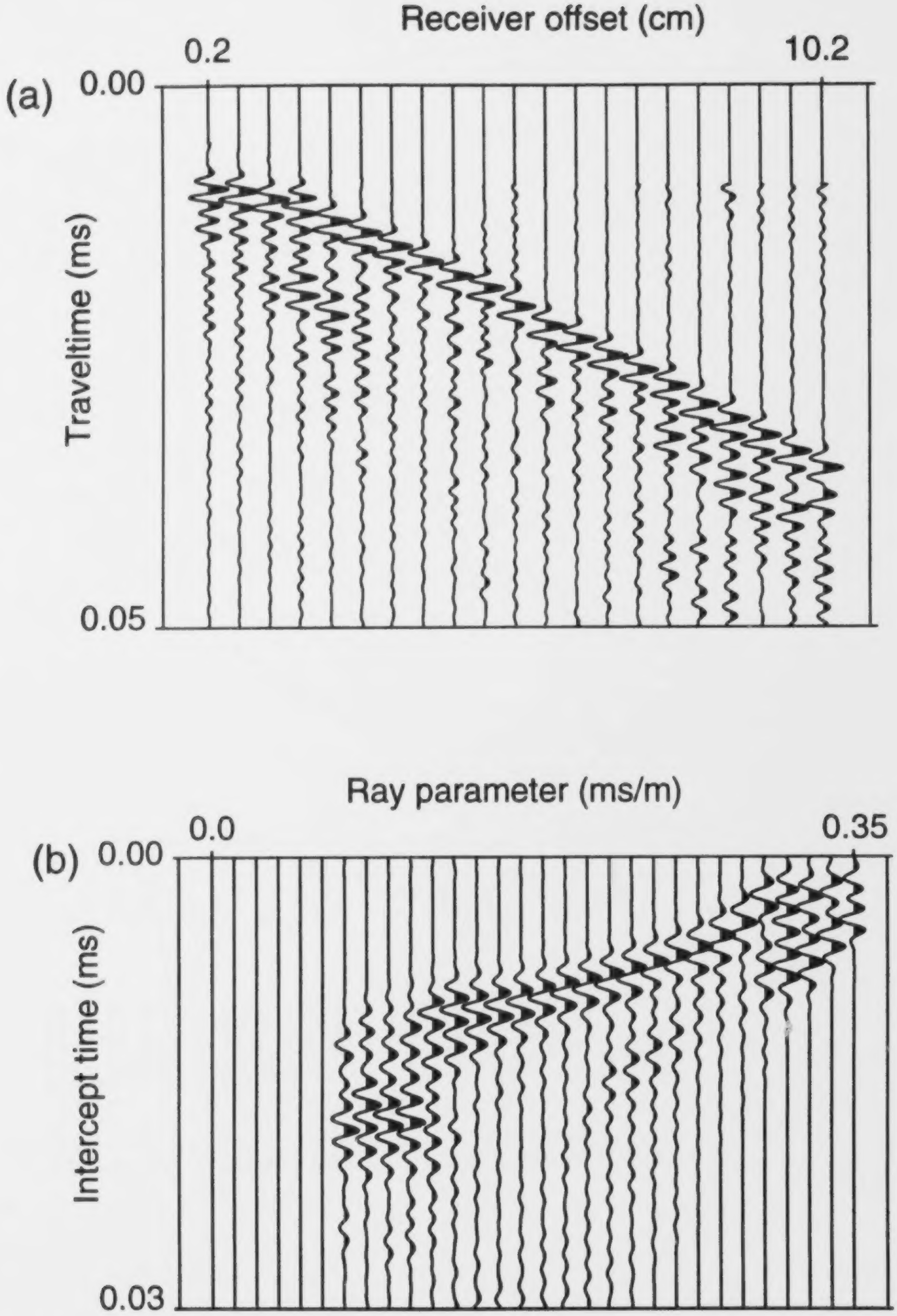

Figure A7. (a) Wave-forms observed for a transmitter on the side of the phenolic specimen at 2 cm from the top surface where 21 receivers are placed along a line in the *x-y* plane that contains the transmitter. (b) τ-p mapping of the wave-forms in (a).

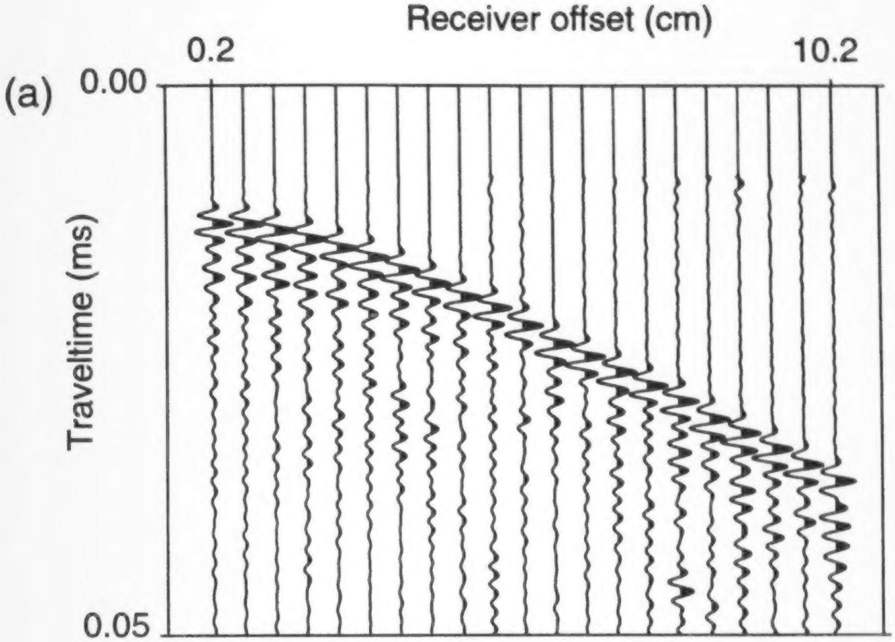

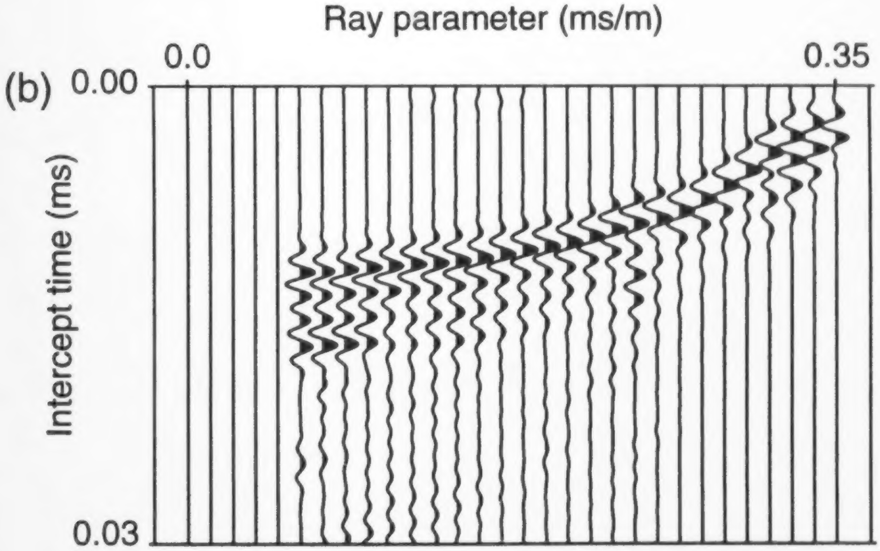

Figure A8. (a) Wave-forms observed for a transmitter on the side of the phenolic specimen at 3 cm from the top surface where 21 receivers are placed along a line in the *x*-*y* plane that contains the transmitter. (b) τ-p mapping of the wave-forms in (a).

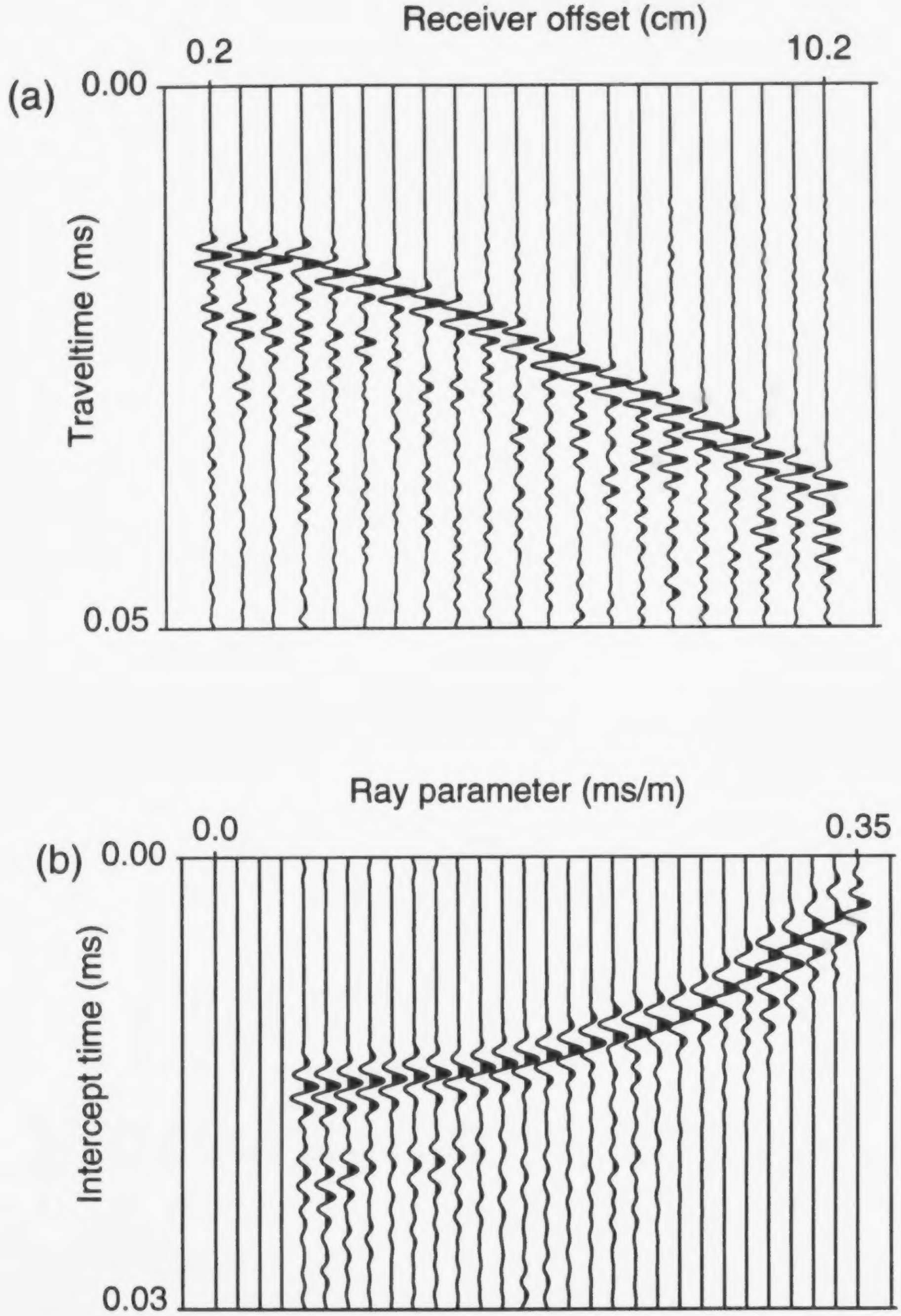

Figure A9. (a) Wave-forms observed for a transmitter on the side of the phenolic specimen at 4 cm from the top surface where 21 receivers are placed along a line in the x-y plane that contains the transmitter. (b) τ-p mapping of the wave-forms in (a).

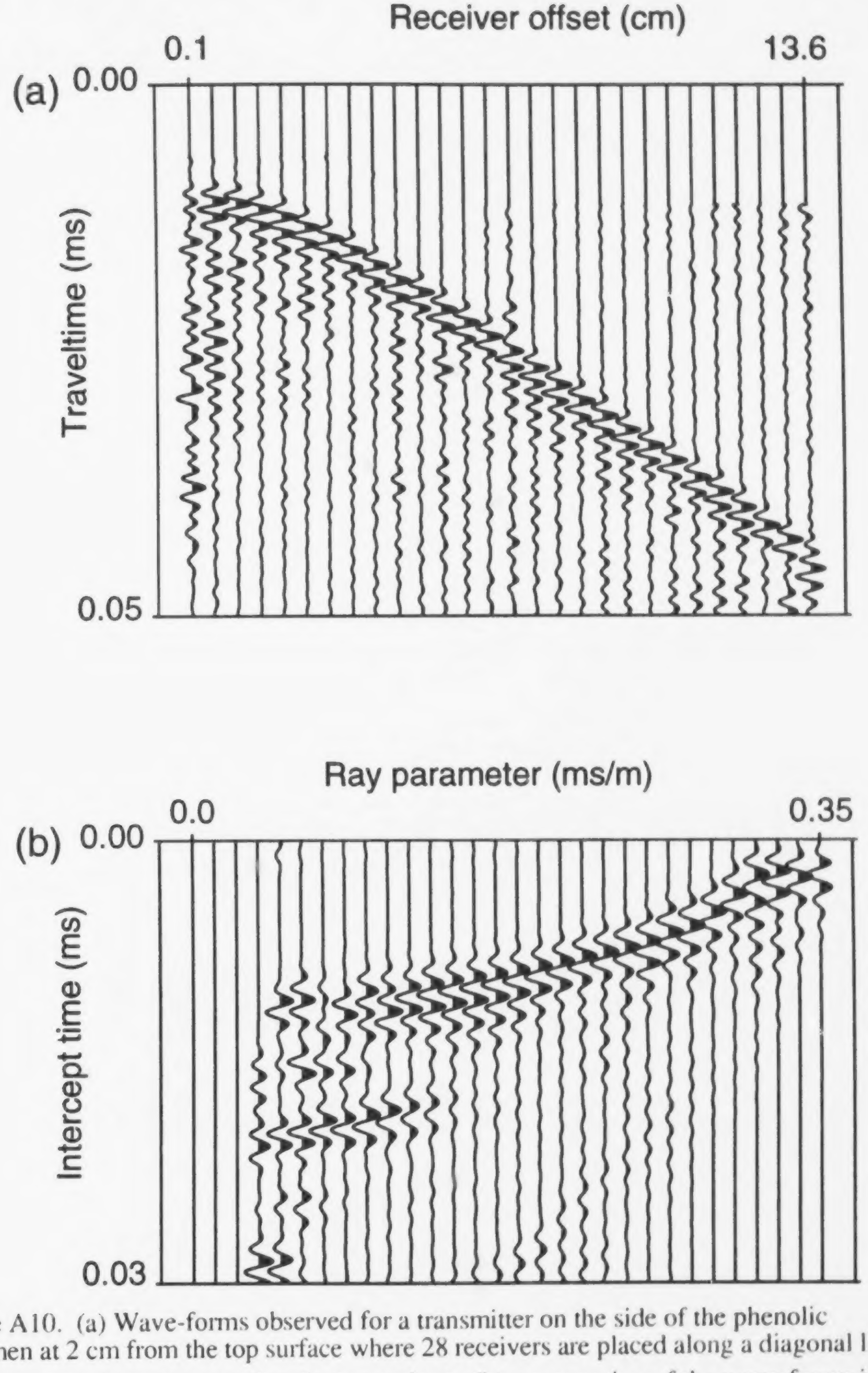

Figure A10. (a) Wave-forms observed for a transmitter on the side of the phenolic specimen at 2 cm from the top surface where 28 receivers are placed along a diagonal line in the vertical plane that contains the transmitter. (b) τ-p mapping of the wave-forms in (a).

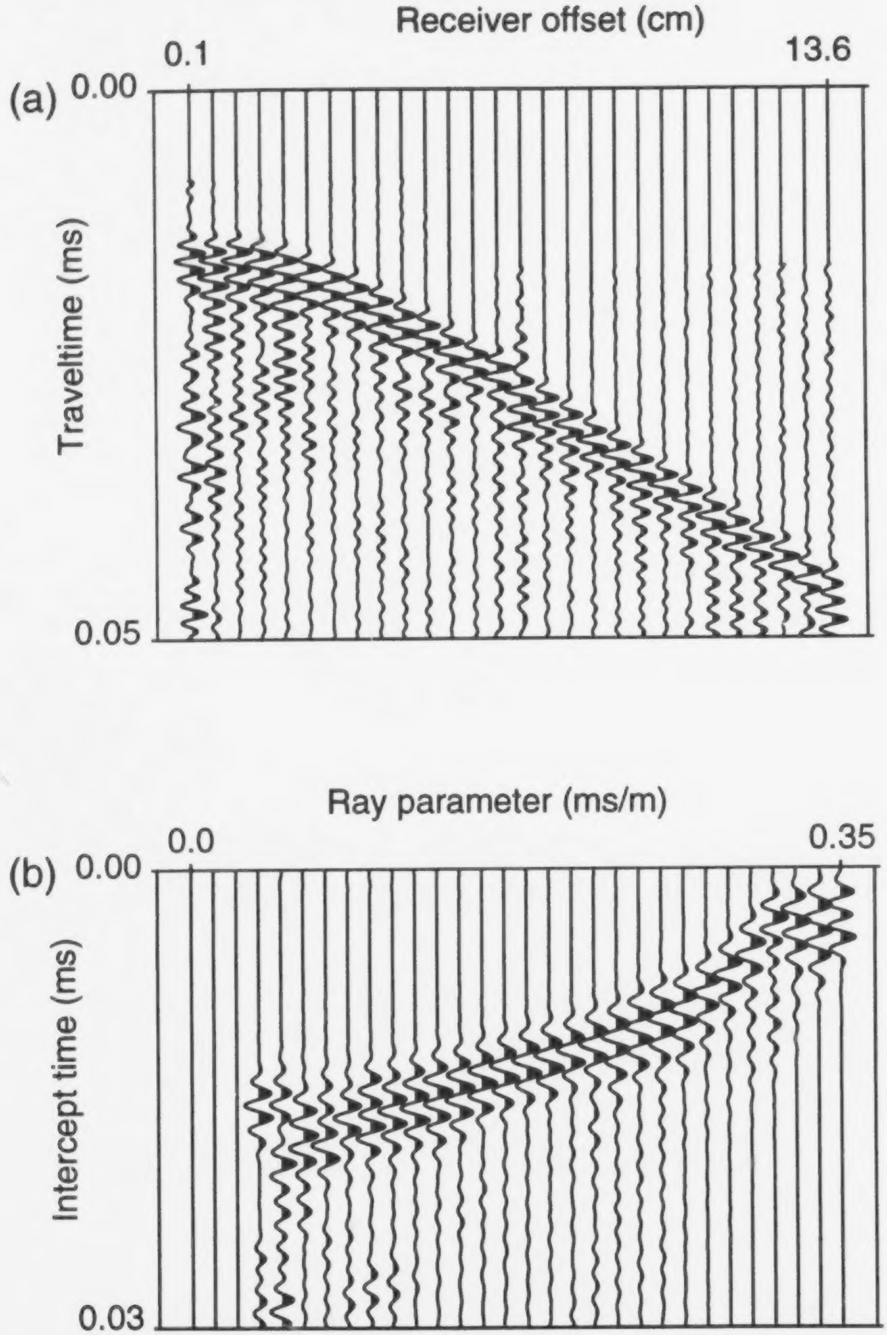

Figure A11. (a) Wave-forms observed for a transmitter on the side of the phenolic specimen at 3 cm from the top surface where 28 receivers are placed along a diagonal line in the vertical plane that contains the transmitter. (b) τ-p mapping of the wave-forms in (a).

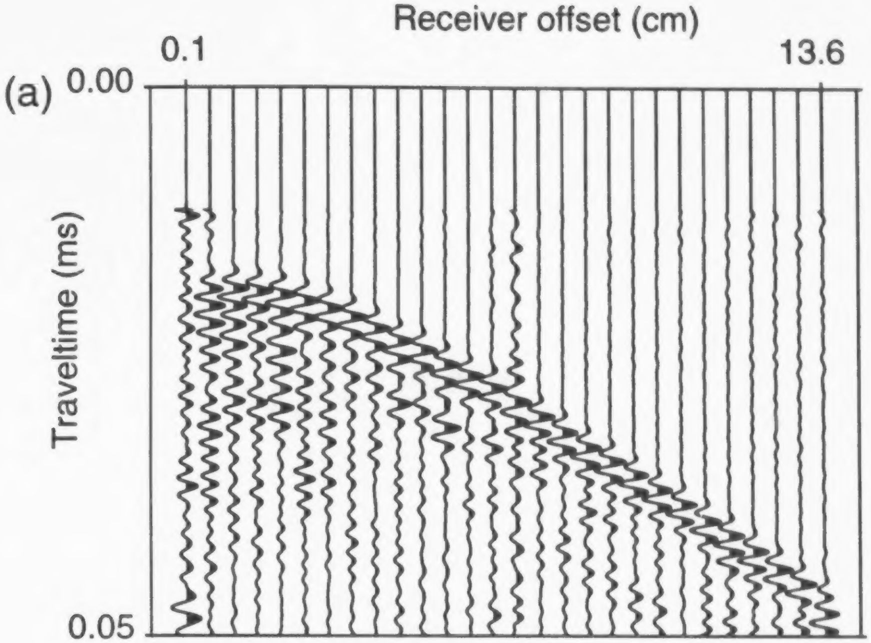

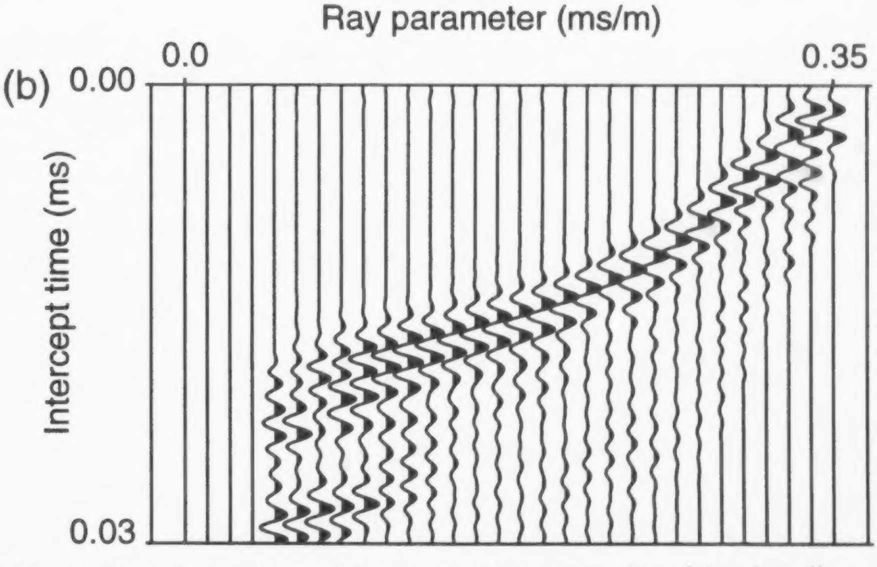

Figure A12. (a) Wave-forms observed for a transmitter on the side of the phenolic specimen at 4 cm from the top surface where 28 receivers are placed along a diagonal line in the vertical plane that contains the transmitter. (b) τ-p mapping of the wave-forms in (a).

Appendix B

The following pages have some of the programs I wrote to process the VSP data.

```
c      This program SYNT_VSP.F generates VSP synthetic data by simple convolution
c      of the time series with a Richer wavelet
c
c *****************************************************************
c
c             nlm  = number of layers of the model
c             v    = velocities
c             thic = thicknesses
c             npts =  number of  samples per trace
c
c
******************************************************************
       dimension  t(48) , x(48) , tr(1000,48),ns(48),tsq(48),xsq(48)
       dimension  wave(100),z(10) , v(10) , ang(10),xx(48),xc(48)
       dimension slp(48),vel(48),thic(10),rdp(20)
       dimension p(48),tao(48),nsp(48),p(48)
       character AA*6 , BB*6, CC*6, DD*6 , EE*10 ,FF*24, GG*12 , HH*12
       character PP*6 , QQ*8 ,RR*6
c
       data  nlm,v/4,2000.,2300.,2500.,2800.,6*0.0/
       data  thic/200.,300.,200.,200.,6*0.0/
       data nt,pmin/48,0.0/
       data tau,npts,nbp/2.0,500,48/
       write(6,*) 'enter xmin , xmax'
       read(5,*) xmin,xmax
c
       write(6,*) 'enter number of Geophone positions '
       read(5,*) ng
       write(6,*) 'enter Geophone positions in depth  (m)'
       read(5,*)  (rdp(i),i=1,ng)
c
       write(6,*) 'enter freqency of ricker wavelet'
       read(5,*) freq
c
       if (nt.GT.1) then
       xinc=(xmax-xmin)/float(nt-1)
         else
        xinc=0.0
          endif
       do 30 i=1,nt
       x(i)=xmin+(xinc*float(i-1))
30     continue
c
        do 20 ig = 1,ng
       write(6,*) 'Geophone  position  #  ', ig
c
c
*******************************************************************
c      Determination of the Geologic model above the Geophone position
c
*******************************************************************
c
              ss = 0.0
```

```
           ia = 1
1000             prss  = ss
           ss = ss + thic(ia)
           IF(ss.LT.rdp(ig)) then
             ia = ia + 1
             goto 1000
           ELSE
             nl = ia
            z(nl) = rdp(ig) - prss
          ENDIF
         do 1001 i = 1,nl-1
1001           z(i) = thic(i)
c
************************************************************************
*
c  computation of the incident angles and the offset of each emerging ray
c  The offset is computed with an accuracy of 1/100.
c
************************************************************************
*
c
c
       do 40 i=1,nt
       angmin = atan(x(i)/rdp(ig))
       deltax = (1./100.)*x(i)
      angin = 0.0001
c
100        ang(nl) = angmin
c
         call cmpanx(v,z,ang,nl,xcomp)
c
        if(xcomp.LT.x(i)) then
c
           angmin = angmin + angin
             goto 100
        else
c
400        if(abs(xcomp-x(i)).GT.deltax) then
c
           angin=angin/2.0
                 if((xcomp-x(i)).GT.deltax) then
            angmin=angmin-angin
                 else
             angmin=angmin+angin
                endif
c
          call cmpanx(v,z,ang,nl,xcomp)
c
           goto 400
            else
c
           time = 0.0
              do 70 m=1,nl
                 time = time+(z(m)/v(m))*sqrt((tan(ang(m)))**2+1.)
```

```
70                  continue
                  t(i) = time
                 p(i)=sin(ang(1))/v(1)
                  tao(i)=t(i)-p(i)*x(i)
                tsq(i) = t(i)**2
               endif
          endif
         xc(i)=xcomp
        xx(i)=xc(i)/1000.
        xsq(i) = xx(i)**2
40      continue
c
c
************************************************************************
c                creation of an output file  :  result.dat
c
************************************************************************
c
        AA = 'trace#'
        BB = 'time'
        CC = 'x(km)'
        DD = 'tsq'
        EE = 'xsqr'
        FF = 'number of of layers  ='
        GG = 'velocities'
        HH = 'thicknesses'
        PP = 'slope'
        QQ = 'velocity'
        RR = 'Reflector  depth     = '
c
        open(unit=11,file='result.dat')
        write(11,*) 'number of reflectors  =  ',nl
        write(11,108)
108     format(/)
c
        write(11,*) 'reflector depth  =  ',rdp(ig) ,'  m'
        write(11,108)
c
          write(11,fmt=103) GG,HH
c
103       format(10x,A10,10x,A12/)
        do 333 i=1,nl
          write(11,fmt=104)  v(i),z(i)
333              continue
104     format(10x,F10.5,10x,F9.5)
c
        write(11,106)
106     format(//)
        write(11,fmt=101) AA,BB,CC,DD,EE,PP,QQ
101     format(3X,A6,4X,A6,6X,A6,8X,A6,7X,A4,8x,A6,7x,A6/)
        slp(nt)=(tsq(nt)-tsq(1))/(xsq(nt)-xsq(1))
        vel(nt)=sqrt(1./slp(nt))
        do 444 i=2,nt
        slp(i-1) = (tsq(i)-tsq(1))/(xsq(i)-xsq(1))
```

```
      vel(i-1) = sqrt(1./slp(i-1))
444   continue
c
      do 222 i=1,nt
        write(11,fmt=102) i,t(i),xx(i),tsq(i),xsq(i),slp(i),vel(i)
102     format(3X,I3,5X,F8.6,5X,F8.6,5X,F8.6,5X,F8.6,5x,F8.6,5x,F8.6)
222   continue
      write(11,109)
109   format(//////)
c
        do 11 i=1,nt
       ns(i)=nint((1000.*t(i)/tau))
11     nsp(i)=nint(1000.*TAO(i)/tau)
      close(2)
c
      DT = tau/1000.0
      call RICKMOD(DT,freq,LS,t000,wave)
c
      open(unit=9,file='Ricker.dat')
        read(9,fmt=*),(wave(k),k=1,LS)
      close(9)
c
      call conv(nt,npts,LS,ns,tr,wave)


20    continue
      close(11)
c
      open(unit=8,file='data.dat',form='unformatted',access='direct',
   &          recl=npts*4)
        do 45 i=1,nt
          write(8,rec=i) (tr(j,i),j=1,npts)
45    continue
      close(8)
c
      stop
      end
c
c
***********************************************************************
c
c     subroutine  cmpanx computes the angles of incidence and
c     the corresponding offset of the emerging ray
c
c
***********************************************************************
c
      subroutine  cmpanx(v,z,ang,nl,xcomp)
      dimension v(10) , z(10) , ang(10)
            do 50 j=1,nl
              ang(j) = asin((v(j)/v(nl))*sin(ang(nl)))
50            continue
c
              xcomp = 0.0
            do 60 k=1,nl
          xcomp = xcomp +z(k)*tan(ang(k))
60       continue
      return
      end
c
c
***********************************************************************
c
      subroutine wavelet generates a dumped cosine wavelet
      # of samples = np , datafile = cos_dump.dat
      alfa = dumping coeff
c
c     ... choose ... alfa=0.8   ,   w=0.2  ,  np=51  :  np is odd integer
c
c
***********************************************************************
c
      subroutine wavelet(A,B,alfa,w,np)
      dimension A(50),B(100)

      do 10 i=1,(np-1)/2
       beta=-alfa*(i-1)
        A(i)=0.5*(cos(w*(i-1)))*exp(beta)
10    continue
cc
      open(unit=8,file='cos_dump.dat')
c
      do 20 i=1,(np-1)/2
20     B(i)=A((np-1)/2+1-(i-1))
      do 30 i=1,(np-1)/2+1
30     B((np-1)/2+i)=A(i)
      write(8,fmt=*) (B(i),i=1,np)
      close(unit=8)
      return
      end

      subroutine conv(nt,npts,LS,ns,tr,wave)
      dimension tr(1000,48),ns(48),wave(100)
       do 22 i=1,nt
         if(ns(i).GE.npts) then
           goto 22
         endif
             j1=ns(i)-(LS-1)/2
            j2=ns(i)+(LS-1)/2
          if(j2.GT.npts) then
            j2 = npts
           endif
          do 33 j=j1,j2
          IF((j-j1).LE.1) then
             goto 33
           endif
           tr(j,i)= tr(j,i)+wave(j-j1+1)
33        continue
```

```
22     continue
      return
      end
c
      subroutine rickmod(dt,f1,ls,t0,f)
c
c
c  computes modified ricker wavelet
c
c  second derivative of ( gaussian * polynomial window)
c
c  input:
c     dt = time sample interval (in seconds)
c     f1 = frequency of max amplitude of pulse spectrum
c
c  output:
c     ls = number of points in filter
c     t0 = time delay to center point of filter
c     f  = array of filter points
c
      dimension f(500)
      data  pi/3.1415927/
c
       write(6,*) 'enter sampling rate , frequency'
       read(5,*) dt,f1
c
      f0=.87*f1
      t0 = 1. / f0
      ls=.001+(t0/dt)
      t0=ls*dt
      ls=2*ls+1
c
c  define wavelet
c
c
      fmax=0.
      alpha=(pi*f0)**2
      do 100 i = 1, ls
      t = dt * (i-1)
      tau=t/t0
c
c     polynomial window and its drivatives
c
      g=(1.0-(tau-1)**2)**3
      gp=-6.0*(tau-1)*(1.0-(tau-1)**2)**2/t0
      gpp=6.0*(1.0-(tau-1)**2)*(5.0*(tau-1)**2-1.0)/(t0*t0)
c
c     gaussian and its derivatives
c     sign of h changed on purpose
c
      h=-exp(-alpha*(t-t0)**2)
      hp=-2.*alpha*(t-t0)*h
      hpp=-2.*alpha*(1.-2.*alpha*(t-t0)**2)*h
c
```

```
      f(i) = gpp*h + 2.0*gp*hp + g*hpp
      if (abs(f(i)).gt.fmax) fmax=abs(f(i))
100   continue

      fmax=1.0e+06/fmax
      do 200 i = 1, ls
      f(i) = f(i)*fmax
200   continue
       return
      end
```

```
c      This program STATIC.F calculates and applies static corrections
c      writen by A.KEBAILI on December 1991
c
c ..... change nt in parameter and input and output files and compile ..
c
       parameter(nt=18,npts=2501,tau=0.2,vw=1300)
       dimension h(nt),idt(30),tr(2600,48),ctr(2600,48)
c
       data  h/1.33,1.37,1.45,1.46,1.46,1.52,1.63,1.71,1.72,1.93,1.95,
     &         1.88,1.88,1.96,2.09,2.20,2.25,2.53/
c
       do 22 i=1,nt
       do 11 j=1,npts
       ctr(j,i)=0.0
11     continue
22     continue
c
       open(unit=1,file='north.files/n.200/XV_n200',
     &         form='unformatted',access='direct',recl=npts*4)
c
       open(unit=2,file='north.files/n.200/cXV_n200',
     &         form='unformatted',access='direct',recl=npts*4)
c
       do 100 i=1,nt
100       read(1,rec=i) (tr(j,i),j=1,npts)
c
c......................................................................................
c      Apply extra static correction   *  negative (backwards) positive (forwards)
c......................................................................................
c
       write(6,*) ' enter number of traces for extra static correction'
       read(5,*) is
       do 222 k=1,is
        write(6,*) 'enter order of trace    ',k,'  to be corrected and correction time (ms) '
          read(5,*) nbt , tm
            km=nint(ABS(tm)/tau)

c..................     negative  correction   (backwards)   ..............................

        if(tm.LT.0) then
          do 333 j=1,npts
            if((j+km).GT.npts) then
              ctr(j,nbt)=0.0
             else
            ctr(j,nbt)=tr(j+km,nbt)
             endif
333     continue

c.....................     positive  correction   (forward)   ...................................

        else
          do 444 j=1,npts
            if(j.LE.km) then
              ctr(j,nbt)=0.0
```

```
           else
          ctr(j,nbt)=tr(j-km,nbt)
           endif
444     continue
      endif
c
c ....................................... save  the  corrected  traces    ......................
c
      do 1010 j=1,npts
1010        tr(j,nbt)=ctr(j,nbt)
c
222   continue
c
c.............................  end  of  extra  static  correction    ................................
c
c .....  start elevation static correction ........  Note that if {h(i) -h(1)} >0 the stat >0......
c
      do 1011 i=1,nt
      do 1011 j=1,npts
1011        ctr(j,i) = 0.0
c
      do 10 i=1,nt
       tdel = (h(1)-h(i))*1000/(tau*vw)
      write(6,*) 'time delay for trace',  i   ,'     is    ',tdel
        if(tdel.GE.0.0) then
           idt(i)=nint(tdel)
             jmax=npts-idt(i)
         do 20 j=1,jmax
            ctr(j,i)=tr(j+idt(i),i)
20      continue
         write(2,rec=i) (ctr(j,i),j=1,npts)
c
      else
         idt(i)=nint(ABS(tdel))
           jmax=npts-idt(i)
          do 30 j=1,jmax
             ctr(j+idt(i),i)=tr(j,i)
30      continue
           write(2,rec=i) (ctr(j,i),j=1,npts)
      endif
10    continue
      close(1)
      close(2)
      end
```

```
c     This program EQUAL.F  equalizes and normalizes the traces.
c     written by A.KEBAILI on September 1991.
c
      parameter(nt=28,npts=15000,xmin=5,xmax=140.0,tau=0.008)
      dimension tr(npts,nt),x(nt),Amean(100),vmax(100)
c
c     .........................................................
c     CHANGE : nt , xmin , input file , output file ,x(i)???
c     .........................................................
c
      write(6,*) 'enter  alpha , beta '
      read(5,*) alpha,beta
c
c     xinc = (xmax-xmin)/(nt-1)
      xinc = 10.0
      do 10 i=1,nt
      x(i)=xmin+xinc*(i-1)
10    continue
c
      open(1,file='local1/Phenol/x-z.43/depth3/mPh.d3.XZ43.x-t',
     &         form='unformatted',access='direct',recl=npts*4)
        do 20 i=1,nt
          read(1,rec=i) (tr(j,i),j=1,npts)
20    continue
c
      open(unit=2,file='local1/Phenol/x-z.43/depth3/eqmPh.d3.XZ43.x-t',
     &         form='unformatted',access='direct',recl=npts*4)

          do 30 i=1,nt
              do 40 j=1,npts
                time = j*tau/1000.0
                  tr(j,i) = tr(j,i)*exp(alpha*x(i)+beta*time)
40            continue
30        continue

c
c...........................................................................
c  Computation of mean value and maximum absolute value of each trace
c...........................................................................
c
      do 60 i=1,nt
      sum=0.0
      do 70 j=1,npts
      if(vmax(i).LT.ABS(tr(j,i))) then
      vmax(i) = ABS(tr(j,i))
      endif
      sum=sum+ABS(tr(j,i))
70    continue
      Amean(I)=sum/npts
60    continue
c
c...........................................................................
c     Search for maximum mean value and maximum value of seismogram
c...........................................................................
```

```
c
      Amax = 0.0
      valmax = 0.0
      do 80 i=1,nt
        if(Amax.LT.Amean(i)) then
          Amax = Amean(i)
        endif
        if(valmax.LT.vmax(i)) then
          valmax = vmax(i)
        endif
80    continue
c
c..................................................................
c     Normalisation
c..................................................................
c
      do 90 i=1,nt
      if(Amean(i).GT.0.0) then
         do 100 j=1,npts
c         tr(j,i) = (tr(j,i)/vmax(i))*valmax
          tr(j,i) = (tr(j,i)/vmax(i))
100   continue
      endif
90    continue
c........................................................................
c     save  the equalized data
c........................................................................
        do 50 i=1,nt
          write(2,rec=i) (tr(j,i),j=1,npts)
50    continue
c
      close(1)
      close(12)
      end
```

```
c      this programm  "TPMAP.F" performs slant_stack mapping
c      of seismic or borehole data.
c      a ratio filter can be used ...   "ratio" between 0.0 and 1.0
c      to avoid using the ratio filter give to the parameter "ratio" a very low value .
c
c...   Change the following parameters: nt, nbp, npts(for x_t), npts1(for t_p), xinc, xmin ,
c             pmin, pmax, input and output file    ..............................
c      npts = nb samples / x_t traces,      npts1 = nb of samples / t_p trace

       parameter(nt=18,npts=2501,npts1=751,nbp=60)
       parameter(tau=0.2,xmax=100.0)
       dimension tr(npts,nt),tp(npts,nbp),x(nt),p(nbp),jdat(nt)
c
       data pmin,pmax/0.0000,0.0007/
c
       open(unit=8,file='north.files/n.200/eqcXV_n200',
     &        form='unformatted',access='direct',recl=npts*4)
c
       open(unit=12,file='/Cougar/users/ahmed/tp70_n200',
     &        form='unformatted',access='direct',recl=npts1*4)
c
c      ......................................................................................
c      CHANGE : nt , x(i) , xmin , xinc , pmin , pmax ,input file , output file
c      ......................................................................................
c
c      ...............................................................................
c                  define the offsets
c      ...............................................................................
       do 14 i=1,nt
14     x(i) = 0.0

       nt1=nt
c      nt2=2
c      nt3=3

       xmin = 20.0
       xinc = 10.0
       do 10 i=1,nt1
10     x(i)=xmin+xinc*(i-1)

c      xmin = 100
c      xinc=20
c      do 12 i=1, nt2
c12    x(i+nt1)=xmin+xinc*(i-1)

c      xmin = 150
c      xinc=30
cc     do 13 i=1, nt3
c13    x(i+nt1+nt2)=xmin+xinc*(i-1)


       write(6,*) (x(i),i=1,nt)
c..........................................................................................
c                read x-t data from data file
```

```
c..............................................................................

        do 20 i=1,nt
          read(8,rec=i) (tr(j,i),j=1,npts)
20      continue
        close(8)
c..............................................................................
c             trace  inversion
c..............................................................................
c
c       do 111 i=1,7
c       do 111 j=1,npts
c111          tr(j,i)=tr(j,i)*(-1)
c
c....................     trace  editing      ......................................

c       do 121 i=1,7
c       do 121 j=1,npts
c121          tr(j,13)=0.0

c..............................................................................
c       define the traces not to be includeed in the tau-p calculation
c..............................................................................
c
c       do 124 i=1,10
c       do 124 j=1,npts
c124          tr(j,i)=0.0
c
        pinc = (pmax-pmin)/(nbp-1)
        write(6,*) 'pinc   =   ',pinc
        write(6,*) 'enter ratio '
        read(5,*) ratio
c
        do 30 j=1,npts
          do 40 i=1,nbp
           p(i) = pmin+pinc*(i-1)
c
            do 50 k = 1,nt
             jdat(k) = j + nint(p(i)*x(k)*1000.0/tau)
50          continue
              do 60 k = 2,nt
                if(jdat(k).GE.npts) then
              goto 40
            endif
          datrat = tr(jdat(k),k)/tr(jdat(k-1),k-1)
            if(datrat.GE.ratio.AND.datrat.LE.(1./ratio)) then
              tp(j,i) = tp(j,i) + tr(jdat(k-1),k-1)
              goto 60
              else
                goto 60
              endif
60      continue
40      continue
30      continue
```

```
c..............................................................................
c      save tau-p data
c..............................................................................

         do 70 i=1,nbp
           write(12,rec=i) (tp(j,i),j=1,npts1)
70     continue
       close(11)
       close(12)
       stop
       end
```

```
c       This program WINDOW.F uses a Gaussean function to window the datap
c
        parameter(nt=60,npts=751,tau=0.2)
        dimension tr(npts,nt),itr(10),t1(10),t2(10)
        dimension ntmax(100),vmax(100),t(100),ctr(npts,nt)
        character*20 input
        character*20 output
        write(6,*) 'enter input filename '
        read(5,*) input
c
        write(6,*) 'enter output filename '
        read(5,*) output
c
        open(unit=1,file=input,form='unformatted',
     &          access='direct',recl=npts*4)

        open(unit=9,file=output,form='unformatted',
     &          access='direct',recl=npts*4)
c

        write(6,*) 'enter number of windows including those of first and last traces'
        read(5,*) nw
c       write(6,*) 'enter trace number,beginning time(ms),ending time(ms) of each window'
        do 10 i=1,nw
        write(6,*) 'window  ',i,'  : enter  trace # , initial time(ms) , final time(ms)'
        read(5,*) itr(i),t1(i),t2(i)
10      continue
c
        open(unit=1,file='wftp70_n210.norm',form='unformatted',
     &          access='direct',recl=npts*4)
        open(unit=9,file='wftp70_n210.nrm',form='unformatted',
     &          access='direct',recl=npts*4)
c
          do 20 i=1,nt
            read(1,rec=i) (tr(j,i),j=1,npts)
20      continue
        close(1)
        write(6,*) 'data read and data_file closed'
c
        inw = nw - 1
        do 30 i=1,inw
          delt1 = t1(i+1) - t1(i)
           delt2 = t2(i+1) - t2(i)
              deltr = itr(i+1) - itr(i)
                 slop1 = delt1/deltr
                 slop2 = delt2/deltr
        i1 = itr(i)
        i2 = itr(i+1)
c
        do 40 j = i1,i2
         tt1 = t1(i) + slop1*float(j-i1)
         tt2 = t2(i) + slop2*float(j-i1)
                 k1 = nint(tt1/tau)
                 k2 = nint(tt2/tau)
```

```
      wmax = 0.0
c
      do 50 ii = k1,k2
         IF(wmax.LE.tr(ii,j)) THEN
             wmax = tr(ii,j)
             iwmax = ii
         ENDIF
50    continue
          vmax(j) = wmax
           ntmax(j) = iwmax
      t(j) = (ntmax(j)*tau/1000.)

40    continue

30    continue

c100       format(10x,I4,10x,f10.7,10x,f10.7,10x,f14.5/)

      ntt=nt-2
c
c.........................................................................
c          windowing of the data
c.........................................................................
c
      write(6,*) 'enter  alpha for exp(-(t/alpha)**2)'
      read(5,*) alpha
             do 60 i =1,nt
                do 70 j=1,npts
                     time = (j-ntmax(i))*tau
                     tr(j,i) = tr(j,i)*exp(-(time/alpha)**2)
70    continue
60    continue
c
c**********************************************************************
c          up time shift of the windowed data
c**********************************************************************
c
      write(6,*) 'enter time shift in msec'
      read(5,*) dt
      it = nint(dt/tau)
             do 110 i =1,nt
                do 120 j=1,npts
      jj = j+it
         if(jj.LE.npts) then
             ctr(j,i) = tr(jj,i)
         else
             ctr(j,i) = 0.0
          endif
120   continue
110   continue
c.............................      save  windowed  data     ..............................
        do 80 i=1,nt
          write(9,rec=i) (ctr(j,i),j=1,npts)
80    continue
```

```
close(9)
end
```

```
c     this programm "LSTRIP.F" performs the layer stripping
c     of the data in the tau_p domain
c     written by Ahmed Kebaili on March 1991
c
c     change pmin and pmax to the actual values . change input and output datafiles
c
      parameter(nbp=60,npts=751,tau=0.2)
      dimension tps(npts,nbp),tp(npts,nbp) , p(nbp)
      dimension t0(10) , vl(10)
      data pmin,pmax/0.000,0.0005/

      write(6,*) 'enter  v1 , depth of first geophone position'
      read(5,*) vinit,z1

      write(6,*) 'enter depth '
      read(5,*)  npts,tau,nbp
      pmin=sin(atan(xmin/z1))/vmax
        pmax=sin(atan(xmax/z1))/vinit
      pinc = (pmax-pmin)/(nbp-1)
c
      write(6,*) 'enter number of layers to strip '
      read(5,*) ls
      open(unit=12,file='eqwtoP_n50',form='unformatted',access='direct',
     &         recl=npts*4)
c
        do 100 i=1,nbp
          read(12,rec=i) (tp(j,i),j=1,npts)
100   continue
      close(12)
      write(6,*) 'enter time (in ms) to which samples are put to zero'
      read(5,*) temps
      jzero = nint(temps/tau)
      do 130 i=1,nbp
      do 140 j=1,jzero
      tp(j,i)=0.0
140   continue
130    continue
      endif
c
       do 30 i=1,ls
        write(6,*) 'enter vertical time(ms) and velocity(m/s) of layer ',i,'   to be stripped'
         read(5,*) t0(i),vl(i)
30     continue
c
      do 50 i=1,nbp
      do 60 j=1,npts
      tps(j,i)=0.0
60    continue
50     continue
c
      do 10 i = 1,nbp
        p(i)=pmin+pinc*(i-1)
        deltau = 0.0
         do 40 k=1,ls
         value = 1-p(i)**2*vl(k)**2
       if(value.LT.0.0) then
         goto 10
        else
          deltau = deltau + t0(k)*(1.0 - sqrt(value))
        endif
40       continue
          ncor = nint(deltau/tau)
        do 20 j=1,npts
          jj = j-ncor
          if(jj.LT.1) then
              tps(j,i)=0.0
          else
              tps(j,i) = tp(jj,i)
            endif
20       continue
10    continue

c
      *******************************************************************
*
c
c                   mute of the some of remaining noise
c
c
      *******************************************************************
*
c
      write(6,*) 'pmax =  ',pmax
      write(6,*) 'pinc =  ',pinc
      write(6,*) 'enter tmax (in sec)of first P and  ppmax  (to find slop of muting line)'
      read(5,*) ttmax,ppmax
      ipmax = nint(ppmax/pinc)
        if(ipmax.LT.nbp) then
          do 70 i=1,ipmax
            it = nint(1000.0*((-ttmax*p(i)**2/ppmax**2)+ttmax)/tau)
           do 80 j = it,npts
             tps(j,i) = 0.0
80          continue
70         continue
         imax = ipmax+1
      do 90 i=imax,nbp
      do 91 j=1,npts
      tps(j,i) = 0.0
91    continue
90    continue
         else
      do 95 i=1,nbp
            it = nint(1000.0*((-ttmax*p(i)**2/ppmax**2)+ttmax)/tau)
           do 96 j = it,npts
             tps(j,i) = 0.0
96          continue
95         continue
        endif
      open(unit=13,file='seqwtoP_n50',form='unformatted',access='direct',
     &        recl=npts*4)
c
        do 110 i=1,nbp
          write(13,rec=i) (tps(j,i),j=1,npts)
110   continue
      close(13)
c
      stop
      end
```

```
c     This program TPICK.F picks automatically the intercept times used to computes
c     the velocities.
c
      dimension tr(2600,90),itr(3),t1(3),t2(3),deltat(100),deltax(100)
      dimension ntmax(100),vmax(100),A(2600),t(100),h(100),v(100),hmid1(100)
      dimension v2(100),v4(100)
c
      parameter(npts=2501,tau=0.2)
      data h(1),h(2),h(3)/10,15,25/
      data hmid1(1),hmid1(2),hmid1(3)/17.5,21.5,27.5/
      data nt,nw,itr,t1,t2/83,3,1,61,82,25,100,110,42,120,130/

      do 80 i=4,83
      h(i)=h(3)+2.5*float(i-3)
      hmid1(i)=hmid1(3)+2.5*float(i-3)
80    continue
c
c..........................................................................................
c
c           conversion of read depths to actual depth of geophone
c
c..........................................................................................
c
      do 90 i=1,83
      h(i) = (h(i)/1.009) + 1.5
      hmid1(i) = (hmid1(i)/1.009) + 1.5
90    continue
c
      write(6,*) 'enter total number of traces  (must be an odd integer)'
      read(5,*) nt
      write(6,*) 'enter number of windows including those of first and last traces'
      read(5,*) nw
      write(6,*) 'enter trace number,beginning time(ms),ending time(ms) of each window'
      do 10 i=1,nw
      write(6,*) 'window  ',i,'  : enter  trace # , initial time(ms) , final time(ms)'
      read(5,*) itr(i),t1(i),t2(i)
10    continue
c
      open(unit=1,file='eqVtube',form='unformatted',access='direct',
     &       recl=npts*4)

      read(1,rec=1) (A(j),j=1,npts)
        do 20 i=1,nt
          read(1,rec=i+1) (tr(j,i),j=1,npts)
20    continue
      close(1)
      write(6,*) 'data read and data_file closed'
c
      open(unit=11,file='tube.time')
      inw = nw - 1
      do 30 i=1,inw
        delt1 = t1(i+1) - t1(i)
         delt2 = t2(i+1) - t2(i)
           deltr = itr(i+1) - itr(i)
          slop1 = delt1/deltr
          slop2 = delt2/deltr
      i1 = itr(i)
      i2 = itr(i+1)
c
      do 40 j = i1,i2
       tt1 = t1(i) + slop1*float(j-i1)
       tt2 = t2(i) + slop2*float(j-i1)
          k1 = nint(tt1/tau)
          k2 = nint(tt2/tau)
      wmax = 0.0
c
      do 50 ii = k1,k2
         IF(wmax.LE.tr(ii,j)) THEN
            wmax = tr(ii,j)
            iwmax = ii
         ENDIF
50    continue
         vmax(j) = wmax
          ntmax(j) = iwmax

c..................................................................................
c
c           computation of vertical time
c
c.....................................................................................
c
      t(j) = (ntmax(j)*tau/1000.)*cos(atan(12./h(j)))

40    continue

30    continue

100
      format(8x,I4,4x,f8.3,4x,f8.5,4x,f8.5,4x,f8.3,4x,f10.3,2x,f10.3,2x,f10.3,2x,f10.3
,2x,f10.3/)

      ntt=nt-2
      write(6,*) '     trace #  depth    time     deltat    midpt_depth  Inst.vel    Aver.vel
Aver.vel '
      write(11,*)'     trace #  depth    time     deltat    midpt_depth  Inst.vel    Aver.vel
Aver.vel'

      write(6,200)
      write(11,200)
200   format(/)

      ntt4=(ntt-1)/4
      do 33 i=1,ntt4
         i4=4*i
         v4(i4+1)=(h(i4+1)-h(i4-3))/(t(i4+1)-t(i4-3))
       v4(i4)=v4(i4+1)
      v4(i4-1)=v4(i4)
      v4(i4-2)=v4(i4)
```

```
33    continue
      v4(1)=v4(2)

      ntt2=(ntt-1)/2
      do 22 i=1,ntt2
         i2=2*i
         v2(i2+1)=(h(i2+1)-h(i2-1))/(t(i2+1)-t(i2-1))
        v2(i2)=v2(i2+1)
22    continue
      v2(1)=v2(2)

      do 70 j=1,ntt
      deltat(j)=t(j+2)-t(j)
      deltax(j)=h(j+2)-h(j)
      v(j)=deltax(j)/abs(deltat(j))
        write(6,100) j,h(j),t(j),deltat(j),hmid1(j),v(j),v2(j),v4(j)
        write(11,100) j,h(j),t(j),deltat(j),hmid1(j),v(j),v2(j),v4(j)
70    continue
c
      close(11)
c
      end
```

```
c     this programm "VELAN.F" yields the vertical time and velocity
c     of a chosen layer or a geophone position (tau_p data).
c     it uses the layer stripped data.
c
      parameter(nbp=60,npts=2501,tau=0.2)
      dimension tps(npts,nbp),tpc(npts,nbp),sembl(100,100),t0(100)
      dimension v(100),p(nbp),Ampl(100,100),Ener(100,100),smbmax(100),velo(100)

      dimension Energ(100),VCTY(100)
c
c     **********     change pmin pmax and input and output data files  **********
c
      data pmin,pmax/0.000,0.0007/
      data ngeo,its,alpha/1,1,7/
      character A1*6 , A2*6 ,A3*6 , A4*6
      write(6,*) 'enter  v1 , depth of first geophone , vmax'
      read(5,*)  v1,z1,vmax
      write(6,*) 'enter : start time (ms) , window_length (odd # of samples) , # of
windows'
      read(5,*) startt,lwind,nw
      write(6,*) 'enter :initial velocity (m/s) , velocity increment (m/s) , # of velocities'
      read(5,*) v0,vinc,nvel
      write(6,*) 'enter :# of first (t_p) trace  , # of last (t_p) trace to be taken into account '
      read(5,*) ipi,ipf
c
      write(6,*) 'enter window jump (in # of samples) ,  power of semblance "alpha" '
      read(5,*) its,alpha
        pmax=sin(atan(xmax/z1))/v1
        pmin=sin(atan(xmin/z1))/vmax
        pinc = (pmax - pmin)/(nbp-1)
c
      write(6,*) 'enter  order of geophone position '
      read(5,*) ngeo

        IF(ngeo.EQ.1) THEN
      open(unit=12,file='eqwtoplot_n25.new',form='unformatted',access='direct',
     &         recl=npts*4)

        do 110 i=1,nbp
          read(12,rec=i) (tps(j,i),j=1,npts)
110   continue
      close(12)
        ELSE

      open(unit=13,file='svsp2.top',form='unformatted',access='direct',
     &         recl=npts*4)
        do 300 i=1,nbp
          read(13,rec=i) (tps(j,i),j=1,npts)
300   continue
      close(13)
      nlay = ngeo-1
      write(6,*) 'enter vertical time (ms) to geophone position   ',nlay
      read(5,*) t00
        ENDIF
```

```
c
c*********************************************************
c
      do 10 i=1,nw
      smbma=0.0
      Energy=0.0
       t0(i) = startt+its*tau*(i-1)
      do 20 j = 1,nvel
        v(j)=v0+vinc*(j-1)
         do 100 ii=1,nbp
           do 200 jj=1,npts
             tpc(jj,ii) = 0.0
200          continue
100      continue
      do 30 k = ipi,ipf
        p(k)=pmin+pinc*(k-1)
      sqval=1-p(k)**2*v(j)**2
       if(sqval.LT.0.0) goto 30
         deltau=(t0(i)-t00)*(1.0 - sqrt(sqval))
          ncor = nint(deltau/tau)
         do 40 l=1,npts
           ll = l-ncor
           if(ll.LT.1) then
              tpc(l,k)=0.0
           else
              tpc(l,k) = tps(ll,k)
            endif
40       continue
30    continue
c.....................................................................
c     semblance numerator computation
c.....................................................................
      am=0.0
      sumsq = 0.0
      is = nint(t0(i)/tau)-(lwind-1)/2
      ie = is + lwind - 1
      do 60 n=is,ie
        sum = 0.0
       do 50 m = 1,nbp
        sum=sum+tpc(n,m)
50     continue
      am= am+sum
        sumsq=sumsq+sum**2
60    continue
      Ampl(j,i)=am
c................................................................
c     semblance denominator computation
c................................................................
      sd = 0.0
       do 70 i1 = 1,nbp
         do 80 j1=is,ie
           sd = sd+tpc(j1,i1)**2
80       continue
70     continue
```

```
      Ener(j,i) = sd
c...........................................................................
c     semblance computation
c...........................................................................
      denom = (ipf-ipi+1)*sd

      IF(denom.LT.1.) THEN
         sembl(j,i)=0.
      ELSE
        smblce=sumsq/denom
       sembl(j,i) =smblce**alpha
      ENDIF

      IF(smblce.GT.smbma) THEN
        smbma=smblce
        actvel = v(j)
      ENDIF
c
      IF(sd.GT.Energy) THEN
      Energy = sd
      velct = v(j)
      ENDIF
c
20    continue
      smbmax(i)=smbma
      velo(i)=actvel
      Energ(i) = Energy
      VCTY(i)=velct
      write(6,*) 'window   ',i,'   done'
10    continue

      enern=0.0
      do 123 i=1,nw
      IF(Energ(i).GT.enern) THEN
      enern=Energ(i)
      ENDIF
123   continue
        do 124 i=1,nw
          Energ(i)=Energ(i)/enern
124   continue

      sembl(j,i) = sumsq
      write(20,fmt=104) t0(i),v(j),sembl(j,i),Ampl(j,i)
104   format(4X,F8.3,6X,F8.3,6X,F8.6,6X,F16.2)
c

      close(20)
c
      open(unit=16,file='sembP_n25.S.data',form='unformatted',access='direct',
     &        recl=nvel*4)

      open(unit=17,file='EnerP_n25.S.data',form='unformatted',access='direct',
     &        recl=nvel*4)
```

```
          do 120 i=1,nw
            write(16,rec=i) (sembl(j,i),j=1,nvel)
        write(17,rec=i) (Ener(j,i),j=1,nvel)
120     continue
        close(16)
        close(17)
c
        open(unit=18,file='topc.data',form='unformatted',access='direct',
     &          recl=npts*4)
          do 130 i=1,nbp
            write(18,rec=i) (tpc(j,i),j=1,npts)
130     continue
        close(18)

        do 90 i=1,nw
        write(6,*) (sembl(j,i) , j=1,nvel)
        write(6,*) 'Ampl = ',(Ampl(j,i),j=1,nvel)
        write(6,*) 'Energy = ',(Ener(j,i),j=1,nvel)
        write(6,1001)
1001          format(/)
90      continue
c
        open(unit=11,file='smbl.n25.data')
        write(6,*) '              file n25     '
        write(11,*)'              file n25     '
c       write(6,102)
        write(11,102)

        write(6,*) '  trace #  time      velocity    max.sembl    velocity     Energy'
        write(11,*)'  trace #  time      velocity    max.sembl    velocity     Energy'
        write(6,102)
        write(11,102)
        do  90 i=1,nw
        write(6,fmt=104) i,t0(i),velo(i),smbmax(i),VCTY(i),Energ(i)
c
        write(11,fmt=104) i,t0(i),velo(i),smbmax(i),VCTY(i),Energ(i)
c
90      continue
104     format(4X,I3,4X,F8.3,6X,F8.3,6X,F8.6,6X,F8.3,6X,F8.5)
102     format(/)
        close(11)
c
        stop
        end
```

```
c     This program VELCAL.F picks automatically the intercept times of events on ellipses
c     and calculatesthe velocity corresponding to each ray parameter p
c
      dimension tr(2600,100),itr(3),t1(3),t2(3)
      dimension ntmax(100),vmax(100),t(100),v(100)
      dimension p(100),ang(100)
c
c........................ tau (ms),  p (s/m), z (m) = geophone depth difference ...........
c
      parameter(npts=751,tau=0.2)
      data nt,pmin,pmax/60,0.000,0.0007/

      open(unit=1,file='/Cougar/users/ahmed/east.files/e.25/ftp_e25',
     &        form='unformatted',access='direct',recl=npts*4)
c
      open(unit=11,file='/Cougar/users/ahmed/east.files/e.25/vel.data2')
      write(11,*) 'velocity data for -1 : e_25 '
      write(6,*) 'velocity data for -1 : e_25 '
c
      write(6,*)'enter nb of windows of actual geoph. including the first and last ones'
      read(5,*) nw
c
      write(6,*) 'enter order of traces at  windows'
      read(5,*) (itr(i),i=1,nw)
c
      write(6,*) 'enter the    ',nw,'   initial times (ms) of the windows'
      read(5,*) (t1(i),i=1,nw)
c
      write(6,*) 'enter the    ',nw,'   final times (ms) of the windows'
      read(5,*) (t2(i),i=1,nw)
c
      write(6,*) ' enter depths of previous and actual geophones'
        read(5,*) depth1, depth2
c
      write(6,*) ' enter vertical traveltimes to previous and actual geophones'
        read(5,*) t01,t02

      depth1 = depth1/1.009
      depth2 = depth2/1.009 + 1.5
      write(6,*) 'depth1 =    ',depth1
      write(6,*) 'depth2 =    ',depth2

      write(6,*) ' '
        read(5,*) xmin1, tt1
          write(6,*) ' enter mini.offset & its traveltime for the actual geophone in ms'
            read(5,*) xmin2, tt2
              t01= tt1*cos(atan(xmin1/depth1))
              t02= tt2*cos(atan(xmin2/depth2))
c
      pinc = (pmax - pmin)/(nt-1)
        do 20 i=1,nt
          read(1,rec=i) (tr(j,i),j=1,npts)
      p(i) = pmin + pinc*(i-1)
20    continue
```

```
        close(1)
        write(6,*) 'data read and data_file closed'
c
        inw = nw - 1
        do 30 i=1,inw
         delt1 = t1(i+1) - t1(i)
          delt2 = t2(i+1) - t2(i)
            deltr = itr(i+1) - itr(i)
               slop1 = delt1/deltr
               slop2 = delt2/deltr
        i1 = itr(i)
        i2 = itr(i+1)
c
        do 40 j = i1,i2
         tt1 = t1(i) + slop1*float(j-i1)
         tt2 = t2(i) + slop2*float(j-i1)
               k1 = nint(tt1/tau)
               k2 = nint(tt2/tau)
        wmax = 0.0
c
        do 50 ii = k1,k2
           IF(wmax.LE.ABS(tr(ii,j))) THEN
               wmax = ABS(tr(ii,j))
               iwmax = ii
           ENDIF
50      continue
            vmax(j) = wmax
             ntmax(j) = iwmax

c.......................................................................................
c
c       computation of time and velocity for each ray parameter p
c
c.......................................................................................
c
        t(j) = ntmax(j)*tau/1000
40         continue

30      continue
c
              tdelay = (ntmax(1)*tau -t02 ) + t01
        write(6,*) 'int. time at p=0 is   ',ntmax(1)
        write(6,*) 'time delay (ms)  =    ',tdelay
c
        do 88 j = 1, nt
             t(j) = t(j)-tdelay/1000.
88      continue
c
        write(6,*) '  trace nb     int. time         inc. angle     ray para. p        velocity (m/s)'
        write(11,*) '  trace nb     int. time         inc. angle     ray para. p        velocity (m/s)'
c
        do 19 j=1,nt
        v(j) = 1.0/SQRT(p(j)**2+(t(j)**2/(depth2-depth1)**2))
```

```
      ang(j)=(180/3.14)*asin(p(j)*v(j))
c
        write(6,100) j,t(j),ang(j),p(j),v(j)
        write(11,100) j,t(j),ang(j),p(j),v(j)
19    continue
c
100   format(5x,I5,5x,f10.6,5x,f10.6,5x,f10.8,5x,f10.2)
      close(11)
c
      end
```